Zhemeng Wu

Queen's College

Neuronal mechanisms in prefrontal and temporal lobe cortical areas underlying perceptual and mnemonic processes

Thesis submitted for the degree of Doctor of Philosophy

Trinity Term 2020

Table of Contents

Abstract 2

Detailed Abstract 4

Acknowledgments 8

General Introduction 12

Chapter 1. Frontopolar cortex is a mediator of network modularity in the primate brain . 66

Chapter 2. Dissociation of dorso-lateral and dorso-medial prefrontal cortex contributions to familiarity and recollective processes in primates 122

Chapter 3. Similar time course of fast familiarity and slow recollection processes for recognition memory in humans and macaques 92

Chapter 4. Contributions of prefrontal and temporal lobe cortical areas to recognition memory for novel and familiar visual stimuli in non-human primates 170

Chapter 5. Contributions of prefrontal and temporal lobe cortical areas to recognition memory and perceptual discrimination 230

Chapter 6. Hippocampal-prefrontal theta coherence during the encoding phase signaling successful recognition memory performance (on-going project) 284

General Discussion 314

References 329

Supplemental Materials 362

Abstract

The medial temporal lobe (MTL) cortical areas, including hippocampus, perirhinal and entorhinal cortex and parahippocampal cortex, are known to support recognition memory. Inferotemporal cortex (IT) is involved in processing visual stimulus during recognition memory, and reciprocally projects to some regions of MTL (e.g. perirhinal cortex). Many neuroimaging, neuropsychological and neurophysiological studies have also emphasized the role of the prefrontal cortex (PFC) in maintaining information during working memory. Although the function of MTL was traditionally viewed as containing a system of structures exclusively involved in memory, a recent perceptual-mnemonic debate over MTL indicates some MTL structures (e.g. perirhinal cortex and hippocampus) contribute to perceptual discrimination. Various versions of cognitive tasks have been implemented to investigate different roles of MTL, IT and PFC in memory and perception, such as cognitive tasks with either mnemonic (i.e. memory tasks with delays) or perceptual demands (i.e. simultaneous discrimination tasks without delays). However, it's still unknown i) whether sub-areas of MTL, sub-regions of PFC or IT operate in the same or different manner when contributing to memory tasks with delays versus simultaneous discrimination tasks without delays; and ii) how any of these areas interact when supporting these tasks; and iii) whether the neural mechanisms in NHPs and in humans differ or not when they perform homologous memory tasks. The motivating idea for the body of work in this thesis is that some of the same brain regions in MTL, IT and PFC may interact differently to underlie mnemonic or perceptual

processes, and/or that different combinations of brain areas (networks and sub-networks) may be recruited for different cognitive processes. To investigate interactions both within MTL, IT and PFC and between these areas in a battery of task variants, I recorded neural activities in a range of perceptual and mnemonic tasks using a simultaneous multi-area, multi-electrode recording paradigm in three awake macaques. Then to generalize the neural mechanism of recognition memory from NHPs to humans, I applied a series of homologous behavioral paradigms to both primates to investigate recollection and familiarity, which are two recognition memory processes based on dual-process theory. To bridge the species divide, I implemented NHP electrophysiological recordings and targeted transcranial magnetic stimulation (TMS) in humans in several homologous recognition memory tasks to investigate both the neural substrates and time course of recollection and familiarity processes, as these two processes are key considerations pertaining to human functional anatomy of MTL and PFC regions. Finally, I investigated the interaction between frontopolar cortex (FPC) and other brain regions during resting state using circumscribed FPC lesions in NHPs and network cluster analyses of whole brain functional connectivity analyses, to illustrate NHP FPC might help implement long-standing diverse neural network dynamics.

Detailed Abstract

The MTL cortical regions, including hippocampus, perirhinal cortex, entorhinal cortex and parahippocampal cortex, and IT cortex are essential in recognition memory; and recent literature emphasizes PFC regions, including dorsolateral, ventrolateral, orbital and polar PFC, contribute to maintaining information about stimuli during working memory. A recent perceptual-mnemonic debate over MTL indicates some MTL structures (e.g. perirhinal cortex and hippocampus) contribute to perceptual discrimination. Different cognitive task variants, including memory tasks with delays and simultaneous discrimination tasks without delays, have been implemented in neuroimaging, neuropsychological and neurophysiological studies in humans and animals, to illustrate how sub-cortical areas of MTL, sub-cortical regions of PFC, and IT are implicated in mnemonic and perceptual processes. It's still unknown i) how the above regions operate in the same or different manner when contributing to memory tasks with delays versus simultaneous discrimination tasks without delays; and ii) how any of these areas interact when supporting these tasks; and iii) whether the neural mechanisms in NHPs and in humans differ or not when they perform homologous memory tasks. Therefore my thesis is organized as follows with a General Introduction to the topics considered in my research, then followed by a series of experimental chapters each considering an element of the above general area of scientific advancement, each with its own focused introduction and discussion; finally the thesis is completed by a general concluding discussion that reflects both on the major issues and also broader issues that the experimental work, within and across chapters, speaks to, including discussion of work that needs to be done next to further scientific advancement in these areas.

In Chapter 1, I investigated the affects of FPC lesions on resting state functional connectivity networks in NHPs. Previous neuroimaging and neuropsychological literature in humans has linked human FPC activities with a bewilderingly diverse range of higher-order

cognitive functions, to the extent that it has proved impossible to reach consensus from those studies on a fundamental role of FPC; and recent circumscribed FPC lesion studies in NHPs indicate primate FPC mediates exploration and rapid learning about the relative value of alternatives of a broad kind. As FPC has a unique pattern of reciprocal anatomical connections to other cortical areas beyond prefrontal cortex, to understand the influence of FPC upon whole brain networks may provide clues about its function. In this Chapter, resting-state functional connectivity (rsfc) has been used to examine correlations in spontaneous brain activities in rhesus monkeys with or without intact FPC. For the first time, we found that in absence of FPC, parts of brain regions were organized into two brain networks, which were distinct both functionally and spatially. Moreover, these brain networks extended both within and beyond prefrontal cortex, indicating wide-spread effects of FPC on multiple brain networks. Hence FPC may be causally involved in maintaining diverse network dynamics across the primate brain.

In Chapter 2, I investigated the time course of recollection (i.e. a vivid recall of past episode) and familiarity (i.e. a general feeling of encountering the item) processes in the NHP and humans. Most of the evidence for fast familiarity and slow recollection (FF/SR) come from analyses of receiver operating characteristic (ROC) curves in humans, and recently more in NHPs by analyzing the reaction time patterns of recognition errors (Basile and Hampton 2013). However, how good the link is between response time and relative contribution of recollection and familiarity in either species, and how comparable the FF/SR methodology across species has been repeatedly questioned. Here, a broadly similar recognition memory task was designed and exploited in both humans and the NHP to investigate the time course of familiarity and recollection processes. The similarities in patterns of recognition errors as a function of response time have been demonstrated in both NHP and humans to suggest species similarities. To address the supportive relationship of FF/SR to recollection and familiarity components calculated from dual-process model, the

time-course analyses of these two components indices derived from the binned ROCs have been made in humans. The lines of evidence in this study proves a similarity of FF/SR existing in both humans and the NHP.

In Chapter 3, I investigated the effects of prefrontal transcranial magnetic stimulation on recognition memory performance in humans. Neural oscillations play essential roles in recognition memory, which is drawn upon familiarity and recollection. It remains unclear how primate PFC contributes to these two processes, but frequency-specific neuronal oscillations are considered to play a key role. Here, NHP electrophysiological recordings first showed that a subregion of macaque dorsolateral PFC (dlPFC) was implicated at a specific frequency (i.e., increased beta power) in the encoding phase of a recognition memory task, and this beta power occurring in the early stage of sample presentation was beneficial for NHP recognition memory performance. Then, to assess the role of beta oscillations in human recognition memory, in a homologous recognition memory task, I targeted left human dorsolateral PFC (dlPFC, BA 9/46) as well as left dorsomedial prefrontal cortex (dmPFC, BA 8/9) and vertex using non-frequency-specific and frequency-specific low-beta patterns of TMS to causally investigate the memory outcomes after modulations. Using a dual process signal detection model, based on analysing ROC curves, I revealed a beta-frequency-related decrease of recollection in left dorsolateral prefrontal cortex, and a beta-frequency-related enhancement of familiarity in left dorsomedial prefrontal cortex. No behavioural changes followed either non-frequency-specific patterns of stimulation to the same sites, or beta-frequency stimulation over vertex. This provides evidence that the above behavioural effects in prefrontal cortex were driven by beta-frequency modulations in humans.

In Chapter 4, I investigated the dynamic interaction between PFC and MTL in an object recognition memory task for novel and familiar images using simultaneous multi-area, multi-electrode recordings in the NHP. I analyzed spike activities from macaque dlPFC, and the local field potentials (LFPs) from dlPFC, perirhinal cortex (PrC) and inferotemporal cortex

(IT) in the encoding, delay and choice phases of the recognition memory task. The neural data analyses indicate that prefrontal and temporal neural activities (particularly beta power) were related with encoding or decoding the visual stimulus; and LFP-LFP coherence analysis across all the recorded regions further illustrated the dynamic flow between PFC and MTL throughout the recognition memory task.

In Chapter 5, I investigated the role of MTL, particularly PrC, in both the mnemonic and perceptual processes. Here, a delayed mnemonic task and a hybrid mnemonic and perceptual task have been developed for simultaneous multi-area, multi-electrode recordings in the NHP. There was a matched behavioral performance between the two tasks. LFPs and LFP-LFP coherence analysis between temporal and prefrontal regions showed low-frequency LFP activities (i.e. theta and low-beta activities) in temporal and frontal regions were important for encoding, maintaining and retrieval of visual stimuli in the memory task; while high-frequency gamma activities in temporal regions during choice phase were more related to perceptual discrimination, suggesting a task-dependent modulation of neural activities in temporal and frontal regions.

In Chapter 6, I investigated the interaction between hippocampus and lateral prefrontal cortex using semi-chronic GrayMatter microdrive to target both deep areas of MTL and PFC and superficial parietal and prefrontal cortical areas in two awake NHPs. This is an ongoing project as I completed recordings of one monkey and still recorded another monkey with a post-doc in different task variants. In this Chapter, I analyzed both the spike activities and LFPs from the macaque hippocampus and PFC during an object recognition memory task and focused on the hippocampal-PFC interaction during the sample phase of the memory task. I preliminarily illustrated an important role of theta coherence between hippocampus and PFC during the sample presentation signaling recognition memory performance.

Acknowledgments

Academic acknowledgments

First of all, I would like to thank my supervisor, Prof. Mark Buckley, for his guidance on all aspects of the research work presented in this thesis, and for his feedback on each chapter of the thesis and each draft paper. Without his help and support, none of the chapters/papers would have been completed.

For Chapter 1, I would like to thank Prof. Buckley for performing the lesion surgeries on macaques. I would also like to thank Dr. Matthew Ainsworth for his advice on analyzing fMRI data, and thank Dr. Andrew Bell for helping me to conduct fMRI data pre-processing, and thank Dr. Helen Browncross for collecting the fMRI data. I carried out all data analysis and interpretation for this chapter.

For Chapter 2, I would like to thank Prof. Buckley for discussions on the research proposal and task programming. I would also like to thank the three final year research project undergraduate students, Martina Kavanova, Lydia Hickman and Fiona Lin, who participated in the human testing part of this study each helping me gather a subset of the human participant data. I carried out all task design, animal training and testings, supervision of the three undergraduates to conduct the human testing, and I alone did the data analysis and interpretation for this chapter.

For Chapter 3, I would like to once again thank Prof. Buckley for discussions on the research proposal and for programming the behavioral tasks in Turbo Pascal. I would also like to thank three undergraduate students, Martina Kavanova, Lydia Hickman and Fiona Lin, who participated in human TMS research and who each helped gather a subset of the data with me (they each analyzed a small subset of the data independently, with my support, for their individual research projects). I would also like to thank Dr. Erica Boschin, Dr. Juan M. Galeazzi, Dr. Lennart Verhagen, Olof van der Werf and Alberto Lazari for TMS support.

And finally, I would like to thank the Oxford Centre for Human Brain Activity (OHBA) and Prof. Matthew Rushworth for access to TMS facilities. I carried out all task design, animal training and recordings, supervised the three undergraduates during the human testing, and I alone conducted the data analysis of the entire combined data-set and interpreted it for this chapter.

For Chapter 4 and Chapter 5 (both are electrophysiological research), I would like to thank Prof. Buckley for giving me the great opportunity to work on this non-human primate project, and for the detailed discussions on each part of the studies. I would like to thank Prof. Buckley and Dr. Martin O'Neill for implanting the head-posts, Prof. Buckley for implanting the Utah arrays, and Dr. Kusunoki for implanting the chambers and microdrive implantation and perfusion surgeries. Thanks to all the support and help from my supervisor Prof. Buckley and my lab members (Dr. Carlos Pedreira, Dr. Erica Boschin, Dr. Juan Galeazzi Gonzalez, and Dr. Martin O'Neill); with their support I have successfully recorded data from the very first NHP in our lab to ever have Utah arrays for 2 years (whose data contributed to Chapter 4 and Chapter 5) and of course there were many technical challenges to overcome along the way setting up a brand new electrophysiology labs for these projects. Meanwhile, great thanks to Dr. Makoto Kusunoki for performing the chamber and microdrive implantation surgery and helping us to set up recording protocols, I was also the first in Prof Buckley's lab to successfully record from a NHP using the 96 channel Gray Matter microdrive recording system, which I did for six months. Due to the time limitation of my DPhil. study, and due to the long-term nature of NHP projects (typically 4-5 years), and also due to the fact that the 2nd animal required to complete the semi-chronic GrayMatter microdrive studies for publication is still being recorded from through 2020 by a post-doc (Dr. Ainsworth), those data from the two animals have not yet been thoroughly analyzed and so are not all included in this thesis. I do however present initial data from two animals sufficient to show advancement of scientific knowledge in Chapter 6. I would also like to thank the team of

expert animal technicians from Biomedical Services and veterinary staff and anaesthetists for their very high standards of animal care and husbandry throughout. I would also like to thank Stuart Mason for initial animal training. And finally, thanks again to my supervisor Prof. Buckley for all the support and encouragement (especially during the hard and challenging times with our first array animal); technical and NHP challenges notwithstanding I learnt and acquired all the skills to carry out state-of-the art multi-area multi-electrode electrophysiological studies starting from the position of a complete novice, which proved to be a very valuable experience for my doctorate and will clearly benefit my future academic career and its aim of furthering scientific understanding of brain function. I carried out all task design, daily animal training, testings and daily recordings, data analysis and interpretation and write-up for these two chapters.

Finally, I would also like to my lab members (Dr. Erica Boschin, Dr. Matthew Ainsworth, Dr. Juan Galeazzi Gonzalez, Dr. Martin O'Neill and Dr. Carlos Pedreira) and office mates (Dr. Makoto Kusunoki, Dr. Mikiko Kadohisa, Dr. Valentia Mione and Dr. Simon Baumann) for all the support and advice when I conducted the above experiments.

All the research was supported by Wellcome Trust Strategic Award Grant (Ref: WT101092MA), a MRC Project Grant (Ref: MR/K005480/1) to Prof Buckley, and the Department of Experimental Psychology. I would also like thank University of Oxford and The Queen's College for their generous financial support which enabled me to undertake my Dphil research.

Personal acknowledgments

I would like to thank my parents for providing lots of moral supports throughout the period of my Dphil study. Without their continuous patience and encouragement, I cannot take the courage to complete the journey of my doctorate. And a million thanks to my husband, Haoyu Fan, who has fulfilled his doctorate and acted as my strongest backup.

Although we were thousands of miles apart, he always gave me the greatest support and encouragement whenever I needed. And thanks to all my friends, for being there to give me encouragement over the last five years. And in the end, thanks to all my trainers in Buzz Gym, who instructed me in each class and enabled me to find a way of releasing the pressure from my doctorate study.

General Introduction

Recognition memory (RM) is the cognitive ability to recognize whether an episode or a fact has been encountered previously, and according to Squire and colleagues this is a key function of the Medial Temporal Lobe (MTL) Long-Term Declarative Memory System (Squire and Zola-Morgan 1991). Indeed, one behavioural task, commonly known as the recognition memory task, has long been used to investigate RM in amnesic patients and in animal models (Squire and Wixted 2011). The recognition memory task has various versions and names; in the MTL literature it is referred to as delayed matching-to-sample (DMS) or delayed nonmatching-to-sample (DNMS), whereas in the prefrontal cortex (PFC) literature it is more often referred to a 'delayed response tasks', that is an object delayed response task if it tests object RM for example. Note that the task, irrespective of name, is a short-term memory task, even though it is often used to assess the contribution of brain structures in the MTL traditionally thought by Squire and colleagues to exclusively support their MTL long-term declarative memory theory (Squire and Zola-Morgan 1991). Another key issue of debate and controversy is to what extent RM, and the tasks that assess it, draw upon recollection as opposed to simply familiarity (both of which according to Squire and colleagues are declarative memory processes); whether or not there are such process specific subdivisions of the MTL (e.g. hippocampus more involved in recollection and perirhinal cortex more involved in familiarity) is hotly debated not least because Squire's theory claims the MTL is homogenous in function (Squire and Zola-Morgan 1991) and also because there is also significant evidence that the MTL may be divided by stimulus domain instead (e.g. hippocampus more involved in spatial/temporal relational mnemonic encoding and perirhinal cortex more involved in object memory processes). Finally, returning to the issue of MTL structures contributing to short vs long-term memory, that debate has evolved into one also

considering the extent to which MTL structures contribute to perceptual discrimination (Baxter 2009; Buckley et al. 2001; Buckley 2005; Bussey et al. 2002a; Bussey and Saksida 2002; Bussey et al. 2003, 2005, 2006; Bussey and Saksida 2007; Eacott et al. 1994; Lee et al. 2005a, 2005b, 2005c; Murray and Bussey 1999; Murray and Richmond 2001). The work in this thesis is influenced by all these considerations and controversies, for example using mnemonic tasks with delays as well as simultaneous discrimination tasks with novel stimuli that may be solved using perceptual discrimination, and by using different stimuli too (objects for the most part and scenes in the latest ongoing work). These issues of domain and process division of function also apply to PFC where it is even less clear which divisions along those dimensions exist. One general overarching and motivating idea for the body of work in this thesis, and in my lab in general, is that some of the same brain regions may interact differently to underlie different processes, and/or that different combinations of brain areas (networks and sub-networks) may be recruited for different processes. Therefore to make scientific advancement we need to investigate interactions both within MTL and PFC and also between MTL and PFC in a range of perceptual and mnemonic tasks. Each experimental chapter takes up an element of this scientific endeavor and so for the first part of the thesis I provide a thorough and detailed 'general introduction' to the main themes (including those alluded to above) that concern the work in each experimental chapter.

FPC interactions with other brain areas during resting state (Chapter 1)

Frontopolar cortex (FPC) is occupied by area 10, a cytoarchitectonic area exclusive to the human and non-human primate brain (Carmichael and Price 1994). Rodents do not contain an equivalent cytoarchitecturally defined cortical zone to primate area 10. Both human and macaque FPC occupy the most anterior area of the frontal lobe. Semendeferi et al. (2001) confirm that human FPC occupies a larger proportion of prefrontal cortex than in other non-

human primates (Semendeferi et al. 2001), although Petrides and Pandya have later noted a similar cytoarchitectonic structure of area 10 between humans and NHPs (Petrides and Pandya 1999). Öngür et al. (2003) identify three separate sub-regions of area 10 in humans: area 10p (polar subdivision), 10r (rostral subdivision) and 10m (medial subdivision). It should be noted that only area 10p occupies the frontal pole, while area 10r and 10m extend caudally on the ventral cingulate gyrus and occupy most of the ventromedial PFC (Carmichael and Price 1994). Figure 1 a-b shows these three sub-regions (filled in red color) in the orbital (Figure 1.a) and medial (Figure 1.b) cortical surface of human PFC. In macaques, Carmichael and Price (1994) identify two distinct sub-regions of area 10: 10o (orbital) and 10m (medial) (Carmichael and Price 1994), although Semendeferi et al. (2001) point out the dorsal macaque area 10 include parts of Broadman area 9 (Semendeferi et al. 2001). Figure 1 c-e shows the two sub-regions (filled in red color) in the orbital (Figure 1.c), medial (Figure 1.d), and dorsal (Figure 1.e) cortical surface of macaque PFC.

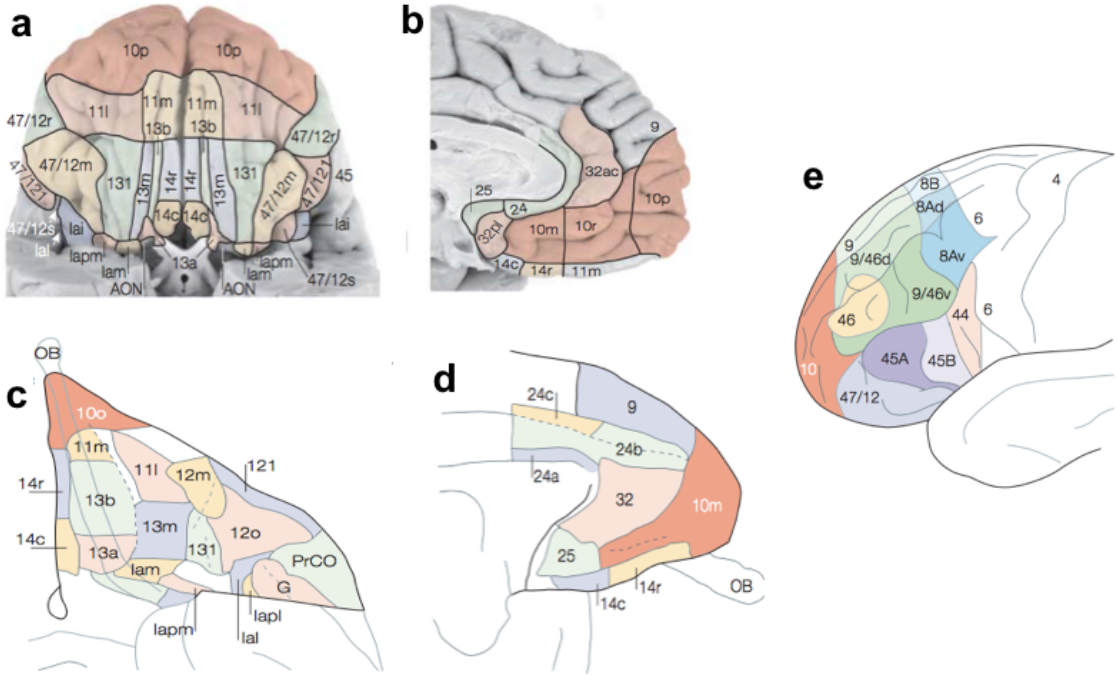


Figure 1. *Different views on the orbital (a, c), medial (b, d) and dorsal (e) extent of area 10 in human and non-human primates. Panel a-b: human FPC; Panel c-e: macaque FPC (adapted from Ramnani and Owen, 2004, and Petrides and Pandya, 2007).*

FPC has a unique pattern of afferent connections from multimodal subcortical and cortical areas in NHPs (Petrides and Pandya 2007; Markov et al. 2014) and in marmosets (Burman et al. 2011a, 2011b). For example, Markov et al. (2014) applied retrograde tracing to thoroughly identify connections to macaque FPC with different strengths from a wide range of cortical brain structures: strong projections have been identified to come from prefrontal (e.g. area 9, 12, 11, 13, 46) and temporal areas (e.g. temporal pole), while weak projections have been noted to come from occipital and parietal areas (Markov et al. 2014). Petrides and Pandya (2007) used anatomical tracing in NHPs to identify connections to FPC from other cortical regions: FPC has prominent reciprocal projections *via* external capsule to multimodal regions in superior temporal sulcus and superior temporal gyrus region, *via* uncinate fasciculus to select regions in

the anterior and medial temporal lobe including perirhinal cortex, and *via* cingulate fasciculus to anterior and posterior cingulate and retrosplenial cortices (Petrides and Pandya 2007). FPC also connects to some subcortical regions, which are amygdala in macaques (Markov et al. 2014) and claustrum and thalamus in marmosets (Burman et al. 2011a). The above anatomical tracing studies suggest a broad connection between FPC and subcortical and cortical areas in NHPs (shown in Figure 2), indicating that FPC may sit atop a hierarchy of prefrontal regions in the macaque brain. A recent MRI-based tractography (DTI) study in humans (Sallet et al. 2013) and functional connectivity studies in macaques (Neubert et al. 2014, 2015) further indicate that many brain regions (i.e. some of the regions are beyond PFC) are functionally connected to FPC.

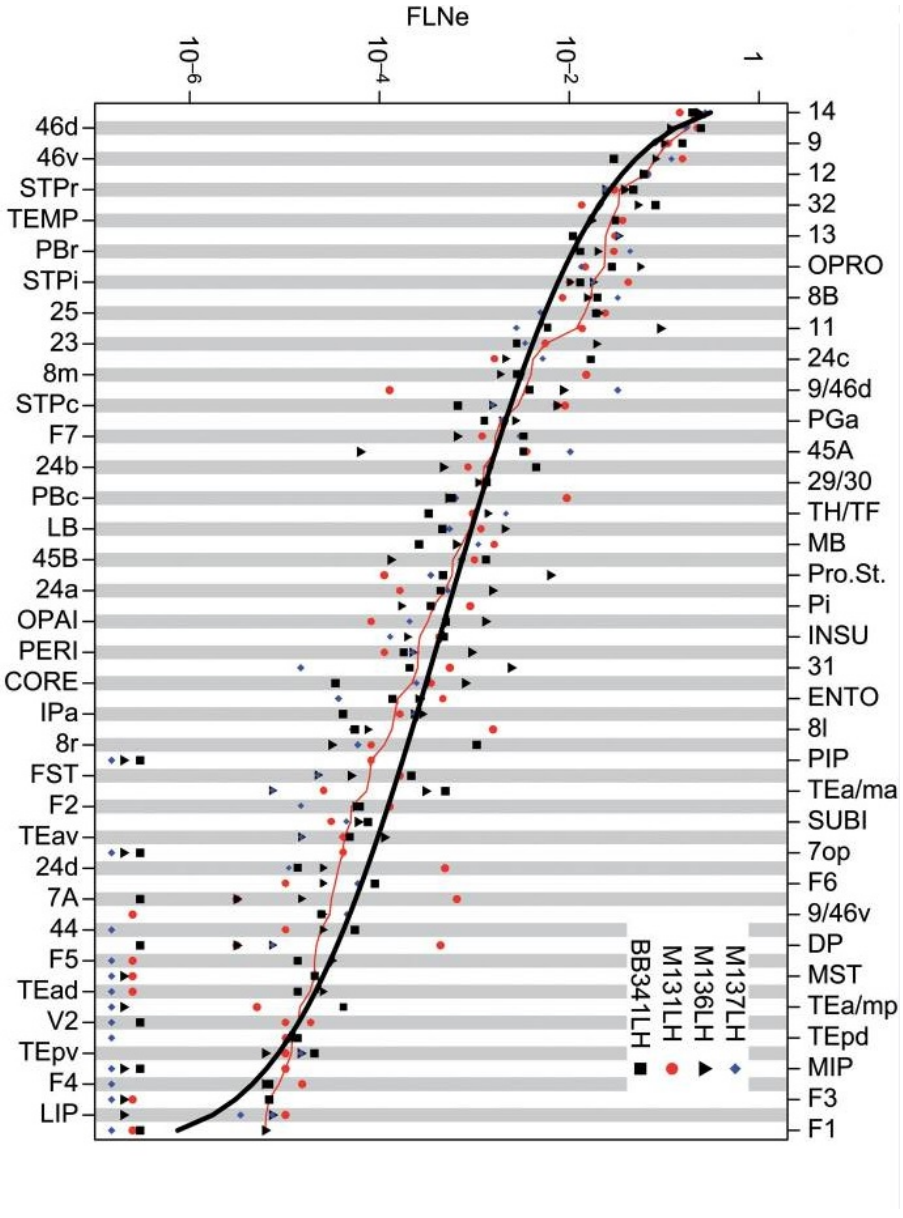


Figure 2. *Anatomical connections to macaque FPC (data from four animals) from a wide range of brain regions. Notably, strong connections to FPC are identified to come from prefrontal and temporal regions (adapted from Markov et al., 2014).*

The contributions that primate FPC makes to cognition are not fully understood. Human studies using non-invasive neuroimaging and transcranial magnetic stimulation methods have linked FPC activities with a wide range of higher-order cognition. Human neuroimaging literature suggests FPC is essential in maintaining and integrating subgoals to fulfil the final behaviour outcomes (Badre and Wagner 2004; Bunge et al. 2009; Christoff et al. 2001, 2003). For instance, human FPC has been found to be engaged in both response selection and managing subgoals for further integrating information representation (Badre and Wagner 2004). Bunge et al. found human left rather than right rostrolateral PFC (i.e. lateral Broadman area 10) was engaged in higher-order relations between individual object representations (Bunge et al. 2009; Christoff et al. 2001). Moreover, human rostrolateral PFC has been found to be involved in the evaluation of internally self-generated information (Christoff et al. 2003). In an uncertain environment posing conflict between exploiting existing information and exploring new information, FPC has been found to play a key role in explorative behaviour (Boorman et al. 2009; Daw et al. 2006; Koechlin et al. 1999). Additionally, Koechlin et al. (2000) measured human participants' fMRI signals when they performed a series of tasks with either expected or unexpected sequences, and they found human FPC was involved preferentially when human participants performed tasks in sequences that were not expected, leading to the author's view that human FPC is engaged in prospective planning (Koechlin et al. 2000). Okuda et al. (2003) confirmed this view and they measured regional cerebral blood flow (rCBF) in healthy participants while they were talking about their future prospects or past experiences, and found human FPC showed greater activation

during the future tasks than the past tasks (Okuda et al. 2003). Besides the role of FPC in prospective thinking (Koechlin et al. 2000; Okuda et al. 2003), Ryals et al. (2015) used theta-burst transcranial magnetic stimulation (TBS) to temporarily modulate human FPC activities during a recognition memory task, and found frontopolar TBS affected participants' associative memory awareness (Ryals et al. 2015); additionally, in another short-term recognition memory task, human participants' frontopolar cortex exhibited higher activities if their confidence judgment correlated with their recognition memory performance. (Yokoyama et al. 2010). Both studies of Ryals et al. (2015) and Yokoyama et al. (2010) suggest a role of human FPC in memory. However, no consensus has yet been reached on the common role of human FPC to cognition. In addition, there is only one report of patients with selective FPC lesions (Hoffmann and Bar-On 2012), and that adds little significant insight to the crucial contributions that FPC makes to cognition.

The similar anatomical connections and subdivisions of FPC verify the use of NHPs as a valid animal model to investigate FPC functions. Targeted lesion and electrophysiological studies in animal models have provided insights to understanding the function of FPC. To-date there are still only two NHP circumscribed lesion studies of FPC, which together indicate that FPC lesions in macaques produce a deficit in first-trial learning about novel objects and novel rules (Boschin et al. 2015) and an even enhancement in exploiting the current task when interruptions were introduced (Mansouri et al. 2015), which together may be interpreted as evidence that FPC mediates exploration and rapid learning about the relative value of alternatives of a broad kind (Mansouri et al. 2017). Relatedly, one study administered reversible silencing of a sub-region of macaque FPC, rather than acute lesions of all of FPC as in the above studies, and found that FPC inactivation in this way impaired metacognitive evaluation of non-experienced events (Miyamoto et al. 2018). In a recent review on function of FPC, a functional model of FPC in macaques in goal-directed behaviour has been proposed, in which FPC contributes to disengaging cognitive control from current task and redistributing resources to

other potential goals for ‘exploration’; while the posterior parts of the prefrontal cortex are involved in staying on the focus on the current task for more ‘exploitation’ (Mansouri et al. 2017). The balance between the ‘exploration’ and the ‘exploitation’ drive behavioural switch across different cognitive tasks indicate a close functional connection between FPC and other prefrontal regions. Neuronal activities of FPC makes little contribution to on-going decision making but the two papers from Tsujimoto et al. (2010, 2012) have given some clues to the function of FPC on feedback. For instance, Tsujimoto et al. (2010) found macaque FPC cells did not encode the monkeys’ decisions when they made responses but encoded their decisions prior to feedback (Tsujimoto et al. 2010); and in other cue instructed tasks, they found macaque FPC cells evaluated decision outcomes prior to feedback according to the cued strategy, contrary to other prefrontal regions involved in goal-directed behaviour (Tsujimoto et al. 2012).

Compared to other prefrontal cortical areas, FPC has a unique pattern of reciprocal connections to other cortical areas in that while its connections to prefrontal cortex are extensive, its connections to posterior regions are not and appear to be exclusive to multimodal regions (Petrides and Pandya 2007). Moreover, Sakai and Passingham (2006) demonstrated that FPC interacted differently with different posterior cortical regions depending on the intended cognitive operation held in working memory (i.e. items to be remembered in a forward or backward sequence) (Sakai and Passingham 2006). Additionally, Boorman et al. (2009) hypothesized that FPC encoded the evidence in favour of switching to alternative courses of action in a similar way, and they found that FPC entered into a distinct pattern of functional connectivity with the parietal cortex immediately before a behavioural switch occurred, leading to their view that FPC engages the parietal cortex to implement the switch (Boorman et al. 2009). To fully understand the function of FPC, it’s essential to investigate the interactions between FPC and other related brain regions, and how FPC is causally involved in mediating far-reaching networks of brain regions both within and beyond prefrontal cortex. Resting state functional connectivity (rsfc) examines the correlations in spontaneous brain activities in

absence of external stimuli or task demands. In Chapter 1, I investigated the above questions using circumscribed FPC lesions and network cluster analyses of whole brain functional connectivity analyses during resting state, aiming to understand the FPC-mediated functional organization of whole brain networks in NHPs.

Recollection and familiarity processes of recognition memory (Chapters 2 and 3)

A large body of literature has maintained that recognition memory draws upon two processes: familiarity and recollection (Parks and Yonelinas 2007; Wixted 2007; Yonelinas 2001, 2002; Yonelinas and Parks 2007; Scalici et al. 2017). Familiarity is defined as a general sense of knowing the item/object was encountered before but independent of the contextual environment; while recollection is characterized by vivid recall of the contextual information about the episode in which the item/object was previously encountered (Parks and Yonelinas 2007; Wixted 2007; Yonelinas 2001, 2002; Yonelinas and Parks 2007; Scalici et al. 2017). Models of memory with these aforementioned two processes are referred to as dual-process theories.

To assess and differentiate contributions of recollection and familiarity to performance of recognition memory, various experimental methods have been applied across different recognition memory tasks. Previously, a task-dissociation method has been proposed with the assumption that only one of the two memory processes were required according to particular task demands (Yonelinas 2002; Scalici et al. 2017). For example, in an associative memory task in which participants are required to remember the co-occurrence of different items, it is assumed that they should rely on recollection as they need to recall detailed contextual information relevant to separated items; on the contrary, in a simple single-item recognition task, in which they are required to distinguish between studied and not-studied items, they are assumed to rely on familiarity as their judgements are based on the memory strength of single items (Yonelinas 2002). Obviously, the efficacy of this task-dissociation hypothesis is

doubted by many studies as it is not credible that the sole contribution of recollection is to remembering lists of different items and the sole contribution of familiarity is to single-item memory tasks (Scalici et al. 2017). Another widely-used task approach to differentiate recollection and familiarity is the remember-know (R/K) procedure (Gardiner et al. 1998; Tulving et al. 1995). In this paradigm, participants answer "remember" if they can recollect the items which they have encountered, and answer "know" if their judgments are based on a feeling of knowing. The subjective differentiation of R and K responses among participants has been acknowledged as a limitation in this approach.

Another approach to distinguish between recollection and familiarity is based on a process-estimation method (Yonelinas 2002; Scalici et al. 2017). This method involves observed behavioural measurements in combination with a set of corresponding model equations to separate the contribution of recollection and familiarity to overall performance (Yonelinas 2002). Receiver operating characteristics (ROC) is one such operational method to differentiate recollection and familiarity. In the ROC curve, which is plotted cumulatively on the proportion of correct 'old' judgments ('hits') against incorrect 'old' judgments ('false alarms') across a range of confidence levels. Typical ROC curves are generated from humans performing a recognition memory task (Parks and Yonelinas 2007; Wixted 2007; Yonelinas 2001, 2002; Yonelinas and Parks 2007; Scalici et al. 2017). The human ROC curve fitting approach has been applied in many studies based on their particular model assumptions, such as equal-variance signal detection model (EVSD), unequal variance signal-detection model (UVSD), dual-process signal-detection model (DPSD), and mixed signal-detection model (MSD) (Koen et al. 2017).

Single-process theory

EVSD and UVSD single process models assume that the ROC function arises from a single signal detection process in which memory strength of both old and new items falls into a

continuum with overlapping Gaussian functions, in which the old item distribution has a higher average strength compared to the new item distribution (see Figure 3) (Koen et al. 2017; Yonelinas 2001, 2002; Yonelinas and Parks 2007).

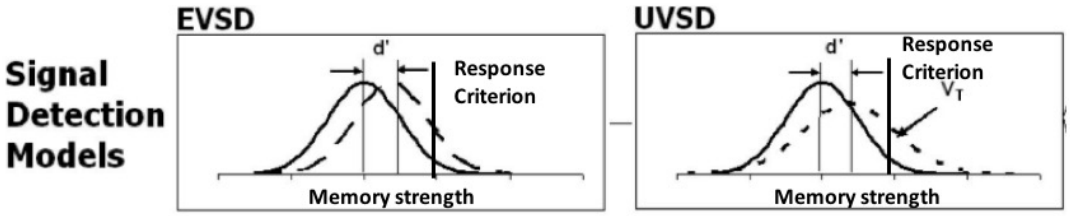


Figure 3. *Illustrations on memory strength distributions in signal-detection models. In both EVSD (left panel) and UVSD (right panel) models, the new (dark line) and old item (dotted lines) distributions are Gaussian function along the dimension of memory strength. In both models, d' is the separation between new and old item distributions, and response criterion is subjects' internal criterion to judge new item, in which whenever internal response is greater than criterion, subject considers it as an old item, and vice versa. (adapted from Yonelinas, 2007).*

The difference between EVSD and UVSD models merely concerns whether the variance of old and new item distributions (V_T in Figure 3) is the same or not (Koen et al. 2017; Yonelinas 2001, 2002; Yonelinas and Parks 2007). The parameter outputs of both the EVSD and UVSD models are d prime (d') and response criterion. Specifically, d' is calculated as the distance (i.e. difference between means) between the Gaussian distributions of old and new items, which reflects subject's discrimination ability in judging old and new items. Response criterion is a parameter presumed to be internally set by subjects when a recognition decision is being made, in which responding to old items exceeds that criterion (Koen et al. 2017;

Yonelinas 2001, 2002; Yonelinas and Parks 2007). The assumptions of both EVSD and UVSD models are based on the single process theory, which suggests that the subjective experiences of recollection and familiarity are the expressions of recognition memory processes resulting from memory traces of different strength: recollection is associated with stronger memory traces, while familiarity is associated with weaker traces (Yonelinas 2001, 2002).

Dual-process theory

According to the dual-process theory, performance on tests of recognition memory may draw upon two processes, commonly referred to as recollection and familiarity. The DPSD model is generated based on the dual-process theory. In the assumptions of the DPSD model (see Figure 4), recollection and familiarity are assumed to have different characteristics and contributions to ROC functions: recollection is considered to be a threshold process which generates high confidence-level memories; while familiarity is thought to be a signal-detection process which generates memories of varying confidence-levels (Yonelinas 2001, 2002). The confidence levels required for ROC plotting (across cumulative confidence levels) are measured by asking participants to state their confidence in the accuracy of their judgment that the stimulus has been viewed before ('old judgments'). For example, a 6-level confidence scale (i.e. 6 – "absolutely sure old", 5 – "moderately sure old", 4 – "somewhat sure old", 3 – "somewhat sure new", 2 – "moderately sure new", 1 – "absolutely sure new") has been commonly used to construct ROC. In ROC curve fitting, two distinct indices can be extracted: a symmetrical and curvilinear component associated with familiarity, and an asymmetrical and linear component related to recollection. By analyzing the shape of ROC curves in the recognition memory task, differential contributions of recollection and familiarity to the recognition memory task can be separated (see Figure 4 below), formally by

deriving the recollection and familiarity indices that result from curve fitting (Koen et al. 2017; Yonelinas 2001, 2002; Yonelinas and Parks 2007).

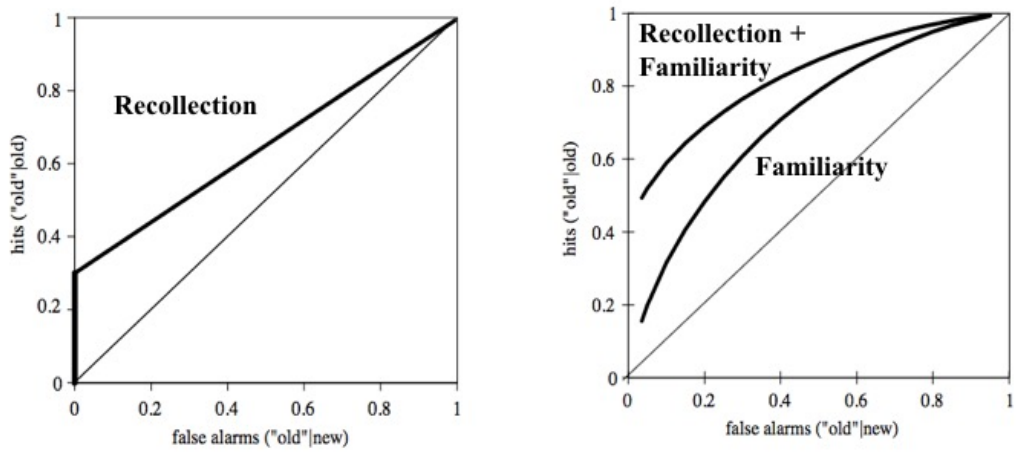


Figure 4. *Receiver operating characteristics (ROC) curves in dual-process signal-detection model. Left panel, the predicted ROC curve of a pure recollection process; right panel, the lower curve is the predicted ROC curve of a pure familiarity process while the upper curve is a combined ROC curve showing both the recollection and the familiarity component in the recognition memory task (adapted from Yonelinas, 2001).*

Debates over single- and dual-process theory in recognition memory

The debate over whether recognition memory reflects a single-process, with assumptions derived from EVSD and UVSD models, or dual-processes, with assumptions associated with DPSD models, are still ongoing (Koen et al. 2017; Malmberg 2008; Wixted and Stretch 2004; Wixted 2007). One of the noted differences is that the single-process and dual-process models predict different shapes of ROC curves (Yonelinas 1994) and different shapes of z-transformed ROC curves (Yonelinas and Parks 2007). Specifically, the ROC is symmetrical to the diagonal in EVSD single-process model (Figure 5A) but is asymmetrical in dual-process model (Figure 5B). The z-transformed ROC curves (zROCs) in EVSD model is

linear with a slope of less than 1 (Figure 5C), and zROCs in DPSD model is characterized as a U-shape (Figure 5D).

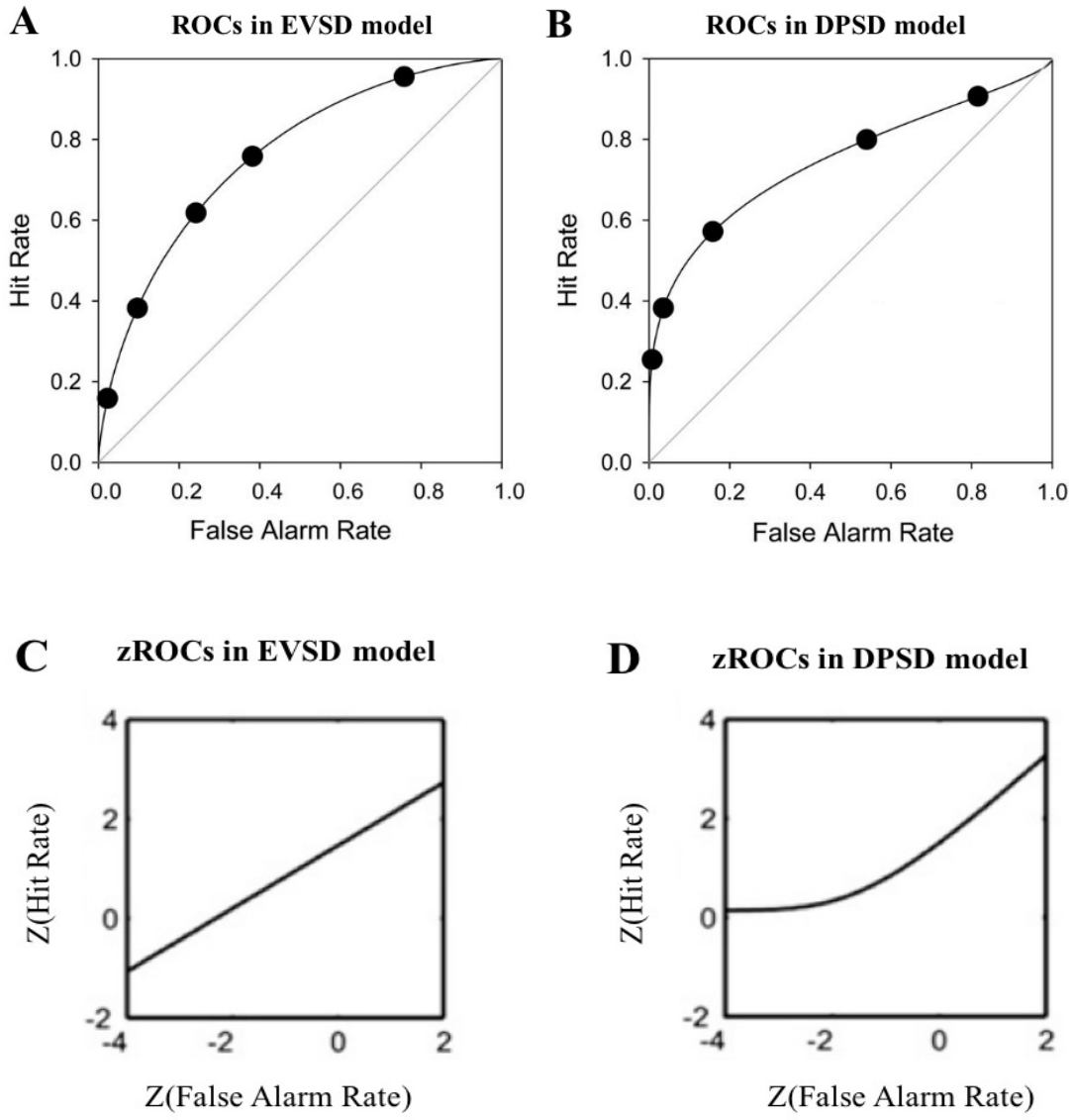


Figure 5. *ROCs and zROCs in EVSD and DPSD model. A symmetrical ROCs and a linear zROCs are found in EVSD model, while an asymmetrical ROCs and a U-shaped zROCs are shown in DPSD model (adapted from Wais, 2006).*

However, there is no consensus upon which model best fits the shape of ROC data (Glanzer and Adams 1990; Yonelinas 1994; Wais et al. 2006; Wixted and Stretch 2004;

Wixted 2007), with some authors proposing none of the two models do a sufficiently good job (Sherman et al. 2003). In comparisons of different models to interpret ROC data, goodness-of-fit tests have been used in many human and animal research (Healy et al. 2005; Guderian et al. 2011; Yonelinas and Parks 2007). However, the goodness-of-fit values of competing models can be exceptionally high (Malmberg 2008). For example, in one human study, the fits of UVSD and DPSD models to human ROC curves differ by less than one or two percent (Healy et al. 2005). Even in fitting macaque ROC curves using UVSD and DPSD models, the goodness-of-fit values are exceptionally high for both models and the value difference are less than one percent (Guderian et al. 2011). So far, any attempts to outright disconfirm either single-process models or dual-process models in normal human participants have failed (Malmberg 2008). In human patient and animal studies (see Figure 6 below), both the EVSD and UVSD single-process models have been challenged due to lack of explanations for the differences of ROC function shapes in patients or animals with selective hippocampal damage versus those in normal control people or animals (Eichenbaum et al. 2007). Specifically, Yonelinas et al. have noted a more symmetrical ROC in patients with hippocampal damage, but an asymmetrical ROC in the normal control group (Yonelinas et al. 1998, 2002). Additionally, in rodents with selective lesions of hippocampus, they also show a more symmetrical ROC compared with non-lesioned control animals (Fortin et al. 2004). These parallel lines of evidence in patients and animals can be readily interpreted according to the assumptions of dual-process models, that is, hippocampus integrity supports recollection, and following hippocampal damage both patients and animals to rely more on familiarity-based recognition memory (Eichenbaum et al. 2007; Malmberg 2008). In another study of Wais et al. (2006), they controlled the overall memory strengths equally for control group (50 items to remember) and hippocampal-impaired patients (10 items to remember) as both groups didn't show any significant difference in their recognition performance. They found the slopes of ROC from two groups were indistinguishable based on EVSD model, so

they argued that any worsening of performance results in ROC getting closer to diagonal and look like a reduction in asymmetry without really being due to selective loss of recollection (Wais et al. 2006). However, some oppositions should be brought up: firstly, when they fitted the data into DPSD model from the same two groups, a decrease of familiarity in hippocampal-impaired patients was still found when compared with control group; additionally, when Wais et al. stated they controlled the overall memory strengths equally for the two groups, they didn't specify why the fact of no difference of recognition performance between two groups was identical to the concept of the same memory strengths controlled across two groups; furthermore, a 1-tailed t-test has been applied to compare the slopes of ROCs in EVSD model between the two groups, making their results less convincing. Hence, we feel the dual-process model seems to provide a better account of ROC from patients and animals with intact vs damaged hippocampus as compared with single-process models (in Chapter 2 and 3, the DPSD model was chosen to fit our human ROC data and was used to interpret recollection and familiarity processes).

Recent animal studies have investigated familiarity and recollection-like memory processes by analyzing the ROC curves based on dual-process signal-detection (DPSD) model (Fortin et al. 2004; Guderian et al. 2011; Sauvage et al. 2008). A fundamental difficulty to overcome in animal models using ROC is that one cannot simply ask for a confidence judgment after the recognition memory judgment. The first application of ROC curves to distinguish familiarity and recollection-like processes in animals was in the rodent model wherein Fortin et al. (2004) plotted ROC in rodents by varying the reward and effort required to make old versus new judgments so to allow responses to be assessed across different levels of 'confidence'. Fortin et al. (2004) showed that these ROC looked like ROC in normal humans; moreover, in rodents with hippocampal lesions the changed shape of the ROC resembled the changed shape of ROC in human patients with hippocampal lesions (i.e. asymmetrical curvilinear ROC became curved symmetrical ROC, shown in Figure 6). In

patients this change may be interpreted as loss of recollection but spared familiarity; hence in rodents with hippocampal lesions Fortin et al (2004) showed that they too possibly lost a recollective-like component to their memory but their familiarity remained intact (Fortin et al. 2004). Subsequently, Sauvage et al. (2008) used an associative recognition paradigm and ROC to show recollection is reduced and familiarity increased after hippocampal lesions in rodents (Sauvage et al. 2008). Later, Guderian et al. (2011), by biasing macaques to respond to new and old stimuli by altering reward amounts they could obtain for their correct responses, further confirmed, using ROC, that recognition memory draws upon separate familiarity and recollection-like processes in macaques (Guderian et al. 2011). Up to date, only three animal studies using DPSD model to investigate familiarity and recollection-like processes in animals, as these types of manipulation are complex and time-consuming. In Chapter 2, I applied a new method (i.e. by analyzing response time of false alarm and miss errors) to investigate these two memory processes in both animals and humans. This method is procedurally easier in animals, which can be used as a decent proxy to investigate these two recognition processes in future animal studies.

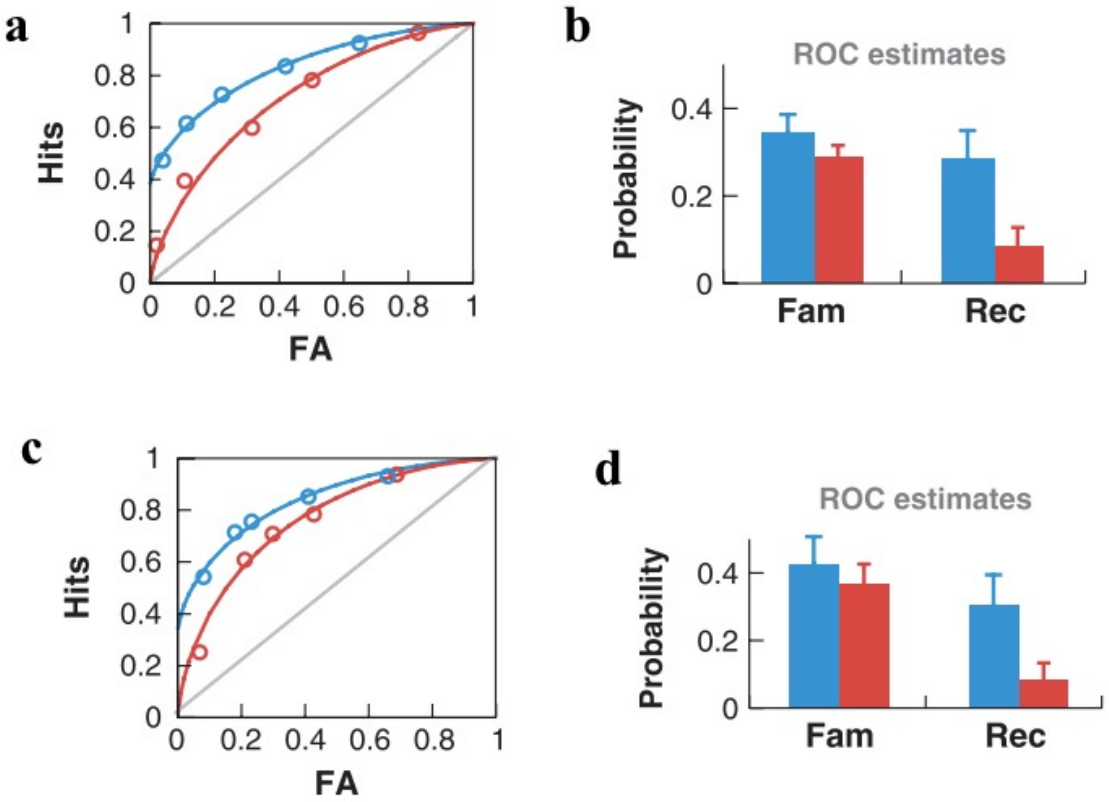


Figure 6. *Investigations on recollection and familiarity in patients with hippocampal damage (Yonelinas et al. 2002) and in rats with selective hippocampal lesions (Fortin et al. 2004). (a) ROC curves from patients with selective hippocampal damage (red line) and from healthy control group (blue line). In both cases, ROC curves are plotted cumulatively on the proportion of correct 'old' judgments ('hits') against incorrect 'old' judgments ('false alarms', FA) across a range of confidence levels. (b) A decrease of recollection (Rec) and intact familiarity (Fam) in patients with hippocampal damage compared with healthy control. (c) ROC curves from rats with lesions to hippocampus (red line) and from control animal group (blue line). (d) A decrease of recollection (Rec) and intact familiarity (Fam) in rats with lesions of hippocampus compared with control animals (adapted from Eichenbaum et al., 2007).*

Neural substrates of recollection and familiarity

Although the debates of single- and dual-process theories of recollection and familiarity still exist and some influential opposition remains (Squire et al. 2007), the neural substrates for recollection and familiarity are generally presumed to be different, or at least dependent upon different interacting networks of regions despite some overlap (Aggleton and Brown 1999; Eichenbaum et al. 2007; Skinner and Fernandes 2007). Evidence from previous neuropsychological studies of human patients and rodents (see Figure 6 above) suggest an involvement of the hippocampus in recollection and recollective-like memory, respectively (Fortin et al. 2004; Yonelinas et al. 1998, 2002). Furthermore, a double dissociation of familiarity impairment following perirhinal disruption and recollection impairment following hippocampal disruption have been found in human patients with temporal lobe epilepsy (Bowles et al. 2010). Neuroimaging studies have further confirmed a neurobiological dissociation of hippocampus activity in recollection and rhinal cortex activity in familiarity in humans (Ranganath et al. 2004; Skinner and Fernandes 2007). For instance, a fMRI study shows that the encoding-related BOLD activities in the rhinal cortex during an encoding phase can predict the performance in the familiarity-based recognition memory, while activities in both the hippocampus and posterior parahippocampal cortex can predict the performance related to recollection-based memory (Ranganath et al. 2004). The above findings of functional brain imaging, together with recent studies of amnesia and animals, indicate different brain networks (i.e. interactions between different brain areas such as hippocampus and perirhinal cortex) are involved separately for familiarity and recollection processes (Aggleton and Brown 2006). In a recent review, Eichenbaum and colleagues summarized evidence from neuropsychological, neuroimaging, and neurophysiological studies of humans and animals and concludes that '*hippocampus is critical for recollection but not familiarity. The parahippocampal cortex also contributes to recollection, whereas perirhinal cortex contributes to and is necessary for familiarity-based recognition*'

(Eichenbaum et al. 2007). And on the related topic of cross-species comparisons and whether animals truly show episodic recollection in a similar manner as humans, Eichenbaum and colleagues opinionated in the title of their review on this issue, "*If it walks like a duck, and quacks like a duck…*" (Eichenbaum et al. 2005).

Besides distinct roles of sub-regions of MTL in recollection and familiarity, prefrontal cortex (PFC) also clearly contributes to the two processes of recognition memory. There is a long-standing literature on PFC function and working memory tasks (i.e. delayed-response tasks such as delayed matching or delayed non-matching to sample tasks), which are often the exact the same tasks used by MTL researchers who more typically refer to them as recognition memory tasks. First of all, different sub-regions of PFC receive substantive projections from different sub-areas of MTL (Barbas et al. 1999; Cavada 2000). For instance, in macaques, the medial section of the orbitofrontal cortex is selectively connected with the hippocampus and posterior parahippocampal cortex (Cavada 2000); and macaque medial prefrontal regions are interconnected with the hippocampus (Barbas et al. 1999). Eichenbaum et al. have persuasively argued that the hippocampus supports episodic memory in the spatial and temporal domains, associating information over space and over time, and for example in forming episodic networks of overlapping sequences of events (Eichenbaum et al. 2007); however, it has been argued that the PFC exerts cognitive control over such episodic memories, for example by suppressing memories for inappropriate contexts/events (DeVito and Eichenbaum 2011; Place et al. 2016). Neural oscillatory dynamics in multiple brain regions, especially in PFC and MTL, are associated with different aspects of memory encoding and retrieval. For example, one recent study has suggested three thalamo-cortical circuits link recognition memory and neural oscillations; to be specific, it is suggested the anterior thalamus connects the hippocampus with the PFC in theta synchrony for recollection, the medial dorsal thalamus connects the MTL with the PFC in beta synchrony for familiarity, and the pulvinar connects the visual cortex and parietal cortex with the PFC in alpha

synchrony for gating (Ketz et al. 2015). In another review focusing on PFC-MTL interactions in recollection/familiarity, a "multi-effect multi-nuclei" model was proposed, in which inputs to PFC directly from hippocampus, and indirectly from hippocampus *via* the anterior and midline thalamic nuclei, are related to recollection process, while connections to PFC from perirhinal cortex and mediodorsal thalamic nucleus are related to familiarity process (Aggleton et al. 2011). Many lesion studies in animals also support the role of PFC in recognition memory. For example, lesions of macaque ventromedial rather than dorsolateral prefrontal cortex impairs their performance in a delayed object nonmatching-to-sample recognition memory task (Bachevalier and Mishkin 1986; Kowalska et al. 1991). Further studies have also shown that lesions of either orbitofrontal cortex or anterior cingulate cortex impairs macaque performance in recognition memory (Meunier et al. 1997). Although the issue of whether rodent frontal areas and primate PFC are homologous in function has been raised (Preuss 1995; Brown and Bowman 2002), it has been found rodent medial frontal cortex is involved in encoding and retrieval processes of recognition memory (Morici et al. 2015). In addition, by enhancing glutamatergic neuronal activities in rodent medial frontal cortex using an optogenetic approach, performance of recognition memory can be improved in rodents (Benn et al. 2016).

However, there is no consensus on distinct involvement of different sub-areas of PFC in recollection or familiarity and the extent to which they may dissociate. Evidence from circumscribed PFC-lesioned patients demonstrated conflicting results based on DPSD modeling. For example, patients with lateral PFC damage, either in left or right or both hemispheres, show behavioral deficits in familiarity rather than recollection (Aly et al. 2011). Similar behavioral deficits in familiarity were found in other two studies on patients with unilateral lesions of PFC (Duarte et al. 2005; MacPherson et al. 2008). Some contrasting results have shown that patients with focal lesions of anterior PFC (Wheeler and Stuss 2003) and patients with lesions of right lateral PFC demonstrate impairments in recollection leaving

familiarity intact (Hay et al. 2002). The divergent deficits in recollection/familiarity in PFC-lesioned patients may be related to the volume of lesioned areas but may also indicate that different sub-regions of PFC contribute to the two memory processes differently. More evidence from human neuroimaging studies have confirmed this view, but still show inconsistent results even for the same sub-region of PFC. For example, it has been found that stronger activities of dorsolateral PFC (dlPFC, BA area 9/46) is more associated with familiarity (judgment of 'knowing') than recollection (judgment of 'remembering) in a R/K memory paradigm (Henson et al. 1999a). A meta-analysis of fMRI studies has further confirmed the caudal dlPFC is associated with familiarity (Horner et al. 2015). However, another fMRI study based on DPSD model has shown that activities of both left and right dorsolateral PFC are related to recollection (Kafkas and Montaldi 2012). A recent review has summarized the evidence from neuroimaging using R/K paradigm and confirmed that dorsolateral PFC is involved in both recollection and familiarity as activations in this region may be related to the search and monitoring of contextual information, which does not solely depend on familiarity (Skinner and Fernandes 2007). Another sub-region of PFC, ventrolateral PFC (vlPFC, BA area 44/45/47), has got mixed results about whether it is more associated with recollection or familiarity. For example, in a high-resolution fMRI study focusing on the retrieval phases, activations of left vlPFC are associated with recollection (Johnson et al. 2013). In another fMRI study, by modulating the feelings of familiarity for scenes to subjects to differentiate recollection and familiarity processes, stronger activations of vlPFC are associated with recollection (Montaldi et al. 2006). Other contrasting evidence from neuroimaging show that activities in vlPFC are stronger in familiarity than recollection in a R/K procedure (Henson et al. 1999b). A recent review of previous neuroimaging studies involving PFC, using a meta-analysis method, has reported a mixture of involvement in recollection/familiarity in lateral, medial and anterior parts of PFC (Scalici et al. 2017), which suggests a complicated characterization of PFC in association with these

two memory processes. To be specific, it has been suggested that a mixture of activation peaks related to recollection-based and familiarity-based memory in lateral PFC (including both dlPFC and vlPFC), while activation peaks related to recollection fall within the more rostral portion of the brain, namely BA 10 and BA 11; whereas all but two of the activation peaks related to familiarity processing have been found more caudally, corresponding to dorsomedial PFC, including BA 8 and BA 9 (Scalici et al. 2017).

It is our interest to know how different sub-areas of PFC contribute to recollection and familiarity in recognition memory, and in which ways (i.e. neural oscillations) they contribute. In Chapter 3, by recording macaque local field potentials I first observed modulation of beta-frequency power in dorsolateral PFC during the sample stimulus encoding, and further showed the post-sample beta power was related to macaque recognition memory performance. Then, in an analogous recognition memory task in humans, I used targeted transcranial magnetic stimulation (TMS) to causally influence PFC mnemonic function during encoding. I investigated different frequency-specific and non-frequency-specific roles of human left dorsolateral prefrontal cortex (BA 9/46) and left dorsomedial prefrontal cortex (BA 8/9) in recollection and familiarity processes using a dual process signal detection model based on analysing ROC curves, to illustrate how the function of the two PFC sub-areas diverged in recollection and familiarity processes.

Time course of recollection and familiarity in humans and animals

The time course of recollection and familiarity has been largely investigated in human studies. Yonelinas and Jacoby (1994) calculated the peak time of familiarity and recollection in a source memory task and showed that the peak time of familiarity was between 600 and 800 ms, while the time of the highest point of recollection was between 800 and 1000 ms, which indicates familiarity is faster (Yonelinas and Jacoby 1994). In addition, a faster response to retrieving familiar words (i.e. familiarity process) has been found compared to retrieving

details of words in a word list (i.e. recollection process) (Hintzman et al. 1998). Some neurological studies have confirmed an earlier process of familiarity compared to a later process of recollection in recognition memory. For instance, Curran (2000) found the components of event-related brain potentials (ERPs) related to familiarity appeared at 300-400 ms; while the other parietal components associated with recollection appeared at 400-800 ms (Curran 2000).

Several behavioural paradigms have been applied to investigate the time course of familiarity and recollection processes in humans. Dosher and his colleagues applied a speed-accuracy trade-off paradigm to interpret the time course of these two processes, in which human participants must respond within a brief window following a go-signal, which is presented at various delays after the offset of the encoded sample items (Dosher 1984; Dosher and Rosedale 1991). In this paradigm, a plot of false alarm errors against retrieval time can be drawn. The retrieval time is being calculated as a sum of lag time between sample and test items and participants' response time. An inverted U-shaped curve of false alarm errors against retrieval time has been found in human subjects, with a rise of errors at extremely short retrieval time and reaches a summit in the moderate retrieval time then decreases in the longer retrieval time (Brainerd and Reyna 2005; Dosher 1984; Dosher and Rosedale 1991; Gronlund and Ratcliff 1989; Hintzman and Curran 1994; Matzen et al. 2011; Rotello and Heit 2000; Rotello et al. 2000). The peak time of false alarm errors has been considered as the onset of familiarity, and those errors are suppressed during moderate retrieval time as evidence of onset recollection, conducive to correcting false alarm errors (Brainerd and Reyna 2005; Dosher 1984). Taken together, there is a large consensus on "fast familiarity" and "slow recollection" (FF/SR) in human literature, although the methodology of speed-accuracy trade-off paradigm has been questioned in other human studies (Brainerd et al. 2014, 2019).

In animal research, the debate over whether animals can 'recollect' per se is still ongoing; and there has been limited evidence on the time course of familiarity and recollection processes in animal recognition memory. The delayed matching-to-sample (DMS) and delayed nonmatching-to-sample (DNMS) tasks were traditionally viewed to test animal recognition memory. Both tasks are initiated by requiring animals to view the sample picture (or as occurred in many earlier studies, by presenting real objects briefly to animals in a Wisconsin General Test Apparatus), and then after a delay in which no stimuli is presented on the screen, typically two choice pictures are presented in which animals should select the stimulus seen earlier as sample (i.e. the 'match') in a DMS task while animals should choose the picture different from the sample (i.e. the 'non-match') in a DNMS task. By manipulating the length of delay between sample and test images, which is often varied within an experiment to test for delay-dependent deficits that might index memory processes; and/or by increasing the number of items to be remembered, the difficulty and cognitive demands on both tasks increase. As in both tasks, studied images will be represented in the test phase, animals may make use of familiarity to differentiate studied and unstudied images. As familiarity is often considered as an automatic process (Jacoby 1991), animals may just rely on familiarity of studies images to solve recognition tests. Whereas animals can clearly judge relative familiarity of stimuli, the issue of whether animals can 'recollect' discrimination per se has been a more contentious issue historically but one for which there is now more supporting evidence (Eichenbaum et al. 2007). Recent animal studies have investigated familiarity and recollection-like memory processes by analyzing the ROC curves based on DPSD model (Fortin et al. 2004; Guderian et al. 2011; Sauvage et al. 2014). To be specific, Fortin et al. (2004) have found that the hippocampus only mediates recollection rather than familiarity by analysing the ROC curves in an odour recognition memory task in rodents (Fortin et al. 2004). This was the first application of ROC curves to distinguish familiarity and recollection-like processes in animals. After that, Sauvage et al. (2008) have applied a

similar testing paradigm in rodents but using stimulus pairs composed of various orders mixed in different digging mediums to investigate associative recognition memory. Rats with hippocampal damage showed decreased recollection whereas increased familiarity in this associative recognition task (Sauvage et al. 2008). Then Guderian et al. (2011) have further confirmed recognition memory is drawn upon two separate processes to be characteristic of familiarity and recollection-like processes in macaques (Guderian et al. 2011). However, ROC analysis on animals' recognition memory performance based on DPSD model is very complicated as to generate ROC is difficult and time-consuming (Fortin et al. 2004; Guderian et al. 2011; Sauvage et al. 2014).

More recently, similar to the speed-accuracy trade-off paradigm used in human studies (Dosher and Rosedale 1991; Dosher 1984), Basile and Hampton have introduced a modified recognition memory paradigm for NHPs in which animals select a standard non-match button if the test image does not match the studied image, or touch the test image if it matches. This paradigm allows miss and false-alarm errors to be distinguished which better facilitates application of signal detection theory to the NHP DMS task. By plotting false alarm errors against animals' response time, Basile and Hampton have found recognition choices in the recognition memory task to be made in three different ways depending on response time: short-latency errors are induced by false alarms to familiar lures, indicating the process of familiarity; medium-latency responses are less likely to be affected by false alarms and are more accurate, suggesting the onset of recollective-like process that could correctly reject familiar lures; long-latency responses are guesses (Basile and Hampton 2013). Thus, they have reported that "FF/SR" in patterns of recognition errors against response time exist in NHPs.

To further investigate whether the "FF/SR" exist in both humans and NHPs, in Chapter 2, I adopted Basile and Hampton's basic recognition memory paradigm, but further refined

the paradigm to probe intra-species comparisons across humans and NHPs. Basile and Hampton only used very familiar stimuli (i.e. two images were repeatedly presented to animals), as certainly small sets are likely to elicit greater proactive interference and the task essentially becomes a recency memory task which weakens the interpretation of Basil and Hampton's data. I applied both novel (i.e. trial-unique) and familiar stimuli in the refined paradigm to further investigate the effects of set-size of stimuli on animal recognition memory performance. Additionally, I investigated whether the FF/SR approach, procedurally easier in animals by Basile and Hampton (2013), can be used as a decent proxy to investigate these two recognition processes in future animal studies, given that scant data exists based on analysing ROCs in animal models.

Contributions of different sub-regions in MTL and in PFC to recognition memory (Chapter 4)

The medial temporal lobe (MTL) includes the hippocampus, amygdala and underlying entorhinal, perirhinal and parahippocampal cortices (Buckley and Gaffan 2006). The rhinal cortex surrounds the rhinal sulcus and is located in the anterior MTL beneath the amygdala and hippocampus. It is made up of the entorhinal cortex and the perirhinal cortex (Buckley and Gaffan 2006). It has been widely acknowledged that the MTL contributes to recognition memory. In the past decades, a wide range of neuropsychological studies in animals, especially on lesion studies in non-human primates (NHPs), have highlighted the different contributions of sub-areas of MTL to recognition memory. In animal studies, the delayed matching-to-sample (DMS) and delayed nonmatching-to-sample (DNMS) tasks have been widely used to investigate recognition memory. In both tasks, a sample image appears, and then after a delay, a same test image and a novel image are shown to animals. In DMS task, the animals select the test image if they think this image has been encountered; while in DNMS task, they select the novel image. Although the rules of both tasks are reversed, DMS

and DNMS task were traditionally viewed as recognition memory tasks to investigate the memory performance in animals.

The rhinal cortex is essential in recognition memory. For instance, the combined amygdalo-hippocampal aspiration lesions in NHPs impair their performance in the DNMS, but this impairment is not found by removal of hippocampus and amygdala separately (Mishkin 1978). However, ibotenic acid neurotoxic lesions of the combined amygdala and hippocampus (without damage to the underlying rhinal cortices) do not impair the performance in DNMS if the animals are trained on the task pre-operatively (Murray and Mishkin 1998). This shows that the rhinal cortical component of the combined ablations in Mishkin's study, as the large aspiration lesions certainly damaged the underlying rhinal cortex extensively, can account for the recognition memory deficits in DNMS task (Mishkin 1978). Subsequently, Meunier et al. confirmed this idea by showing that the combined perirhinal and entorhinal lesions, in which the amygdala and hippocampus remain intact, cause impairments in DNMS as severe as those found in Mishkin's study (Meunier et al. 1993).

In macaques, the perirhinal cortex (PrC) is the posterior section of rhinal cortex and located laterally to the rhinal sulcus (Suzuki 1996a, 1996b); and in humans, the PrC is rostral to the collateral sulcus, which appears in the ventromedial aspect of the brain (Insausti et al. 1998). It has been found that combined perirhinal and entorhinal ablations result in deficits in object recognition memory performance, whereas ablations of the entorhinal cortex alone result in only mild (Meunier et al. 1993) and transient effects (Leonard et al. 1995) on the performance in DNMS task. Thus, compared with entorhinal cortex, PrC is much more involved in object recognition memory task. In macaques, the cortical inputs to PrC are predominantly from the visual area TE and TEO (part of inferotemporal cortex, IT). Some inputs are from parahippocampal and entorhinal cortex within the MTL, and other inputs are

from the frontal lobe (e.g. orbitofrontal cortex, cingulate cortex) and sensory regions (e.g. somatosensory insular cortex) (Suzuki 1996a, 1996b). Since the PrC receives sensory information *via* projections from a range of unimodal and polymodal cortical areas in the ventral stream (Miyashita 2019) and also a range of inputs from outside of the ventral stream as well as from within the visual system (Suzuki 1996a, 1996b), it is concerned with processing visual and non-visual aspects of objects (Buckley 2005).

The parahippocampal cortex (PhC) is a cortical region, which underlies the hippocampus and is posterior to the entorhinal and perirhinal cortex. Many studies support the role of PhC in recognition memory task. For example, bilateral lesions of both PrC and PhC impair performance in both visual and tactual versions of DNMS task (Suzuki et al. 1993). Other studies suggest PhC is highly involved in spatial processing (Aguirre et al. 1996; Epstein and Kanwisher 1998; Janzen et al. 2007). For example, removal of PhC impairs patients' landmark identifications (Ploner 2000). Besides processing spatial information alone, PhC is involved in linking a target object with its surrounding context to form an intact contextual scene (Aminoff et al. 2013). In macaques, PhC contains the medial TH regions and lateral TF areas (Suzuki 1996a, 1996b, 2009), which have reciprocal connections within the MTL, such as temporal pole, entorhinal cortex and PrC (Aminoff et al. 2013). Moreover, PhC receives other inputs from frontal (e.g. media prefrontal cortex, dorsolateral prefrontal cortex, orbitofrontal cortex) and parietal areas in the dorsal stream (Aminoff et al. 2013). Different from PrC which has strong interconnections with other visual areas (Miyashita 2019), PhC receives little information from visual area TE and TEO, and other regions processing sensory information (Suzuki 2009). It has been found damage to macaque TH/TF regions impairs performance of the delayed nonmatching-to-location task (i.e. DNML, a spatial memory task) at all delays but only impairs performance of the delayed nonmatching-to-sample task (i.e. DNMS, an object memory task) at long delays; while damage to macaque PrC only impairs performance of the DNMS but not DNML (Alvarado and Bachevalier

2005). These results indicate a more spatial role of PhC verses a more object role of PrC in recognition memory. How PhC interacts with other regions (e.g. PrC) in recognition memory task is still unknown but on the basis of the different connections one might reasonably hypothesize a more spatial (PhC) versus object (PrC) dissociation, perhaps with more direct interaction for object-in-place tasks.

The hippocampus lies above the rhinal cortex (see Figure 7 below), which is divided into four sub-fields: CA1, CA3, dentate gyrus and subiculum (Giap et al. 2000). Hippocampus receives projections from the entorhinal cortex and other brain regions *via* the perforant pathway (a major input-output pathway) and from a range of subcortical (e.g. diencephalic) and cortical areas *via* the fornix (another major input-output pathway) (Saunders and Aggleton 2007). The role of hippocampus in memory is hotly debated. Some researchers support its role in recognition memory. For example, bilateral ibotenate acid lesions of hippocampus impair performance in DNMS but noticeably in animals that learn the task after lesions (Baxter and Murray 2001; Beason-Held et al. 1999; Zola et al. 2000). However, other researchers argue that hippocampus is mainly involved in processing spatial/scene information. One recording study has demonstrated that hippocampal neuronal activities represent spatial information about the contextual environment (Brown and Aggleton 2001). Many neuroimaging studies have further confirmed the contribution of hippocampus to scene processing (Hodgetts et al. 2016; Mundy et al. 2013). Moreover, lesions of hippocampus do not always affect recognition memory performance (Meunier and Barbeau 2013). For example, hippocampal lesions alone have mild effects on the performance in DNMS (Zola-Morgan et al. 1994).

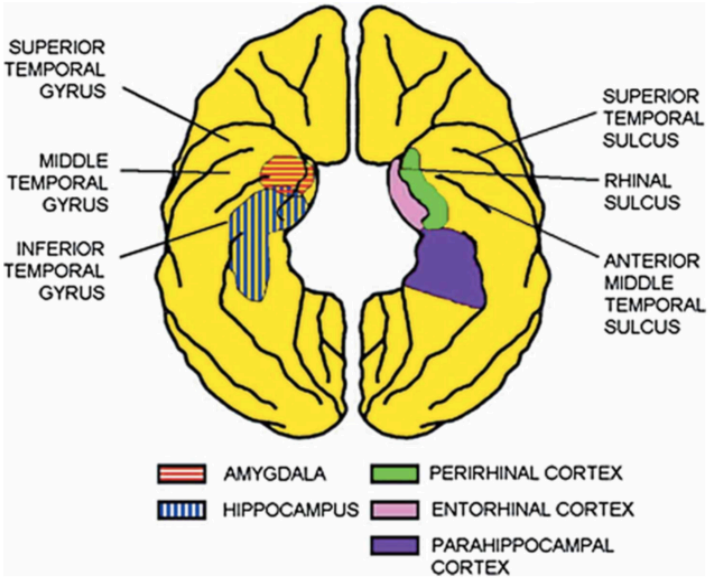


Figure 7. *Drawings of anatomical structures in macaque medial temporal lobe from a ventral view. The extent and location of hippocampus (blue stripe) and amygdala (red stripe) is depicted on the left side. The extent and location of underlying cortical regions, including perirhinal cortex (green), entorhinal cortex (pink) and parahippocampal cortex (purple), is depicted on the right side (adapted from Buckley, 2005).*

Besides the involvement of different sub-regions of MTL in memory, the prefrontal cortex (PFC) also contributes to recognition memory. For instance, lesions of rodent medial prefrontal cortex results in their behavioural deficits in the DNMS task (Kolb et al. 1994). Additionally, rats with focal lesions of the ventral medial PFC, including anterior cingulate and medial prefrontal cortex, show severe impairments in the DMS task, even at the shortest delays (Kesner et al. 1996). Similarly, lesions of macaque ventromedial rather than dorsolateral prefrontal region impair their performance in the DNMS task (Bachevalier and Mishkin 1986). The dissociable roles of ventromedial and dorsolateral PFC in recognition memory may lie in that ventromedial PFC receives thalamic projections from the limbo-diencephalic system, which is critical for visual recognition memory; whereas the

dorsolateral PFC lies outside this system and may contribute little to this type of memory both anatomically and functionally (Bachevalier and Mishkin 1986). Both lesions of macaque inferior prefrontal convexity alone and combined lesions of macaque inferior and dorsolateral PFC impair their performance in the DNMS task (Kowalska et al. 1991). Additionally, lesions of macaque orbitofrontal cortex (OFC) also impair their recognition memory performance in the DNMS task (Meunier et al. 1997). The above animal literature suggests different sub-regions of PFC play essential roles in recognition memory. One of the key functions of the PFC in recognition memory is executive control. For instance, a macaque single-unit recording study shows that dorsal and ventral PFC neurons encode abstract rules in a DMS task, in which macaques are required to indicate whether two successively presented pictures are the same or different depending on the current rule (Wallis et al. 2001). In a similar rule-guided task, neurons throughout PFC demonstrate rule-selective activities in the delay period when the animals follow the abstract rules (Muhammad et al. 2006). The above rule-guided activities in macaque PFC may be essential for selectively encoding, maintaining, reading out the information held in recognition memory and even forgetting those information when no longer needed.

Evidence from the frontal-temporal disconnection experiments show that the memory acquisition is not solely dependent on the MTL but on the widespread brain networks, including the PFC (Gaffan and Wilson 2008). For instance, macaques' performance in the DMS task are impaired both by crossed unilateral prefrontal and temporal lesions (Parker and Gaffan 1998) and by uncinate fascicle section (Gaffan and Eacott 1995). A functional disconnection between the PFC and the rhinal cortex in macaques results in their deficits in estimating expected rewards in a cue-reward association task, which indicates an interaction between PFC (i.e. signaling information about rewards) and MTL (i.e. signaling information about objects and contexts) is essential in recognition memory (Clark et al. 2013). Human neuroimaging studies suggest a role of ventrolateral PFC in recognition memory in which

right ventrolateral PFC exhibits stronger functional connectivity with PrC (O'Neil et al. 2012), and its involvement in the ventral polysynaptic pathway supports PFC-MTL interactions during episodic memory retrieval (Barredo et al. 2015). Both the disconnection studies in animals and neuroimaging studies in humans highlight the interaction between PFC and MTL plays important roles in recognition memory. Below is a table which summarizes different functions of MTL and PFC in recognition memory tasks in animal lesion studies (Alvarez-Royo et al. 1992; Bachevalier and Mishkin 1986; Beason-Held et al. 1999; Boschin et al. 2015; Buckley et al. 1997; Bussey et al. 2002b; Eacott et al. 1994; Kesner et al. 1996; Kolb et al. 1994; Kowalska et al. 1991; Leonard et al. 1995; Levy and Goldman-Rakic 1999; Málková et al. 2000; Meunier et al. 1993, 1997; Mishkin and Manning 1978; Mishkin 1978; Murray and Mishkin 1998; Petrides 1995, 2000; Suzuki et al. 1993; Voytko 1985; Zola-Morgan et al. 1994; Zola et al. 2000).

Table 1. *Animal lesion studies on different regions in MTL and PFC, which are proved to be involved in recognition memory tasks (e.g. DMS and DNMS task).*

	Target Regions	**Manipulation**	**Task**	**Delay Interval /sec**	**Set Size**	**List Length**	**Intertrial Interval/ sec**	**Result**
Mishkin, 1978	Hippocampus	Bilateral Lesion	DNMS	10/30/60/120		3/5/10	30	Intact
	Amygdala	Bilateral Lesion	DNMS	10/30/60/120		3/5/10	30	Intact
	Amygdalo-hippocampus	Bilateral Lesion	DNMS	10/30/60/120		3/5/10	30	Impaired
Murray and Mishkin, 1998	Amygdalo-hippocampus	Bilateral ibotenic acid Lesion	DNMS	10/30/60/120	20/40	3/5/10	30	Intact
Eacott et al., 1994	Rhinal Cortex	Bilateral Lesion	DMS	5/15/30	4	3/4/5/8-10		Not significantly impaired
			DMS	5/15/30	500 million	3/4/5/8-10		Impaired

			SMS	0	500 million	3/4/5/8-10		Impaired
Zola-Morgan et al., 1994	Hippocampus	Bilateral Lesion	DNMS	15/60/600	300	Trial-unique		Mild Impaired
	Perirhinal-Entorhinal-Hippocampus	Bilateral Lesion	DNMS	15/60/600	300	Trial-unique		Impaired
Zola-Morgan et al., 2000	Hippocampus	Bilateral ibotenate acid lesion	DNMS	15/60/600/2400	400	Trial-unique	20	Impaired
Beason-Held et al., 1999	Hippocampal Formation	Bilateral ibotenate acid lesion	DNMS	10/120/600	400	Trial-unique		Impaired
Buckley, Gaffan and Murray, 1997	Middle temporal gyrus	Bilateral Lesion	DNMS	10/30/60/120		3/5/10		Mildly Impaired
	Perirhinal Cortex	Bilateral Lesion	DNMS	10/30/60/120		3/5/10		Impaired
Alvarez-Royo et al., 1992	Parahippocampal-Hippocampus	Bilateral Lesion	DNMS	0.5/180/600				Impaired at longer delays
Meunier et al., 1993	Perirhinal Cortex	Bilateral Lesion	DNMS	10/30/60/120	1120	3/5/10	30	Impaired
	Entorhinal Cortex	Bilateral Lesion	DNMS	10/30/60/120	1120	3/5/10	30	Mildly Impaired
	Rhinal Cortex	Bilateral Lesion	DNMS	10/30/60/120	1120	3/5/10	30	Impaired
Leonard et al., 1995	Entorhinal Cortex	Bilateral Lesion	DNMS	8/15/60	300	10		Intact
				600/2400	300	10		Impaired
Suzuki et al., 1993	Perirhinal-parahippocampal cortex	Bilateral Lesion	DNMS	15/60/600		70	15	Impaired immediately and 2 years after surgery
Kolb et al., 1994	Rat Medial prefrontal cortex	Bilateral Lesion	DNMS	10/20				Impaired

Kesner et al., 1996	Rat Ventromedial prefrontal cortex	Bilateral Lesion	DMS	1-4/15/30				Impaired
Levy & Goldman-Rakic, 1999	Dorsomedial convexity	Bilateral Lesion	DNMS	10	1000			Improved
Kesner et al., 1996	Dorsolateral prefrontal cortex	Bilateral Lesion	DNMS	10	1000			Intact
Bussey et al., 2002	The orbital and ventral prefrontal cortex and inferotemporal cortex	Unilateral Lesion	MS	0			7	Impaired
Mishkin & Manning, 1978	Cortex in the principle sulcus	Bilateral Lesion	DMS	10		2	30	Mildly impaired
Bachevalier and Mishkin, 1986	Ventromedial prefrontal cortex	Bilateral Lesion	DNMS	10/30/60/120	1300	3/5/10	20	Impaired
	Dorsolateral prefrontal cortex	Bilateral Lesion	DNMS	10/30/60/120	1300	3/5/10	20	Not significantly impaired
Kowalska et al. 1991	Inferior frontal Convexity	Bilateral Lesion	DNMS	10/30/60/120	1300	3/5/10	20	Impaired
	Combined Inferior and Dorsolateral prefrontal cortex	Bilateral Lesion	DNMS	10/30/60/120	1300	3/5/10	20	Impaired
Voytko, 1985	Orbitofrontal cortex	Bilateral Lesion	DMS	0/15/30/45/60				Intact
Petrides, 1995	Mid-dorsolateral prefrontal cortex	Bilateral Lesion	DNMS	10		Trial-unique	10	Impaired

	Posterior dorsolateral prefrontal cortex	Bilateral Lesion	DNMS	10		Trial-unique	10	Intact
Petrides, 2000	Mid-dorsolateral prefrontal cortex	Bilateral Lesion	DMS	10/90/120		200/600		Impaired as the number of stimuli increases
	Anterior inferotemporal cortex	Bilateral Lesion	DMS	10/90/120		200/600		Impaired as the delay increases
Málková et al., 2000	Inferior frontal convexity	Neonatally Bilateral Lesion	DNMS	5/10/30/60/120		3/5/10	20	Mildly Impaired at 2 years; No impaired at 3 months
	Medial temporal lobe	Neonatally Bilateral Lesion	DNMS	5/10/30/60/120		3/5/10	20	Impaired
Meunier et al. 1997	Orbitofrontal cortex	Bilateral Lesion	DNMS	10/30/60/120	1400	3/5/10	20	Impaired
	Anterior cingulate cortex	Bilateral Lesion	DNMS	10/30/60/120	1400	3/5/10	20	Not significantly impaired
	Ventromedial prefrontal cortex	Bilateral Lesion	DNMS	10/30/60/120	1400	3/5/10	20	Impaired
Boschin et al., 2015	Frontopolar cortex	Bilateral Lesion	DMS	5/10/30/60/120		Trial-unique	10	Intact
			DNMS	5/10/30/60/120		Trial-unique	10	Intact

As the dynamics of neural interactions between PFC and MTL, and also inferotemporal cortex (IT), during the encoding and retrieval stages of recognition memory are not fully understood, in Chapter 4-6, we recorded neural activities in a visual recognition memory task using a simultaneous multi-area, multi-electrode recording paradigm in three NHPs to

determine how these areas interact at the neural level when the animal encode, maintain and discriminate between stimuli in recognition memory.

The memory versus perception debate: function of the medial temporal lobe (MTL) (Chapter 5)

According to the canonical MTL memory system theory, the MTL is exclusively involved in declarative memory (Squire 2004). This influential view of MTL functional organization assumes that the MTL (composed of the hippocampus, amygdala, and perirhinal, entorhinal, and parahippocampal cortices) constitutes a functional homogenous memory system, which plays no part in perception (Squire and Zola-Morgan 1991; Buffalo et al. 1998, 1999, 2000; Squire 2004; Squire et al. 2004, 2006; Suzuki 2009). However, there has since been a long-standing debate as to whether some MTL structures, most notably the perirhinal cortex (PrC) also extending to the hippocampus too, contribute to perception (Baxter 2009; Buckley et al. 2001; Buckley 2005; Bussey et al. 2002a; Bussey and Saksida 2002; Bussey et al. 2003, 2005, 2006; Bussey and Saksida 2007; Eacott et al. 1994; Lee et al. 2005a, 2005b, 2005c; Murray and Bussey 1999; Murray and Richmond 2001).

The PrC is lateral to the rhinal sulcus in macaques, located in the very anterior area of the medial temporal lobe (Suzuki 1996a, 1996b). The role of PrC in memory is distinct from other areas of MTL as the function of PrC is more associated with object memory. For example, lesions of PrC in macaques impair object recognition memory but not simple colour discrimination (Buckley et al. 1997). Additionally, a double dissociation of PrC and fornix in the function of spatial and memory process has been found: lesions of PrC impair the performance in a DMS task but not in a spatial discrimination task; while lesions of fornix lead to a reversed pattern of those deficits (Gaffan 1994a, 1994b). In macaques, the cortical inputs to PrC are predominantly from the visual area TE and TEO (Aminoff et al. 2013), and also from other sub-regions of MTL (e.g. entorhinal cortex, PhC, hippocampus), the PFC and

other sensory cortical areas (Suzuki 1996a, 1996b). The above findings suggest PrC is functionally distinct from other MTL structures as it is heavily interconnected both with the ventral visual processing stream (e.g. area TE) and with other structures in the MTL (e.g. hippocampus), which makes it a prominent target for experiments and discussion in the context of debates about perceptual-mnemonic theory versus MTL declarative memory system theory (Buckley 2005).

Studies supporting the canonical memory system theory of MTL

Although PrC has been proven to have closer functional relationship with area TE (a region highly involved in visual processing) (Aminoff et al. 2013), Buffalo and the colleagues argue that area TE is more involved in visual perception while PrC is more engaged in recognition memory (Buffalo et al. 1998, 1999, 2000). For example, Buffalo et al. (1998) demonstrated that in a concurrent discrimination learning task, the correlation between the extent of damage to area TE and number of errors was higher than the correlation between the extent of damaged PrC and number of errors in human patients (Buffalo et al. 1998). However, the stimuli used in this study are quite simple and can be easily discriminated on basis of simple features, hence it's not surprising extent damage of TE correlated with the performance in a task involving simple feature discrimination. Moreover, Buffalo et al. (1999) showed that lesions of area TE impaired the performance in a visual but not a tactile recognition memory whereas lesions of PrC impaired both (Buffalo et al. 1999). A more recent study by Buffalo and colleagues (2000) demonstrated that no behavioral difference between monkeys with lesions of PrC and unoperated monkeys has been found in a delayed nonmatching-to-sample (DNMS) task with very short delay (i.e. 0.5 s), while monkeys with ablations of area TE showed impairments in the same task compared with unoperated animals (Buffalo et al. 2000). Although the delay of 0.5 s is pretty short, it cannot exclude any mnemonic factor in

this DNMS task so the interpreting on the opposite perceptual discrimination patterns induced by damage to area TE and PrC (Buffalo et al. 2000) is limited. Additionally, one of the three control animals performed much worse than the rest two control animals when the delay was very short, which indicates no behavioral difference between the PrC-lesioned and control animal groups detected in this study may be related with the worse performance of the outlier animal in the control group. Again, the stimuli used in these studies are very simple as monkeys can solve the task by discriminating the stimuli on the basis of single feature rather than combining or conjunction of different features. To summarize the above three studies from Buffalo et al., although their interpretation on the role of PrC is controversial, they suggest the function of area TE and PrC are distinct in visual perception and recognition memory and support the canonical memory system theory of MTL (Suzuki 2009).

Studies supporting the perceptual-mnemonic theory of MTL

The perceptual-mnemonic theory of MTL claims an underlying representation at object level of complexity is found in PrC and this contributes to object-level perception and object-level memory. This perceptual-mnemonic theory of MTL has been supported by a series of animal studies, which confirm that PrC is essential in perceptual discrimination (Baxter 2009; Buckley et al. 2001; Buckley 2005; Bussey et al. 2002a; Bussey and Saksida 2002; Bussey et al. 2003, 2005, 2006; Bussey and Saksida 2007; Eacott et al. 1994; Lee et al. 2005a, 2005b, 2005c; Murray and Bussey 1999; Murray and Richmond 2001). The set-size effects both in recognition memory (Eacott et al. 1994; Gaffan and Eacott 1995) and in concurrent discrimination learning (Buckley et al. 1997; Buckley and Gaffan 1998a) have been investigated. The original study from Eacott et al. (1994) showed that macaques with bilateral ablations of rhinal cortex (including entorhinal and perirhinal cortex) preserved recognition

memory in a delayed matching-to sample (DMS) task with small set-sizes but showed impairments in both a DMS task and a simultaneous matching-to sample task with large set-sizes (Eacott et al. 1994), which indicates a role of rhinal cortex not only in recognition memory but in a general visual processing. Eacott et al. (1995) further found lesion of uncinate fascicle (i.e. an area connecting visual association cortex and prefrontal areas) had no effect on monkeys' performance in DMS task with small or large set-sizes (Gaffan and Eacott 1995), which indicates one possible explanation of the intact memory after removal of rhinal cortex in the DMS task with small set-sizes (Eacott et al. 1994) is that the remaining visual association cortex (i.e. located medial and posterior to the rhinal cortex) can subserve normal recognition memory with a small stimulus population after removal of rhinal cortex (Gaffan and Eacott 1995). In the later studies from Buckley and Gaffan, it has been found that monkeys with lesions of PrC demonstrate impairments in concurrent visual discriminations between pairs of colored shapes, especially when the number of foils from which the stimulus has to be selected is increased (Buckley et al. 1997). Additionality, damage to macaque PrC impairs object concurrent discrimination learning in large-set sizes (Buckley and Gaffan 1998a) but not in recognition memory task with small set-sizes (Eacott et al. 1994; Zola-Morgan et al. 1993). As damage to PrC impairs performance in both concurrent learning task and recognition memory task if set-size is large, but removal of PrC does not impair performance if set-size is small, which implies task category does not matter and set-size of stimulus matters more. That is a clue to PrC being important for object identification. Lesions of macaque PrC also impair discriminating real objects presented in different views which cannot be easily discriminated based on simple features but on the basis of feature configurations (Buckley and Gaffan 1998c), and impair configural learning and paired-associate learning (Buckley and Gaffan 1998b). Both of these tasks require macaques combine or configurate features to be associated together, hence the deficits of

combinations/configurations of features in PrC-lesioned macaques indicate PrC is highly involved in an object-level perceptual discrimination (Buckley 2005).

The oddity discrimination task

The changing-view task used in an early study (Buckley and Gaffan 1998c) has implicated essential roles of PrC in an object-level perceptual discrimination. To further investigate how PrC contributes to perceptual discrimination, an oddity discrimination task has been invented by Buckley and Gaffan in rhesus monkey (*Macaca mulatta*) (Buckley et al. 2001) and further applied to human patients (Lee et al. 2005a, 2005b, 2005c; Levy et al. 2005). In the oddity discrimination task (see Figure 8 below), monkeys or humans learn to simultaneously discriminate an oddity stimulus among other same or similar stimuli. It has been first reported that lesions of macaque PrC impair performance in discriminating the oddity object among the same objects with different viewpoints or among degraded images of objects shown in different viewpoints, or discriminating the oddity human or monkey faces among other faces presented from different viewpoints. Damage to macaque PrC also impairs discriminating oddity scenes among other same-view scenes (i.e. both the oddity and same-view scenes has multiple objects and similar background features). It should be noted that ablations of macaque PrC doesn't impair simple discriminations based on color, shape, or size, or same-viewpoint presentations of human or monkey faces (Buckley et al. 2001). This study illustrates an involvement of PrC to perception if an object or a scene cannot be discriminated based on a single feature but more on a combination of different features (Buckley et al. 2001). The early research from Buckley et al. (1997) detected perceptual deficits in a simple colour discrimination task have been found by damage to area TE but not area PrC, the recent study indicates that simple object discriminations based on different colors do not rely on PrC (Buckley et al. 2001). Taken together, these two studies (Buckley and Gaffan 1997; Buckley et al. 2001) indicate that distinct roles of area PrC and area TE in visual discrimination as

area TE may be more involved in processing of elemental visual features of objects while area PrC may play more crucial roles in discriminating objects based on different combinations of features (Buckley 2005). Lee and his colleague further applied this oddity task paradigm to human patients, and they found patients with hippocampal lesions and extensive MTL lesions (including PrC) demonstrate impairments in discriminating oddity scene from other scenes with different views. Only patients with extensive MTL lesions demonstrate impairments in discriminating oddity object or face from same objects or faces with different views. Both groups don't show any impairments in oddity brightness, shape, size, and same-view face discriminations. (Lee et al. 2005b). These results in human patients in the same oddity task indicate both human hippocampus and PrC are associated with oddity judgments based on an object level rather than a single feature level (Buckley and Gaffan 2006; Lee et al. 2005a, 2005b, 2005c).

The key manipulation in the macaque and human oddity task is to use stimuli (e.g. objects, faces, and scenes) in different rotated views so perceptual discrimination cannot be made based on a single feature of those stimuli (Buckley et al. 2001; Buckley 2005; Buckley and Gaffan 2006). Indeed, stimuli used in previous perceptual discrimination paradigms in animal lesion and human patient studies are pictures with simple features so subjects can count on the single feature of those stimuli to solve the problem. For instance, Hampton and Murray have found lesions of macaque PrC doesn't impair general discriminative abilities to familiar images with being enlarged, shrunk, rotated, masked and without colour, although those PrC-lesioned monkeys show impairments in acquisition of discrimination of new images (Hampton and Murray 2002). Another human study shows an intact visual discrimination in patients with bilateral lesions of PrC in discrimination among degraded objects and faces (Stark 2000). The failure to detect discrimination impairments after perirhinal damage in both macaque (Hampton and Murray 2002) and patient studies (Stark 2000) may lie on the fact that manipulations on distorting images, such as rotation, resizing,

degrading/masking and decolorization, transform images along with two dimensions, are not thought to be sensitive to PrC. Instead, discriminating items with different 3D viewpoints involve discriminating overlapping features between items, which are thought to involve the function of PrC (Buckley et al. 2001; Buckley 2005; Buckley and Gaffan 2006). In human studies using oddity task, there is an inconsistent result from Lee et al. (2015) and from Stark (2000), in which Lee et al. found a deficit of face oddity discrimination in patients with extensive damage to MTL (including PrC) (Lee et al. 2005b) whereas Stark and Squire have shown an intact perceptual discrimination in patients with damage to bilateral PrC in a face oddity task (Stark 2000). An influential review from Graham et al. (2010) have compared the performance of three groups of participants (individuals with selective hippocampal damage; individuals with more extensive lesions to the MTL and controls) from both human patient studies (Lee et al. 2005b; Stark 2000) in the face oddity task. It shows that neither the performance of patients with hippocampal damage nor performance of patients with MTL damage differs, but the performance of the control groups differs between the two studies (Graham et al. 2010). Consequently, the intact perceptual discrimination after extensive removal of MTL compared with control group (Stark 2000) may be attributable to a worse performance of the control group rather than the patients per se.

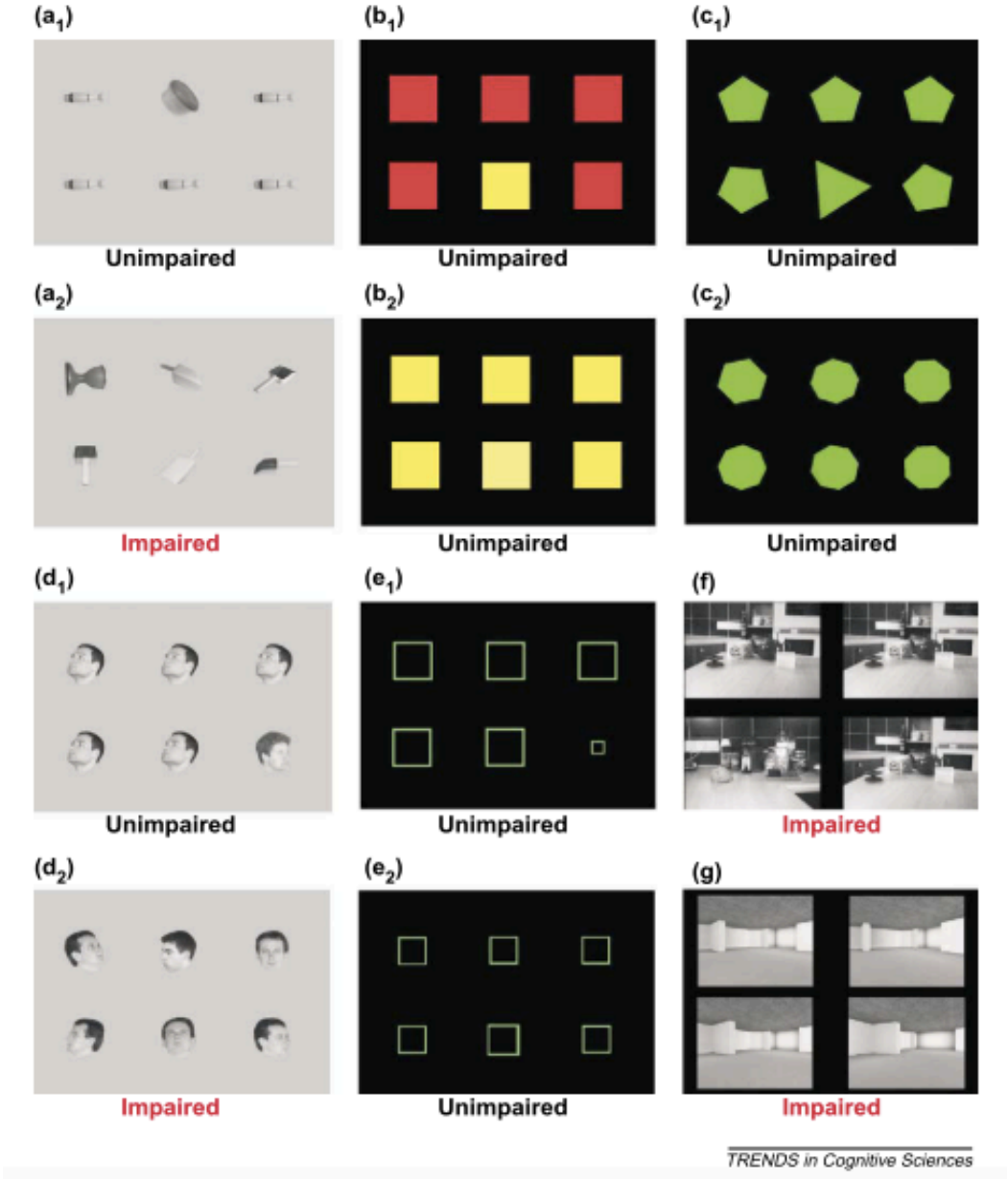


Figure 8. *Example stimuli used in the oddity task. In this task developed by Buckley and colleagues for macaques* (Buckley et al. 2001) *and subsequently used in human patients* (Lee et al. 2005b; Stark 2000)*, subjects are presented with an array of visual stimuli on a screen from which they have to select the oddity stimulus that is different from others. Monkeys with lesions of PrC don't show impairments in same-view object oddity (a_1), same-view face oddity (d_1), and in very different color (b_1), brightness (b_2), shape (c_1, c_2) and size (e_1, e_2) oddity discriminations; while they show impairments in discriminating an oddity object from*

same objects with different views (a_2), an oddity human face from same faces with different views (d_2), and an oddity scene from other scenes with unchanging views (f)(Buckley et al. 2001). *Human patients with hippocampal lesions and extensive MTL lesions (including PrC) demonstrate impairments in discriminating oddity scene from other scenes with different views (g), and patients with extensive MTL lesions also demonstrate impairments in discriminating oddity object from same objects with different views (a_2) and oddity face from same faces with different views (d_2), but both groups show no impairment in discriminating oddity brightness (b_2), shape (c_2), size (e_1,) and same-view face (d_1)* (Lee et al. 2005b) *(adapted from Buckley and Gaffan, 2006).*

There are several criticisms to interpretation on the role of PrC in the macaque oddity discrimination task (Buckley et al. 2001). Firstly, as PrC is also involved in associative learning based on previous literature (Buckley and Gaffan 1998b; Messinger et al. 2001; Staresina and Davachi 2008), Suzuki and Hampton argued that in the oddity task, discriminating an oddity object requires animals to associate other different views of the same object with one another. This argument indicates that the behavioral impairments induced by damage to PrC may reflect a deficit in associative learning (Hampton 2005; Suzuki 2009). However, Buckley and Gaffan later suggest that animals or humans if exposed to the same stimuli repeatedly, they learn to associate the different views as being views of an object and this helps them discriminate; however, if exposed to trial-unique stimuli, subjects cannot rely on associative learning to solve the problem (Buckley and Gaffan 2006). As in human study from Lee et al. (2005b), patients with extensive MTL damage (including perirhinal damage) demonstrate impairments in oddity judgment of trial-unique faces or objects from others with different views, which cannot be associated with a deficit in associative learning. In addition, Hampton and Suzuki criticized the smaller set-size of

stimuli used in macaque oddity task in Buckley et al. (2001) but not in human oddity task in Lee et al. (2005b) (as they used trial-unique stimuli), as the set-size is not large so animals are exposed with repeated presentation of certain stimuli, which results in a learning effect in the oddity task (Hampton 2005). Additionally, pre-operative task trainings in both control and PrC-lesioned animals in the early stage will benefit control animals to remember those stimuli, which results in a deficit of PrC in long-term memory accounting for the post-operative behavioral difference between the two groups (Suzuki 2009). Indeed, in macaque oddity task, using the trial-unique and larger set-size stimuli (as I have used to compare macaque perceptual and mnemonic processes in Chapter 5-6) is needed for excluding any effects of long-term memory and learning (Buckley 2005; Buckley and Gaffan 2006).

The morph discrimination task

The morph discrimination task has been pioneered by Bussey and his colleagues to assess the role of MTL in perceptual discrimination (Bussey et al. 2003, 2006; Bussey and Saksida 2007). In this task, greyscale pictures are morphed or blended to increase feature overlap between original pictures, so the morphed new pictures present high degrees of feature ambiguity. It has been found monkeys with lesions of PrC demonstrate discrimination impairments in discriminating pictures with high feature ambiguity, but not show any impairment in the simple visual discrimination on normal pictures, which indicates PrC contributes to feature-ambiguous discriminations (Bussey et al. 2003, 2006; Bussey and Saksida 2007).

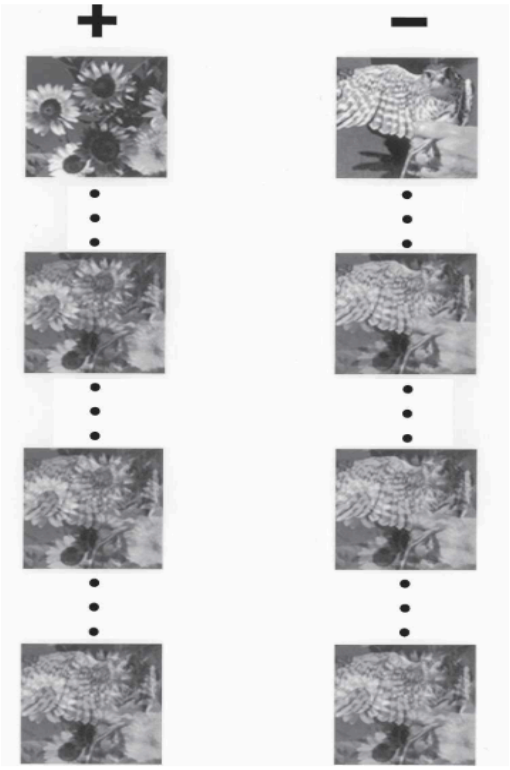


Figure 9. *Example stimuli used in the morph task. For each pair of stimuli excluding the top two pictures, two original pictures (i.e. flower picture and eagle picture on the top) are 'morphed' (blended) together. The '+' indicates the rewarded stimuli, and '-' indicates the unrewarded stimuli in the pair (adapted from Bussey et al., 2003)*

However, Suzuki (2009) and even Bussey et al. (2006) criticized the data interpretation of their study from Bussey et al. (2003). Both of them suggest both PrC-lesioned and control animals are trained to discriminate a series of simple picture pairs at the first stage, and then those pictures are morphed to create feature-ambiguous pictures for both monkey groups to discriminate. It's obvious that long-term memory of initially presented simple pictures may weaken the interpretation of PrC-damage induced impairments in discrimination between morphed stimuli. In other words, animals from both the lesion and control groups can still make use of memory strategies to solve the later difficult morph task, so the memory

component cannot be excluded from perception (Bussey et al. 2006; Suzuki 2009). To exclude the mnemonic effect in the morph task, Lee et al. (2005c) have designed both a mnemonic version and a hybrid mnemonic and perceptual of the morphed tasks in human patients. Specifically, in the first task, subjects are required to remember the original target image and then select the target image with another morphed image; while in the second task, in order to rule out the mnemonic effect on performance in the first task, the original target image is continually present on top of the screen (as subjects are not required to remember it) along with the two choice stimuli on the bottom, and subjects still select the bottom image that looks most similar to the displayed original image. In both the mnemonic and hybrid morphed tasks, Lee et al. found damage to MTL impaired discriminating morphed objects, scenes and faces (Lee et al. 2005c). Inspired by this study design, in Chapter 5-6, I established both a mnemonic version and a hybrid perceptual/mnemonic version of tasks, where I compared neural activities of MTL in the two cognitive demanding tasks. Some studies reported conflicting findings in humans with MTL damage in the morph discrimination task (Levy et al. 2005; Shrager et al. 2006). Levy et al. (2005) used morphed images in small set-sizes and didn't detect discrimination difference between patients with extensive MTL lesions and control group although one patient showed severe discriminative impairment (Levy et al. 2005). Both Lee et al. (2005b) and Shrager et al. (2006) used trial-unique presentations of 'morphed': Lee et al. (2005b) found patients with extensive MTL damage significantly impaired in discriminating morphed items; while Shrager et al. (2006) failed to find impairments in their population of amnesic patients. In Baxter's review on these inconsistent results in the above morphed discrimination studies, he suggests one problem in the morph discrimination task is that discrimination can be solved based on identification of single features among simultaneously presented morphed images, hence discrimination in this task do not solely depend on feature ambiguity (Baxter 2009).

The biconditional discrimination task

Bussey and his colleagues (2002) have also developed a biconditional discrimination task, in which high feature ambiguous problems can only be solved based on a combination of features. For instance, prior to the task, animals learn which stimuli (i.e. A, B) are rewarded. In the minimum feature ambiguous problem, four stimuli are presented in a pairwise manner, in which AB+, CD+ are accompanied with reward (+) and EF-, GH- are followed without reward (-). In this problem condition, each feature of stimuli is unambiguous as this problem can be solved on the basis of individual features, for example, A always indicates the stimulus AB is rewarded. In the intermediate feature ambiguous problem, some features are rewarded when they appear as part of one pair but not when part of another. For example, AB+, DE+, AC-, DG- are presented in which stimulus feature A and E are ambiguous as they cannot always indicate other pairs containing them (e.g. AC, DG) are rewarded but there are some features (e.g. E, G) are unambiguous. In the maximum feature ambiguous problem, AB+, DC+, AC-, DB- are shown in which all the features are ambiguous, and animals need to conjunct different features together to judge this stimulus pair is rewarded or not. It has been found that damage to PrC impairs in discriminating both the intermediate and maximum feature ambiguity but not the minimum feature ambiguity (Bussey et al. 2002a; Bussey and Saksida 2002).

Both Baster and Suzuki evaluates this biconditional discrimination paradigm but don't reach an agreement on interpretation of the role or PrC in this perceptual paradigm. Baxter claims that the minimal, intermediate and maximal conditions have the same task demands on both learning and memory as the number of stimulus pairs to be associated with reward or no reward are equal in those three conditions (Baxter 2009). Otherwise, Suzuki (2009) suggests there is difference of memory demands upon discriminating items based on simple features and items with overlapping features over multiple trials. As for the later difficult

discrimination, additional information and details of the items need to be maintained over trials and used when comparing with other items with similar features, hence the memory strength increases over trials (Suzuki 2009). However, as suggested in previous paragraph on the oddity task, it is of importance to compare first-trial discrimination in control and PrC lesioned animals in both morph and biconditional discrimination tasks to exclude the effects of learning and memory over multiple trials (Buckley 2005; Buckley and Gaffan 2006).

A similar pattern of impairment to PrC-lesioned macaques has been found in amnesia patients. Similar to biconditional discrimination task used in macaques, a concurrent object discrimination task with minimum, intermediate and maximal feature ambiguous problem is introduced to human patients with hippocampal damage and patients with larger ablations of MTL, including PrC. It has been found hippocampal damage doesn't impair discrimination in all the three feature ambiguous problems; while patients with ablations of extensive MTL show specific impairments in solving both the intermediate and maximal feature ambiguous problem (Barense et al. 2005). However, Levy and his colleagues (2005) have found there is no behavioral difference between healthy control and patients with large MTL lesions when discriminating within feature-ambiguous and blended pictures in easy, hard and very hard conditions, although one of the two patients demonstrate poorer discrimination of blended images in very hard condition (Levy et al. 2005). Together with the findings from macaques with lesions of PrC (Bussey et al. 2002a; Bussey and Saksida 2002) and MTL-damaged patients (Barense et al. 2005) in solving feature ambiguity problem, although some controversy exists, these findings show that MTL, especially PrC, is necessary for supporting discrimination of objects with overlapping features.

A recent prominent review (Suzuki and Naya 2014) concludes with the statement: "*it will be important to record during oddity or concurrent discrimination as well as during other clear memory-demanding tasks to determine if the perirhinal cortex provides similar*

mnemonic signals across both categories of tasks" and this is a key motivating factor and intention that I have developed a delayed memory task and a hybrid perceptual and memory task for simultaneous multi-area, multi-electrode recordings in NHPs in Chapter 5. In this chapter, I investigated whether neuronal interactions within and between areas of the MTL and PFC (and particularly focusing on the PrC activities) would be similar or different in mnemonic versus perceptual tasks.

Scope of the thesis

The thesis comprised six chapters, aiming to address a number of above issues which have been raised in both animal and human literature.

Chapter 1: Frontopolar cortex is a mediator of network modularity in the primate brain

In the first chapter, I will investigate the role of FPC in mediating brain networks in the primate brain. I will apply resting-state functional connectivity (rsfc) to examine correlations in spontaneous brain activities in rhesus monkeys with or without intact FPC. K-means clustering and multidimensional scaling analyses on the connectivity network will be implemented, to further probe how FPC influences cortical brain networks. A version of this chapter is submitted for publication (a preprint of the first submitted draft manuscript is available on Biorxiv (doi: 10.1101/2019.12.20.882837).

Chapter 2: Similar time course of fast familiarity and slow recollection processes for recognition memory in humans and macaques

In the second chapter, I will investigate whether the time course of recollection and familiarity processes differ or not in humans and macaques. Using a broadly similar recognition memory task in both species, I will firstly apply dual-process model based receiver operating characteristic curves to humans to validate whether fast familiarity and

slow recollection (FF/SR) existing in humans; then I will analyze recognition error response time profiles (adopted in Basile and Hampton, 2013) in both humans and macaques, to further validate FF/SR existing across species. A version of this chapter is submitted for publication and at the point of thesis submission is 'in press' (a preprint of the first submitted draft manuscript is available on Biorxiv (doi: 10.1101/2020.01.10.901975).

Chapter 3: Dissociation of dorso-lateral and dorso-medial prefrontal cortex contributions to familiarity and recollective processes in primates

In the third chapter, I will investigate the prefrontal neural oscillations in recollection and familiarity processes of recognition memory in both humans and non-human primates (NHPs). I will firstly investigate neural activities in macaque dorsolateral prefrontal cortex during the sample presentation in an object recognition memory task and identify which frequency-specific neuronal activities play essential roles when NHPs encode the visual stimuli. Then in a homologous recognition memory task, I will apply both frequency-specific and non-frequency-specific transcranial magnetic stimulation over humans' dorsolateral prefrontal cortex, dorsomedial prefrontal cortex, and vertex (as a no-stimulation control) during occasional sample presentations of the task, to investigate the causal importance for human memory of a location-specific, frequency-specific, and task-epoch-specific intervention derived directly from the NHP electrophysiological observations. Using a dual process signal detection model, based on analysing receiver operating characteristic curves, I will investigate how the frequency-specific patterns of stimulation affect recollection and familiarity processes in human recognition memory, compared with non-frequency-specific patterns of stimulation and no-stimulation control. A version of this chapter is submitted for publication and at the point of thesis submission is 'under review' (a preprint of the first submitted draft manuscript is available on Biorxiv (doi: 10.1101/2020.01.16.909812).

Chapter 4: Contributions of prefrontal and temporal lobe cortical areas to recognition memory for novel and familiar visual stimuli in non-human primates

In the fourth chapter, I will analyze the recorded neural activities in macaque dorsolateral prefrontal cortex (dlPFC) and perirhinal cortex (PrC) and inferotemporal cortex (IT) in a visual object recognition memory task using simultaneous multi-area, multi-electrode recordings in NHPs. I will analyze the local field potentials (LFPs), single-unit (spikes), and multi-unit activities from the three Utah arrays, to investigate the neural activities in prefrontal and temporal regions throughout the recognition memory task. I will also apply the LFP-LFP coherence analysis across different brain regions to illustrate the dynamic interactions between prefrontal and temporal regions throughout the task. Moreover, a non-parametric permutation test will be applied to compare both neural activities of the recorded regions and coherence between the recorded regions in novel and familiar sample presentations, to illustrate how the image familiarity affects the neural activities in recognition memory.

Chapter 5: Contributions of prefrontal and temporal lobe cortical areas to recognition memory and perceptual discrimination

In the fifth chapter, to better illustrate the role of perirhinal cortex (PrC) in perception and memory, both a mnemonic version and a hybrid mnemonic/perceptual version of the tasks will be designed for simultaneous multi-area, multi-electrode recordings in NHPs. To compare the effects of task structures (i.e. mnemonic demand or mnemonic/perceptual demand) on neural activities, I will analyze LFP activities and LFP-LFP coherence from the three Utah arrays in dlPFC, PrC and IT, to illustrate the involvement of PrC in both memory and perception and how the interaction between PrC and other recorded regions (i.e. dlPFC, IT) mediating different cognitive processes.

Chapter 6: Hippocampal-prefrontal theta coherence during the encoding phase signaling successful recognition memory performance (on-going project)

In the last chapter, I will show an ongoing project I led to investigate the interaction between hippocampus and prefrontal cortex in recognition memory using a novel semi-chronic chamber and microdrive recording systems in other two macaques. I will show some preliminary results of unit activities of hippocampus and PFC; and theta-coherence between these two regions during the sample phase of recognition memory task. More through and complicated neural analysis will be carried out in the future to validate our initial findings.

Chapter 1. Frontopolar cortex is a mediator of network modularity in the primate brain

Abstract

Primate frontopolar cortex (FPC), occupied by area 10, sits atop a functional hierarchy of prefrontal cortical regions yet little is known about its causal role influencing cognition and brain networks. We studied resting-state-functional-connectivity (rsfc) networks in rhesus monkeys with or without FPC; 86 cortical regions showed significant differences in inter-area rsfc measures in lesioned animals versus controls. K-means clustering showed these regions were organized into two distinct networks in lesioned animals, whereas the same areas clustered into four networks in control animals. These networks extended within and beyond prefrontal cortex. These results suggest that FPC is involved in mediating cortical networks in the primate brain, both within and beyond prefrontal cortex. Even after 40 months only partial recovery of lesion-induced reduced modularity had occurred. We therefore suggest that FPC might help implement long-standing diverse neural network dynamics.

Introduction

Frontopolar cortex (FPC) is occupied by area 10, a cytoarchitectonic area exclusive to the human and non-human primate brain. Studies using non-invasive neuroimaging methods have previously linked human FPC activities with a bewilderingly diverse range of higher-order cognitive functions, to the extent that it has proved impossible to reach consensus from neuroimaging studies on a fundamental role of FPC. In human neuroimaging studies, for example, FPC has been found to be associated with maintaining and integrating subgoals to fulfil the final behaviour outcomes (Badre and Wagner 2004; Bunge et al. 2009; Christoff et al. 2001, 2003), explorative behaviour (Daw et al. 2006; Boorman et al. 2009), cognitive branching (Koechlin et al. 1999), multi-tasking (Burgess 2000), future planning (Burgess et al. 2011), prospective memory (Koechlin et al. 2000; Okuda et al. 2003, 2007) and memory awareness (Ryals et al. 2015; Yokoyama et al. 2010) amongst many others. Clearly, whatever contributions to cognition are supported by FPC, they involve interactions with other posterior brain regions.

Whilst all these cognitive operations must require inter-area coordination, some human studies have explicitly revealed some FPC interactions. For example, Sakai and Passingham (2006) demonstrated that FPC interacts differently with different posterior cortical regions depending on the intended cognitive operation held in working memory (Sakai and Passingham 2006). In a similar vein, in hypothesizing that FPC encodes the evidence in favour of switching to alternative courses of action, Boorman et al. (2009) found that FPC entered into a distinct pattern of functional connectivity with the parietal cortex immediately before a behavioural switch occurred, leading to the proposal that FPC engages the parietal cortex to implement the switch (Boorman et al. 2009).

Whether such observations of interactions reflect causal influences on posterior regions cannot be determined from correlational neuroimaging studies as to reveal causality one

needs to study interventions. However, naturally occurring selective FPC lesions interventions are extremely rare. Human neuropsychology has traditionally proceeded by considering many patients with varied and overlapping lesions and assigning patients to groups if their lesions encroach significantly on target areas such as FPC irrespective of selectivity. That FPC may have a role in optimizing attentional allocation and controlling or switching attention between alternatives (including in one theory between externally available stimuli and self-generated thoughts) especially in the context of novel, ambiguous, and open-ended situations, or during multi-tasking and cognitive branching, are some of the key insights to have arisen from human neuropsychological investigations of FPC (Burgess 2012; Pollmann et al. 2007; Roca et al. 2011; Dreher et al. 2008). It is hard to draw firm conclusions for patients with such extensive lesions. One way to address this is to take large numbers of patients with non-selective brain lesions and apply voxel-based lesion analyses to see which lesioned voxels are most commonly associated with their behavioural deficits. Using this approach Volle et al. (2011) showed that lesioned voxels in FPC were associated with time-based prospective memory (a task which may be interpreted as one that requires monitoring of the relative value of performing one of two tasks at any given time) (Volle et al. 2011). There exist only extremely rare case studies of individual patients with lesions restricted to within FPC; indeed, we know of only one (Hoffmann and Bar-On 2012) and that adds little significant insight to the issue (other than reported marked indecisiveness and lack of normal response inhibition) as perhaps the most relevant behavioural tests were not administered.

Therefore, we turn to animal models (in non-human primates (NHP) as rodents do not have area 10 of FPC) wherein both highly circumscribed lesions and electrophysiology may be targeted specifically to NHP FPC. Only two published studies have targeted neuronal recordings of FPC and these indicate that while FPC makes little contribution to on-going decision making it appears to be engaged in evaluating decision outcomes prior to feedback

(Tsujimoto et al. 2010, 2012), contrary to other prefrontal regions involved in goal-directed behaviour (Tsujimoto et al. 2012). Until very recently there were no circumscribed FPC lesion studies in NHPs but three recent studies now indicate that FPC lesions in macaques produce a pattern of spared, impaired, and enhanced behaviour which together may be interpreted as evidence that FPC mediates exploration and rapid learning about the relative value of alternatives of a broad kind (Boschin et al., 2015; Farshad A. Mansouri, Buckley, Mahboubi, & Tanaka, 2015; Farshad A Mansouri, Buckley, Fehring, & Tanaka, 2019). Relatedly, one study administered reversible silencing of a sub-region of macaque FPC, rather than acute lesions of all of FPC as in the above studies, and found that FPC inactivation in this way impaired metacognitive evaluation of non-experienced events (Miyamoto et al. 2018). Moreover, a recent review on the function of FPC, taking into account the NHP and human literature, proposes a functional model of FPC in which FPC contributes to disengaging cognitive control from the current task and redistributing resources to other potential goals for 'exploration'; while the posterior parts of the prefrontal cortex are involved in staying on the focus on the current task to facilitate 'exploitation' (Mansouri et al. 2017). Setting the optimum balance between 'explorative' and 'exploitative' tendencies, especially in dynamic volatile environments, is likely to be a key process common across many different cognitive tasks and this is likely to necessitate a close functional connections and interactions between FPC and multiple other prefrontal and posterior brain networks. Anatomical connections between FPC and other brain regions are broadly similar across human and NHPs (Barbm and Pandya 1989; Sallet et al. 2013). However, compared to other prefrontal cortical areas, FPC has a unique pattern of reciprocal connections to other cortical areas in that while its connections to prefrontal cortex are extensive, its connections to posterior regions are not and appear to be exclusive to multimodal regions (i.e. prominent reciprocal projections: *via* external capsule to multimodal regions in superior temporal sulcus and superior temporal gyrus region, *via* uncinate fasciculus to select regions in

the anterior and medial temporal lobe including perirhinal cortex, and *via* cingulate fasciculus to anterior and posterior cingulate and retrosplenial cortices (Petrides and Pandya 2007) suggestive that FPC my sit atop a hierarchy of prefrontal regions in the primate brain. Accordingly, we hypothesize that FPC is causally involved in mediating far-reaching networks of brain regions within and beyond prefrontal cortex. This study investigates this using circumscribed FPC lesions and network cluster analyses of whole brain functional connectivity analyses. Resting state functional connectivity (rsfc) examines the correlations in spontaneous brain activities in absence of external stimuli or task demands and offers a tool for understanding the functional organization of whole brain networks. Seven adult macaque monkeys received bilateral lesions to the entire FPC; three of them had MRI scans 2 months post-lesion and four of them had scans 40 months post-lesion (Boschin et al. 2015). We first compared extra-FPC rsfc in 13 control animals (i.e. with intact FPC) with the same measures in the FPC lesioned animals scanned 2 months post-lesion to investigate how presence versus absence of FPC affects widespread brain networks (using cluster analyses to distinguish networks). We ran the same analyses with the 40 months post-FPC lesion group to investigate how robust the observed disturbances in FPC-mediated brain networks were across years.

Methods

Animals

Resting state fMRI and structural scans were collected under anaesthesia from seven macaque monkeys (Macaca mulatta) after bilateral lesions of FPC (area 10) (Fig. 1). Monkeys were scanned either 2 months post-operatively (three female monkeys with an average age and weight of 4.4 years and 7.8 kg at time of scanning) or 40 months post

operatively (four female monkeys with an average age and weight of 8 years and 6.7 kg at time of scanning). In addition, we collected resting-state fMRI data from a control group of thirteen monkeys (one female and twelve males, with an average age and weight of 4.5 years and 7.6 kg at time of scanning). All animals were socially housed in enriched environments with a 12hr light/dark cycle and had *ad libitum* water access. Prior to participation in this study all animals received basic training on an identical set of behavioural tasks reported elsewhere (Boschin et al. 2015). All animal surgery, anaesthesia and experimental procedures were carried out in accordance with the guidelines of the UK Animals (Scientific Procedures) Act of 1986, licensed by the UK Home Office, and approved by Oxford's Committee on Animal Care and Ethical Review.

Surgery

Bilateral lesions of FPC (macaque area 10) was carried out by aspiration of cortical tissue under sterile conditions. During the FPC lesion surgery, a bone flap was raised over the left and right anterior prefrontal cortex, the dura mater was cut and reflected. Using rongeurs, a craniotomy was made anteriorly to give access to perform the lesion. Then using a small-gauge metal aspirator, all cortical areas anterior to the limit of the lesion on the dorsal, medial, and orbital surfaces was removed by aspiration. Specifically, the caudal limit of the lesion on the dorsolateral surface was 2 mm posterior to the rostral tip of the principal sulcus; on the orbital and medial cortical surfaces, the lesion extended caudally to match the same anterior-posterior extent of the lesion on the dorsolateral surface. The white matter was spared during the surgery although some of them (e.g. most rostral part of the lesion) may be slightly distorted during the lesion. After the lesion operation was completed, the dura mater was sewn back, the bone flap was replaced, and the wound was closed in layers.

The operations of lesion surgery were performed in aseptic conditions with the aid of an operating microscope. The animals were first sedated with both ketamine (10 mg/kg) and xylazine (0.25-0.5 mg/kg) given i.m., intubated, and then artificially respirated and anesthetized throughout the surgery. Surgical depth of anaesthesia was maintained throughout the surgery with isoflurane (1.0-2.0% to effect). At the night before surgery, steroids (methylprednisolone 20 mg/kg i.m.) were given to the animals. On the day of surgery, three doses of steroids (methylprednisolone 20 mg/kg i.v. or i.m. every 4-6 hrs) were given to the animals to protect against intraoperative edema and postoperative inflammation. The animals were also given an antibiotic (8.75 mg/kg of amoxicillin) for prophylaxis of infection, an atropine (0.05 mg/kg) to reduce secretions, an opioid (0.01 mg/kg of buprenorphine given i.v., repeated twice i.v. or i.m. every 4-6 hrs), a nonsteroidal anti-inflammatory (0.2 mg/kg of meloxicam given i.v.) agent for analgesia, and an H2 receptor antagonist (1 mg/kg of ranitidine given i.v.) to protect against gastric ulceration as a side effect of the combination of steroid and nonsteroidal anti-inflammatory treatment. Heart rate, oxygen saturation of hemoglobin, mean arterial blood pressure, end-tidal CO2, body temperature, and respiration rate were monitored continuously throughout surgery (Boschin et al. 2015).

Histology

At the conclusion of the experiments, the FPC-lesioned animals were deeply anesthetized and then perfused through the heart with saline, followed by formol-saline solution. Their brains were blocked in the stereotaxic plane, removed from the skull, put in sucrose-formalin solution until the block sank, and subsequently cut in 50-μm horizontal sections on a freezing micro-tome. Every fifth or tenth section was retained and stained with cresyl violet. The histological slides so prepared and mounted were subsequently scanned at high resolution from which drawings of the actual extent of the lesion were prepared alongside matched

drawings of the intended extent (Fig. 1). Such drawings of four of the FPC lesioned animals (those in the 40-month post-FPC lesion group) have already been presented previously (Boschin et al. 2015) and are represented again here, now with accompanying drawings of the additional three FPC lesioned animals (those in the 2-month post-FPC lesion group).

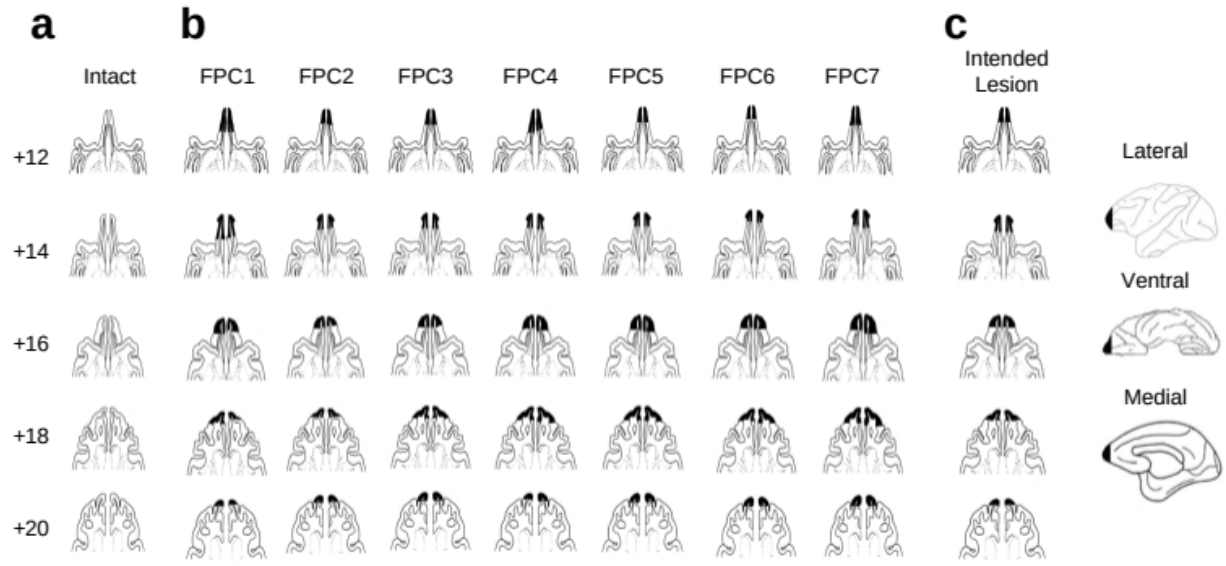


Figure 1. *Intended and actual extent of the bilateral FPC lesion. Drawings of horizontal sections of macaque prefrontal cortex showing the intact FPC (**a**), and the actual lesion extent from all seven FPC lesioned animals (**b**, FPC 1-4: 40-month post-FPC lesion group; FPC 5-7: 2-month post-FPC lesion). The intended extent of the lesion is shown on the same horizontal sections and summarised in drawings of the lateral, ventral, and medial surfaces (**c**). Numbers represent the approximate distance in millimeters above the interaural plane.*

Anaesthesia and MRI data acquisition

The fMRI data in the two animal groups were collected under sevoflurane anaesthesia. Anaesthesia was induced with intramuscular injection of ketamine (10 mg/kg), xylazine (0.125 - 0.25 mg/kg) and midazolam (0.1 mg/kg) two hours prior to the start of scanning,

which allowed ketamine to leave in the monkey's bodies before data acquisition. After induction, anaesthesia was maintained using sevoflurane. Commonly used volatile anesthetics including sevoflurane have been shown to modulate functional connectivity in the brain in a dose dependent manner (Peltier et al. 2005). Therefore, to preserve connectivity and minimize variation in the data EPI data was collected during light anaesthesia, with a targeted sevoflurane concentration of 2.3% across the entire project. There was no significant difference between the sevoflurane concentrations while data was collected for control animals (mean = 2.0%), FPC-lesioned animals with 2-month scanning interval (mean = 2.4%), and FPC-lesioned animals with 40-month scanning interval (mean = 2.4%, $F_{(2,17)}$ = 1.225, $p > 0.05$, $\eta^2 = .126$). Physiological parameters (e.g. heart rate and blood pressure) were used to assess the depth of anaesthesia throughout the scanning sessions (For further details of anesthesia maintenance and monitoring see Mars et al. 2011; Mitchell et al. 2016).

fMRI scans were conducted using a horizontal 3T scanner using a custom-made 4-channel phased array coil (H. Kolster, MRI Coil Laboratory, Laboratory voor Neuron Psychofysiologie, KU Leuven). High-resolution structural scans (0.5 mm isotropic voxels) were acquired using a T1-weighted high-resolution magnetization-prepared rapid-acquisition gradient echo (MPRAGE) sequence (128 slices, TR=2500ms; TE=4.01ms). Whole-brain resting-state EPI fMRI data were collected at a 2x2x2mm resolution (36 axial slices, TR=2000 s, TE=19 ms), with an approximate duration of 54 minutes for each animal (1600 volumes).

MRI data pre-processing and calculation of functional connectivity

All fMRI data pre-processing and analysis was conducted using a combination of MATLAB (The MathWorks Inc.), SPM8 (Statistical Parametric Mapping; www.fil.ion.ucl.ac.uk/spm),

FSL (fMRI of the Brain (FMRIB) Software Library; http://fsl.fmrib.ox.ac.uk/fsl/fslwiki/), Caret (Computerized Anatomical Reconstruction Toolkit (Van Essen et al. 2012)) and aa software (automatic analysis (Cusack et al. 2015); www.automaticanalysis.org). High resolution structural images for each animal were aligned to a standard space (F99 Rhesus macaque template - in the space of the atlas of Saleem and Logothetis (2012) (Saleem and Logothetis 2012) using affine and nonlinear transformations). Images were subsequently segmented into grey matter, white matter and cerebrospinal fluid (CSF) masks (McLaren et al. 2009). Resting-state fMRI data were aligned to standard space through a two-stage process and then spatially-smoothed with a 3mm Gaussian kernel (full-width half maximum). Grey-matter masks were defined on a monkey by monkey basis as voxels with grey-matter probability > 0.5 within each animal.

Physiological noise covariates were calculated by extracting up to 6 principal components (sufficient to explain 99% of the variance) from the BOLD time-series for white-matter and CSF tissue masks (Behzadi Y et al. 2007). An additional vascular covariate was defined as the mean time-course within a mask encompassing the superior sagittal sinus. A motion covariate was calculated from the EPI data (prior to smoothing and registration) and was defined as the time-course of the average displacement over the expected brain volume. These confound time-series and their first derivatives were then regressed from each grey-matter time-series, and the mean time-series was calculated for each cortical region within the derived from the CC atlas (the LV-FOA-PHT composite atlas) for macaques (Van Essen et al. 2012). Finally, functional connectivity was estimated by calculating pairwise correlation coefficients (Pearson's r) for each pair of CC areas (260 areas, 130 in each hemisphere) and transformed using Fisher's r-to-z transform. For further details of the pre-processing of structural images & resting state data see Ainsworth et al. 2018; Mitchell et al. 2016).

Nonparametric connectivity analysis

To calculate significant changes in functional connectivity between control and 2-month post-FPC-lesioned animals, we tested the mean difference between the two groups using a standard assumption-free nonparametric permutation-based approach (Nichols and Holmes 2002). The test involved a comparison of the observed difference against a reference distribution of differences, under the null hypothesis of no significant change in the functional connectivity between the two animal groups. For each connection, the reference distribution was obtained by performing 10,000 permutations on the animal labels to randomly assign them to two groups. On each loop of the permutation the mean functional connectivity between these randomly assigned groups was calculated and only the minimal and maximal difference was stored. This resulted in both a minimal and maximal matrix (each 260 by 260). The upper and lower thresholds were defined as the 97.5th percentile of the maximal matrix and the 2.5th percentile of the minimal matrix, respectively. Any observed mean difference between the two animal groups greater than the upper threshold or smaller than the lower threshold was deemed significant at the 0.05 level ($p < 0.05$, two-tailed). By selecting the maximal/minimal value from the permutation distribution, this two-sided nonparametric permutation-based test was sensitive to both positive and negative changes in connectivity and therefore controlled for global type I errors associated with multiple comparisons.

Multi-dimensional scaling analysis

Further analysis was carried out all possible connections between 86 ROIs revealed by the previous non-parametric analysis. To visualize changes in connectivity between these regions,

multi-dimensional scaling analysis was applied to the connectivity matrices from all 20 animals in the study. For each experimental group (control, 2-month post-FPC-lesion, and 40-month post-FPC-lesion) 3 dissimilarity matrices was calculated from the mean connectivity matrix from each group (normally distribution). Classical multi-dimensional scaling was then carried to generate an x and y position for each ROI in 2-D space. Clustering of ROIs based on these 2-D coordinates was then calculated by K-means clustering. The number of clusters for each group was found using the elbow method, and set to explain 80% of total variance.

To provide a more precise explanation of what drives changes in an ROIs connectivity in the absence of FPC further correlation analysis was conducted. In this analysis the Euclidean distance between an ROIs position in space in the control group and both post lesion groups were compared with two rules; firstly the strength of an ROIs connection to FPC in control animals and secondly an ROIs within/between ratio. An ROIs within/between ratio is defined as the average distance to within cluster ROIs divided by average of distance to ROIs in other clusters. The relationship between these two rules (FPC-connectivity and within/between ratio) and the change in an ROIs position was tested by calculation of a correlation coefficient (Pearson's r) and the significance of the correlation tested by a standard general linear model.

Results

We collected resting state fMRI data and structural scans under anaesthesia from a total of 20 animals. These included 13 control animals with intact FPC, 3 FPC-lesioned animals scanned 2-month post-lesion and 4 FPC-lesioned animals scanned 40-month post lesion. All seven lesioned animals received complete bilateral aspiration lesions of the FPC (Fig.1). Resting

state functional connectivity (rsfc) was calculated between 260 cortical regions by pairwise correlation from the mean BOLD time series.

Changes of functional connectivity across the brain after circumscribed lesions to FPC

To investigate the changes in functional connectivity after lesions to FPC, we constructed matrices of the pairwise correlations between all 260 cortical regions. Matrices of mean functional connectivity in unoperated control animals versus in 2-month post-FPC-lesioned animals are shown in Fig. 2a and Fig. 2b respectively.

To probe significant differences in functional connectivity between the two animal groups, a standard assumption-free nonparametric permutation test was applied to these rsfc data (see methods) (Nichols and Holmes 2002). In this test the difference in connection strength between the lesion and control group was compared to a surrogate distribution of the maximal/minimal difference observed after random re-labelling of the lesion and control groups (repeated 10,000 times). Testing in this way revealed 469 functional connections which were significantly different between control animals and the 2-month post-FPC-lesioned animals (two-tailed permutation test, $p < 0.05$). Of the 469 functional connections deemed to have significantly changed, the majority were found to have enhanced functional connectivity following FPC lesion: 369 connections increased while 100 connections decreased in strength (Fig. 2c). These significant connections linked a subset of 86 cortical regions-of-interest (ROIs), distributed both within and beyond prefrontal cortex (see Table 1 in supplementary material of the thesis for full list and MRI coordinates of selected ROIs). To further explore changes in connectivity following lesion of FPC we therefore considered only connections between these 86 ROIs (Fig. 2d and 2e functional connectivity matrices).

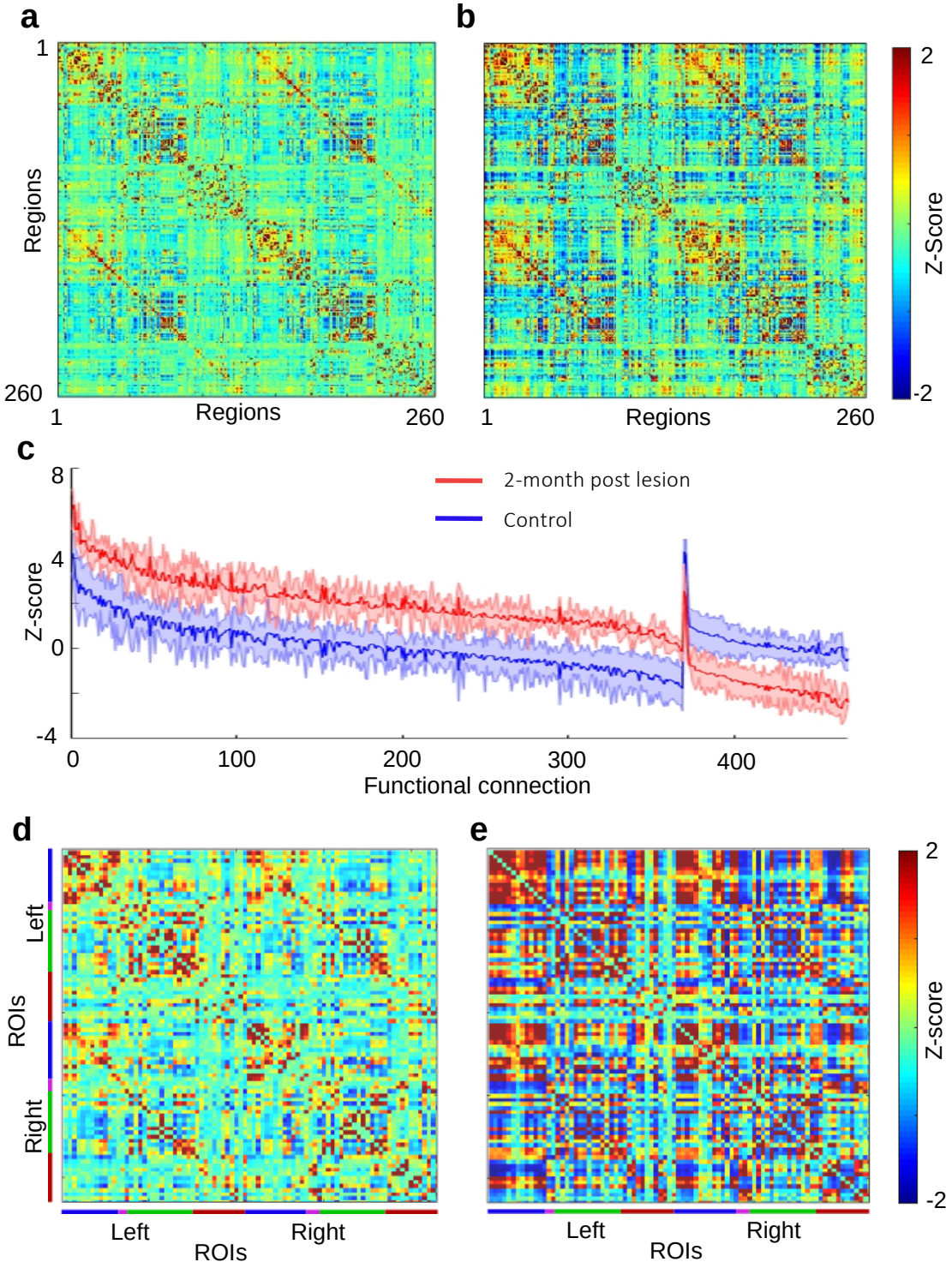


Figure 2. *The impact of lesions to Frontopolar cortex on resting state functional connectivity. Matrices of functional connectivity between 260 cortical regions for control group (**a**) and 2-month post-FPC lesion group (**b**). A total of 469 functional connections (linking 86 cortical regions) were revealed by a nonparametric permutation test to be significantly different*

*between the two animal groups (two tailed test, $p<0.05$, see methods for details of the test). The majority of connections were enhanced in the 2-month post-FPC lesion group (red) when compared with control group (blue). Matrices of functional connectivity between the 86 identified regions reveal marked differences between the control group (**d**) and 2-month post-FPC lesion group (**e**). Colour bars (left and below matrices) indicate ROIs within the frontal (blue), occipital (pink), parietal (green), and temporal (red) lobes respectively.*

Multidimensional scaling reveals a striking lesion effect of FPC

To aid in the visualization of the significant changes in functional connectivity between control animals and 2-month post-FPC-lesioned animals, we applied a multidimensional scaling (MDS) analysis to the pairwise correlations between these 86 identified ROIs in both groups. In this analysis we projected all connections into a 2-dimensional space, where ROIs with similar overall patterns of functional connectivity across the overall matrix are plotted with greater proximity to one-another (Fig. 3 a-b). We then used K-means clustering (with the variance to be explained fixed at 80%) to define clusters within the 2-dimensional space for both the control and the 2-month post FPC-lesioned animals' scaled data (Fig. 3 a-c).

In control animals this projection revealed the existence of four clusters (Fig. 3a) whereas only two distinct clusters were evident in the projection of 2-month post-FPC lesion animals (Fig. 3b). Moreover, visualization of the 2-dimensional space of all ROIs in the FPC-lesioned animals revealed a large spatial separation between the two clusters (Fig. 3b). In addition, these clusters showed physical separation in the brain when the anatomical locations of the regions were considered. Specifically, there was a distinct anterior versus posterior clustering of brain regions (Fig 3e). The first cluster included frontal regions, areas of insula cortex, somatosensory cortex, premotor and motor cortex, anterior parietal cortex and regions

of the anterior temporal lobe; while the second cluster predominantly included posterior cortical regions including posterior parietal cortex, cingulate cortex, retrosplenial cortex, occipital cortex and posterior temporal lobe regions. In contrast, in the control group, the four clusters show less obvious spatial separation on the 2D plot (Fig. 3a) and less obvious gross anatomical separation between networks (Fig. 3d).

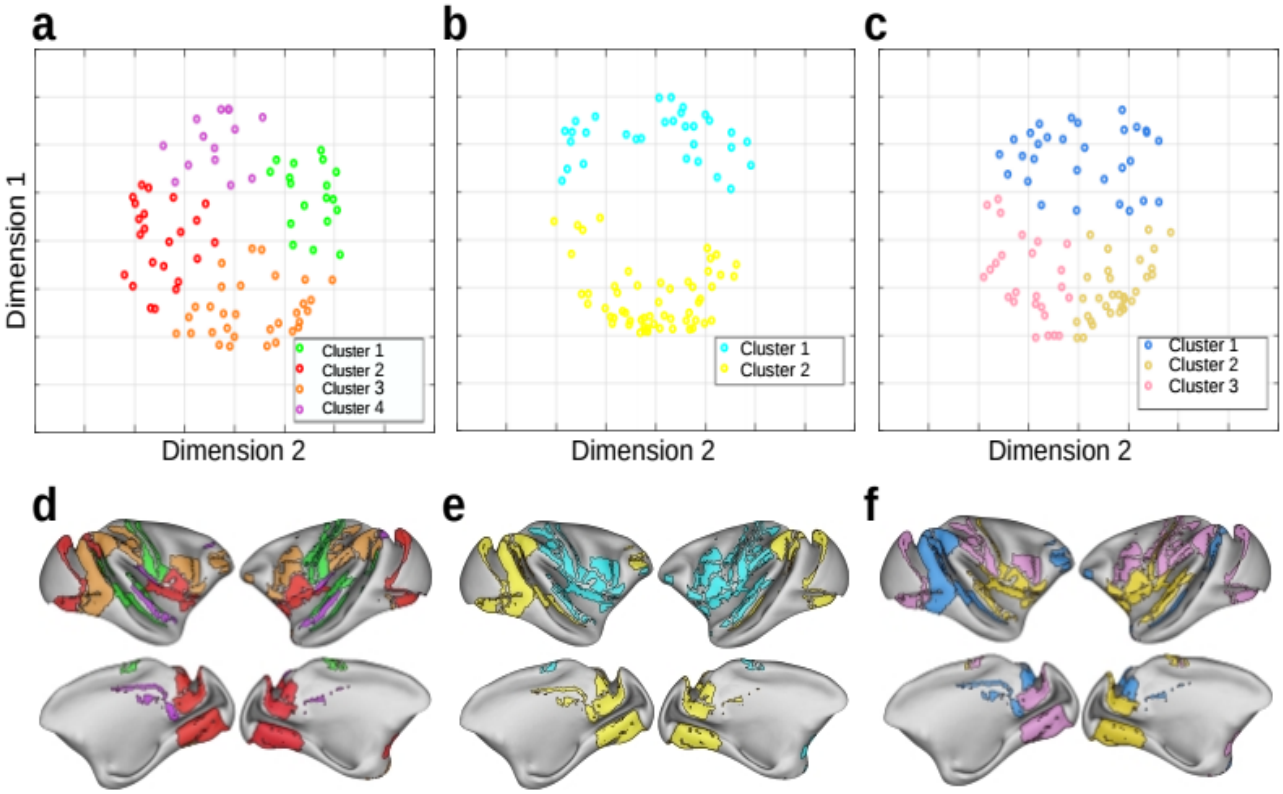


Figure 3. *Multidimensional scaling reveals reduced network modularity in the absence of Frontopolar cortex. Multidimensional scaling and cluster analysis of the functional connectivity between the 86 previously identified ROIs for animals in the control group (**a**), 2-month post-FPC lesion group (**b**), and 40-month post-FPC lesion group (**c**). Clustering of ROIs was defined by K-means clustering (into sufficient clusters to explain 80% of total variance). Each ROI is represented with a single dot, with cluster class denoted by colour. The distance between ROIs corresponds to the similarity/dissimilarity in the patterns of*

*functional connectivity of each ROI respectively. Differences in the cluster classes of all ROIs in the control (**d**), 2-month post-FPC lesion (**e**), and 40-month post-FPC lesion group (**f**) was visualised on the surface of the macaque brain, adopting the same colour conventions as in a-c.*

Differences in cluster-based analyses between 2-month versus 40-month post-FPC lesion groups

To explore how robust are our observed FPC-lesion mediated changes in rsfc clusters (mindful of the possibility of recovery/plasticity in the brain after some brain insults), we compared these results to corresponding rsfc and MDS projections from the 40-month post-FPC-lesion group.

We observed three clusters in the 40-month post-FPC lesion group (Fig. 3c). The spatial (i.e. Fig 3c versus Fig3a/Fig3b) and anatomical (i.e. Fig 3f versus Fig3d/Fig3e) separations appeared to fall between the control group and the 2-month post-FPC lesion group. This suggests some but not complete restoration of functional organization after 40 months compared to control animals.

To better illustrate the similarities and differences in cluster organization between the three groups of different animals (control, 2-month post FPC lesion, 40-month post FPC lesion), we made a 3D plot to link the three 2-dimensional projections for the 86 ROIs across groups (Fig. 4). Fig. 4 shows that the four clusters observed in control animals appear to collapse into two distinct clusters (shown in blue and yellow) in 2-month post FPC-lesion animals, with dramatic changes in the position of individual ROIs. The three clusters, observed in the 40-month post-FPC-lesion group, appeared more integrated than for the two clusters in the 2-month post-FPC-lesion group. However, there were limited changes in the

position of individual ROIs between these two group, particularly when compared with the more robust differences observed between controls and 2-month post-FPC-lesion group. This provides evidence that the 40-month period, a relatively long time in terms of brain plasticity and recovery of function, did not result in anything more apparent than a relatively small and partial recovery of network structure.

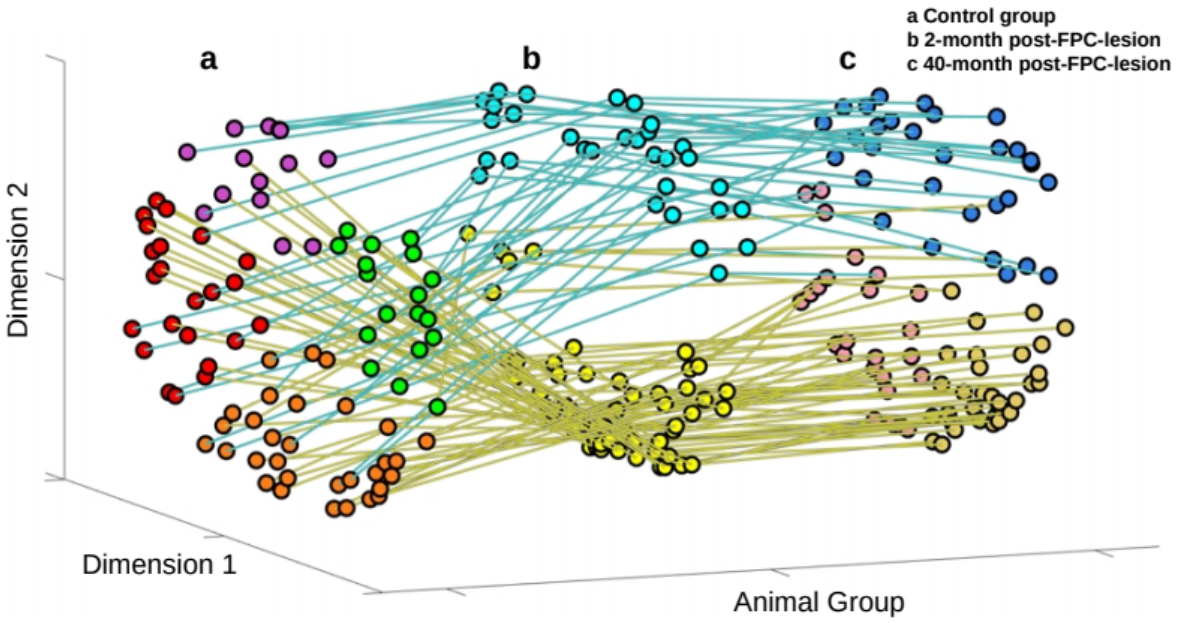


Figure 4. *Visualisation of changes in the relationship between ROIs explored by multidimensional scaling. Multi-dimensional scaling plots of the relationship between all 86 ROIs in the control group (a), 2-month post-FPC-lesion group (b), and 40-month post-FPC-lesion group (**c**). Changes in the location occupied by each ROI are visualised by linking across lesion groups. ROI scatter plots follow the conventions in Figure 3a-c. Line linking ROIs between lesion groups are coloured based on whether the ROI was in cluster 1 (blue) or cluster 2 (yellow) in the 2-month post-FPC-lesion group.*

Predictors of changed rsfc patterns across the brain in absence of FPC

We next sought to enquire whether the specific patterns of observed changes of rsfc induced by FPC lesions might be predicted by brain organization observed in the control animals with intact FPC.

Our first hypothesis is that the magnitude of rsfc between FPC and other ROIs in control animals predicts (i.e., with a positive correlation) the extent of repositioning of ROIs in the 2D projection (and therefore changes in the pattern of connectivity between ROIs) in the FPC lesioned animals. To test this hypothesis, for each of the 86 ROI's, we computed the Euclidean distance (in 2D space) between the position occupied by that region in control animals and the position occupied by that region in 2-month post-FPC-lesioned animals. Correlation of the Euclidean distance between these two groups, with the absolute connection strength between each ROI and FPC in control animals revealed a significant positive correlation (Pearson's $r = 0.233$, $p = 0.031$, Fig. 5a). This suggests that the stronger rsfc of one brain region to FPC in control animals, the greater the separation between that regions position in 2-dimensional space in control animals and FPC-lesioned animals. In other words, FPC-induced lesion effects on functional connectivity can predict how brain networks may adapt in the absence of FPC.

Our second hypothesis is that in the absence of FPC, connectivity between ROIs can be predicted according to the relationship between ROIs in control animals. In this scenario the separation between an ROIs position in 2D space in control and FPC lesioned animals would be dependent on its relative location within the four clusters observed in control animals, with ROIs more loosely or peripherally related to the relevant cluster demonstrating the greatest change in position (and therefore connectivity) after FPC lesions. Therefore, we investigated whether *centrality* versus *peripherality* of a ROI within the four clusters observed in control animals might predict the change in rsfc between a ROI and other areas after FPC lesions. To

calculate the relative location of each ROI in the 2-dimensional scale in control animals, we defined an index, called the within/between ratio. This ratio was calculated as the average of distances (in the 2-dimensionally scaled data) between each ROI and other ROIs within their local cluster divided by average of distances between the ROI and other ROIs in other clusters; hence the within/between ratio was larger for ROIs situated towards the margins of its own cluster and smaller if the ROIs were located more centrally in its own cluster. We did this for each of the 86 ROIs in control animals compared to the same ROIs in the 2-month post-FPC lesioned animals. Correlation of the within/between ratio with the Euclidean distance between the control and 2-month post-FPC lesioned animals was not significant (Pearson's $r = 0.025$, $p = 0.822$, Fig. 5B), therefore our second hypothesis was not supported.

We also tested these two hypotheses in the 40-month post-FPC-lesioned animals, as compared to controls, and found that neither of the correlations was significant (strength of rsfc to FPC: Pearson's $r = 0.134$, $p = 0.220$; within/between ratio: Pearson's $r = 0.156$, $p = 0.152$, Fig. 5c and 5d). This suggests that the network state that exists in the 40-month post-FPC lesion animals and that likely includes any plasticity-mediated recovery of function occurring over a few years is no longer predictable from the aforementioned parameters of the control animals network state. This further suggests that even after several years, plasticity such that it exists is insufficient to return the network to a nearly normal state. Hence the effects of FPC lesions on extended brain networks may be robust for several years (and although our data cannot speak to longer periods than 40 months, 40 months appears to be a long time in terms of brain plasticity and recovery of function, especially in light of our own previous studies of functional recovery after frontal lesions in macaques (Ainsworth et al. 2018)), so it is not unreasonable to predict that FPC-lesion mediated changes to brain network structure may indeed extend to decades or even to the lifetime).

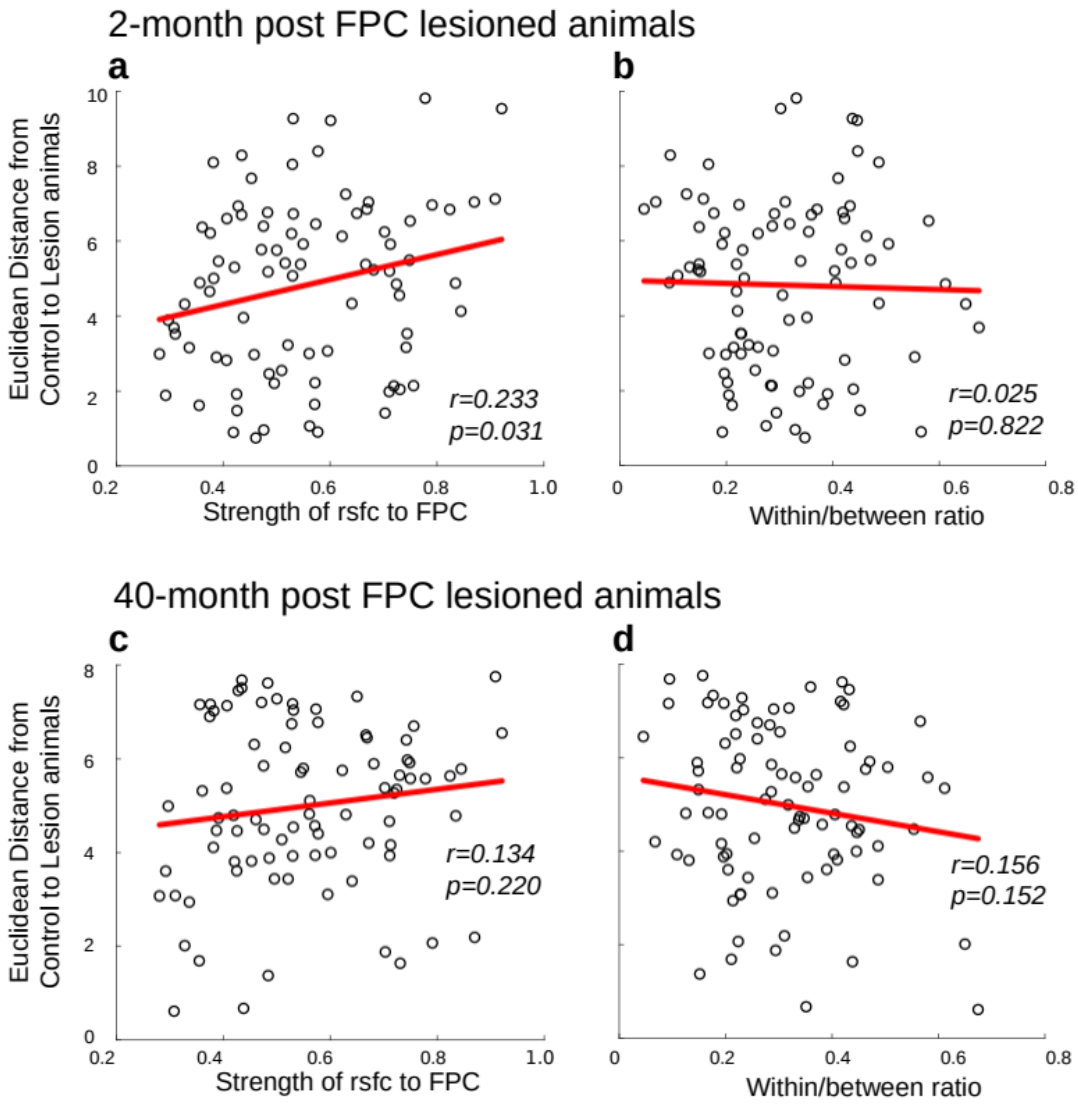


Figure 5. *Remodeling of ROI connectivity after lesion of frontopolar cortex is predicted by ROI to FPC connectivity in control animals. Scatter plots showing the relationship between the strength of an ROIs connection to FPC in control animals and the difference between an ROIs position in 2-D space (calculated as Euclidean distance) in control animals vs. in 2-month post-FPC-lesion animals* ***(a)*** *and the relationship between the within/between ratio of an ROI in control animals with the Euclidean distance between control animals vs. in 2-month post-FPC-lesion animals* ***(b)***. *The same relationships, FPC connection strength vs. Euclidean distance* ***(c)*** *and within/between ratio vs. Euclidean distance* ***(d)*** *are shown for*

ROIs between control animals and 40-month post-FPC-lesion animals. An ROIs within/between ratio is defined as the average distance to within cluster ROIs divided by average of distance to ROIs in other clusters). Correlation coefficient (Pearson's r) and the significance of the correlation shown for each test.

Discussion

Circumscribed bilateral lesions to the macaque FPC produced a distinctive change in rsfc across multiple brain networks extending both within and beyond prefrontal cortex. Analyses of the patterns of changes suggest FPC lesions reduce the number of distinct networks as compared to the intact animals. In control animals our cluster-based analyses of rsfc revealed the following four networks: (i) a primary auditory cortex, somatosensory, occipital, superior and middle temporal cortical network (cluster 1); (ii) a gustatory cortex, piriform cortex, ventral premotor cortex, insular, occipital, posterior parietal and middle temporal cortical network (cluster 2); (iii) a ventral prefrontal, premotor, motor, somatosensory, occipital, anterior areas of posterior parietal and perirhinal cortical network (cluster 3); and (iv) a posterior prefrontal, somatosensory, superior temporal sulcal, cingulate, and retrosplenial cortical network (cluster 4). Notably each of these clusters extended over multiple cortical lobes. This indicates that animals with an intact FPC can maintain several distinct and complex cortical networks. By contrast, in the absence of FPC, the ROIs collapsed into two brain networks: a frontal-temporal-anterior parietal network and a cingulate-occipital-posterior parietal network, with each demonstrating disparate resting state connectivity patterns according to our cluster analyses. The frontal-temporal-anterior parietal network occupied more anterior parts of the brain, which included prefrontal cortex, premotor and motor cortex, gustatory cortex, piriform cortex, somatosensory cortex, insular regions, anterior regions in parietal cortex, anterior regions in temporal cortex and perirhinal cortex.

This brain network is typically associated with executive control (Cochin 1999), somatosensory and olfactory perception (Stettler and Axel 2009; De Araujo and Simon 2009), motion and body movement (Kiyoshi Kurata 1991) and mnemonic processing (Suzuki and Naya 2014; Brown and Aggleton 2001) . The cingulate-occipital-posterior parietal network occupied more posterior parts of the brain, which included posterior cingulate cortex, retrosplenial cortex, posterior parietal cortex, occipital cortex, medial superior temporal areas and middle temporal areas. The regions involved in these networks are typically associated with emotional (Vogt 2005), visual (Boussaoud et al. 1992; Kaas and Collins 2004), and spatial processing (Lewis and Van Essen 2000).

The relationship between functional connectivity and anatomical connectivity is not precise (directly connected areas need not oscillate in synchrony, and it is not necessarily the case that areas without direct anatomical connections cannot exhibit synchrony as posterior areas without direct connections to FPC may be strongly connected to other posterior areas and 'recruited' into a FPC-mediated networks indirectly). Nonetheless, anatomical tracing studies (see below) and functional connectivity studies in macaques (Neubert et al. 2014, 2015) do indicate that many brain regions are in fact both anatomically and functionally connected to FPC. Petrides and Pandya (2007), Markov et al. (2014) used anatomical tracing to identify cortical and subcortical efferent and afferent connections to and from FPC in macaques (Petrides and Pandya 2007; Markov et al. 2014). Despite the different techniques and different species used, a broadly similar range of connections were found in these tracing studies. FPC has dense interconnections with other prefrontal areas (e.g. area 8Ad, 9, 11, 12, 13, 14 and 32); and robust cortical connections with temporal lobe regions, including insula, rostral superior temporal gyrus and superior temporal gyrus regions (e.g. area Ts, TAa and TPO) *via* the external capsule; and anterior and medial temporal lobe (e.g. perirhinal cortex) *via* the uncinate fasciculus; and anterior and posterior cingulate and retrosplenial cortex (Petrides and Pandya 2007; Markov et al. 2014) *via* the cingulate fasciculus. Moreover,

Markov et al. (2014) identified a much wider range of posterior connections with area 10, including connections with parietal and occipital cortex, in which connections were observed with lateral, medial and posterior inter-parietal and with V2 (Markov et al. 2014), although these connections have not been observed in other studies and in some cases the projections are very light. In summary, these evidence of cortico-cortical connections to/from FPC in tracing studies showed a wide range of cortical regions are involved in the cortical networks related to FPC, and most of them have been detected in the frontal-temporal-anterior parietal and cingulate-occipital-posterior parietal network in our rsfc study.

As reviewed in the introduction, the three studies that have investigated macaques with bilateral and circumscribed lesions to FPC have demonstrated that FPC is necessary for considering the relative values of (unchosen) alternatives of a broad kind. This can lead to deficits in some contexts (e.g., specific impairments in the one-trial learning phase of both concurrent objects-in-scenes learning and successive single problem learning wherein animals chose between novel alternative stimuli; and impairments in learning to choose between novel alternative abstract rules (Boschin et al. 2015) yet can also lead to enhancements in other contexts (e.g., macaques with FPC lesions showed enhancements in a Wisconsin Card Sort Test analog involving conflict between two well learnt rules in terms of being less distractible than control animals by to intentional distraction between trials and hence better ongoing performance on the focused-upon task (Mansouri et al. 2015)). Together these studies showed that FPC is necessary for disengaging executive control from the current task/goal/stimuli and redistributing it to explore any other potential tasks/goals/stimuli (Mansouri et al. 2015, 2017). It is understandable then that the kinds of behavioural changes induced by FPC lesions are both broad in scope, yet also specific to certain kinds of situations such as those where exploration versus exploitation of chosen versus unchosen alternatives is required. Accordingly, the effects of FPC lesions cannot be

simply understood as a loss of function of the specific area removed; to understand FPC function one has to consider how FPC causally interacts with a broad range of posterior areas.

The current study contributed to this goal by demonstrating how brains with an intact and functioning FPC influence network cohesion are able to maintain more posterior networks compared to brains without a functioning FPC. We propose that FPC may be considered a mediator of modularity. We show that in addition to changes in behaviour following FPC lesions (Boschin et al. 2015; Mansouri et al. 2015, 2019), we also observe changes to rsfc. But we do not know if the robust changes in rsfc patterns themselves had any influence upon (long-term) behaviour, or whether changed behaviour influenced long-term rsfc (or both).

Speaking to the latter possibility in broad terms it has been shown that such effective connectivity can at least predict cognitive flexibility in humans (Chén et al. 2019). Speaking to the former, resting state networks have themselves been linked to memory consolidation processes that may also be active in the resting state (Albert et al. 2009) and indeed, patients exhibiting episodic memory loss who had lesions to more polar than dorsolateral prefrontal areas have been observed to have greater deficits in remembering than knowing (Wheeler and Stuss 2003). Given we have shown a clear causal influence of FPC lesions on posterior network organization, the next set of studies should investigate the influences of FPC on posterior network organization during behaviour itself by conducting rsfc in the awake state. Causal influences of dynamic network states on behaviour may be determined by selective intervention in the dynamic network states (e.g. *via* microstimulation to drive or disrupt oscillations in target areas) in the presence and absence of FPC.

As the control and FPC-lesioned animals scanned after 2 months versus after 40 months post-lesion demonstrated distinct patterns of brain network organizations, we investigated what, if any, factors inherent to network organization on controls might influence network

organization in FPC-lesioned animals. Our supported hypothesis, that brain regions with the greatest change in their connectivity pattern following an FPC lesion (measured as change in position in 2-D space) were those that exhibited stronger effective connectivity to FPC in control animals. This was true for 2-month post-FPC lesion but no longer true in the 40-month post-FPC lesioned animals. These findings imply that FPC is important not only in influencing select key areas that it robustly interacts with but is also important for shaping wider posterior brain networks involving those key areas. After 40 months without the influence of FPC the brain's network organization has evolved, this is unsurprising, but the fact that the post-lesion network structure has not returned to normality after a few years only indicates how FPC plays a critical long-standing role in brain functional organization in primates.

Animals with an intact FPC can maintain more distinct sets of brain networks than animals without FPC. Moreover, the functional connections of regions robustly interacting with FPC are predictive of the changed network structure within and beyond prefrontal cortex in absence of FPC. The predictive changes last at least 2 months and even after 40 months the network structure has not returned to normality. Future work should investigate how these FPC-related brain networks in awake behaving animals influence essential cognitive processes, such as learning, memory and decision making by combining neuroimaging and electrophysiology with reversible targeted interventions during behaviour.

Chapter 2. Similar time course of fast familiarity and slow recollection processes for recognition memory in humans and macaques

Abstract

According to dual-process theory, recognition memory performance draws upon two processes, familiarity and recollection. The relative contributions to recognition memory are commonly distinguished in humans by analyzing receiver-operating-characteristics (ROC) curves; analogous methods are more complex and very rare in animals but fast familiarity and slow recollective-like processes (FF/SR) have been detected in non-human primates (NHPs) based on analyzing recognition error response time profiles. The relative utility of these methods to investigate familiarity and recollection/recollection-like processes across species is uncertain; indeed, even how comparable the FF/SR measures are across humans and NHPs remains unclear. Therefore in this study a broadly similar recognition memory task was exploited in both humans and a NHP to investigate the time course of the two recognition processes. We first show that the FF/SR dissociation exists in this task in human participants and then we demonstrate a similar profile in the NHP which suggests that FF/SR processes are comparable across species. We then verified, using ROC-derived indices for each time-bin in the FF/SR profile, that the ROC and FF/SR measures are related. Hence we argue that the FF/SR approach, procedurally easier in animals, can be used as a decent proxy to investigate these two recognition processes in future animal studies, important given that scant data exists as to the neural basis underlying recollection yet many of the most informative techniques primarily exist in animal models.

Introduction

Recognition memory, a form of declarative memory according to some authors (Squire and Zola-Morgan 1991), allows us to make judgements as to the prior occurrence of stimuli based on previous encounters. The delayed matching-to-sample (DMS) and delayed nonmatching-to-sample (DNMS) tasks of recognition memory have been used extensively in animal models. Both tasks are initiated by requiring animals to view the sample picture (or as occurred in many earlier studies, by presenting real objects briefly to animals in a Wisconsin General Test Apparatus), and then after a delay in which no stimuli are presented on the screen, typically two choice pictures are presented in which animals should select the stimulus seen earlier as sample (i.e. the 'match') in DMS task while animals should choose the picture different from the sample (i.e. the 'non-match') in DNMS task. By manipulating the length of delay between sample and test images, which is often varied within an experiment to test for delay-dependent deficits that might index memory processes; and/or by increasing the number of items to be remembered, the difficulty and cognitive demands on both tasks increase. As in both tasks, studied images will be represented in the test phase, animals may make use of familiarity to differentiate studied and unstudied images. As familiarity is often considered as an automatic process (Jacoby 1991), animals may just rely on familiarity of studies images to solve recognition tests. Whereas animals can clearly judge relative familiarity of stimuli, the issue of whether animals can 'recollect' discrimination per se has been a more contentious issue.

Dual-process signal detection (DPSD) theory suggests recognition memory may draw upon two processes, commonly referred to as familiarity and recollection (Dede et al. 2014; Parks and Yonelinas 2007; Scalici et al. 2017; Wixted 2007; Yonelinas 2001, 2002; Yonelinas and Parks 2007). In recollection, if the item/object is judged as being encountered previously, the related contextual information about the item/object can be recalled with more

details. For instance, recollection of an item/object may prompt retrieval of information about when and where one was when one encountered the item/object, what one was doing, thinking or feeling, as well as the surrounding environments. By contrast, familiarity is simply a feeling of the item/object has been encountered and generates a feeling of familiarity or knowing but without too much details (Dede et al. 2014; Parks and Yonelinas 2007; Scalici et al. 2017; Wixted 2007; Yonelinas 2001, 2002; Yonelinas and Parks 2007). Accordingly, recollection versus familiarity is often characterized as remembering versus knowing. The receiver-operating-characteristics (ROC) analysis in humans has shown two different components in human recognition memory: a symmetrical and curvilinear component associated with familiarity, and an asymmetrical and linear component related to recollection (Parks and Yonelinas 2007; Eichenbaum et al. 2007; Yonelinas and Jacoby 1994; Yonelinas 2001, 2002; Yonelinas and Parks 2007; Yonelinas et al. 2010).

Recent animal studies have also investigated familiarity and recollection-like memory processes by analyzing the ROC curves based on DPSD model (Fortin et al. 2004; Guderian et al. 2011; Sauvage et al. 2008). A fundamental difficulty to overcome in animal models using ROC is that one cannot simply ask for a confidence judgment after the recognition memory judgment. The first application of ROC curves to distinguish familiarity and recollection-like processes in animals was in the rodent model wherein Fortin et al. (2004) plotted ROC in rodents by varying the reward and effort required to make old versus new judgments so to allow responses to be assessed across different levels of 'confidence'. Fortin et al. (2004) showed that these ROC looked like ROC in normal humans; moreover, in rodents with hippocampal lesions the changed shape of the ROC resembled the changed shape of ROC in human patients with hippocampal lesions (i.e. asymmetrical curvilinear ROC became curved symmetrical ROC). In patients this change may be interpreted as loss of recollection but spared familiarity; hence in rodents with hippocampal lesions Fortin et al (2004) showed that they too possibly lost a recollective-like component to their memory but

their familiarity remained intact (Fortin et al. 2004). Subsequently, Sauvage et al. (2008) used an associative recognition paradigm and ROC to show recollection is reduced and familiarity increased after hippocampal lesions in rats (Sauvage et al. 2008). These issues are not without controversy and opposing views generated lively debate (Eichenbaum et al. 2005, 2008; Wixted and Squire 2008). Later, Guderian et al. (2011), by biasing macaques to respond to new and old stimuli by altering reward amounts they could obtain for their correct responses, further confirmed, using ROC, that recognition memory in animals draws upon separate familiarity and recollection-like processes in macaques (Guderian et al. 2011).

A key alternative approach to investigating the relative contributions of familiarity and recollection have investigated the time course of familiarity and recollection processes. Time courses of recollection and familiarity have also largely been investigated in human studies. For example, Yonelinas and Jacoby (1994) calculated the peak time of familiarity and recollection in a source memory task and showed that whilst the peak time of familiarity is faster, between 600 and 800 ms, the peak time of recollection is slower, between 800 and 1000 ms; this gives rise to the concept of faster familiarity and slower recollection (Yonelinas and Jacoby 1994). A faster response to retrieving familiar words (i.e. familiarity process) has likewise been found in comparison to retrieving details of words in a word list (i.e. recollection process) (Hintzman and Curran 1994). Some neurological studies have also confirmed an earlier process of familiarity compared to a later process of recollection in recognition memory. For instance, Curran (2000) found the components of event-related brain potentials (ERPs) related to familiarity appears earlier at 300-400 ms than other later parietal components associated with recollection at 400-800 ms (Curran 2000).

Dosher and his colleagues applied a speed-accuracy trade-off paradigm to interpret the time course of these two processes, in which human participants must respond within a brief window following a go-signal, which is presented at various delays after the offset of

the encoded sample items (Dosher and Rosedale 1991; Dosher 1984). In this paradigm, a plot of false alarm errors against retrieval time shows a rise of errors across extremely short retrieval time that reaches a summit in the intermediate retrieval time then decreases in the longer retrieval times (Brainerd and Reyna 2005; Dosher 1984; Dosher and Rosedale 1991; Gronlund and Ratcliff 1989; Hintzman and Curran 1994; Matzen et al. 2011; Rotello and Heit 2000; Rotello et al. 2000). The peak time of these false alarm errors has been considered to relate to the onset of familiarity, and the suppression of false alarm errors during the longer moderate/intermediate retrieval times is considered to reflect the onset of recollection which is conducive to minimizing false alarms (Brainerd and Reyna 2005). Taken together, there is significant consensus as to "fast familiarity" and "slow recollection" (FF/SR) across the human literature, although the methodology of speed-accuracy trade-off paradigm has been questioned in some other human studies (Brainerd et al. 2014, 2019).

More recently, Basile and Hampton (2013) have reported similar FF/SR profiles in non-human primates (NHPs). Their study is similar to the speed-accuracy trade-off paradigm used in human studies (Dosher 1984; Dosher and Rosedale 1991), wherein the time course of familiarity and recollection are investigated by plotting false alarm errors against retrieval time. Basile and Hampton (2013) introduced a modified recognition memory paradigm for NHPs in which animals were trained to select/touch a standard non-match button on the touch-screen if they wished to indicate that the test image did not match the studied image, but were trained to select/touch the test image itself if they wished to indicate that the test item was a match to the studied image. By this approach this paradigm allowed miss and false-alarm errors to be distinguished which better facilitates application of signal detection theory to the NHP DMS task. By plotting false alarm errors against animals' response time, the authors found that recognition choices in the recognition memory task could be categorized in three different ways depending on response time: (i) short-latency errors induced by false alarms to familiar lures, deemed to indicate the process of familiarity; (ii)

medium-latency responses are less likely to be affected by false alarms and are more accurate, suggesting the onset of recollection-like process that could correctly reject familiar lures; and (iii) long-latency and low accuracy responses which are deemed to be guesses (Basile and Hampton 2013).

There have been criticisms of applying the DPSD model to differentiate familiarity and recollection-like processes in animals. Firstly, the DPSD model assumes that recollection is a threshold process with high confidence judgments in which human subjects either recollect or do not recollect a stimulus; while familiarity is a signal-detection process with various confidence judgments. Whether animals can 'recollect' discriminanda per se is still debated as discussed above, though at least some studies are favorable to this view (Fortin et al. 2004; Guderian et al. 2011; Sauvage et al. 2008). Secondly, animal models have had to develop proxies for humans' reported confidence judgments. As outlined above, rats were biased to respond to new and old odour by altering the amounts of rewards in different heights of test cups (Fortin et al. 2004; Sauvage et al. 2008); and macaques were biased to respond to new and old stimuli by altering different amounts of rewards they could obtain for their correct responses (Guderian et al. 2011). In the above three animal studies, it is assumed that animals have to be sufficiently confident to overcome any given level of bias, so the bias levels can be used to estimate their confidence. However, training animals to respond to correct new and old stimuli based on such bias levels so as to generate ROC is difficult and time-consuming and we are not aware of other studies that have achieved this to-date; whilst an important and influential methodology it is unlikely to become a frequently used methodology in animal models.

Other criticisms on interpreting animal recognition memory using DPSD models are focused upon the model itself. Malmberg (2008) points out the lack of consistency in the measurements of recollection and familiarity derived from DPSD model even across different

human studies (Malmberg 2008). A review from Yonelinas and Parks (2007) raised several issues related to this inconsistency which should be carefully considered when applying DPSD to animal models. A first considers the average performance rate; either performing too well or too poorly will result in the ceiling and floor effects, which will lead to the difficulties in ROC curve fitting in the DPSD model and makes the interpretation of familiarity index based on slope of ROC less certain (Yonelinas and Parks 2007). Secondly, as with human participants, if the entire scale of confidence judgments is not utilised, then ROC curve fitting is less reliable and parameter estimates extracted from ROC curve will be less meaningful (Yonelinas and Parks 2007). Moreover, in animal models, if animals showed significant preferences to trials with certain biases values (i.e. trials with higher biases values representing larger rewards in studies of Fortin et al., 2004 and Guderian et al., 2011) then the number of reliable data points to fit ROC curves may decrease. Additionally, curve fitting results are easily influenced when hits or false alarm rates on the extreme ends of the ROC approach 0.0 or 1.0 (Yonelinas and Parks 2007); negative values of R (recollection index) or F (familiarity index) may be reported but are meaningless considering the nature of recollection and familiarity process. All the above issues are challenges for DPSD model-based interpretation of human ROC and have arguably larger impact upon animal ROC studies of recognition memory.

The FF/SR paradigm on the other hand is relatively easy to implement in both humans and NHPs (Dosher 1984; Dosher and Rosedale 1991; Basile and Hampton 2013). In the NHP version of this paradigm reviewed earlier (Basile and Hampton 2013) only two images were used repeatedly, in each trial, so in each trial one was the studied image to remember while the other one was the lure (or vice versa). Basile and Hampton (2013) argued that this was appropriate larger sets which are easier to remember (i.e. to avoid too few errors for analysis) and also that large sets may be too easily discriminabale on basis of familiarity; however this was not verified in that study. Certainly small sets are likely to elicit

greater proactive interference but this is expected to be very limiting indeed for recollection and familiarity per se; the task essentially becomes a recency memory task which weakens the interpretation of Basil and Hampton's data. Therefore our study of FF/SR here expands upon Basil and Hampton (2013) by looking at both small sets and larger sets (trial-unique) of stimuli, to overcome the aforementioned limitation and more importantly, seek generalization of FF/SR effects across a range of set-sizes.

In this study, we adopted Basile and Hampton's basic recognition memory paradigm, but further refined the paradigm to probe intra-species comparisons across humans and NHP. Firstly, in human subjects, we used the tasks to assess whether response time derived measurements of recognition errors could be used to differentiate fast familiarity and slow recollection processes in humans using similar paradigms to that we used in the NHP. Then, to probe the relationship between recognition error response time (FF/SR) derived and ROC derived estimates of familiarity and recollection indices in humans, we first sorted trials from slowest to fastest in order to assign trials to a series of response time bins (ranging from fast to slow), and then fitted human ROC data to the DPSD model and extracted familiarity and recollection index independently across the different response time bins. To enable comparison of approaches we then plotted recognition errors (i.e. miss errors and false alarm errors) independently across similar response time bins to those used in the ROC approach. We compared the plots of recognition errors to plots of ROC derived familiarity/recollection indices along a common time course. Following Basile and Hampton (2013) we hypothesized a peak of false alarm errors associated with the short latency bins and we further hypothesized this 'fast-familiarity' behaviour would correspond with a peak of ROC-derived familiarity index; accordingly we also hypothesized that a peak in recognition accuracy (d prime) would correspond in time-course with the peak of the ROC-derived recollection index in the medium-latency bins. If the aforementioned hypotheses were supported then, this would suggest that the time course analyses of patterns of recognition errors are

phenomenologically related to the ROC-derived familiarity and recollection indices. Then, benefiting from using a similar recognition memory paradigm in both humans and macaque (Fig.1), we were able to compare plots of recognition errors against response time in humans to those in the NHP on a similar task so to investigate the time course of familiarity and recollection across species; accordingly we hypothesized similar "fast familiarity" (peak of false alarm errors) and "slow recollection" (peak of accuracy) profiles across response time in both species. If our first hypothesis about a relationship between recognition error-derived and ROC-derived familiarity/recollection indices holds then this significantly increases the validity of the response time approach derived from recognition errors in the NHP for probing their familiarity and recollective-like (i.e. dual-process) contributions to recognition memory (of clear benefit to future behavioural neuroscience research in animal as to the neural basis of recollection given the inherent difficulties associated with fully exploiting ROC approaches in animals as we reviewed earlier).

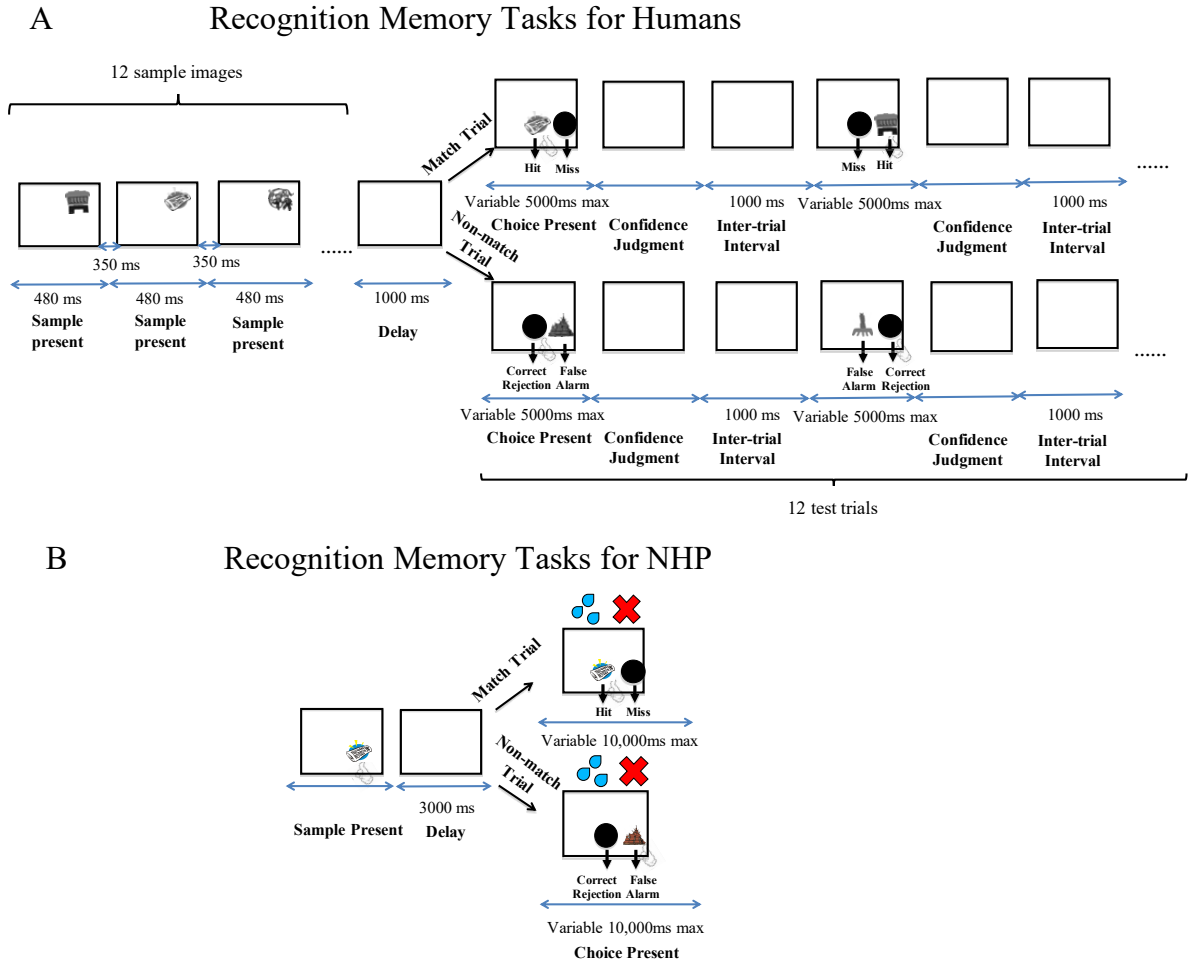


Figure 1. *Diagram of the match/non-match recognition memory paradigms for human participants (top panel, A) and a NHP (bottom panel, B). A, in the recognition memory tasks for humans, participants were instructed to remember 12 gray-scale sample images, then after a delay of 1000 ms, they were instructed to touch the test image if it matched the sample image; or selected the standard 'non-match button' if not match (the maximal responding time for humans was 5,000 ms); and then report their confidence judgments using hand gestures in each test trial; they completed blocks of 12 sample trials and then 12 test-trials in this way (15 blocks in total per session). B, in the NHP recognition memory tasks the NHP viewed one sample image, and experienced a delay of 3000 ms, and then was trained to touch the test image if it matched or to select a standard non-match button if not match (the maximal responding time for animal was 10,000 ms); this trial structure repeated throughout*

the session with some samples and test-items being novel (trial-unique) and others familiar within (but not between) daily sessions.

Materials and Methods

Experiment 1: Human behavioural study

Participants

27 participants (18 male, 9 female, age range 18-30 years) took part in this study. Participants were fluent English speakers, right-handed, and had normal or corrected-to-normal vision. Prior to the study, all the participants provided written consent and went through safety screening check to make sure they had no history of previous or current neurological or psychiatric conditions and were not taking any psychoactive medication. All the participants received monetary compensation for their participation at a standard rate for volunteers in Oxford. This study was carried out with the approval of Medical Sciences Interdivisional Research Ethics Committee, University of Oxford.

Task Stimuli and Apparatus

The task was an object recognition memory task similar to the one used in the NHP, similarly programmed using Turbo Pascal (Borland), run under DOS on a desktop PC and presented on a 20.1" colour touchscreen (TFT LCD TS200H GNR). The object images used in the task were clip-art images as in NHP study, but in order to increase difficulty (in light of a pilot study wherein performance was close to ceiling) the images were all converted to grey-scale and the contrast toned down in an attempt to make them harder to discriminate from each other. Additionally, the samples were presented in lists followed by lists of choice trials, again to reduce ceiling effects in the human version of the NHP task. Each image subtended

10° of visual angle in width and 10° in height to the participant sitting facing the screen. The sample image was always presented on the right top of the screen, positioned +12 ° horizontal and -12 ° vertical from the center of the screen. The test images were presented on the right bottom of the screen: one was positioned 0 ° horizontal and +5 ° vertical from the center of the screen; and the other one was positioned +23 ° horizontal and +5 ° vertical from the center of the screen. The background colour to the screen was white.

Participants sat with their eyes a distance of 25 cm from the screen, wearing earplugs, resting their chins on a chin-rest and their foreheads on a head holder to stabilize their head position throughout the experiment. They were instructed to respond to items by touching them on the screen and gestured their confidence ratings using their right hands. For example, they indicate by raising fingers (1, 2 or 3) whether their opinion corresponding to their being somewhat confident (1), moderately confident (2), or absolutely confident (3) in their judgment as to whether they considered the test-item to be old (i.e. presented before in the preceding list as a sample) or new (not seen before in the preceding list as sample). None of the samples in this task were used in more than one list so all stimuli were trial-unique (and hence compared to the novel/trial-unique stimuli in the NHP task).

Behavioural task

Prior to the experiment, participants were given instructions on how to perform the task, and how to indicate their confidence judgments (see above), and then they were introduced to the behavioural task in a short training/practice session (comprised of one list of 12 samples and then 12 test-item trials) of the task without stimulation to provide an opportunity to become familiarized with task procedure. We used lists in the human version to avoid ceiling effects as pilot investigations revealed the NHP task with single samples and single test-trials to be too easy for participants. The experimental session itself contained 3 sub-sessions, with each sub-session containing 15 blocks of trials. Participants took a 10-15 min break between each

sub-session. Each block contained an encoding phase (i.e. a list of 12 sample images), and then a short delay, and then a test phase (i.e. a list of 12 test-item trials). The task structure is depicted, for one block, in Figure 1 (top panel, A); during the encoding phase, 12 sample images were presented sequentially on the screen (individually for 480 ms), with inter-stimulus-interval as 350 ms. Participants were instructed to view and try to remember each sample image. After the sample phase (all 12 sample items) was completed, a blank screen was presented for 1 s (delay), and then the test phase commenced (all 12 test trials). Test trials were either 'match trials' or 'non-match trials'. In each test trial, either an identical stimulus to one of the preceding12 samples (i.e. 'match trials') was shown as a test image, or a novel and previously unseen image (i.e. 'non-match trials') was shown as a test image, and that test image appeared on the screen together with a black circle (the left/right position of the black circle and the test-trial image were randomized between trials). The maximal time allowed for a response for human participants was 5,000 ms. The match and non-match trials were also counter balanced (6 of each per test phase of 12 test-trials) and were put in a random order. Just as in the NHP version of the task (Experiment 2) participants were instructed to touch the test image if they thought it matched one of the 12 sample images, or touch the standard 'non-match button' (i.e. the black circle) if they thought the test image was not a match. After responding to the test image, participants were instructed to rate their confidence as to whether the test item was new or old using a scale of 1-3 by making three different movements with their fingers, corresponding to somewhat, moderate, and absolute confidence. Participants were further instructed to try to use the entire range of confidence responses as best they could and not simply select the extremes of confidence as defaults.

Experiment 2: Macaque behavioural study

Subject

One adult female rhesus macaque (*Macaca mulatta, age 8 years, weigh 10-13 kg*) participated in this experiment. All animals in our lab are socially housed (or socially housed for as long as possible if later precluded, for example, by repeated fighting with cage-mates despite multiple regrouping attempts) and all are housed in enriched environments (e.g. swings and ropes and objects, all within large pens with multiple wooden ledges at many levels) with a 12hr light/dark cycle. The NHP always had *ad libitum* water access 7 days/week. Most of its daily food ration of wet mash and fruit and nuts and other treats was delivered in the automated testing/lunch-box at the end of each behavioral session (this provided 'jack-pot' motivation for quickly completing successful session performance; supplemented by trial-by-trial rewards for correct choices in the form of drops of smoothie delivered via a sipping tube) and this was supplemented with fruit and foraging mix in the home enclosure. All animal training and experimental procedures were performed in accordance with the guidelines of the UK Animals (Scientific Procedures) Act of 1986, licensed by the UK Home Office, and approved by Oxford's Committee on Animal Care and Ethical Review.

Task stimuli and apparatus

The object recognition memory task was programmed using Turbo Pascal (Borland), run under DOS on a desktop PC. Visual stimuli used in the task were clip-art images in colour, which were presented on a 20.1" colour touch-sensitive screen (TFT LCD TS200H GNR). Those clip-art images used in the task were from a large pool of several thousand unique images. Each image subtended 5° of visual angle in width and 5° in height to the subject when presented on the screen. Both the sample image and test images were presented on the right bottom of the screen. The sample image was positioned +10 ° horizontal and +5 ° vertical from the center of the screen, with equal distance to the two test images. The test images were presented at the same horizontal level as the sample image: one was positioned

0° horizontal and +5 ° vertical from the center of the screen; and the other one was positioned +20 ° horizontal and +5 ° vertical from the center of the screen. The background colour to the screen was white. In each session, images were randomly chosen from the pool without replacement and were not re-used on the other testing days.

The animal was seated in a primate chair (Rogue Research Inc.) in front of the touch screen with its head-fixated and whilst it performed the recognition memory task in a magnetic-shielded, and partially sound-attended, testing-box. A window in the front of the chair provided its access to the touch-screen itself. The distance between the monkey and touch screen was fixed at 50 cm enabling the animal to touch the screen easily. An infrared camera was used to monitor the general status of the monkey in the box. A peristaltic pump device located on top of the box fed smoothie reward through a tube and to a spout positioned in the vicinity of the animal's mouth. Below the screen was also an automated lunch-box which contained the majority of the animal's daily meal (wet mash and fruits and nuts etc.) and which opened immediately at the end of the task.

Behavioural task

In the NHP study, a similar task design has been exploited with the main difference being samples and test phases were not blocked. In each trial, animal viewed a sample image (shown in the right bottom of the screen) to remember and touched it to progress. Then after the 3000 ms delay period, the NHP was tested with two choice stimuli (one an object image and the other a black circle, left-right randomized between trials). The NHP was required to make a choice to the touchscreen to either the object test-image stimulus or to the black circle stimulus. The object stimulus was either the identical stimulus to the sample seen earlier in the trial or it was not identical to the sample. The animal was rewarded by delivery of 10 ml of smoothie for touching the test-item image if it matched the sample image (these we refer to as 'match trials'), or it was rewarded for selecting the standard 'non-match button' (i.e. the

black circle) if the test-item was a non-match (these we refer to an 'non-match trials'). The maximal time allowed for a response for animal was 10,000 ms. The next trial started after a 3000 ms inter-trial interval after a correct response, or after a 10 s 'time-out' after any kind of error response. A schematic of the recognition memory task is illustrated in Figure 1 (bottom panel, B). Accordingly on *match trials* the animal could either make a correct response ('hit') or an incorrect response ('miss') whereas on *non-match trials* the animal could either make a correct response ('correct rejection') or an incorrect response ('false alarm'). The use of the black circle allowed hit/miss rate to be calculated independently of correct rejection/false-alarm rate; in this way the paradigm is similar to one previously use by Basile and Hampton (Basile and Hampton 2013). A key element of task design in this paradigm for the macaque, enabled by the non-match 'button' (i.e., black circle), is that miss errors and false-alarm errors may be distinguished independently in which their latencies can be used for estimating the time of familiarity and recollection in the macaque. We also varied the degree to which stimuli were either familiar or novel in the session (typically there were up to 80 pairs of novel stimuli that were trial-unique in each session, and six other familiar stimuli, grouped into three pairs, that repeated many times through the session). This allows us to investigate how the image familiarization (repetition of novel sample images) change the relationship between recognition errors and response time.

Results

Experiment 1: Human behavioural study

Performance data from all 27 participants were included in the analysis; each participant completed 180 trials (12 test trials in each of 15 blocks). For analysis of recognition errors, for each participant, we first grouped their 180 trials into 10 response time (RT) bins (therefore each bin contained 10% of each participant's trials), and then calculated false

alarm error rate, miss error rate, and d prime (an index of discriminability/accuracy) independently for each RT bin.

D prime (d') was calculated according to the output of an equal-variance signal-detection (EVSD) model wherein new-items and old-items are represented by two Gaussian distributions along the dimension of memory strength with equal variance. The d' measure depends both on the separation (difference in standardized means of new-item and old-item distributions) and the spread (standard deviation) of new-item and old-item distributions. As the EVSD model assumes the variance of new-item and old-item distributions are equal, d' is effectively the distance between new-item and old-item distributions (expressed as a z score with respect to its magnitude relative to the standard deviations of the distributions), reflecting sensitivity or discriminative ability to judging old-items from new-items. In our recognition error analysis, d′ was calculated in each RT bin, as an indication of discriminability/accuracy (see Table 1 EVSD model for mean RTs represented in each bin).

Similar to plots of recognition errors and d' found in Basile and Hampton's macaque study (Basile and Hampton 2013), we found that our human participants (Fig. 2) exhibited a slight U-shaped function: their false alarm error rate was significantly higher in our shortest latency RT bin than in the next two RT bins in which RT was lower (first vs. second bin: paired t-test, $t_{(26)} = 2.431$, $p = 0.022$; first vs. third bin: paired t-test, $t_{(26)} = 3.338$, $p = 0.003$), after the third RT bin it rose again (third vs. forth bin: paired t-test, $t_{(26)} = -2.656$, $p = 0.013$; third vs. tenth bin: paired t-test, $t_{(26)} = -5.896$, $p < 0.001$). On the other hand their miss error rate increased (left to right on Fig. 2) from the fastest RT bins to the slowest RT bines (first vs. tenth bin: paired t-test, $t_{(26)} = -6.214$, $p < 0.001$). Discriminability/accuracy, measured as d′, demonstrated an increasing then decreasing trend across the 10 latency bins, whose peak-to-valley value was significantly larger than zero (second vs. tenth bin: paired t-test, $t_{(26)} = 6.958$, $p < 0.001$). It should be noted that the peak value of d' (d' = 2.57) appeared in the second RT bin (average time: 1225 ms). The peak time of false alarm error occurrence has

been considered to correspond to the onset of familiarity (Basile and Hampton 2013), and the peak time of discriminability/accuracy (in parallel with a suppression of false alarm rate due to recollection/recollective-like memory processes) was considered to evidence the onset of recollection (Basile and Hampton 2013); accordingly, the patterns and time profiles of recognition errors against response time in humans were similar to the ones found in the previous macaque study of Basile and Hampton (2013) which also showed evidence for fast-familiarity and slow-recollection (FF/SR) in a similar behavioural task.

To further investigate the latency of recollection and familiarity in human participants, we looked for correspondence between the aforementioned analyses and the ROC-derived approach for deriving familiarity and recollection indices. So we next applied the DPSD model to ROC data derived from each of the ten RT bins separately. The DPSD model is more complex form of model containing a single threshold process of recollection and a pure signal-detection process of familiarity. For all trails with confidence levels equal to or larger than the ith confidence rating bin (i.e. $CL \geq CL_i$), the DPSD model predicts the cumulative false alarm rate in lure-item trials and hit rate in target-item trials as follows:

$$p(Lure|CL \geq CL_i) = R_n + (1 - R_n) * \Phi(-c_i)$$

$$\mathrm{p}(Target|CL \geq CL_i) = R_0 + (1 - R_0) * \Phi(\frac{d'_F - \mathrm{c_i}}{\sigma_F})$$

Briefly, in the target and lure distributions (Φ is the cumulative normal distribution), the parameters for the response criterion are designated as c_i. In the target distribution, R_0 is a target threshold parameter being labeled recollection of old stimuli, which is that the target items that have a strength above the R_0 are classified as old. If the target item strength is below the R_0, its classification is governed by the familiarity component of the model, which is a Gaussian distribution with the mean of d'_F and standard deviation of σ_F.

In the lure distribution, R_n is a lure threshold parameter being labeled falsely recollection of old stimuli, which is that the lure items that have a strength above the R_n are classified as old (i.e. false alarm response), while the classification for those with strength below the R_n threshold would be governed by a standard Gaussian distribution, with a mean of 0 and a unit standard deviation. It should be noted that the meaning of R_n is different from the one in the paper of Koen et al. (2017), in which they assume R_n is a lure threshold that lure items above this threshold will be classified as new.

In our DPSD model, we further make the R_n parameter is constrained to equal 0 (i.e. assuming that participants would never recollect something they never saw), and σ_F parameter is constrained to equal 1. Based on the above assumptions, the algorithm of DPSD model becomes:

$$p(Lure|CL \geq CL_i) = \Phi(-c_i)$$

$$p(Target|CL \geq CL_i) = R_0 + (1 - R_0) * \Phi(d'_F - c_i)$$

When fitting ROC data to the DPSD model, sufficient trials are required to make ROC curve fitting sufficiently reliable (Yonelinas 2002; Yonelinas and Parks 2007). Therefore, for each human participant, we took the 180 trials divided into 10 RT bins from fastest to slowest and to ensure sufficient trials in each RT bin for curve fitting, trials in the corresponding RT bins of different participants were all combined. So, for example, the 10% fastest trials from each participant came to bin 1, and 10% slowest trials from each participant came to bin 10. Therefore, for analysis, there were 486 trials (i.e. 10% of total number of trials from all 27 participants) in each RT bin. Then for each RT bin independently, a ROC was plotted cumulatively for each confidence level according to the proportion of correct 'old' judgements against proportion of incorrect 'old' judgements. The recollection index (R_0) and familiarity index (d'_F) were extracted by fitting the model to data minimizing the squared difference between the observed and predicted data in each cumulative confidence rating bin. Yonelinas' research group provides an Excel worksheet which facilitates ROC curve fitting

and index extraction (website link: https://yonelinas.faculty.ucdavis.edu/roc-analysis/). In this way, we calculated recollection and familiarity index across 10 RT bins and plotted the values on the same figure as the error-rates (and EVSD derived d′) given both analysis approaches considered 10 RT bins (Fig. 2, see Table 1 DPSD model for average latencies represented by each RT bin).

The recollection index demonstrated an inverted U-shape across the 10 latency bins, whose peak value (recollection index = 0.70) was in the second RT bin (average time: 1209 ms), whilst the familiarity index showed a decreasing trend from a peak value (familiarity index = 2.13) in the first RT bin (average time: 1049 ms). The mean RTs for recollection/familiarity indices in each bin is shown in Table 1. It should be noted that the time-course of a significant switch from clearly high familiarity and clearly low recollection to somewhat lower familiarity values accompanied by somewhat higher recollection values appeared from the first to the second RT bin, thereafter both indices decreased as RT prolonged consistent with the longest latency RT bins being associated with increased rates of 'guessing', and also consistent with our observed steady decline in discriminability/accuracy (see plot of d′ on Fig. 2) as RT increases. This is also consistent with the aforementioned evidenced that miss rate steadily increases to 50% across higher RT bins. Notably, the average time of peak value of accuracy or d' in EVSD model was in the second RT bin (average time: 1225 ms) and this corresponded to the RT bin (average time: 1209 ms) in which the peak recollection index occurred. Taken together our observations provide strong evidence that FF/SR processes exist in humans just as observed by Basile and Hampton in macaques, using broadly similar paradigms. Moreover, the interpretation/conclusions from the FF/SR approach appear consisted with the time profile of indices of recollection and familiarity derived from the ROC approach, further validating the approach.

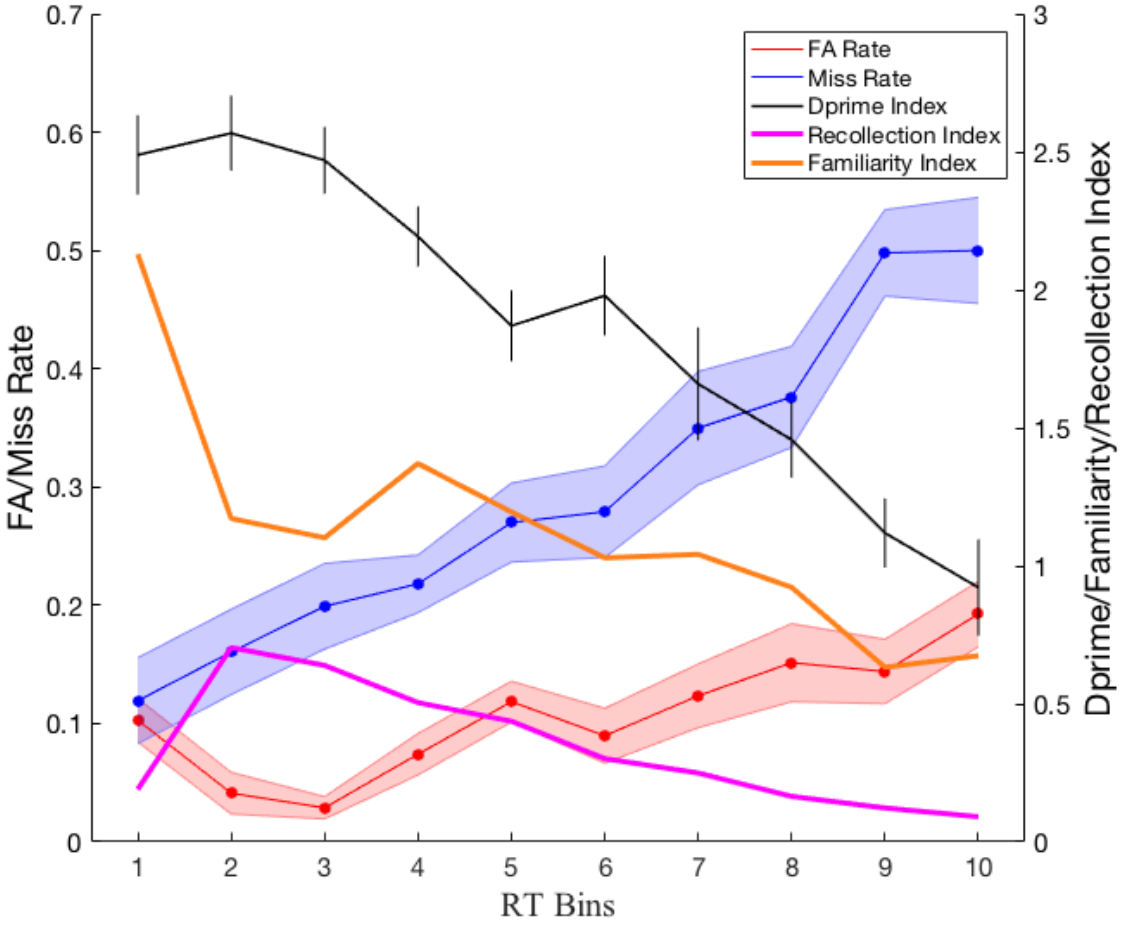


Figure 2. *Recognition errors, discriminability/accuracy d prime, and familiarity/recollection indices as a function of response time in humans. Each bin contains 10% of each participant's trials (ranging from bin 1 which contains the fastest 10% of trials to bin 10 which contains the slowest 10% of trials). Error bars are ± 1 SEM. False alarm errors (red solid line) and miss errors (blue solid line) were almost the same in the first RT bin; then miss errors increased, while false alarm errors initially decreased and then later increased across RT bins. Based on EVSD model, accuracy (d prime, black solid line) demonstrated an increasing then decreasing trend across RT bins and reached the summit in the second RT bin. Based on DPSD model, recollection index (magenta solid line) demonstrated an inverted U-shape against the 10 latency bins; while familiarity index (orange solid line) showed a decreasing trend, whose peak value appeared in the first RT bin.*

Table 1. Mean response latencies for binned human data in Fig.2.

Bin Number	1	2	3	4	5	6	7	8	9	10
EVSD model	1075 ± 24	1225 ± 31	1337 ± 36	1443 ± 42	1559 ± 48	1685 ± 54	1835 ± 62	2051 ± 72	2358 ± 87	3089 ± 119
DPSD model	1049 ± 29	1210 ± 38	1327 ± 46	1443 ± 57	1555 ± 65	1677 ± 73	1840 ± 84	2067 ± 100	2358 ± 119	3059 ± 170

Legends. Each bin contained 10% of the responses of each participant. For each response bin, we calculated the mean response latency in milliseconds for each human participant, and then averaged those mean latencies to produce a group mean latency for each bin.

Experiment 2: NHP behavioural study

In this experiment, the animal had completed 5 sessions with more than 300 trials per session, and all of the data from these 5 sessions were put into the analyses. Similar to our above analyses on recognition errors in humans, we next analyzed macaque behavioural data across 5 sessions in a similar task; we likewise grouped trials into 10 RT bins, with each bin containing 10% of macaque's trials. In each RT bin, we calculated false alarm rate, miss rate and d' (discriminability/accuracy index based on EVSD model). This analysis was done separately for sample images that were novel (Fig. 3B) and those that were familiar (Fig. 3C) to the macaque (also see Table 2 for mean RTs represented in each bin for images as being novel and familiar to the monkey separately).

Consistent with previous results from Basile and Hampton (2013)'s macaque study which considered only highly familiar stimuli consisting of a repeating small set of just two stimuli (Fig. 3A), our plots of recognition errors for viewing larger numbers of familiar images (Fig. 3B) and also novel images (Fig. 3C) both demonstrated a U-shape function in the false alarm error rate profile across the 10 RT bins whereas the miss error rate profile increased. Discriminability/accuracy, measured as d′ in the EVSD model, produced an inverted U-shape from the fastest RT bin to slowest RT bin, whose peak-to-valley value was larger than zero. Consistent with the main conclusion in Basile and Hampton's study and with the pattern of recognition errors in our human study (Experiment 1), we found a similar pattern of recognition errors and d′ (discriminability/accuracy) in the macaque: at the short response latencies, errors were mostly false alarms consistent with performance being driven primarily by familiarity; at moderate response latencies, the false alarm rate dropped and accuracy was higher consistent with longer-latency recollective-like processes reducing the false alarm rate; and at the longest response latencies, both false alarm rate and miss rate increased and accuracy reached its lowest point consistent with monkeys guessing.

Although the familiarity level of sample pictures didn't affect the U-shape function of false alarm errors and the inverted U-shape function of d' as a function of RT, the RT bins in which the minimal values of false alarm errors and the RT bins in which the maximum accuracy (d') were different for the different familiarity levels. To be specific, the first valley value of false alarm errors (FA rate = 0.1) and the peak value of d'(d' = 2.66) were in the second RT bin (average time 901 ms) for familiar pictures (Fig. 3B); while the first valley value of false alarm errors (FA rate = 0.1) and the peak value of d'(d' = 2.56) were in the fourth RT bin (average time 1071 ms) for novel pictures (Fig. 3C). The mean RTs for novel and familiar stimuli in each RT bin is shown in Table 2. As the peak value of d' (also corresponding to the first decrease in false alarm error rate) may indicate the start of recollection, it appears that novel images induce a switch from familiarity driven to

recollection/recollective-like driven contributions to recognition memory later with respect to time-course, compared with familiar pictures.

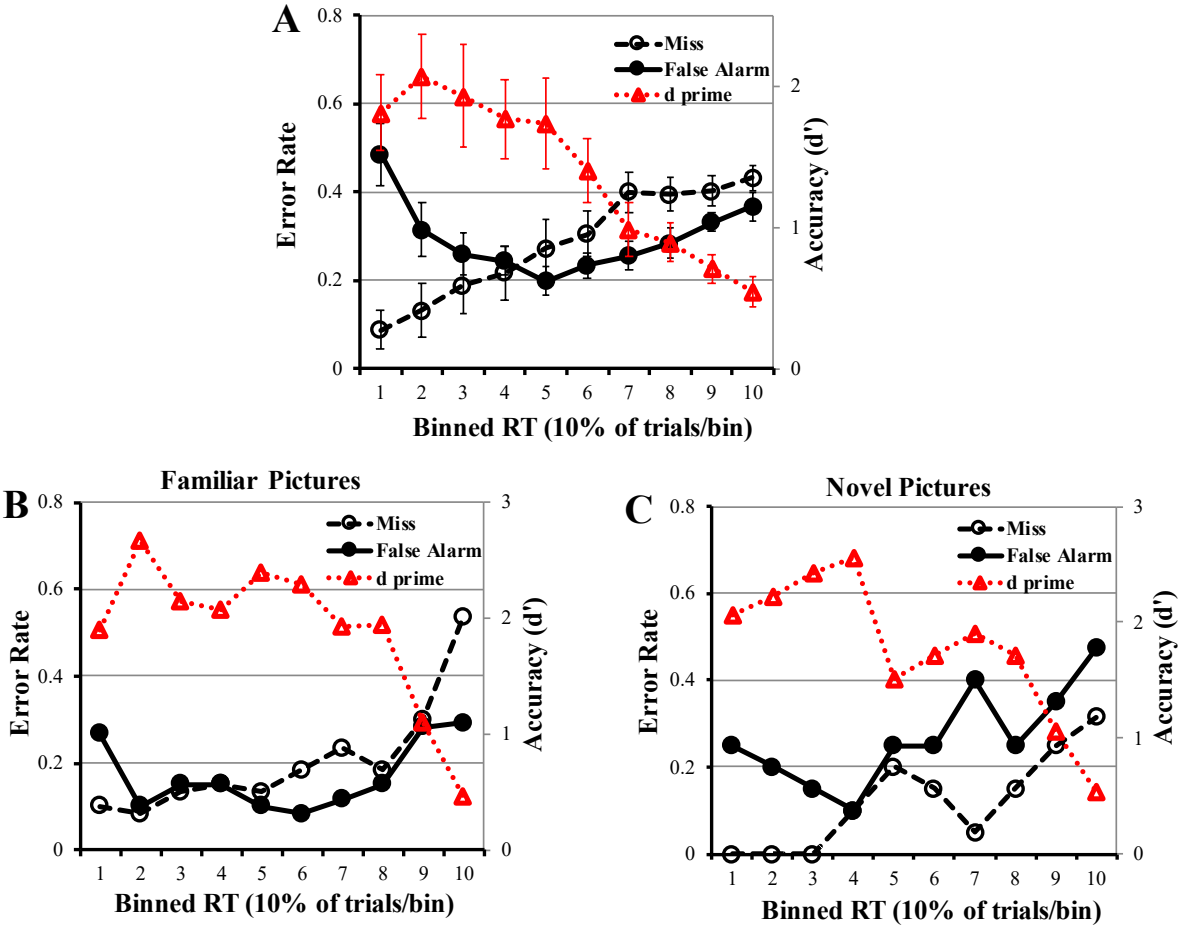


Figure 3. *False alarm error rate (solid line with filled circles), miss error rate (dashed line with hollow circles) and discriminability/accuracy d prime (dashed line with hollow triangles) as a function of response time bin in the macaque. Each bin contains 10% of each macaque's trials (ranging from bin 1 which contains the fastest 10% of trials to bin 10 which contains the slowest 10% of trials). Panels A-C depict recognition errors and discriminability/accuracy from: (A) data re-plotted from Basile and Hampton, 2013; (B) from our macaque when viewing familiar pictures; and (C) from our macaque when viewing novel pictures. All the panels show that false alarm errors revealed a U-shape function, miss errors increased, and d prime produced an inverted U-shape in relative incidence across the 10 RT latency bins in the NHP.*

Table 2. Mean response latencies for binned macaque data in Fig. 3.

Bin Number	1	2	3	4	5	6	7	8	9	10
Novel Image	782 ± 174	936 ± 84	1002 ± 103	1071 ± 111	1180 ± 129	1306 ± 163	1464 ± 173	1657 ± 211	1928 ± 256	3215 ±1889
Familiar Image	715 ± 208	901 ± 51	973 ± 55	1048 ± 60	1133 ± 70	1246 ± 67	1384 ± 58	1564 ± 93	1941 ± 286	3690 ±1688

Legends. Each bin contained 10% of the responses of the monkey. For each response bin, we calculated the mean response latency in milliseconds for images as being novel and familiar to the monkey.

Discussion

This study investigated the time course of familiarity and recollection/recollection-like processes contributing to recognition memory in both humans and NHP. A first key aim was to examine relationships between ROC derived indices of recollection and familiarity with recognition errors derived measures of 'fast-familiarity' and 'slow-recollection' (FF/SR) in humans. A second key aim was to compare FF/SR analyses in humans and NHP. A major motivation for these aims was to strengthen interpretations that may be made from FF/SR studies pertaining to recollective-like behaviour in animals, in existing behavioural studies and future neuroscientific enquiries; this is important because FF/SR data is markedly easier to obtain in animals than ROC data (Fortin et al. 2004; Guderian et al. 2011; Sauvage et al. 2008). In the current study, using a similar task structure across species, human participants and a macaque performed an object recognition memory task (with distinct match and non-match trials, see methods, to distinguish two types of errors, false alarms and misses). Our expectations were that: at the shortest response latencies, false alarm errors would be high, attributed to familiarity; intermediate-latency responses would be more accurate and

associated with fewer false alarm errors, which is attributed to an onset of recollection or recollection-like processes reducing the false alarm errors; at the longest response latencies, both false alarm errors and miss errors would increase in frequency and accuracy would reach its lowest point suggestive of guessing to a greater degree. Prior evidence from human studies suggest that familiarity arises earlier than recollection, for example in studies in which participants used slow recollection to countermand false alarm errors induced by familiarity (Rotello and Heit 2000; Rotello et al. 2000). In our macaque study, most of the short-latency errors were false alarm errors; and at the intermediate response latencies, false alarm rate decreased along with an increase of d', consistent with a slow recollective-like process to suppress false alarm errors and increase accuracy. In humans, the short-latency errors were occupied by miss and false alarm errors equally; at intermediate response latencies, false alarm errors showed a decreasing trend along with an increasing of d', which indicates a similar start point of recollection-driven memory. Thus, it is concluded that both humans and macaque can use "recollect to reject" to override false alarm errors driven by familiarity and their response profiles are broadly similar on the FF/SR paradigm.

Robust evidence in support of "fast familiarity and slow recollection" has been provided by many human recognition memory studies (Brainerd and Reyna 2005; Dosher 1984; Dosher and Rosedale 1991; Gronlund and Ratcliff 1989; Hintzman and Curran 1994; Matzen et al. 2011; Rotello and Heit 2000; Rotello et al. 2000). For example, Gronlund and Ratcliff (1989) found little or no evidence for familiarity-based retrieval of studied items at extremely brief retrieval time (i.e. less than 200 ms), but as retrieval time lengthened (i.e. 300-500 ms), familiarity-based evidence accumulated accompanied by increasing false alarm rates, and.as retrieval time became longer (i.e. more than 500 ms), recollection-based evidence was taken into account and accumulated to suppress false alarm rates (Gronlund and Ratcliff 1989; Brainerd and Reyna 2005). Consistent with these studies, our human and macaque results showed a U-shaped curve of false alarm errors against response time as detailed earlier (and

see Figs. 2 and 3); however we did not find the corresponding very low false alarm probability at extremely low response times as Gronlund and Ratcliff (1989) and other showed. One possible reason for this might be that our studies didn't include such extreme short response time periods. Indeed, in the study of Gronlund and Ratcliff (1989) their very short (< 600 ms) latencies included both sample-to-test item delay plus response time (also see the review by Brainerd and Reyna, 2005) but in our macaque study, the delay between sample and test image was already 3000 ms and in our human study was 1000 ms. Instead, the U-shaped functions in our study, seen also in the macaque study of Basile and Hampton (2013), are consistent with the higher response times (wherein an inverted U-curve in seen) in the study of Gronlund and Ratcliff, in which false alarm errors reached highest point at short response latency and then decreased.

In this study we compared the response time profiles for fast-familiarity (FF) and slow-recollection (SR) in macaque and humans; for each species we plotted recognition errors and discriminability/accuracy (indicated by d' in EVSD model) against response time (see Figs. 2 and 3). The summit of accuracy for humans appeared in the second RT bin, which indicates that a switch from relying primarily upon familiarity to relying upon recollection has already occurred by around 1225 ms (see Table 1 EVSD model for mean RTs represented in the second bin). In Figure 2, to compare ROC-derived indices of recollection and familiarity to the FF/SR interpretations we also plotted curves through the values obtained from deriving familiarity and recollection indices on the data in each bin from fitting ROC data to the DPSD model. The peak values of the ROC-derived familiarity index occurred much earlier in RT Bin 1 (corresponding to average peak time of familiarity index of 1049 ms) than the peak values of the ROC-derived recollection index in RT Bin 2 (corresponding to average peak time of recollection index of 1209 ms). The timing profiles of the ROC-derived indices of recollection and familiarity correspond with and corroborate the timing profiles of the FF/SR based interpretations further supporting and validating the FF/SR approach in humans.

Moreover, the peak ROC-derived recollection index based on DPSD model fell in the second RT bin in which the discriminability/accuracy (d', calculated based on recognition errors in EVSD model) was also in peak, suggesting recognition error distributions can be used as a proxy for estimating the onsets of recollection processes in humans. In our macaque study, the trends of recognition errors and accuracy were similar to those in humans (compare Figs 3B, C with Fig 2). Accordingly, if the peak time of accuracy can be used as a proxy to estimate the onset of recollection processes within the response time profile, then we estimate that an analogous switch from relying primarily upon familiarity to relying upon recollection in the macaque was at an average time of around 901 ms for familiar sample images (Fig. 3B), and with average time of 1071 ms for novel sample images.

The extent to which image repetition affects familiarity or recollection is an issue of debate. In some studies with humans repetition of studied items improves both familiarity and recollection; image repetition was found to increase false alarm errors if participants were under pressure to respond quickly but had no effects on false alarm errors if participants had more time to respond (Jacoby et al. 1998; Jacoby 1999; Jones and Jacoby 2001). Other studies using the remember-know (R/K) procedure (Tulving 1985) found that repetition of items enhanced recollection/remembering rather than familiarity/knowing (Mántylá and Cornoldi 2002; Pitarque et al. 2015). In our macaque study, as mentioned above, the estimate switch time from familiarity to recollective-like processes occurred earlier for familiar than novel sample images. It appears that image repetition expedites the onset of recollection-like process so as to enhance the performance of recognition memory in the NHP. In a recent macaque electrophysiological and human ERP study, image familiarization sharpened the response dynamics of inferotemporal neurons of macaques and of human extrastriate visual cortex (Meyer et al. 2014). This finding illustrates that repeated viewing of an image modulated neural responses in both macaque and human visual areas, which may be conducive for efficient coding of stimuli. However, as only one animal was involved in this

current study, and as we didn't carry out a similar investigation of image repetition effects on familiarity/recollection effect in humans, our conclusions as regards the difference between familiar and novel images should be appreciated as being limited and so we encourage future studies to follow up on investigations on whether this intriguing behavioural pattern can be replicated in both species.

A small number of influential animal models (with rodents and more recently macaques) used the ROC approach to assess contributions of familiarity and recollection-like processes to recognition memory. These studies manipulated animals' biases to respond "old" or "new" to stimuli by varying the relative amount of reward corresponding to correct old and correct new responses across various levels (Fortin et al. 2004; Guderian et al. 2011; Sauvage et al. 2008). As stated earlier, these types of manipulation are complex and time-consuming to train but most importantly the bias levels cannot be treated equivalently to humans' confidence judgments, with the result that interpretation of ROC curves in animals has been questioned and hotly debated (Eichenbaum et al. 2008; Wixted and Squire 2008). We consider those animal models important and influential but at the same time we recognize both the practical and theoretical limitations. Indeed, this has been a major motivation for the current study which we consider successful in strengthening the interpretation of a proxy for differentiating between familiarity and recollection-like processes in animals, namely by investigating the time-course patterns of recognition errors. Our data further validates this FF/SR approach as providing valuable insight into these processes and hence future investigations of familiarity and recollection-like processes in animals, which are in need of advancing given the scarcity of animal models of recollection/recollective-like memory processes (see also (Basile et al. 2009; Basile and Hampton 2011; Paxton and Hampton 2009; Hampton 2001; Hampton et al. 2004; Hampton and Hampstead 2006) for some other approaches to look at other elements of episodic memory in animals).

In summary, the conclusions from this study are that i) "fast familiarity" and "slow

recollection" provide comparable measures in both humans and macaque performing similar tasks; ii) both species applied a similar strategy of "recollect to recall" to countermand false alarm errors based on recollection/recollective-like memory processes; and iii) image familiarization expedites switches from familiarity to recollection-like processes in the macaque; and iv) the time course of familiarity and recollection can be estimated relative to the time-to-peak value of discriminability/accuracy based on recognition errors, and this estimation method is validated by DPSD models used in humans.

Chapter 3. Dissociation of dorso-lateral and dorso-medial prefrontal cortex contributions to familiarity and recollective processes in primates

Abstract

According to dual-process theories, recognition memory draws upon both familiarity and recollection. It remains unclear how primate prefrontal cortex (PFC) contributes to familiarity and recollection processes but frequency-specific neuronal activities are considered to play a key role. Here, non-human primate (NHP) electrophysiological local field potential (LFP) recordings first showed that a specific subregion of macaque PFC (i.e., dorsolateral PFC, dlPFC) was implicated in task performance at a specific frequency (i.e., increased alpha/beta power in the 10-15 Hz range observed in correct versus error trials) in a specific phase of a recognition memory task (i.e., during sample presentation). Then, to assess generalization to humans and causality we targeted left human dlPFC (BA 9/46) as well as left dorsomedial prefrontal cortex (BA 8/9) for comparison, and also vertex as a control, with transcranial magnetic stimulation at a frequency in the middle of the low-beta range observed in NHP (i.e. 12.5 Hz) and compared that to non-frequency-specific stimulation, and also to a no-stimulation control, during occasional sample presentations within a similar task. Hence we investigated hypotheses about the causal importance for human memory of a location-specific, frequency-specific, and task-epoch-specific intervention derived directly from the NHP electrophysiological observations. Using a dual-process signal detection (DPSD) model based on analysing receiver operating characteristics (ROC) curves, we showed beta-frequency TMS caused decreased recollection when targeted to human dlPFC, but enhanced familiarity when targeted to dorsomedial prefrontal cortex. Non-frequency-specific patterns

of stimulation to all sites, and beta-frequency stimulation to vertex, were all without behavioural effect. We also found a beta-frequency specificity of rTMS effect on recollection upon targeted and non-targeted samples, although no behavioral difference in match trials containing targeted and non-targeted samples suggests a spread of rTMS effect. This study provides causal evidence that PFC-mediated contributions to object recognition memory are modulated by beta-frequency activity; more broadly it provides translational evidence bridging NHPs and humans by emphasizing functional roles of beta-frequency activity in homologous brain regions in recognition memory.

Introduction

There is also a long-standing literature on the necessity of PFC for supporting object recognition memory based on lesion studies in macaques (Bachevalier and Mishkin 1986; Kowalska et al. 1991; Levy and Goldman-Rakic 1999; Mishkin and Manning 1978; Meunier et al. 1997; Parker 1998; Petrides 1995, 2000). Early neuronal recording studies in macaque prefrontal cortex (PFC) suggested sustained neuronal spiking might encode stimuli across delays in object recognition memory tasks (Fuster and Alexander 1971; Rao et al. 1997; Wilson et al. 1993). More recently other mnemonic mechanisms for this kind of working memory task in PFC have since been proposed (Stokes 2015; Lundqvist et al. 2016). Consideration as to the role of neuronal synchrony (e.g. within and between-area oscillatory coherence), including at different frequencies, and their importance in helping mediate cognition including learning and memory has also become a key area of systems neuroscience research (Benn et al. 2016; Buzsáki and Schomburg 2015; Fries 2015; Fell and Axmacher 2011; Gregoriou et al. 2009; Herweg et al. 2016; Köster et al. 2014; Pipa 2009; Womelsdorf et al. 2007).

In this context the local field potential (LFP) electrophysiological signal is thought to reflect a summation of local transmembrane currents (Buzsáki et al. 2012) such that LFP amplitude may reflect local synchrony within an area. One influential theory is that neuronal synchrony also facilitates inter-area neuronal communication; for instance, given rhythmic inhibition within local networks, two neuronal ensembles may have a greater influence on each other when their temporal interaction windows open at the same times (i.e. rhythmic synchronization *within* areas also synchronized *between* areas) (Womelsdorf et al. 2007). Relatively few studies to-date have analysed LFP activity in non-human primate (NHP) PFC during working memory tasks. One recent electrophysiological LFP recording study in NHPs indicated discrete and dynamic modulation of beta (20-35 Hz) and gamma oscillations (45-100 Hz) in lateral PFC during encoding period of working memory, which suggests beta

oscillations in PFC reflect a default network state while are interrupted by gamma oscillations when encoding or decoding the stimuli (Lundqvist et al. 2016). Kornblith et al. (2016) have found that beta synchrony (16-30 Hz) in lateral PFC increases (although beta power decreases) during multiple stimulus presentation while decreases (although beta power increases) during memory delay; moreover, both gamma synchrony and power (50-100 Hz) in lateral PFC increase during multiple stimulus presentation. The results of this study indicate that roles of low-frequency oscillations in top-down processing and higher-frequency oscillations in bottom-up processing (Kornblith et al. 2016). Another electrophysiological study shows that small groups of neurons in macaques probably comprising a cortical column participate in high-gamma oscillations around 80 Hz and their activity carries partial information about the memorized stimulus, while larger networks in and most likely beyond PFC appear to be coordinated by coherent low-gamma- and beta-oscillations (14-45 Hz) which are correlated with performance but not stimulus content (Pipa 2009). Although studies have analysed LFP activity in macaque PFC during recognition memory they facilitate comparison between PFC regions and even cortical layers (Bastos et al. 2018). Moreover, in humans, a significant body of research maintains that human recognition memory draws upon two processes: familiarity and recollection (Wixted 2007; Yonelinas 1994; Yonelinas et al. 1998; Yonelinas 2001; Yonelinas et al. 2002; Yonelinas 2002; Yonelinas and Parks 2007). One influential neuropsychology review concluded that PFC patients were numerically worse than controls at recognition but deficits in recall were more profound (Tulving et al. 1995). However, there is no consensus as to whether different sub-areas of PFC contribute differently to familiarity and recollection. Using paradigms that aim to dissociate recollection from familiarity (e.g. receiving operating characteristic (ROC) curve plotting across confidence levels, or dissociations of subjective reports of ‘remembering’ versus ‘knowing’), human neuropsychological investigations present conflicting results. In some, lateral PFC lesions cause deficits in familiarity rather than

recollection (Aly et al. 2011; Duarte et al. 2005; MacPherson et al. 2008), whereas others (Wheeler and Stuss 2003) report that dorsolateral PFC (dlPFC) lesions don't impair either, in contrast to frontopolar lesions which only impaired recollection. Evidence from human neuroimaging studies also provides mixed evidence as to the relative contributions of PFC sub-regions to familiarity/recollection (Henson et al. 1999b, 1999a; Horner et al. 2015; Johnson et al. 2013; Kafkas and Montaldi 2012; Solstad et al. 2006; Skinner and Fernandes 2007). A recent review of previous neuroimaging studies involving human PFC similarly reports a mixture of involvement in recollection/familiarity in different parts of PFC (Scalici et al., 2017), which suggests a complicated characterization of PFC in association with these component memory processes supporting recognition memory. In a combined fMRI-EEG study in humans, an alpha-theta synchronization (4-13 Hz) during recollection is associated with increased functional connectivity between the PFC and hippocampus, indicating low-frequency oscillations support the PFC-hippocampal network dynamics during recollection process (Herweg et al. 2016). Another human electroencephalography study shows that a coupling between prefrontal theta and parietal gamma oscillations occur during successful memory retrieval, which suggests an essential role of an interaction between low- and high-frequency oscillations in memory retrieval (Köster et al. 2014).

The homologies between NHP PFC and human PFC, as evidenced by long-standing comparative cytoarchitectural analyses (e.g. Petrides and Pandya, 2007) and from more recent comparative functional connectivity profiles (Neubert et al. 2015), help confirm NHPs as a good animal model to investigate the neural activities and synchronies underlying recognition memory although the debate over whether animals can 'recollect' per se is still ongoing. Nonetheless, the neural signals (e.g. finer grained information on LFPs) available in NHPs that are recorded direct from electrodes within specific brain regions may provide important information about the neural mechanisms that may give rise to recollection and familiarity in humans.

In this study we aimed to investigate the causal role of subregions of human PFC in recollection and familiarity using non-invasive transcranial magnetic stimulation (TMS). TMS can be used to intervene in on-going neural processing by administering either single pulse or several repetitive pulses (rTMS) either before or during task performance to modulate ongoing neural oscillations (Huang et al. 2005; Rossi and Rossini 2004). It has previously been observed that behavioural performance in humans can be either disrupted or enhanced by adopting TMS in a frequency-specific manner (Albouy et al. 2017; Chanes et al. 2013; Elkin-Frankston et al. 2011; Thut et al. 2011). For example, perceptual discrimination has been enhanced by applying TMS over a frontal eye field (an area of human PFC) at high-beta frequency, while response criterion has been lowered by delivery of TMS over the same region at gamma frequency (Chanes et al. 2013). In order to generate narrower hypotheses about causality as to which specific PFC area might be targeted and at what point in the working memory task and at what frequency we sought insight from a simple preliminary investigation in a single NHP that we previously trained to perform a similar task and from which we recorded LFP activity from a multi-electrode array implanted in dlPFC (additional animals were not available as the NHP data was a pilot/parameter defining stage for a subsequent larger-scale longer-term NHP project still in progress).

In the present NHP observations, we found a strong correspondence between increased beta LFP power from electrodes in dlPFC around the time of sample presentation onset in our object recognition memory paradigm and memory performance; the significant sample phase activity was transient, lasting no more than 200 ms and with a frequency range of 10-15 Hz. It's relation to performance was determined by confirming that the power was significantly higher in trials than proceeded to be correct trials (in the subsequent choice phase) than in trials that proceeded to be error trials. The desynchronization hypothesis (Hanslmayr et al. 2012a; Holmes et al. 2018) suggests that PFC neurons desynchronize to retain stable memories. We observed robust beta power that was greater in correct trials but

which didn't persist throughout the entire sample presentation; therefore it may be hypothesized accordingly that transient robust beta power coupled with subsequent efficient beta power desynchronization supports effective memory encoding. To assess both causality and generalizability across primate species we hypothesized that targeting the homologous human region with beta TMS in the same low beta frequency range observed (i.e. our TMS stimulation frequency was chosen as 12.5 Hz being right in the middle of beta range observed in NHP dlPFC) throughout the entire sample presentation in a similar task may lessen desynchronization and disrupt effective memory encoding for those samples. As a control for this hypothesis we included a randomly timed stimulation condition in other blocks (same number of pulses, same duration, but with no inherent frequency) as this non-beta (random) frequency stimulation was presumed to be less likely to prevent beta desynchronization. As human activation peaks related to familiarity were previously generally found to be located more caudally, corresponding to dorsomedial PFC (dmPFC), in meta-analyses (Scalici et al. 2017), we further hypothesized that targeting dlPFC would primarily affect recollection indices, while targeting dmPFC (our chosen comparison target for this reason) would primarily affect familiarity indices. We included vertex as a control region wherein we hypothesized no effect of TMS by either of the two stimulation protocols.

Materials and Methods

Experiment 1: NHP electrophysiological study.

Subject

Neural data was recorded in one young adult female macaque monkey (*Macaca mulatta, age 8 years, weight 10-13 kg*). All animals in our lab are socially housed (or socially housed for as long as possible if later precluded, for example, by repeated fighting with cage-mates despite multiple regrouping attempts) and all are housed in enriched environments (e.g. swings and ropes and objects, all within large pens with multiple wooden ledges at many levels) with a 12hr light/dark cycle. The NHP always had *ad libitum* water access 7 days/week. Most of its daily food ration of wet mash and fruit and nuts and other treats was delivered in the automated testing/lunch-box at the end of each behavioral session (this provided 'jack-pot' motivation for quickly completing successful session performance; supplemented by trial-by-trial rewards for correct choices in the form of drops of smoothie delivered via a sipping tube) and this was supplemented with fruit and foraging mix in the home enclosure. All animal training, array implantation surgery, and experimental procedures were performed in accordance with the guidelines of the UK Animals (Scientific Procedures) Act of 1986, licensed by the UK Home Office, and approved by Oxford's Committee on Animal Care and Ethical Review.

Surgical procedures

After the basic behavioural and initial task training phase was complete the animal first received a titanium head-post, implanted posteriorly and secured to the cranium with titanium cranial screws through the legs of the post (the legs of the head-post were pre-shaped to fit the precise morphology of the skull in the region according to a 3D printed skull model based

on pre-operative structural MRI scans); the reflected skin and galea was sutured and the wound closed around the base of the head-post.

Later, after more behavioural training with head-fixation was complete and task-performance satisfactory, the NHP received surgical implantation of microelectrode arrays (Utah arrays, Blackrock Microsystems). A bone flap was raised over the left anterior prefrontal cortex, the dura mater was cut and reflected, and Utah arrays implanted directly into the cortex; the dura mater was sewn back over the arrays where possible and the bone flap was replaced. Two reference wires connecting to the pedestals were left under the dura away from the site of the array and these and the wire bundle connecting to each electrode in the Utah array exited the cranium through a gap at the edge of the craniotomy and ran from there to the pedestal which was secured to the cranium (located away from the edge of the craniotomy) with titanium cranial screws through its base; to complete the procedure the wound was then closed in layers. A pedestal cap was screwed on to the top of the pedestal to protect the gold contacts (the cap was subsequently removed each day, while the NHP in the recording session, to connect the digital head-stage direct to the pedestal's connectors at which point recording commenced).

The operations to implant the head-post and later to implant the microelectrode arrays were performed in aseptic conditions with the aid of an operating microscope for intra-cranial surgeries. The monkeys were first sedated with ketamine (5 mg/kg), medetomidine (20mcg/kg) and midazolam (0.1 mg/kg) given i.m., intubated, and then artificially respirated using a mixture of carrier gases (oxygen/medical air) and volatile anaesthetic. Surgical depth of anaesthesia was maintained throughout the surgery with sevoflurane (1.0-2.0% to effect) and injectable adjuncts (fentanyl 5 mcg/kg/hr i.v., dexmedetomidine 0.5 mcg/kg/hr i.v.). On average three doses of steroids (methylprednisolone 20 mg/kg i.v. every 4-6 hrs) and in the case of intra-cranial surgery a bolus of mannitol (1000 mg/kg i.v.) were given on the day of

surgery to protect against intraoperative brain edema and postoperative inflammation. Steroids were continued in the postoperative phase (dexamethasone 0.2 mg/kg s.c., daily for 5 days). The animals were given an antibiotic (30 mg/kg of amoxicillin intraoperatively every 2 hours, and 17.5 mg/kg daily postoperatively) for prophylaxis of infection. Additional intraoperative medication included atropine (10 mcg/kg i.v. as required), an H2 receptor antagonist ranitidine (1 mg/kg i.v.), meloxicam (0.2 mg/kg i.v.) and crystalloid fluids (Hartmann's solution 3-5 ml/kg/hr). Heart rate, oxygen saturation of hemoglobin, mean arterial blood pressure, end- tidal CO2, body temperature, and respiration rate were monitored continuously throughout surgery. Postoperative analgesia was provided via opioids (methadone 0.3 mg/kg i.m. or buprenorphine 10 mcg/kg i.m.) and nonsteroidal anti-inflammatory agents (0.1 mg/kg of meloxicam, p.o./i.m., 10 mg/kg acetaminophen p.o.). A proton pump inhibitor (Omeprazole 0.5 mg/kg) was given daily to protect against gastric ulceration as a side effect of the combination of steroid and nonsteroidal anti-inflammatory treatment.

This study records data from one 32-electrode Utah array inserted into dlPFC (area 9/46, just dorsal to the principal sulcus, see Fig. 1B); the electrodes were arrange on a 6 × 6 grid embedded in silicone; the electrode length was 1.0 mm with interelectrode spacing of 0.4 mm. All the microelectrodes were made of platinum (Pt). This Utah array was connected to one pedestal (with 128 output channels) affixed externally to the cranium. The four corner electrodes of this pedestal were 2 reference electrodes and 2 ground electrodes.

Task stimuli and apparatus

The object recognition memory task was programmed using Turbo Pascal (Borland), run under DOS on a desktop PC. Visual stimuli used in the task were clip-art images in colour, which were presented on a 20.1" colour touch-sensitive screen (TFT LCD TS200H GNR). Those clip-art images used in the task were from a large pool of several thousand unique

images. Each image subtended 5° of visual angle in width and 5° in height to the subject when presented on the screen. The sample image was always presented on the right top of the screen, positioned +9 ° horizontal and -9 ° vertical from the center of the screen. The test images were presented on the right bottom of the screen: one was positioned 0 ° horizontal and +3 ° vertical from the center of the screen; and the other one was positioned +17 ° horizontal and +3 ° vertical from the center of the screen. The background colour to the screen was white. In each session of recordings, images were randomly chosen from the pool without replacement and were not re-used on the other recording days.

The animal was seated in a primate chair (Rogue Research Inc.) in front of the touch screen with its head-fixated and whilst it performed the recognition memory task in a magnetic-shielded, and partially sound-attended, testing-box. A window in the front of the chair provided its access, both to the touch-screen itself and also to a touch-sensitive knob which we refer to as a 'key-touch' which was positioned low down in front of the touch screen; the animal had to steadily hold the keytouch at various times in each trial (to control for arm movement/position whilst it waited for stimuli, looked at stimuli, and waiting for a visual cue to release keytouch and touch the screen to make a choice). The distance between the monkey and touch screen was fixed at 50 cm enabling the animal to touch the screen easily. An infrared camera was used to monitor the general status of the monkey in the box. A peristaltic pump device located on top of the box fed smoothie reward through a tube and to a spout positioned in the vicinity of the animal's mouth. Below the screen was also an automated lunch-box which contained the majority of the animal's daily meal (wet mash and fruits and nuts etc.) and which opened immediately at the end of the task.

Behavioural task

The task is a variant of the well-established delayed-matching-to-sample (i.e. recognition-memory) paradigm in which a stimulus in a sample phase has to be judged as familiar or not

in a subsequent choice phase after a short delay; the form of the task used is similar to that used by Basile and Hampton (2013) in that in the choice phase, to allow separation of hits, misses, false alarms, and correct rejections, one choice image is presented with one non-match button (black circle) such that the animal selects the choice image if it considers the choice image a match and selects black circle if it considers it is a non-match (see Fig.1A). In each trial, the animal initiated the task by holding the key-touch when cued to do so by a small red circular keytouch cue (located towards upper centre of screen; Fig. 1A) presented on the screen. The NHP was required to keep holding the keytouch device through a variable delay of 1000-1500 ms (if the keytouch hold was broken the trial aborted) after which a central sample (object image) appeared behind the red key-touch cue. The NHP was required to keep holding the keytouch device through another variable delay of 1000-1500 ms (again, if the keytouch hold was broken the trial aborted) after which the red keytouch cue disappeared which was the cue to the animal it could release its hand from the keytouch at which point the delay (1000ms) between sample and choice-phases began (the maximal time for releasing key-touch was 5000 ms else the trial aborted and the animal received a time-out for 10 s). Then after the 1000 ms delay period another red keytouch cue appeared, this time in the bottom of the screen (close to, and equidistant, from where the two choice items would appear) and animal was required to hold the key-touch again. The NHP was again required to keep holding the keytouch device through a variable delay of 1000-1500 ms (if the keytouch hold was broken the trial aborted) after which two choice stimuli appeared (one an object image and the other a black circle, left-right randomized between trials). The NHP was required to keep holding the keytouch device through another variable delay of 1000-1500 ms (again, if the keytouch hold was broken the trial aborted) after which the red keytouch cue disappeared which was the cue to the animal that it could release holding the keytouch and now make a choice to the touchscreen to either the object test-image stimulus or to the black circle stimulus. The object stimulus was either the identical stimulus to the sample seen

earlier in the trial or it was not identical to the sample. The animal was rewarded by delivery of 10 ml of smoothie for touching the test-item image if it matched the sample image (these we refer to as 'match trials'), or it was rewarded for selecting the standard 'non-match button' (i.e. the black circle) if the test-item was a non-match (these we refer to an 'non-match trials'). After a correct response, the intertrial interval was 3 s. However, following any error trial (including both incorrect response and aborted trials), the intertrial interval was 10 s Accordingly, on *match trials* the animal could either make a correct response ('hit') or an incorrect response ('miss') whereas on *non-match trials* the animal could either make a correct response ('correct rejection') or an incorrect response ('false alarm'); in this way the paradigm is similar to one previously used by Basile and Hampton (2013) but a key difference is that we did not restrict the stimulus set to just two stimuli as we used larger sets moreover we also varied the degree to which stimuli were either familiar or novel in the session. Specifically, in any given session 50% of the trials used trial-unique stimuli and 50% were 'repeat' stimuli used previously in the session (but not used in any previous session); in each session there were six repeat stimuli sorted into 3 pairs such that in each trial with repeat stimuli one pair was chosen at random and one member of the pair was randomly chosen to be the sample. Each session typically consisted of 150 trials so the six repeat stimuli got steadily more familiar across the session.

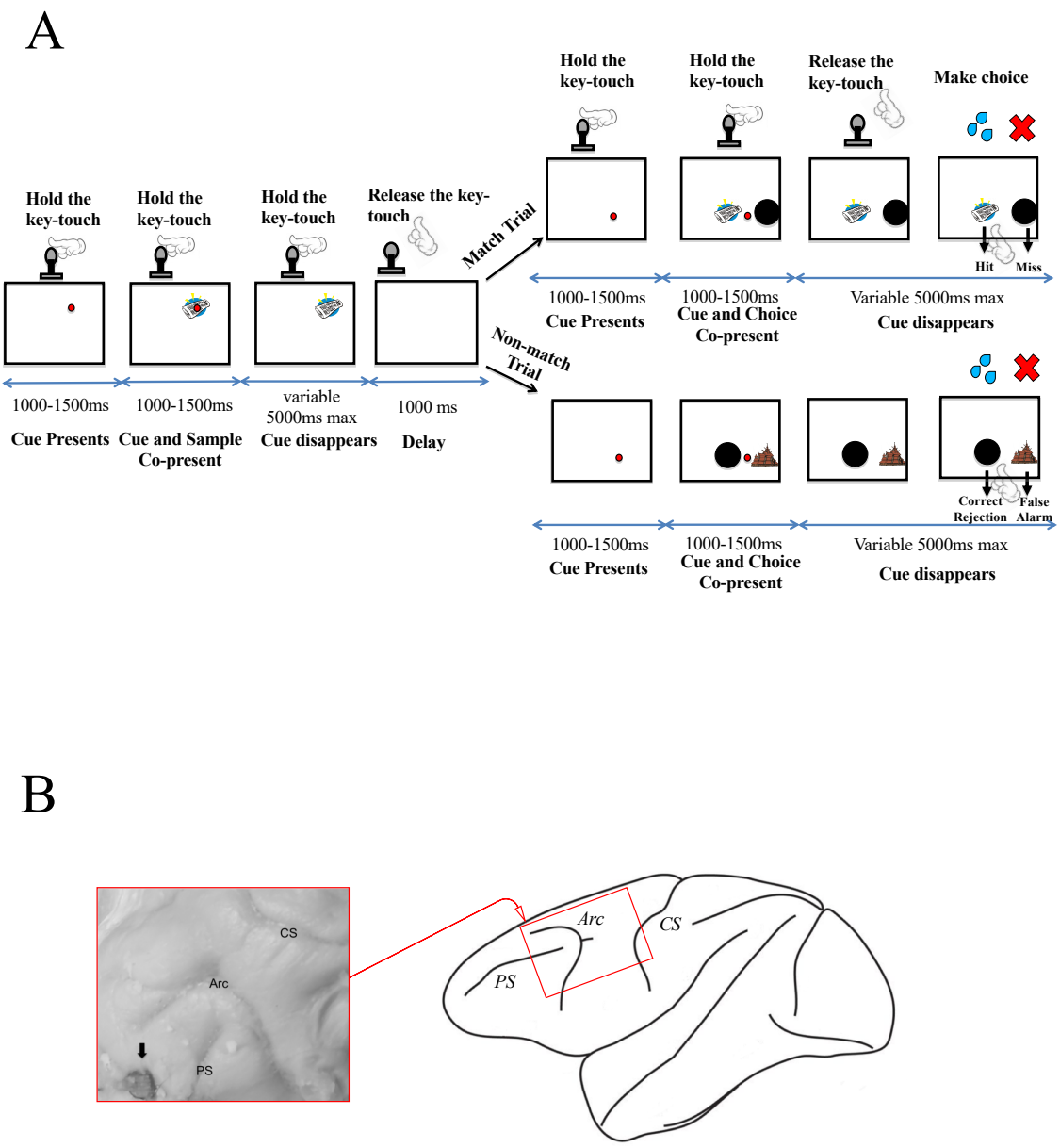


Figure 1. *NHP recognition memory task structure and recording sites from dlPFC array in in NHP. Panel A depicts one trial in the electrophysiological study. The NHP initiated the task by holding the key-touch device once the red dot cue appeared through a variable time of 1000-1500 ms, after which a sample object image was shown on the screen behind the red dot cue (encoding phase). The NHP was required to keep holding the keytouch device through another variable delay of 1000-1500 after which the red keytouch cue disappeared then the NHP was trained to release its hand from the keytouch prompting the commence of*

the delay (1000ms) between sample and choice-phases. Then after the 1000 ms delay period another key-touch red dot cue, this time in the bottom of the screen, and the animal was required to hold the key-touch again. The NHP was again required to keep holding the key-touch device through a variable delay of 1000-1500 ms after which two choice stimuli (one an object image and the other a black circle, left-right randomized between trials) appeared. The NHP was required to keep holding the keytouch device through another variable delay of 1000-1500 ms after which the key-touch red dot cue disappeared cueing the animal that it could release holding the key-touch and make a choice to the touchscreen to either the object test-image stimulus or to the black circle. Just as in the human task in Figure 2, in 'Match Trials' the black circle was presented with an identical image to one of the preceding sample; in 'Non-match Trials' the black circle was presented with a novel stimulus not seen before. Animals were trained to touch the test-item if they remembered the test-item was a match but to touch the black circle if they thought the test-item was a non-match; accordingly the responses could be separated into hits, misses, correct rejections, and false alarms as indicted. Panel B: drawing of a lateral view of the NHP brain; the Utah array was placed above the principle sulcus (PS) and anterior to the arcuate sulcus (Arc); the enlarged insert (red square) shows photographic verification of the array's position.

Electrophysiological Recordings

Data were recorded simultaneously from the 32-electrodes in the microelectrode array implanted in dlPFC throughout the recognition memory task. We only considered the trial-unique stimuli in these analyses as we used the trial-unique stimuli in human TMS study. The NHP performed, on average, 35 trials (with trial-unique stimuli) per day; the total average session duration was 45 minutes. In this study we analysed data recorded over 29 sessions approximately 8-12 weeks after the array implantation. The NHP had learnt the task in full

prior to array implantation. Neural signals from each microelectrode were amplified, digitized at 30 kHz using a 256-channel Cerebus™ Neural Signal Processor (Blackrock Microsystems). The local field potential (LFP) was analyzed off-line using the FieldTrip toolbox (*http://www.fieldtriptoolbox.org*, details see Oostenveld et al., 2011) for MATLAB (R2017b, MathWorks), as well as custom scripts (available upon request from corresponding author).

Signal analysis

We investigated the power of the induced LFP responses during the encoding (i.e. sample presentation) phase of the NHP recognition memory task. A notch filter, the second-order infinite impulse response (IIR), was applied to the raw data signals, to remove the power from line noise (i.e. 50 Hz) and its harmonics (i.e. 100, 150 Hz). Then the data signals were down sampled from 30 kHz to 1 kHz. To obtain the power spectrums of LFPs for each of the 32 channels, a time-frequency decomposition analysis based on Morlet wavelet transform was performed. The frequency range in LFP spectral analysis was chosen to start at 4 Hz (to exclude slow-wave LFP components) and terminate at 120 Hz, in steps of 1 Hz.

For the 32 channels in the dlPFC array, the induced power spectra from LFPs were limited to data segments which contained completed trials and inter-trial intervals (ITIs). In each trial the duration of sample image presentation was 1000-1500 ms while the NHP held the key-touch throughout to control for hand movement; our analyses of LFPs considered a point 1000 ms before stimulus onset until 1000 ms after stimulus onset were analyzed. The LFP power around the stimulus onset was calculated as follows:

1) Wavelet transform of the signals around the stimulus onset and during the ITI baseline (i.e. a 1000 ms segment) were calculated, yielding $O_{stimulus}$ *and* $O_{baseline}$;
2) The power of the stimulus was calculated as $P_{stimulus} = O_{stimulus}^2$, and the mean power of the baseline was calculated as $P_{baseline} = \text{avg}(O_{baseline}^2)$;

3) The LFP power of the stimulus was calculated as a ratio of $P_{stimulus}$ to $P_{baseline}$, i.e.:

$$LFP\ power = \frac{P_{stimulus}}{P_{baseline}} = \frac{{O_{stimulus}}^2}{\text{avg}({O_{baseline}}^2)}$$

As both the power of the stimulus and the baseline have the same units (i.e. μV^2), the above calculated LFP power is dimensionless. Then LFP power in dlPFC was calculated by averaging the LFP power across 32 channels of dlPFC array and was combined across sessions. In the recognition memory task, LFPs in both the pre- and post-sample presentation periods (both within a time window of 1000 ms while the NHP held the keytouch) from completed correct trials (N = 646) and completed incorrect trials (N = 241) were selected and analyzed.

Statistical methods

To test for statistical significance of differences of the induced LFP power spectra between pre- and post-sample presentations during the recognition memory task, we performed a nonparametric permutation test, with the median difference between the above two conditions (i.e. pre and post-sample) as our test statistic. The non-parametric permutation test is an assumption-free method without prescribing underlying distributions (Maris and Oostenveld 2007). As described above in *signal analysis*, channel-averaged LFPs in dlPFC were calculated. In each trial, the time window of pre- and post-sample condition for nonparametric permutation test was 800 ms (i.e. time zero was the stimulus onset), to avoid the spectral leakage of LFP power when calculated near the margin of a 1000 ms time-window. This nonparametric permutation test was performed separately for correct trials and incorrect trials. In each trial type, the null hypothesis of this test was assumed that, for each frequency and time bin, there was no significant difference of the LFP power when comparing the observed median difference between the two conditions (i.e. pre- and post-

sample) against a reference distribution. The permutation test for the LFP data was performed in the following steps:

1. The observed median difference between the two conditions was obtained for each time and frequency bin, i.e. $D_{t,f}$;
2. A reference distribution for each time and frequency bin was obtained by performing 10,000 permutations on trial labels to randomly assign the two conditions. That is, each time and frequency bin had its own reference distribution, in the format of $[d_{t,f}] = (d_{t,f,1}, d_{t,f,2}, d_{t,f,3}, \ldots d_{t,f,10000})$.
3. For each time and frequency bin, its $D_{t,f}$ was compared to its own refence distribution (i.e. $[d_{t,f}]$). This bin would be selected if the observed median difference was either larger than the 97.5th or smaller than the 2.5th percentile of its reference distribution.
4. All these selected time and frequency bins were then clustered in connected sets based on adjacency in time and frequency.
5. We calculated the sum of the median differences within each cluster, and kept only the largest cluster (with the largest sum of the median difference) in the cluster-level statistics (Maris and Oostenveld 2007).

It's acknowledged that as comparisons between observed data and permutated data have been carried out in all the time and frequency bins separately, multiple comparison problem still exists in this method. To be reasonably conservative, I picked the largest cluster in the real data among other clusters, although by doing so, the sensitivity for detecting smaller clusters is reduced.

To test for statistical significance of differences of the induced LFP power spectra between correct trials (N=646) and incorrect trials (N=241) during sample presentations, we performed a similar nonparametric permutation test, with the median difference between the above two conditions (i.e. correct and incorrect conditions) as our test statistic. In each trial, the time window of correct and incorrect conditions for the permutation test was 0-400 ms

(i.e. time zero was the stimulus onset) as the above nonparametric permutation test confirmed a significant cluster appearing from the sample image onset until 300 ms in both correct and incorrect conditions. As specified in the above permutation test steps, briefly, the null hypothesis of this test was assumed that, for each frequency and time bin, there was no significant difference of the LFP power when comparing the observed median difference between the two conditions (i.e. correct and incorrect condition) against a reference distribution. This reference distribution was obtained by performing 10,000 permutations on trial labels to randomly assign the two conditions. A time and frequency bin would be selected if its observed median difference was larger than the 97.5th or smaller than the 2.5th percentile of its permutated data ($p < 0.05$, two-tailed). Then the selected time and frequency bins were clustered in connected sets on the basis of frequency and temporal adjacency. We calculated cluster-level statistics by taking the sum of the observed median difference values within a cluster and took the largest of the cluster-level statistics as the significant differences between the two conditions (Maris and Oostenveld 2007).

Experiment 2: Human TMS study

Participants

27 participants (18 male, 9 female, age range 18-30 years) took part in the TMS study. Participants were fluent English speakers, right-handed, and had normal or corrected-to-normal vision. Prior to the study, all the participants provided written consent and went through safety screening check to make sure they had no history of previous or current neurological or psychiatric conditions and were not taking any psychoactive medication. All the participants received monetary compensation for their participation at a standard rate for volunteers for TMS studies in Oxford. This study was carried out with the approval of Medical Sciences Interdivisional Research Ethics Committee, University of Oxford.

Stimulation Brain Sites

In this study, we investigated the differential effects of rTMS to dlPFC and dmPFC in recollection and familiarity in a recognition memory task designed to be similar to that used with NHP in Experiment 1. We chose left dlPFC which approximately corresponded to area BA46 or BA9/46 (referred to as BA 9/46) in light of Experiment 1, and we chose dmPFC along the midline as an area the literature led us to expect to provide a contrast with respect to consideration of contributions to recollection and familiarity, this more medial area corresponded to area BA 8 or BA9 (referred to as BA 8/9). A further control brain site was chosen to be vertex, which we had no reason to expect to be important for either memory process, and which was localized at center point of the head. The three targeted sites were measured using Beam F3 localization system (Beam et al. 2009). This system allows the measurement of the location of the F3 electrode position in the 10-20 EEG coordinate system, and takes into account individual skull variations. Based on this system, BA 9/46 was localized 1 cm caudal to F3. Both vertex and BA8/9 sit on the midline, in which vertex was localized at a site corresponding to location of electrode Cz (measured as half the distance between inion and nasion and intersecting with half the distance between the two aural tragus); and BA8/9 was localized 7cm rostral to the vertex and 6 cm medial to F3. The relative positions of three stimulation sites are illustrated in Fig. 4A. The participants were assigned to one of the three brain site groups to equalize numbers per group: dlPFC group (BA 9/46, 9 participants), dmPFC group (BA8/9, 9 participants) and control group (9 participants).

Defining Participant's Motor Threshold

Prior to the experiment, all the participants were invited to a taster session, in which the individual's Resting Motor Threshold (RMT) was obtained for each participant. To measure

RMT, stimulation was applied over the site of left primary motor cortex (M1) (localized 5 cm laterally and 5 cm rostrally to the vertex), where the largest twitch in right index finger of the participant was found. Site search was initially started at the lowest stimulator output. By gradually increasing output, the RMT of the participant was determined when 5 out of 10 TMS pulses caused a twitch in the right index finger (Rossini et al. 1994).

A stimulation intensity of 90% of RMT was used in the study. This intensity was within an appropriate range taking into account the average scalp-cortical surface distance between M1 and stimulation areas and a 2.8% reduction in stimulator output for every mm closer to the skull (Stokes 2005; Stokes et al. 2007, 2013). The mean RMT of dlPFC group was 44.33 μV (SE = ± 3.61 μV), and of dmPFC group was 51.33 μV (SE = ± 5.52 μV), and of vertex group was 49.11 μV (SE = ± 7.39 μV).

Task Stimuli and Apparatus

The task was an object recognition memory task similar to the one used in NHPs, similarly programmed using Turbo Pascal (Borland), run under DOS on a desktop PC and presented on a 20.1" colour touchscreen (TFT LCD TS200H GNR). The object images used in the task were clip-art images as in NHP study, but in order to increase difficulty (in light of a pilot study wherein performance was close to ceiling) the images were all converted to grey-scale and the contrast toned down in an attempt to make them harder to discriminate from each other. Additionally, the samples were presented in lists followed by lists of choice trials, again to reduce ceiling effects in the human version of the NHP task. Each image subtended 10° of visual angle in width and 10° in height to the participant sitting facing the screen. The sample image was always presented on the right top of the screen, positioned +12 ° horizontal and -12 ° vertical from the center of the screen. The test images were presented on the right bottom of the screen: one was positioned 0 ° horizontal and +5 ° vertical from the center of the screen; and the other one was positioned +23 ° horizontal and +5 ° vertical from the center of the screen. The background colour to the screen was white.

Participants sat with their eyes a distance of 25 cm from the screen, wearing earplugs in order to avoid audio disturbance of TMS pulses, resting their chins on a chin-rest and their foreheads on a head holder to stabilize their head position throughout the experiment. They were instructed to respond to items by touching them on the screen and gestured their confidence ratings using their right hands. For example, they indicate by raising fingers (1, 2 or 3) whether their opinion corresponding to their being somewhat confident (1), moderately confident (2), or absolutely confident (3) in their judgment as to whether they considered the test-item to be old (i.e. presented before in the preceding list as a sample) or new (not seen before in the preceding list as sample). None of the samples in this task were used in more than one list so all stimuli were trial-unique (and hence compared to the novel/trial-unique stimuli in the NHP task).

Transcranial Magnetic Stimulation (TMS) was carried out using a biphasic Magstim Super Rapid^2 magnetic stimulator (Magstim, Dyfed, UK) with a double 70-mm figure-of-eight coil. The TMS coil was clamped in line with participants' assigned brain sites and localized at a 45° angle off the midline with the handle pointing to the posterior direction throughout the experiment.

Behavioural task

Prior to the experiment, participants were given instructions on how to perform the task, and how to indicate their confidence judgments (see above), and then they were introduced to the behavioural task in a short training/practice session (comprised of one list of 12 samples and then 12 test-item trials) of the task without stimulation to provide an opportunity to become familiarized with task procedure. We used lists in the human version to avoid ceiling effects as pilot investigations revealed the NHP task with single samples and single test-trials to be too easy for participants. The experimental session itself contained 3 sub-sessions, with each sub-session containing 15 blocks of trials. Participants took a 10-15 min break between each

sub-session. Each block contained an encoding phase (i.e. a list of 12 sample images), and then a short delay, and then a test phase (i.e. a list of 12 test-item trials). The task structure is depicted, for one block, in Figure 2; during the encoding phase, 12 sample images were presented sequentially on the screen (individually for 480 ms), with inter-stimulus-interval as 350 ms. Participants were instructed to view and try to remember each sample image. After the sample phase (all 12 sample items) was completed, a blank screen was presented for 1 s (delay), and then the test phase commenced (all 12 test trials). Test trials were either 'match trials' or 'non-match trials'. In each test trial, either an identical stimulus to one of the preceding 12 samples (i.e. 'match trials') was shown as a test image, or a novel and previously unseen image (i.e. 'non-match trials') was shown as a test image, and that test image appeared on the screen together with a black circle (the left/right position of the black circle and the test-trial image were randomized between trials). The match and non-match trials were also counter balanced (6 of each per test phase of 12 test-trials) and were put in a random order. Just as in the NHP version of the task (Experiment 1) participants were instructed to touch the test image if they thought it matched one of the 12 sample images, or touch the standard 'non-match button' (i.e. the black circle) if they thought the test image was not a match. Participants could touch the screen to make responses once the test image and black circle were on the screen, with a maximum responding duration set to 5000 ms (i.e. test trial ended if participants didn't make responses within 5000 ms). After responding to the test image, participants were instructed to rate their confidence as to whether the test item was new or old using a scale of 1-3 by making three different movements with their fingers, corresponding to somewhat, moderate, and absolute confidence. Participants were further instructed to try to use the entire range of confidence responses as best they could and not simply select the extremes of confidence as defaults. The inter trial interval was 1000 ms.

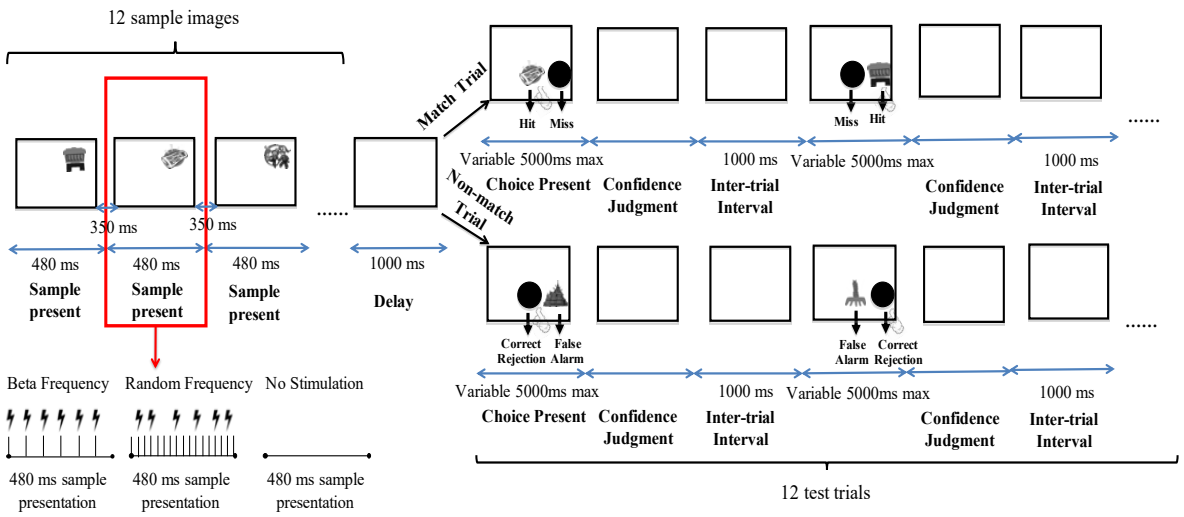


Figure 2. *Human recognition memory task structure. The figure depicts one block in the TMS study. Twelve sample object images were sequentially presented for 480 ms with an inter-stimuli-interval of 350 ms (the figure shows the procedure for one of these 12). Six rTMS pulses (at beta frequency or at random frequency) or no stimulation were given during the 480ms sample presentation for 4 out of the 12 samples in the list. Then after a delay of 1000 ms, 12 test trials followed (the figure shows the procedure for one of these 12). Just as in the NHP task in Figure 1, in 'Match Trials' the black circle was presented with an identical image to one of the preceding sample; in 'Non-match Trials' the black circle was presented with a novel stimulus not seen before. Participants were told to touch the test-item if they remembered the test-item was a match but to touch the black circle if they thought the test-item was a non-match; accordingly the responses could be separated into hits, misses, correct rejections, and false alarms as indicted. Each test-trial in this human version of the task lasted maximally 5000 ms and ended with a confidence judgment indicated by the participant by their making a finger gesture as described in the main text. The inter test-trial interval was 1000 ms.*

Repetitive TMS Protocol

As our local field potential (LFP) investigations in the NHP (Experiment 1) revealed heightened beta power in dlPFC when macaques viewed and encoded sample images in a similar recognition memory task, the extent of which was associated with success or error in subsequent macaque recognition memory performance, rTMS stimulation in this human study was targeted during the encoding phase of the memory task so as to assess whether that activity in that region at that time may be necessary for successful encoding and subsequent recognition in humans.

In line with the safety guidelines for TMS by Rossi et al. (2009) to avoid seizure risks caused by too much sequential high-frequency stimulation, a restriction was implemented that there were at least 2 non-stimulated images in between every stimulated image in each sample list of 12 items. Therefore, we determined all the possible combinations wherein 4 out of 12 sample images might be targeted, with at least 2 non-targeted intervening samples, and each block's sample phase took one of those schedules selected randomly each time. During beta-stimulation condition blocks, each of the four rTMS targeted samples in the list (each with a duration of 480 ms as detailed above) were targeted with the delivery of 6 pulses every 80 ms (hence at 12.5 Hz and within the range of beta frequency); while in the random-frequency stimulation blocks, the same total number of pulses (6) were delivered less regularly over the same period of presentation time (specifically, the 480ms sample presentation epoch was divided into 30ms intervals and 6 of those, with the constraint that no two consecutive 30ms intervals could be chosen, were chosen at random to trigger a TMS pulse delivery). All these considerations of TMS frequency ensured we always kept well within the known safe ranges of TMS stimulation at high frequency and over extended durations of stimulation in line with the safety guidance of Rossi et al. (2009). Each sub-session contained 15 blocks, with each of the three 'types' of stimulation (i.e. beta-stimulation, random-stimulation, and no-stimulation) occurring 5 times per sub-session, randomly ordered. Each participant received the same sets of stimuli and same stimulation

order. As there were 3 sub-sessions in total each stimulation condition was repeated 15 times per participant and so participants performed a total of 540 trials (i.e. 3 sub-sessions x 15 blocks per sub-session x 12 trials per block). As we were interested in the effects of stimulated sample items on the subsequent memory performance, in each participant, 126 trials in beta-stimulation condition (i.e. excluding unstimulated old items appearing in the test phase), 123 trials in random-stimulation (i.e. excluding unstimulated old items appearing in the test phase) and 180 trials in no-stimulation (i.e. 15 blocks per sub-session x 12 trials per block) were used for our between-block analyses.

Data analysis

Behavioural effects of TMS were evaluated based on dual-process signal detection (DPSD) theory model. According to this model, both familiarity and recollection contribute to recognition memory (Yonelinas 2001, 2002). A recollection index (R) and familiarity index (F) were extracted by fitting the model to data using a standard approach that minimized the squared difference between the observed and predicted data in each cumulative confidence rating bin. Specifically, participants were asked to express their confidence in each of their decision using a 6-point scale, where 1 implies absolutely certain old, 2 for moderately certain old, 3 for slightly certain old, 4 for slightly certain new, 5 for moderately certain new, and 6 for absolutely certain new. The cumulative hit rate was then plotted against the cumulative false alarm rate to create the ROC plot of each participant. To be more specific, the first point at the left-hand side of the plot was the hit rate and false alarm rate at confidence level 6. After that, the second point was for the combination of confidence levels 6 and 5, the third point for confidence levels 6 to 4 and so on. The cumulative hit rate and false alarm rate of all confidence levels was constrained to 1.0. Accordingly, we had five coordinate points for each ROC plot.

The ROC data was analyzed using the DPSD model. This model assumes recognition memory to be contributed towards by two distinct processes referred to as recollection and familiarity. For all trails with confidence levels equal to or larger than the ith confidence rating bin (i.e. $CL \geq CL_i$), the DPSD model predicts the cumulative false alarm rate in lure-item trials and hit rate in target-item trials as follows:

$$p(Lure|CL \geq CL_i) = R_n + (1 - R_n) * \Phi(-c_i)$$

$$\mathrm{p}(Target|CL \geq CL_i) = R_0 + (1 - R_0) * \Phi(\frac{d'_F - \mathrm{c_i}}{\sigma_F})$$

Briefly, in the target and lure distributions (Φ is the cumulative normal distribution), the parameters for the response criterion are designated as c_i. In the target distribution, R_0 is a target threshold parameter being labeled recollection of old stimuli, which is that the target items that have a strength above the R_0 are classified as old. If the target item strength is below the R_0, its classification is governed by the familiarity component of the model, which is a Gaussian distribution with the mean of d'_F and standard deviation of σ_F.

In the lure distribution, R_n is a lure threshold parameter being labeled falsely recollection of old stimuli, which is that the lure items that have a strength above the R_n are classified as old (i.e. false alarm response), while the classification for those with strength below the R_n threshold would be governed by a standard Gaussian distribution, with a mean of 0 and a unit standard deviation. It should be noted that the meaning of R_n is different from the one in the paper of Koen et al. (2017), in which they assume R_n is a lure threshold that lure items above this threshold will be classified as new.

In our DPSD model, we further make the R_n parameter is constrained to equal 0 (i.e. assuming that participants would never recollect something they never saw), and σ_F parameter is constrained to equal 1. Based on the above assumptions, the algorithm of DPSD model becomes:

$$p(Lure|CL \geq CL_i) = \Phi(-c_i)$$

$$p(Target|CL \geq CL_i) = R_0 + (1 - R_0) * \Phi(d'_F - c_i)$$

Each pair of the free parameters, d'_F (F) and R_0 (R), defines a ROC curve. These parameters were obtained by minimizing the sum of squared residuals in both the abscissa and the ordinate of all the five points (that is, the sum of squared errors of prediction, or SSE, method for both axes). Based on the assumptions of the DPSD model, the range of R is between 0 and 1 while the range of F is between 0 and infinity (a theoretical maximum that is; practically it is much less, around 3-4 as a maximum). If the best fit of the *R* value turns out to be negative in the initial fitting of ROC and thus meaningless, we fixed it to be 0 and refit the model to get F. In each stimulation type and in each stimulation site condition, a ROC is plotted cumulatively for each confidence level by the proportion of correct 'old' judgements against the proportion of incorrect 'old' judgements, and both R and F in each stimulation type and stimulation site condition were extracted from DPSD model.

Statistical methods

All the statistical analysis on human behavioral data was carried out using SPSS software (IBM). The above calculated indices (i.e. R and F) were subjected to 2×3×3 mixed model repeated measures ANOVAs with 3 levels of the within-group factor stimulation-type (beta-frequency, random-frequency, and no-stimulation) and with 3 levels of the between-subject factor stimulation-site (dlPFC, dmPFC, and vertex).

Accuracy was assessed for each human participant in each stimulation condition by calculating the area under each ROC curve (AUC). AUCs were calculated using the parameters from a fit of the DPSD model to the individual ROCs. Response time (RT) for correct responses were also evaluated for each participant under each stimulation condition.

Then performance (i.e. accuracy or response time) was subjected to a 3×3 mixed model repeated measures ANOVAs with 3 levels of the within-subject factor stimulation-type (beta-frequency, random-frequency, and no- stimulation) and with 3 levels of the between-subject factor stimulation-site (dlPFC, dmPFC, and vertex).

Results

Experiment 1: NHP electrophysiological study.

During the NHP recognition memory task, we focused only on the encoding (i.e. sample presentation) phase. A nonparametric permutation test as described earlier revealed a significant cluster ranging from 7-24 Hz starting after the sample image onset in macaque dlPFC in sample presentations preceding correct choices in subsequent choice-trials (two-tailed permutation test, $p < 0.05$) whereas a significant cluster ranging from 8-21 Hz was revealed starting after the sample image onset in macaque dlPFC in incorrect condition (two-tailed permutation test, $p < 0.05$). This post-sample alpha/beta power lasted roughly 300 ms in correct trials (Fig. 3A) and in incorrect trials (Fig. 3B). When comparing the difference between correct and error trials a further nonparametric permutation test (two-tailed permutation test, $p < 0.05$) revealed a cluster ranging from 10-15 Hz starting after the sample image onset in macaque dlPFC that was significantly higher in correct trials compared to incorrect trials. The analysis highlighter another small cluster ranging from 59-87 Hz (which was very brief, from 199 ms to 221 ms) found to be lower in beta power correct trials compared to incorrect trials. Therefore a stimulation frequency that was intermediate within this range (we chose 12.5 Hz, i.e. low beta) and that was, importantly, also well within the safety guidelines (with respect to duration and frequency considerations for repetitive stimulation) for humans (Rossi et al. 2009) was selected to be used in Experiment 2, our repetitive TMS (rTMS) study examining the effect of intervention at this frequency in the corresponding encoding phase of a homologous recognition memory task in humans.

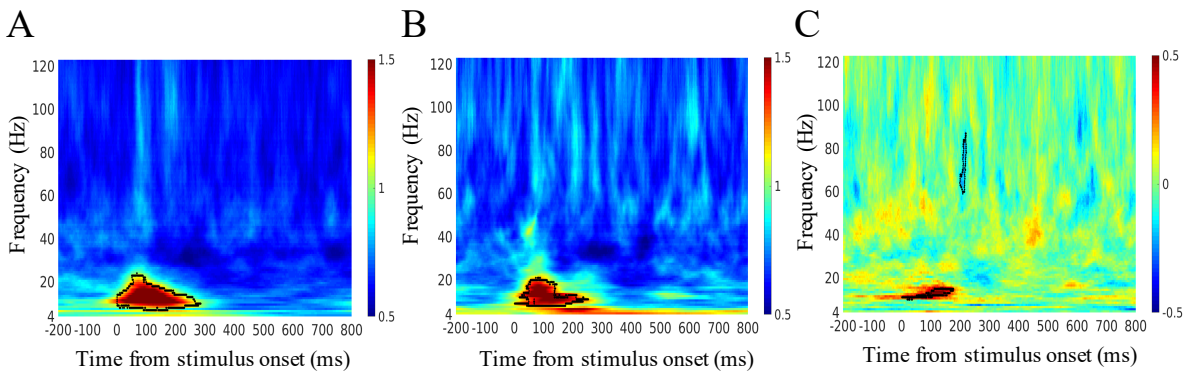


Figure 3. *Time-frequency spectrogram for induced local field potential (LFP) power from dlPFC array in the sample presentation epoch in NHP in Expt.1. Panel A-B: the area of statistically significant differences of LFPs between pre- and post-sample periods in macaque dlPFC is highlighted by a black outline in trials that ended up being correct trials (A) and in trials that ended up being error trials (B). In both trials types we observed transient beta frequency power increase for around 300 ms from sample onset (indicated by zero ms on this figure). Panel C: the area of statistically significant higher LFPs in trials that ended up being correct trials compared to in trials that ended up being error trials in macaque dlPFC is highlighted by a black outline and includes low-beta frequencies in the 10-15 Hz range for around 200 ms from sample onset ms (indicated by zero ms on this figure); another area of statistically significant higher LFPs in error trials compared to correct trials is highlighted by another black outline and includes a very transient gamma peak in the 59-87 Hz range for around 20 ms. The data depicted in this figure is averaged across 32 electrodes in dlPFC, and across 29 daily sessions, and across 646 correct trials and 241 error trials.*

Experiment 2: Human TMS study.

To summarise the results (statistical analyses described in detail below) we observed that only rTMS at beta frequency to dlPFC drove down the recollection index, and only rTMS at beta frequency to dmPFC drove up the familiarity index.

Impact of TMS on accuracy and response time in the human recognition memory task

Participants were highly accurate in their recognition memory task; mean performance (calculated as AUCs) is shown in Table 1. A mixed-model repeated measures ANOVA, with stimulation-site as the between-subjects factor and stimulation-type as the within-subject factors, showed that neither the main effects (i.e. stimulation-site, stimulation-type) nor their interaction was significant (main effect of stimulation-site: $F_{(2,24)} = 2.035$, $p = 0.153$, $\eta^2 = 0.145$; main effect of stimulation-type: $F_{(2,48)} = 1.252$, $p = 0.295$, $\eta^2 = 0.050$; interaction: $F_{(4,48)} = 0.529$, $p = 0.715$, $\eta^2 = 0.042$) with respect to AUC.

Response times (RTs) were also calculated for each participant group in beta frequency, random frequency, and no-stimulation TMS conditions (Table 1). The aforementioned mixed-model repeated measures ANOVA applied to RT also showed neither the main effects (i.e. stimulation-site, stimulation-type) nor their interaction was significant (main effect of stimulation-site: $F_{(2,24)} = 2.255$, $p = 0.127$, $\eta^2 = 0.158$; main effect of stimulation-type: $F_{(2,48)} = 1.184$, $p = 0.315$, $\eta^2 = 0.047$; interaction: $F_{(4,48)} = 1.387$, $p = 0.253$, $\eta^2 = 0.104$).

Table 1. Descriptive statistics: accuracy (AUCs) and response time of correct responses for each participant group across each stimulation condition

Brain Area	Stimulation	Accuracy	Response Time (ms)
dlPFC	Beta frequency	0.85 ± 0.02	1727 ± 147
(n = 9)	Random frequency	0.84 ± 0.01	1742 ± 157
	No Stimulation	0.84 ± 0.02	1738 ± 154
dmPFC	Beta frequency	0.92 ± 0.02	1900 ± 113
(n = 9)	Random frequency	0.89 ± 0.03	1856 ± 98
	No Stimulation	0.88 ± 0.03	1836 ± 95
Vertex	Beta frequency	0.88 ± 0.02	1546 ± 66
(n = 9)	Random frequency	0.89 ± 0.02	1503 ± 73
	No Stimulation	0.88 ± 0.02	1538 ± 76

Legend: Accuracy and response time of correct responses for each participant group across each stimulation condition; neither accuracy nor response time differed significantly across different stimulation-sites and stimulation-types in each group of human participants.

Impact of TMS on recollection and familiarity in the human recognition memory task

The recollection index (R) and familiarity index (F) were calculated for each participant in each of the three stimulation types. A mixed-model repeated measures ANOVA was conducted on the indices data, with stimulation-site (3 levels: dlPFC, dmPFC, and vertex) as the between-subjects factor and stimulation-type (3 levels: beta-frequency, random-frequency, and no- stimulation) and index-type (2 levels: recollection-index, familiarity-index) as the two within-subject factors. A significant main effect of index type ($F_{(1,24)} = 65.809$, $p < 0.001$, $\eta^2 = 0.733$) was found, in addition to a significant two-way interaction between index-type and stimulation-type ($F_{(2,48)} = 6.112$, $p = 0.008$, $\eta^2 = 0.203$) with Greenhouse-Geisser correction due to a significant Mauchly's test of sphericity. As tests of the linear trend component of the 3-way interaction between index type, stimulation type, and stimulation site were highly significant ($F_{(2,24)} = 5.190$, $p = 0.013$, $\eta^2 = 0.302$) we submitted the data to further scrutiny.

Therefore we next applied, repeated-measures ANOVAs to each stimulation-site independently, firstly considering the dlPFC site with the aforementioned index-type and stimulation-type within-subjects factors. We found a significant main effect of index-type ($F_{(1,8)} = 82.060$, $p < 0.001$, $\eta^2 = .911$) and a significant two-way interaction between index-type and stimulation-type ($F_{(2,16)} = 3.984$, $p = 0.039$, $\eta^2 = 0.332$), the latter prompted further scrutiny by a repeated-measures ANOVA on R alone, with stimulation type as the within-subjects factor, and this showed that although the main effect of stimulation was marginally

significant ($F_{(2,16)} = 4.432$, $p = 0.055$, $\eta^2 = 0.356$; with Greenhouse-Geisser correction due to a significant Mauchly's test of sphericity) the tests of within-subjects contrasts showed a highly significant effect of the linear component of stimulation type ($F_{(1,8)} = 21.547$, $p = 0.002$, $\eta^2 = 0.729$) which prompted further scrutiny by post-hoc pairwise t-tests with bonferroni correction. These revealed a significant suppression of the R index under beta stimulation compared with R under no-stimulation ($p = 0.005$), although no significant difference of the R index between beta stimulation and random stimulation was found ($p = 0.272$). Another parallel repeated-measures ANOVA, this time only considering the F index, with stimulation type as the within-subjects factor, showed that neither the main effect of stimulation type ($F_{(2,16)} = 2.380$, $p = 0.125$, $\eta^2 = 0.229$) nor the linear trend component ($F_{(1,8)} = 2.680$, $p = 0.140$, $\eta^2 = 0.251$) was significant.

Secondly, we ran another repeated-measures ANOVA this time considering just the dmPFC site, again with aforementioned index-type and stimulation-type as within-subjects factors. We found a significant main effect of index-type ($F_{(1,8)} = 15.964$, $p = 0.004$, $\eta^2 = 0.666$), a significant main effect of stimulation-type ($F_{(2,16)} = 5.430$, $p = 0.016$, $\eta^2 = 0.404$), and a significant two-way interaction between index-type and stimulation-type ($F_{(2,16)} = 5.326$, $p = 0.017$, $\eta^2 = 0.400$). The interaction prompted further scrutiny and so a repeated-measures ANOVA on the R index alone, with stimulation-type as the within-subjects factor, showed the main effect of stimulation type not to be significant ($F_{(2,16)} = 2.185$, $p = 0.145$, $\eta^2 = 0.215$). A parallel repeated-measures ANOVA on the F index alone, similarly with stimulation-type as the within-subjects factor, revealed a significant main effect of stimulation ($F_{(2,16)} = 6.144$, $p = 0.010$, $\eta^2 = 0.434$) and follow-up post-hoc pairwise t-tests with bonferroni correction showed that with respect to the dmPFC site a significant enhancement of the F index under beta stimulation compared to under no-stimulation ($p = 0.012$).

Thirdly, parallel analyses were conducted for the vertex site, again with index-type and stimulation-type as within-subject factors; here a significant main effect of index-type was found ($F_{(1,8)} = 22.931$, $p = 0.001$, $\eta^2 = 0.741$), but neither the main effect of stimulation-type nor the two-way interaction between index-type and stimulation-type were significant (main effect of stimulation-type: $F_{(2,16)} = 0.160$, $p = 0.854$, $\eta^2 = 0.020$; two-way interaction: $F_{(2,16)} = 0.094$, $p = 0.911$, $\eta^2 = 0.012$) so no follow-up analyses were required.

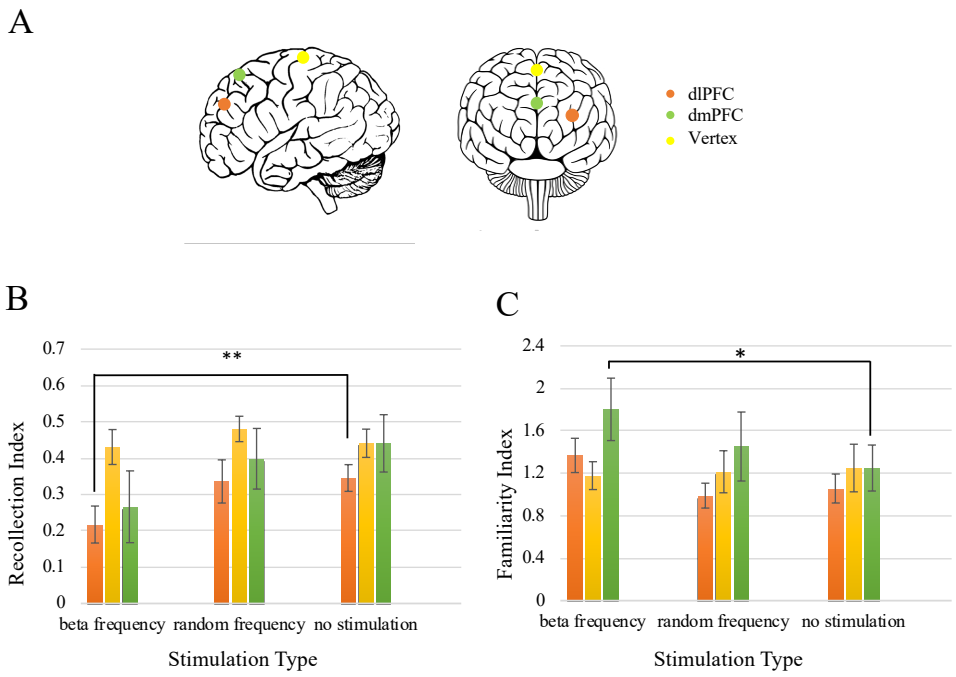


Figure 4. *Stimulation sites for each group of human participants and effects of TMS upon recollection and familiarity indices in a between-block analysis in Expt. 2. Panel A: lateral and frontal view of the human brain. Human stimulation sites for rTMS are shown as dlPFC (orange), dmPFC (green) and vertex (yellow). Panel B-C: Bar graphs presenting the mean recollection index (Panel B) and familiarity index (Panel C) in dlPFC (orange bar), dmPFC (green bar) and vertex (yellow bar) under beta-frequency stimulation, random-frequency stimulation and no stimulation. Note that beta-frequency stimulation (but neither random-*

*frequency stimulation nor no stimulation) suppressed recollection index in dlPFC, and beta-frequency stimulation (but neither random-frequency stimulation nor no stimulation) enhanced familiarity index in dmPFC. * indicates p < 0,05, and ** indicates p < 0.01.*

In summary, the between-block analyses above indicate (see Figure 4) that, when comparing ROC derived R and F indices only calculated from participants' performance in choice trials that included samples that had appeared in the preceding list of samples and that had also been stimulated with rTMS (i.e. in the beta-stimulation and random-stimulation blocks) compared to all trials in the no-stimulation blocks (all choice trials could be included from the no-stimulation block because all were equivalent in that none of them had received rTMS), then the R index appears to be suppressed by beta stimulation in dlPFC (compared to non-stimulated trials in the no-stimulation block) but the F index appears to be enhanced by beta stimulation in dmPFC (compared to non-stimulated trials in the no-stimulation block). This highly intriguing result is limited in interpretational scope, however, because the above analyses clearly do not also show that beta-stimulation significantly suppresses the R index compared to random frequency stimulation rTMS, nor that beta-stimulation significantly enhances the F index compared to random frequency stimulation rTMS. To attempt to address this further we next considered what we refer to as 'within-block' analyses wherein we also calculate a within-block comparison of R and F indices for trials that used samples that had occurred in the sample phase that were targeted with rTMS (denoted +) versus trials that used samples that occurred in the sample phase that were not targeted with rTMS (denoted -); hence we refer to these four indices as R+, R-, F+, and F-. These indices cannot be calculated for the no-stimulation block as all trials are without rTMS so this analysis is restricted to beta-stimulation and random-stimulation blocks. Specifically, we investigated whether the within-block numerical difference between R+ and R- and also between F+ and F- differed between blocks, that is, whether these differences themselves depended upon

whether samples were targeted with beta versus random rTMS. The aim was to further probe whether the beta-stimulation effect on R in dlPFC might, in this more sensitive within-block analysis, be somewhat more distinguished (i.e. statistically significantly as opposed to just numerically) from the random-frequency effect in dlPFC (and not just from the no-stimulation effect previously observed); similarly, we also aimed to probe if the beta-stimulation effect on the F index in dmPFC might be distinguished from the random-frequency effect upon the F index in dmPFC.

Accordingly, a repeated measures ANOVA on the R+/R- difference observed in dlPFC with stimulation-type as a within-subjects factor (2 levels: beta-frequency block and random-frequency block) showed a significant main effect of stimulation-type ($F_{(1,8)} = 6.508$, $p = 0.034$, $\eta^2 = 0.449$) confirming a significant difference in this within-block analysis between the greater suppression of the R index by beta-frequency stimulation than by random-frequency stimulation (no significant difference by stimulus-type ($F_{(1,8)} = 3.060$, $p = 0.118$, $\eta^2 = 0.277$) was observed for the F+/F- statistic). In contrast, with respect to dmPFC, the repeated measures ANOVA on the R+/R- difference with stimulation-type as a within-subjects factor (2 levels: beta-frequency block and random-frequency block) did not show a main effect of stimulation-type ($F_{(1,8)} = 0.143$, $p = 0.715$, $\eta^2 = 0.018$) nor did a corresponding F+/F- analysis ($F_{(1,8)} = 0.303$, $p = 0.597$, $\eta^2 = 0.037$). Then, with respect to vertex, the repeated measures ANOVA on the R+/R- difference with stimulation-type as a within-subjects factor (2 levels: beta-frequency block and random-frequency block) did not show a main effect of stimulation-type ($F_{(1,8)} = 0.996$, $p = 0.347$, $\eta^2 = 0.111$) nor did a corresponding F+/F- analysis ($F_{(1,8)} = 2.551$, $p = 0.149$, $\eta^2 = 0.242$).

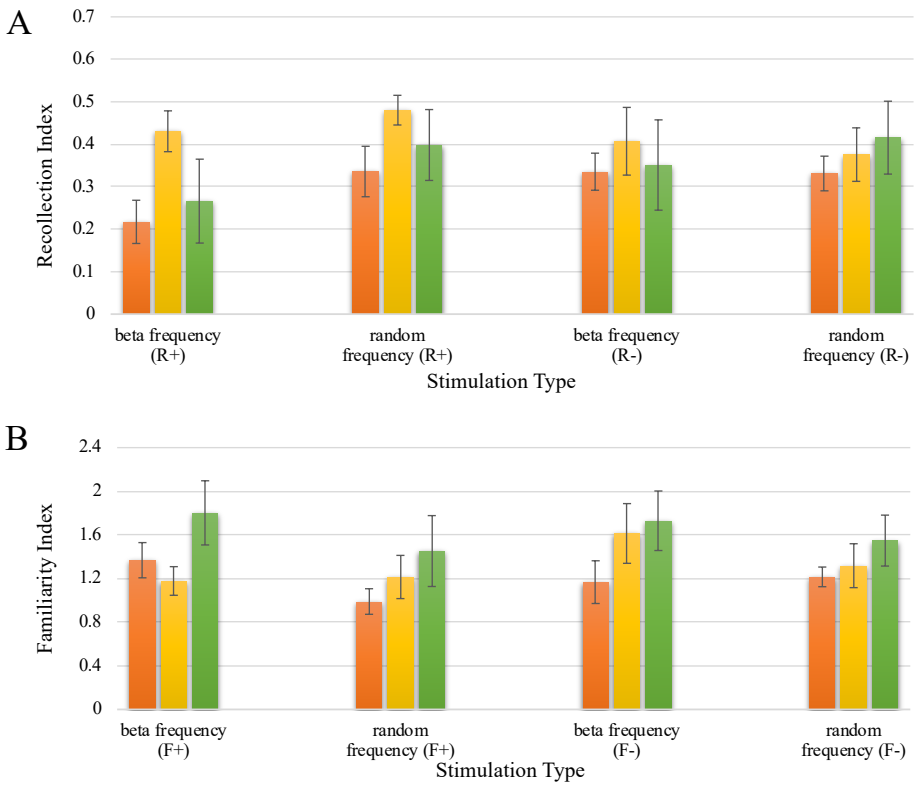


Figure 5. *Stimulation sites for each group of human participants and effects of TMS upon recollection and familiarity indices in a within-block analysis in Expt. 2. Panel A-B: Bar graphs presenting the mean recollection index (Panel A) and familiarity index (Panel B) in dlPFC (orange bar), dmPFC (green bar) and vertex (yellow bar) under beta-frequency stimulation with samples targeted with rTMS (+) or without rTMS (-), and random-frequency stimulation with samples targeted with rTMS (+) or without rTMS (-). Accordingly, the R and F indices were labeled as R+, R-, F+, and F-. Our intended analyses compared the R+/R- and F+/F- difference scores and confirmed that these difference scores were significantly greater for R index dlPFC for beta-stimulation than for random-stimulation, but were not significantly greater for F in dmPFC for beta-stimulation than random-stimulation.*

In summary the overall analyses (a combination of between-block and within-block approaches) provide mixed results and so must be interpreted cautiously; nonetheless the within-block analyses do at least support the notion that that the beta-frequency effect on the R index in dlPFC does not generalize to all rTMS stimulation parameters (as the random-frequency stimulation does not have the same effect) supporting the numerical trend seen in the between-block analyses and raising the possibility that it may be a frequency specific effect (how specific will need to be addressed by future studies); in contrast the beta-frequency effect on the F indices in dmPFC on the other hand appears to be less of a frequency specific effect as the difference between beta-frequency and random-frequency stimulation effects on the F indices did not attain statistical significance.

Impact of TMS on memory performance in match trials that containing samples that were either stimulated or not stimulated by rTMS

Finally, we returned, more directly, to the question of whether our rTMS protocols might be having effects that was clearly seen to be specific to choice trials that contained those particular samples (i.e. the 4 out of 12 in the preceding sample list) that were stimulated, or whether rTMS to those 4 samples might be having a broader effect upon performance across the block in general. We first calculated the hit rate for match trials that contained samples that had been targeted by rTMS in the sample list phase and compared that to the hit rate for match trials that did not contain samples targeted by rTMS in the sample list phase; the hit rate data was subjected to an ANOVA with the within-subjects factor 'targeted' (2 levels: rTMS-to-sample versus no rTMS-to-sample), the within-subjects factor stimulation-type (2 levels: beta-frequency block and random-frequency block), and with stimulation-site as the between-subjects factor (3 levels: dlPFC, dmPFC, and vertex). We found that there was a significant main effect of stimulation-type on this hit rate measure ($F_{(1,24)} = 11.341$, $p = 0.003$, $\eta^2 = 0.321$) and also a significant 3-way interaction between stimulation-type and targeted

and stimulation-site ($F_{(2,24)} = 4.264$, $p = 0.026$, $\eta^2 = 0.262$) which prompted follow-up investigation of each stimulation-site separately which revealed that the main effect of the factor 'target' was not significant in any of the three regions (dlPFC: $F_{(1,8)} = 1.156$, $p = 0.314$, $\eta^2 = 0.126$; dmPFC: $F_{(1,8)} = 0.106$, $p = 0.753$, $\eta^2 = 0.013$; vertex: $F_{(1,8)} = 0.277$, $p = 0.613$, $\eta^2 = 0.034$) nor were interactions with stimulus-type (dlPFC: $F_{(1,8)} = 2.767$, $p = 0.135$, $\eta^2 = 0.257$; dmPFC: $F_{(1,8)} = 0.242$, $p = 0.636$, $\eta^2 = 0.029$; vertex: $F_{(1,8)} = 4.679$, $p = 0.062$, $\eta^2 = 0.369$). These analyses suggest that to some degree rTMS to just 4 out of 12 samples in the list had a broader effect on performance than to those targeted samples alone; this is to be expected as interference with sample encoding may lead to some broader confusion between presented and non-presented samples at choice. On the other hand our earlier within-block analyses reveal that R measures are different for R+ and R- conditions which implies that any effect is not equal to all choice trials. Likely there is both a degree of sample-focused rTMS effect and a degree of diffuse/spread of rTMS effect. Future studies that investigate the persisting effects of rTMS ideally need to also employ simultaneous recordings of EEG/MEG or neuronal responses so to correlate physiological measures with behavioural measures that outlast rTMS presentation.

Discussion

In this study, we first observed in a NHP what frequency-specific and performance related LFP power modulations occurred in dlPFC during sample image presentation in an object recognition/working memory task. An early transient peak in alpha/low-beta power was seen during sample presentation for 300 ms, moreover we observed a significant difference between its power during sample presentations in trials that ended up being correct recognition trials compared to in sample presentations that ended up being incorrect trials; specifically, the 10-15 Hz peak in alpha/low-beta power was significantly greater in the former than in the latter suggesting that the neuronal activity during sample presentation was indeed related to behavioural performance (i.e. subsequent recognition being correct versus incorrect). The significant brief bursts of alpha/low-beta power observed in our LFP signal between correct and error trials had a very early onset and only lasted around 200 ms. Previous electrophysiological investigation in NHPs have also found early involvement of dlPFC in the representation of salient stimuli, for example visual responses in the population peristimulus time histogram were observed with a latency as early as 52 ms and linked to bottom-up visual attention (Katsuki and Constantinidis, 2012). Early signals with a somewhat longer latency (~120ms) observed in dlPFC have also been linked with top-down visual attention (Buschman and Miller 2007). These aforementioned latencies are all well within the time-frame of the heightened alpha/low-beta power observed in our LFP recordings and so it is possible that the early signal we observed in dlPFC reflects both visual and attentional processes that benefited sample encoding and subsequent memory performance of NHPs in accordance with our observations of a behavioural association of signal magnitude with subsequent correct versus incorrect recognition. These LFP observations are limited with respect that to-date the data are from a single NHP providing information about task parameters to be used in a more comprehensive in-depth NHP study in progress but the link

to behaviour gave us confidence to use them to inspire investigation of causality in a human TMS paradigm using a similar task.

Our initial hypotheses for the human TMS study were also inspired by the neural de-synchronization hypothesis, based on information theory, that was previously proposed (Hanslmayr et al. 2012a) to account for a *decrease* of alpha/beta LFP power in frontal and parietal cortex correlating with *successful* memory encoding and retrieval processes across some human studies (Hanslmayr et al. 2009, 2011; Khader and Rösler 2011; Waldhauser et al. 2012). Specifically, power decreases in the alpha/beta frequency band are presumed to reflect a de-synchronization of local neural assembles. A rationale, based on information theory, is that synchronization of neural firings reduces the richness of information transfer which results in information redundancy; in contrast, a de-synchronization of neural firing patterns leads to more potential for carrying information to improve the efficiency of neural communications (Hanslmayr et al. 2012a). The de-synchronization hypothesis, applied to human recognition memory and our paradigm, maintains that a decrease of alpha/beta power may be associated with more efficient encoding, which helps contribute to successful memory retrieval subsequently (Hanslmayr et al. 2012a; Holmes et al. 2018). Therefore we first hypothesized that in our human investigations of a similar task to that performed by the NHP (albeit with lists of samples followed by lists of choice trials to increase memory demands so to avoid ceiling effects) that interfering in efficient beta desynchronization would be deleterious to successful encoding and hence recognition performance. To test this causal hypothesis we targeted rTMS stimulation at a beta frequency, chosen to be intermediate within the significant task-relevant low-beta frequency range found in our NHP observations (namely 12.5 Hz), and targeted to the homologous brain region (dlPFC) in human participants to that we recorded form in the NHP, all while they performed a similar task. We reasoned that artificial entrainment of low-beta frequency activity in dlPFC through 12.5 Hz low-beta rTMS throughout the 480ms of sample presentation might impair subsequent

recognition by preventing effective beta desynchronization linked to effective sample encoding; therefore as a control rTMS stimulation protocol we also employed a random-frequency rTMS stimulation (i.e., with same total number of pulses over same total duration, but with each burst occurring pseudorandomly in time) presumed less likely to be deleterious to efficient and effective beta de-synchronization. We also targeted both rTMS stimulation protocols to both an active comparison site (dmPFC) given previously observed differences in relationship of these areas to recollective and familiarity processes in neuroimaging studies, and also a passive control site (vertex, which we had no reason to think was implicated in recognition memory).

We indeed found functional dissociations between the effects of short bursts of 12.5 Hz low-beta frequency rTMS stimulation (i.e. six pulses lasting 480ms, lasting the entire the duration of the sample presentation) to left dlPFC and left dmPFC. Only 12.5 Hz rTMS to dlPFC during sample presentations in the beta-stimulation block reduced behavioural indices of recollection derived from ROC/DPSD (see Methods) compared to performance in the no-stimulation block; whereas only 12.5 Hz rTMS to dmPFC in the beta-stimulation block enhanced similarly derived behavioural indices of familiarity compared to performance in the no-stimulation block (Figure 4 panel B and panel C). Short bursts of random frequency rTMS had no effect on either recollection or familiarity over either prefrontal regions, nor over the vertex. While intriguing these dissociations of beta-frequency effects between brain regions are limited with respect to claims about frequency specificity of the effects because the effects of beta-frequency stimulation, while differing from no-stimulation control, were not also significantly different from the random-frequency stimulation comparisons in this between-block analysis. To address this further we also conducted within-block analyses that applied ROC/DPSD separately to trials in each block that used samples that were targeted with rTMS and trials in each block that did not use samples targeted with rTMS; this 'within-block' approach was applied to beta-frequency blocks and random-frequency blocks wherein

this distinction could be made. The within-block analyses revealed evidence that the effect of 12.5 Hz beta-stimulation to dlPFC on R index was significantly different from the effects of random-frequency stimulation to the same site on that index, but that the 12.5 Hz beta-frequency stimulation effect to dmPFC on the F index was not significantly different from the random-frequency stimulation effect on the same site on that index (Figure 5 panel A and panel B). Overall, our hypothesis as to the deleterious causal effects of low-beta frequency stimulation to human dlPFC sustained throughout the sample period was supported.

Another issue we considered was whether the rTMS effects we observed were specific to disrupted encoding of those particular samples viewed during rTMS stimulation or whether the causal effect upon subsequent recognition were attributable in part to a spread of effect, for example to all samples in the list given that it is known that rTMS effects can outlast the duration of stimulation (Hallett 2007). Another possible explanation for general effect is that disrupted sample encoding may lead to a general confusion in evaluating familiarity or recollection of stimuli at choice. As we did not have EEG/MEG recording, we sought behavioural evidence to speak to this issue. Firstly we note that our within-block analyses point to some specificity of rTMS effect (as ROC indices differed depending upon whether choice trials contained targeted samples or non-targeted samples), however when we analyzed the proportion of trials at choice that were correct (i.e. 'hits') for trials that used samples targeted with rTMS compared to those that did not we found no significant difference which suggests a spread of effect.

As no online EEG/MEG recording was carried out in our human's task, this hypothesis of a de-synchronization effect of random-stimulation versus beta-frequency stimulations during encoding remains tentative and needs to be validated in future human research (or indeed in NHPs performing the same task wherein, as we showed, electrodes can be placed directly in the relevant regions, so that in future studies recording can be made in and around the regions that are stimulated). Previous studies have however combined EEG

and TMS study, and have provided stimulation over left dlPFC (BA 9) using rTMS at a particular beta frequency (18.7 Hz), but not at other lower frequencies (6.8 Hz and 10.7 Hz), also impaired recall processes (Hanslmayr et al. 2014). This gives support to hence our external source of beta frequency entrainment from rTMS over the same region may have impaired recognition memory performance by lessening natural processes of de-synchronization as this hypothesis predicts. Holmes et al. (2018) also showed a dissociation between LFP beta power and mnemonic tuning and whilst in a spatial task this is also consistent with de-synchronization aiding memory stability (Holmes et al. 2018). Neural attractor network modeling (Compte et al. 2003), in the context of delayed response task performance in NHPs, also suggests mechanisms by which a drop in LFP power may relate to memory processing; asynchronous networks can maintain memory coding for longer durations whereas synchronization leads to an overall instabilities incompatible with stable memory-coding states. According to these models too, frontal memory networks desynchronize to preserve memory states.

The neural communication through coherence hypothesis (Fries 2005) suggests that synchronized neural oscillations within a particular brain region or between distant brain areas provides important mechanisms for mediating cognition. This theory captures the general concept of interaction between spikes and oscillatory LFPs, and brain areas fluctuating between frequencies and/or phase of oscillations with respect to each other in order to '*tune-in*' (Fries 2015; Fell and Axmacher 2011). Inter-area phase synchronization may have other effects too: e.g. facilitating timing of synaptic inputs onto common targets, or inducing spike timing-dependent plasticity of synaptic connections between regions facilitating communication (Fell and Axmacher 2011). In a review focusing on frontal-temporal interactions in recollection/familiarity, a "multi-effect multi-nuclei" model was proposed, in which inputs to PFC directly from hippocampus, and indirectly from hippocampus *via* the anterior and midline thalamic nuclei, are related to recollection process,

while connections to PFC from perirhinal cortex and mediodorsal thalamic nucleus are related to familiarity process (Aggleton et al. 2011). Indeed, a three-circuit model of neural oscillations between PFC and MTL *via* thalamus has been proposed (Ketz et al. 2015). The first theta-circuit model emphasized interaction between PFC and hippocampus through theta oscillations (4-8 Hz) to support core functions of the hippocampus in successful memory encoding and retrieval processes (Ketz et al. 2015). The human neuropsychology and neuroimaging literature highlight the involvement of the hippocampus (Bowles et al. 2010; Eichenbaum et al. 2007; Ranganath et al. 2004; Skinner and Fernandes 2007; Yonelinas et al. 2002) and PFC (Wheeler and Stuss 2003) in recollection, hence theta oscillations within a PFC-hippocampus network may be essential for recollection process. In our TMS study then, the external source of beta frequency from rTMS over dlPFC may disrupt the communication between PFC and hippocampus mediated by theta-oscillation, which may be a plausible mechanism by which our rTMS effected a decrease of recollection process. The theta-circuit model of dlPFC and hippocampus interactions in recollection processes will require further investigations and will shed light on the systems-wide oscillatory mechanisms underlying recognition memory. Recording simultaneously from multiple areas and multiple cortical layers in NHPs will further elucidate these issues.

Other studies have also applied the information theory by de-synchronization hypothesis to investigate voluntary memory suppression. A combined fMRI-EEG-TMS study has shown that an increased BOLD signal in left dlPFC (BA 9) was associated with decreased neural synchrony at beta frequency (11-18 Hz) in a directed forgetting task; moreover, stimulation over dlPFC using a slow train of 1 Hz rTMS pulses in the same task boosted cued forgetting-behaviour and induced a further reduction in neural synchrony at 13 Hz (Hanslmayr et al. 2012b). This study also suggests a causal role for beta desynchrony in dlPFC, this time in a directed forgetting paradigm and also suggests a key role of dlPFC in memory control operates *via* downregulating neural synchrony at beta frequency (Hanslmayr et al. 2012b).

Another fMRI study has shown that voluntary memory suppression was associated with an increased activation of dlPFC and a decreased activation of hippocampus (Anderson et al. 2004), which suggests an interaction between dlPFC and hippocampus in regulating memory suppression.

In our human TMS study, familiarity was enhanced in association with rTMS delivered at beta frequency over dmPFC. This result is in line with human neuroimaging meta-analyses suggesting that more activation peaks related to familiarity processing in PFC were found in dmPFC (BA area 8 and 9) (Scalici et al. 2017). Our study not only shows a causal involvement of dmPFC in familiarity-based recognition, but suggests that the mechanism driving familiarity may operate through a mechanism involving neural synchrony at beta frequency. However, unlike for dlPFC, we didn't detect a difference between beta-stimulation and random-stimulation over human dmPFC in familiarity, so our results indicate a potential mechanism of beta coherence in dmPFC modulating familiarity but they don't rule out modulation effects of other frequency. In terms of potential mechanistic explanations for this finding, a thalamo-cortical circuit (involving entorhinal, parahippocampal, and perirhinal cortical areas connected via the medial dorsal thalamic nucleus to PFC) may synchronise within the beta frequency range and it has been proposed that this beta-circuit model may underlie familiarity judgment processes (Ketz et al. 2015). Indeed, the functional role of rhinal cortex, especially perirhinal cortex, has long been associated more with familiarity-based recognition than recollection (Aggleton and Brown 1999; Bowles et al. 2010; Ranganath et al. 2004; Skinner and Fernandes 2007; Norman and O'Reilly 2003). TMS was a viable methodology in our study due to dlPFC and dmPFC both being accessible on the lateral surface of the frontal lobes, but the TMS approach is not viable for targeting deep structures in the medial temporal lobe. Future work in NHPs will of course be able to target microstimulation in via the same electrodes that record LFPs in the medial temporal lobe and record, simultaneously, the effects on multiple other brain regions.

The current project has helped bridge the species divide in understanding the neural mechanisms supporting object recognition memory between macaques and humans. The site of human rTMS stimulation, the frequency, and the stage of stimulation in the task were all inspired directly by study our NHP observations. Our rTMS study found evidence for dissociable functional roles of beta frequency oscillations in different prefrontal regions. As no online EEG/MEG recordings was carried out in combination with our rTMS stimulation the proposed function of beta coherence or even beta oscillations in human prefrontal regions in recollection and familiarity processes needs to be further validated in future studies using, for example, a combined EEG-TMS or MEG-TMS methodology, and/or for a more detailed neuronal level approach, in NHPs using multi-area multi-electrode neuronal recording combined with intervention methodologies including focal ultrasound, reversible pharmacological inactivation, or direct microstimulation through implanted electrodes. Importantly, our study helps further bridge the species divide and confirms that human and NHP PFC show similarity in function and in underlying neural mechanisms supporting recognition memory performance.

Chapter 4. Contributions of prefrontal and temporal lobe cortical areas to recognition memory for novel and familiar visual stimuli in non-human primates

Abstract

The medial temporal lobe (MTL), including hippocampus, perirhinal cortex, entorhinal cortex and parahippocampal cortex, was traditionally viewed as a long-term declarative memory system. Recent lesion studies in animals indicate MTL cortical regions are involved in short-term recognition memory, which is measured using a delayed matching-to-sample (DMS) or a delayed nonmatching-to-sample (DNMS) paradigm. In addition, many neuropsychological and neurophysiological studies have also emphasized the role of the prefrontal cortex (PFC) in maintaining the information about stimuli in working memory. However, the dynamic interaction between PFC and MTL during the encoding, maintenance and retrieval stages of recognition memory has not been fully understood. Here we simultaneously recorded neural activities in dorsolateral prefrontal cortex (dlPFC), perirhinal cortex (PrC), and inferotemporal cortex (IT) in a recognition memory task in the non-human primates (NHPs). In each trial, a central sample image (object picture) was initially shown to the monkey. Then after a delay, either an identical test image or another new test image appeared on the screen, the monkey touched the test image if it matched; or selected a standard non-match button (always a black circle) if the test image did not match the studied sample image. In our study, we also changed the probabilities of cues being sample images, which were either novel (i.e. presented only once through a session) or familiar (i.e. presented repeatedly across trials) to the monkey. We analyzed spike activities from dlPFC and the local field potentials (LFPs) from dlPFC, PrC and IT in the encoding, delay and choice phases of the recognition memory task. During the encoding phase of the sample

image, brief bursts of low-frequency activities (4-20 Hz) were found in all the three regions. An early modulation of induced LFP power was found after familiar sample presentation compared with novel sample presentation. During the delay phase, the brief bursts of low-frequency activities in temporal regions (4-20 Hz) and in dlPFC (4-40 Hz) were detected around the sample image offset. Moreover, previously-presented novel sample images modulated beta-band LFPs while familiar sample images modulated gamma-band LFPs in temporal and frontal regions. During the choice phase, high-beta oscillations (i.e. 30-40 Hz) were persistent in area IT, PrC and dlPFC prior to the presentation of test image and then became weaker when test image appeared. It seems these beta oscillations in frontal and temporal regions were related to maintenance of items in recognition memory. An early LFP modulation by familiar image than novel image has been found in area IT, PrC and dlPFC during the choice phase, which suggests familiar encoded images may have a priority to be retrieved when comparing them with other test stimuli. In addition, spike analysis in dlPFC showed an increase of spike activities after the onset and offset of visual stimuli and after the reward delivery, all along with the increases of beta power. These preliminary analyses indicate that prefrontal and temporal neural activities (particularly beta power) were related with encoding or decoding the visual stimulus in macaque recognition memory.

Introduction

In both humans and NHPs, the medial temporal lobe (MTL) system consists of the hippocampus and underlying entorhinal (EnC) and perirhinal (PrC) cortical regions (both occupy the rhinal cortex), and parahippocampal (PhC) cortices (Squire and Zola-Morgan 1991). In a recent review, Graham et al. have summarized neuropsychological and neuroimaging findings, and concludes that '*there is now significant evidence of a functional specialization in how MTL structures contribute to memory and perception of objects and scenes'* (Graham et al. 2010). For example, Lee et al. have found a double-dissociation between hippocampus and PrC in processing scenes and processing objects in patients (Lee et al. 2005b). In one macaque study, the extent of impaired performance in a recognition memory task is positively correlated with the extent ablations of rhinal cortex but negatively correlated with the extent of hippocampal lesions (Baxter and Murray 2001). This opposite relationship in recognition memory performance shows that hippocampus and rhinal cortex affect recognition memory in different ways (Baxter and Murray 2001). A recent human neuroimaging study also demonstrates a functional separation within the MTL: in a scene-object associative memory task, the PrC is involved in object processing while the PhC supports the scene processing; the hippocampus doesn't show any preference to either scene or object processing but integrates the information from both PrC and PhC during successful retrieval (Staresina et al. 2013). Another human imaging study supports this idea and shows that encoding-retrieval similarity (i.e. the match between encoding items and test items) are related to frontal activities; and more importantly, hippocampus mediates the relationship between the encoding-retrieval similarity and successful recognition performance, which indicates a potential dynamic interaction between the hippocampus and prefrontal cortical regions (Ritchey et al. 2013). Given the evidence of functional specialization of MTL structures above, investigating the *interaction* among MTL structures (e.g. hippocampus, PrC and PhC) and prefrontal cortex (PFC) is crucial to facilitate the understanding of the neural

mechanism of recognition memory.

Investigation of the interaction between MTL and PFC is not a new issue. In a recent review, three MTL-PFC circuit models *via* thalamus have been proposed to support recognition memory underlying different neural oscillations. Specifically, a theta-oscillation circuit model, based on the hippocampus interacting with medial and orbital PFC *via* the anterior thalamus, supports recollection-based memory (i.e. the related contextual information about the previously encountered item/object can be recalled with more details); a beta-oscillation circuit model, based on other parts of MTL regions (e.g. EnC, PrC and PhC regions) except hippocampus interacting with PFC *via* medial dorsal thalamus, supports familiarity-based memory (i.e. a feeling of the item/object has been encountered which generates a feeling of familiarity or knowing but without too much detail); while the visual and parietal cortex interacting with the PFC *via* pulvinar in alpha synchrony for sensory gating. All these three oscillation pathways are top-down modulated by frontal control, indicating a role of PFC upon different MTL structures through oscillatory activities in different aspects of memory processes (Ketz et al. 2015). Another review supports this viewpoint of an integrated memory system operating between PFC and MTL, and highlights that interaction between the hippocampus and medial prefrontal cortical regions is essential for recognition memory of episodes (Warburton and Brown 2010).

In the traditional recognition memory tasks (e.g. delayed matching-to-sample (DMS) and delayed nonmatching-to-sample (DNMS) paradigms) for animals, after viewing the sample image, two test images (one is the same as the sample image and the other one is a completely new image if the tasks use trial-unique stimuli) are presented to the animals. Animals are trained to select the test image which has been encountered in the DMS task; and select the new image in the DNMS task. Both tasks only allow one type of error (i.e. miss errors to targets or false alarm errors) to be investigated. Recently, Basile and Hampton (2013)

introduced a modified recognition memory paradigm for NHPs: after viewing the sample image, animals are either tested in the match trials in which the same test image is presented along with a non-match 'button' (i.e., black circle) or in the non-match trials in which a novel test image is presented along with this non-match 'button'. Animals are trained to select the non-match 'button' if the test image does not match the studied sample image (i.e. nonmatch trials) or touch the test image if it matches (i.e. match trials). A key element of this task design, enabled by the non-match 'button', is that miss errors and false-alarm errors can be distinguished independently (Basile and Hampton 2013). The first goal of this study is to exploit this recognition memory paradigm (developed by Basile and Hampton, 2013) for NHPs to investigate the interaction between different sub-areas of PFC and sub-regions of MTL, theorized to be involved in recognition memory. By using simultaneous neural recordings from 128 electrodes across multiple areas in the macaque temporal and frontal lobes, I primarily aim to determine how these areas interact at the neural level in the encoding, maintenance (i.e. delay period) and choice phases of recognition memory. As different MTL structures are proposed to be modulated *via* frontal control in recognition memory (Ketz et al. 2015), I hypothesized that PFC would interact with MTL brain regions *via* different neural oscillations in the encoding, delay and choice phases of recognition memory task.

Many neural populations in the ventral temporal lobe demonstrate reduced activities to the exposure of repeated presentations of stimuli (i.e. familiar stimuli). Such adaption has been termed as familiarity effect (Feuerriegel 2016; Ringo 1996). Ringo initially proposed that these decreased firing amplitudes of neurons to familiar stimuli benefited the later processing of novel stimuli in the inferotemporal (IT) cortex (Ringo 1996). IT is an unimodal area in the ventral visual stream (Tompa and Sáry 2010), and includes the unimodal visual areas TE and TEO in macaques and corresponds to middle and inferior temporal gyri in humans (Fujita 2002). It is widely acknowledged that IT is involved in object perception (Brown 1996; Tanaka 1996), including encoding moderately complex features of visual

objects, such as sizes (Vighneshvel and Arun 2015), textures (Zhivago and Arun 2014) and depths (Janssen 2000; Apurva Ratan Murty and Arun 2015). Other studies show that activities of IT neurons can be shaped by visual experience (Brown 1996; Tompa and Sáry 2010). For example, familiar and novel images induce different changes of IT responses. Li et al. found decreased neural responses in anterior IT to the novel image along with its repetitions (Li et al. 1993). Xiang and Brown further confirmed this point of view and found an approximate 40% of neurons in anterior IT (i.e. TE area) demonstrated decremental spike magnitudes to both familiar and recent images (Xiang and Brown 1998). Image familiarization can also sharpen the response dynamics of IT neurons. For instance, Freedman et al. found IT neuronal stimulus selectivity was stronger for visual stimuli presented at the trained orientation than at the rotated orientation (Freedman 2005), indicating IT neural activities can be modulated by explicitly training. Anderson et al. demonstrated that familiar images induced larger amplitudes of local field potentials (LFPs) and smaller amplitudes of multiunit spike activities in IT (Anderson et al. 2008). Consistent with the previous viewpoint from Freedman et al. (2005), the greater LFP activities induced by familiar stimuli could be modulated by rotating the same stimuli in different angles, for example, familiarity effects were weakened by image rotations (Anderson et al. 2008). A recent study further showed that the putative inhibitory IT neurons responded more strongly to familiar images than the putative excitatory IT neurons in a serial visual discrimination task (Meyer et al. 2014). Modulations of IT activities by image familiarization may leave IT neurons ready for processing the ensuing images in a rapid way (Anderson et al. 2008; Freedman 2005; Meyer et al. 2014).

IT is reciprocally connected to different sub-regions of MTL (Suzuki and Amaral 1994a, 1994b). For instance, the PrC receives inputs from the IT cortex (Brown 1996). Xiang and Brown have found that neurons in macaque temporal cortical areas like IT, PrC and EnC, demonstrate reduced spike activities to repeated stimuli rather than to novel stimuli (Xiang

and Brown 1998), although IT neurons demonstrate enhanced activities to the second stimuli in an "ABBA" paradigm, where a target stimulus (A) is followed by a series of other stimuli (B, C,…) and the monkeys are trained to respond when A is repeated (Miller and Desimone 1994; Brown 1996). The role of IT in recognition memory tasks has been extensively investigated. Initially in the DMS task, Fuster and Jervey have shown macaque IT neurons demonstrate larger spike activities during maintenance of the encoded stimuli (Fuster and Jervey 1982). In another single-cell recording study, a consistent spike firing pattern in macaque IT is found during the delay period of recognition memory task (Miyashita and Chang 1988). In a modified DMS task with multiple intervening items between the sample and test stimulus, half of the recorded IT neurons preserve their responses to the test stimulus when it matches the sample stimulus; while other IT neurons demonstrate suppressed responses to the matched test stimulus following intervention (Miller et al. 1993); in contrast, sample-selective activities in dlPFC neurons are maintained during the delay period even when other intervening stimuli present during the delay (Miller et al. 1996). These lines of evidence suggest activities in IT are more involved in processing stimulus information and may be modulated by frontal control during recognition memory (as Miller et al. suggested in their studies). It has been found that macaque ventromedial, orbitofrontal, and anterior cingulate but not dorsolateral prefrontal cortex demonstrate spike activities related to information of encoded images which represent stimulus familiarity (Xiang and Brown 2004). Currently, there is no clear evidence on how the familiarity information of remembered stimulus is transferred from IT to PrC and from IT to other PFC regions in recognition memory.

In order to understand how the familiarity effect benefits recognition memory performance and its relevant neural substrates, it is of importance to investigate the interaction among IT, MTL and PFC during the encoding and maintenance of recognition memory. In our study, we changed the probabilities of cues being samples, some of which

were completely novel to the animal while others were repeatedly presented over trials so the animal became more and more familiar with them during a session. I would investigate whether this image familiarity had any effect on recognition memory performance and related neuronal activities in those regions. The second goal of this study was to investigate whether neural activities within MTL and PFC areas and their interactions would differ depending on whether individual discriminations were being based upon novel or familiar images. As previous electrophysiological evidence indicated IT could be modulated by frontal control (Miller et al. 1993, 1996), I hypothesized that neurons in IT would demonstrate fewer interaction with PFC if the sample and test stimulus matched (i.e. match trials) but would show stronger interaction with PFC if both stimulus differed (i.e. nonmatch trials). As the sample stimulus became more and more familiar to the animal over trials, the difference of the above interactions between match and nonmatch conditions would decrease.

Materials and Methods

Subject

Neural data was recorded in one young adult female macaque monkey (*Macaca mulatta, age 8 years, weight 10-13 kg*). All animals in our lab are socially housed (or socially housed for as long as possible if later precluded, for example, by repeated fighting with cage-mates despite multiple regrouping attempts) and all are housed in enriched environments (e.g. swings and ropes and objects, all within large pens with multiple wooden ledges at many levels) with a 12hr light/dark cycle. The NHP always had *ad libitum* water access 7 days/week. Most of its daily food ration of wet mash and fruit and nuts and other treats was delivered in the automated testing/lunch-box at the end of each behavioral session (this provided 'jack-pot' motivation for quickly completing successful session performance;

supplemented by trial-by-trial rewards for correct choices in the form of drops of smoothie delivered via a sipping tube) and this was supplemented with fruit and foraging mix in the home enclosure. All animal training, array implantation surgery, and experimental procedures were performed in accordance with the guidelines of the UK Animals (Scientific Procedures) Act of 1986, licensed by the UK Home Office, and approved by Oxford's Committee on Animal Care and Ethical Review.

Surgical procedure

The details of *surgical procedures* can be found in Chapter 2. After the basic behavioural and initial task training phase was complete the animal first received a titanium head-post, implanted posteriorly and secured to the cranium with titanium cranial screws through the legs of the post; the reflected skin and galea was sutured and the wound closed around the base of the head-post. Targeted brain areas were chosen on the basis of previous lesion literature which confirmed the areas are relevant in recognition memory task, and their locations were visually guided by the surgeon in surgery. During the implantation surgery, one 64-electrode Utah array (the electrodes were arrange on a 8 × 8 grid embedded in silicone) was subdurally inserted into area TE, and the other two 32-electrode Utah arrays (the 6 × 6 grid of silicone microelectrodes) were inserted into PrC (area 35/36) and dlPFC (area 9/46), separately. All the microelectrodes were made of platinum (Pt). These three arrays were all connected to one pedestal (with 128 output channels) affixed externally to the cranium. The four corner electrodes of this pedestal were 2 reference electrodes and 2 ground electrodes. Recording sites of TE array, PrC array and dlPFC array in the NHP were shown in Figure 1. Another 64-electrode Utah array (the 8 × 8 grid of silicone microelectrodes) was subdurally inserted into area vlPFC (area 45), and the other two 32-electrode Utah arrays (the 6 × 6 grid of silicone microelectrodes) were inserted into area OFC (area 11/13) and temporal pole, separately. All these microelectrodes were made of platinum-iridium mix. These three

arrays were all connected to a second pedestal (with 128 output channels) also affixed externally to the cranium. Unfortunately, the neural signals from vlPFC, OFC and temporal pole arrays could not be obtained due to accidental disconnection of the pedestal connecting to those Utah arrays from the cranium (i.e. pulled off by the animal playing with loosened pedestal before we had completed preparations for surgical stabilization of the pedestal which were underway). All the electrode lengths on all arrays were 1.0 mm and the inter-electrode separation within arrays was 0.4 mm. After array implantation surgery, two reference wires connecting to each of the two pedestals were left under the dura, and both dura and bone flap were sutured back and covered with the skin.

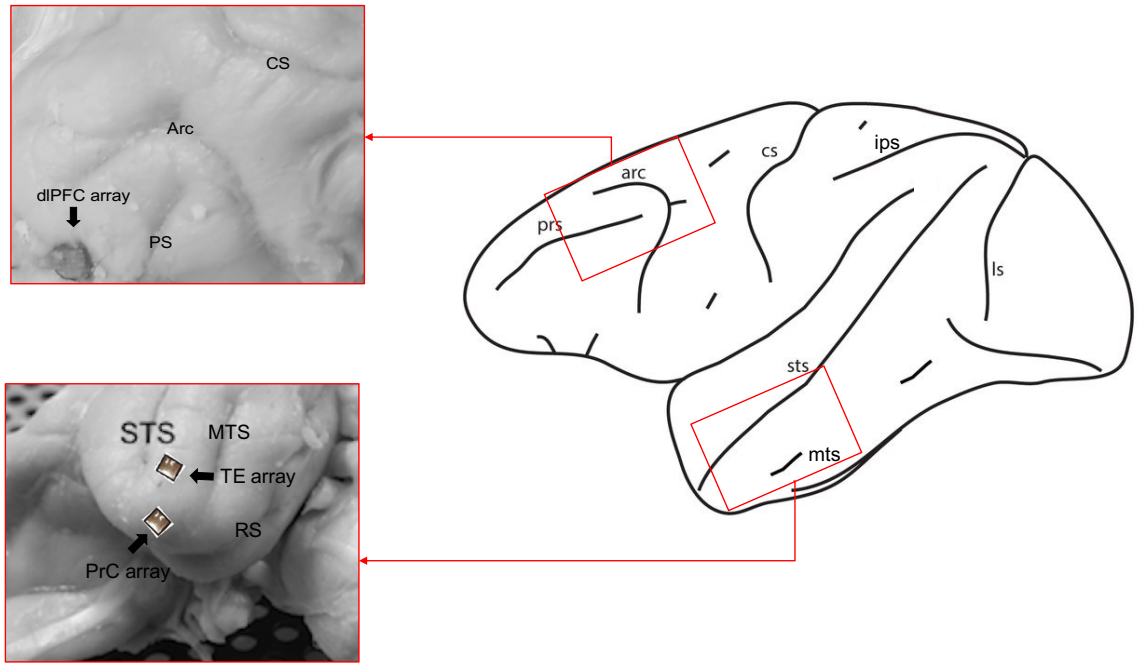


Figure 1. *Recording sites from TE array, PrC array and dlPFC array in the lateral view of the NHP brain. NHP recording sites (shown in the upper red square) using the Utah array of dlPFC was above the principle sulcus (PS) and anterior to the arcuate sulcus (Arc). NHP recording sites (shown in the lower red square) using the Utah array of TE was between the superior temporal sulcus (STS) and anterior to the medial temporal sulcus (MTS), and recording sites using the Utah array of PrC was below the STS and above the rhinal sulcus (RS).*

Task stimuli and apparatus

The object recognition memory task was programmed using Turbo Pascal (Borland), run under DOS on a desktop PC. Visual stimuli used in the task were clip-art images in colour, which were presented on a 20.1" colour touch-sensitive screen (TFT LCD TS200H GNR). Those clip-art images used in the task were from a large pool of several thousand unique images. Each image subtended 5° of visual angle in width and 5° in height to the subject when presented on the screen. The sample image was always presented on the right top of the screen, positioned +9 ° horizontal and -9 ° vertical from the center of the screen. The test images were presented on the right bottom of the screen: one was positioned 0 ° horizontal and +3 ° vertical from the center of the screen; and the other one was positioned +17 ° horizontal and +3 ° vertical from the center of the screen. The background colour to the screen was white. In each session of recordings, images were randomly chosen from the pool without replacement and were not re-used on the other recording days.

The animal was seated in a primate chair (Rogue Research Inc.) in front of the touch screen with its head-fixated and whilst it performed the recognition memory task in a magnetic-shielded, and partially sound-attended, testing-box. A window in the front of the chair provided its access, both to the touch-screen itself and also to a touch-sensitive knob which we refer to as a 'key-touch' which was positioned low down in front of the touch screen; the animal had to steadily hold the keytouch at various times in each trial (to control for arm movement/position whilst it waited for stimuli, looked at stimuli, and waiting for a visual cue to release keytouch and touch the screen to make a choice). The distance between the monkey and touch screen was fixed at 50 cm enabling the animal to touch the screen easily. An infrared camera was used to monitor the general status of the monkey in the box. A peristaltic pump device located on top of the box fed smoothie reward through a tube and

to a spout positioned in the vicinity of the animal's mouth. Below the screen was also an automated lunch-box which contained the majority of the animal's daily meal (wet mash and fruits and nuts etc.) and which opened immediately at the end of the task.

Behavioral Tasks

In each trial, the animal initiated the task by holding the key-touch when cued to do so by a small red circular keytouch cue (located towards upper centre of screen; Figure 2) presented on the screen. The NHP was required to keep holding the keytouch device through a variable delay of 1000-1500 ms (if the keytouch hold was broken the trial aborted) after which a central sample (object image) appeared behind the red key-touch cue. The NHP was required to keep holding the keytouch device through another variable delay of 1000-1500 ms (again, if the keytouch hold was broken the trial aborted) after which the red keytouch cue disappeared which was the cue to the animal it could release its hand from the keytouch at which point the delay (1000ms) between sample and choice-phases began (the maximal time for releasing key-touch was 5000 ms else the trial aborted and the animal received a time-out for 10 s). Then after the 1000 ms delay period another red keytouch cue appeared, this time in the bottom of the screen (close to, and equidistant, from where the two choice items would appear) and animal was required to hold the key-touch again. The NHP was again required to keep holding the keytouch device through a variable delay of 1000-1500 ms (if the keytouch hold was broken the trial aborted) after which two choice stimuli appeared (one an object image and the other a black circle, left-right randomized between trials). The NHP was required to keep holding the keytouch device through another variable delay of 1000-1500 ms (again, if the keytouch hold was broken the trial aborted) after which the red keytouch cue disappeared which was the cue to the animal that it could release holding the keytouch and now make a choice to the touchscreen to either the object test-image stimulus or to the black circle stimulus. The object stimulus was either the identical stimulus to the sample seen

earlier in the trial or it was not identical to the sample. The animal was rewarded by delivery of 10 ml of smoothie for touching the test-item image if it matched the sample image (these we refer to as 'match trials'), or it was rewarded for selecting the standard 'non-match button' (i.e. the black circle) if the test-item was a non-match (these we refer to an 'non-match trials'). The next trial started after a 3000 ms inter-trial interval after a correct response, or after a 10 s 'time-out' after any kind of error response (or after any failure to hold keytouch for the required time, or after failure to release when required). A schematic of the recognition memory task is illustrated in Figure 2. Accordingly on *match trials* the animal could either make a correct response ('hit') or an incorrect response ('miss') whereas on *non-match trials* the animal could either make a correct response ('correct rejection') or an incorrect response ('false alarm'). The use of the black circle allowed hit/miss rate to be calculated independently of correct rejection/false-alarm rate; in this way the paradigm is similar to one previously use by Basile and Hampton (Basile and Hampton 2013). In order to explore the effects of image familiarization on both behavioural performance and neural responses throughout recognition memory, we also varied the degree to which stimuli were either familiar or novel in the session (typically there were up to 80 pairs of novel stimuli that were trial-unique in each session, and six other familiar stimuli, grouped into three pairs, that repeated many times through the session).

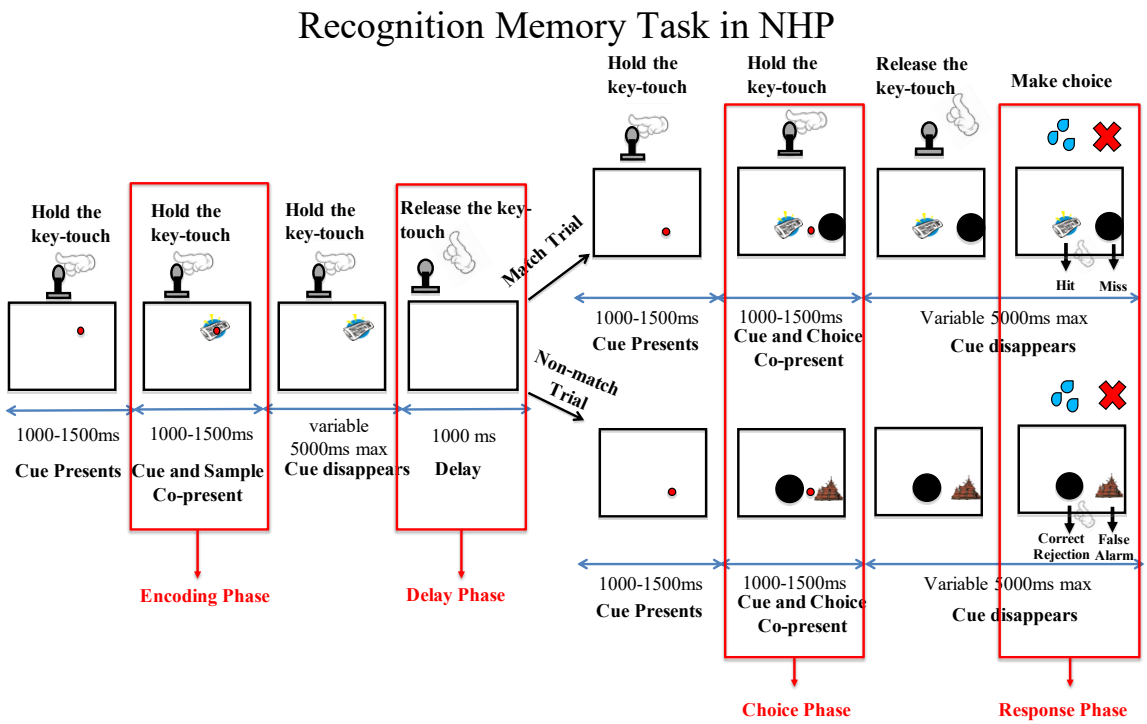


Figure 2. *Recognition memory task in NHP. The animal initiated the task by holding the key-touch within a variable time of 1000-1500 ms, then a sample image was shown on the screen below the red cue (encoding phase). After the red cue disappeared, animal released the key-touch and experienced a delay period of 1000 ms (delay phase). After that, animal was trained to hold the key-touch to wait for the choice stimuli. Two choice images, either an identical image or a novel image along with a black circle were shown on the screen (choice phase). After the red cue disappeared, animal released the key-touch and touched the stimuli to make a choice (response phase). The highlighted sample, delay, choice and response phases were selected to be time windows for neural data analysis.*

Electrophysiological Recordings

Data were recorded simultaneously from the 64-electrodes in the microelectrode array implanted in TE, and the 32-electrodes in PrC and the 32-electrodes in dlPFC throughout the

recognition memory task performance. Neural signals from each microelectrode were amplified, digitized at 30 kHz using a 256-channel Cerebus™ Neural Signal Processor (Blackrock Microsystems), and then sorted off-line. Both the spike analysis and the local field potentials (LFPs) activities were analyzed with the MATLAB (R2017b, MathWorks), Wave_clus toolbox (*https://www2.le.ac.uk/departments/engineering/research/bioengineering/neuroengineering-lab/spike-sorting*), FieldTrip toolbox (*http://www.fieldtriptoolbox.org*, details see Oostenveld et al. 2011), Chronux Toolbox (*http://chronux.org*) and custom-written scripts.

Signal Analysis

The NHP performed, on average, 75 trials (including both trial-unique and repeated stimuli) per day; the total average session duration was 45 minutes. In this study we analysed data recorded over 29 consecutive sessions (these were not always on consecutive days as the NHP always had at least two rest days/week without testing) around 8 weeks after the array implantation. The NHP had learnt the task in full prior to array implantation. I analyzed the local field potentials (LFPs), single-unit (spikes), and multi-unit activities from the three Utah arrays in TE, PrC and dlPFC throughout the encoding, delay, choice and response phases of recognition memory task. To investigate how the activities of IT was modulated by PFC and whether this modulation could be further modulated by sample image familiarity (i.e. to test the second hypothesis), I calculated the induced LFP power spectra for TE, PrC and dlPFC in each task phase, and then compared the difference of LFP activities in those areas between novel sample condition and familiar sample condition across different task phases. To investigate how PFC and MTL brain regions interacted *via* different neural oscillations during recognition memory (i.e. to test the first hypothesis) and how the interaction could be modulated by sample image familiarity (i.e. to test the second hypothesis), I calculated the LFP-LFP coherence for each brain pair (i.e. TE-PrC, TE-dlPFC, PrC-dlPFC) in each task

phase, and then compared LFP-LFP coherence for each brain pair between novel and familiar sample conditions across different task phases. All the data were analyzed from successfully completed trials.

Spike Sorting

Spike detection and sorting was completed using the toolbox Wave_clus (Quiroga et al. 2004). In the 128 recorded channels, 3 units in TE and 25 units in dlPFC (including both single- and multi-units) were sorted in total across all the recorded days. It should be noted that each of the above units appeared in some, rather than all, of the recorded sessions.

LFPs pre-processing and spectral analysis

We investigated the power of the induced LFP responses throughout the NHP recognition memory task. A notch filter, the second-order infinite impulse response (IIR), was applied to the raw data signals, to remove the power from line noise (i.e. 50 Hz) and its harmonics (i.e. 100, 150 Hz). Then the data signals were down sampled from 30 kHz to 1 kHz.

To obtain the power spectrums of LFPs for each of the 128 channels, a time-frequency decomposition analysis based on Morlet wavelet transform was performed. First of all, the pre-processed LFP signals were convolved with a complex Morlet wavelet, which is defined as follow:

$$\Psi(f,t) = \frac{1}{(\sigma^2\pi)^{1/4}} e^{-t^2/2\sigma^2} e^{2\pi i f t}$$

The Morlet wavelet function consists of a wave component $e^{2\pi ift}$ as characterized by the target frequency f_0, and a Gaussian component $e^{-t^2/2\sigma^2}$ as characterized by its standard deviation σ. These two components are connected by the wavenumber $n_c = 2\pi f\sigma$ which is

approximately the number of cycles of the wavelet and is related to its duration. The wavelet function of higher frequencies would have shorter duration, and vice versa. The wavenumber is set to 7, as the default choice adopted in the FieldTrip Toolbox. The result of the transition would take the form:

$$F(t) = \sum_{f} A(f,t) * \Psi(f,t)$$

Where $F(t)$ is the input LFP signal, and $A^2(f, t)$ is the instantaneous power at frequency f and time t, the quantity of real interest in the transition. The frequency range in LFP spectral analysis was chosen to start at 4 Hz (to exclude slow-wave LFP components) and terminate at 120 Hz, in step of 1 Hz.

For the 128 channels (i.e. 64 channels in TE, 32 channels in PrC, and 32 channels in dlPFC), the induced power spectra from LFPs were limited to data segments which contained completed correct trials and inter-trial intervals (ITIs). In the recognition memory task, LFPs in the sample phase (i.e. sample image displayed on the screen for 1000-1500 ms while the macaque held the key-touch), delay phase (i.e. 1000 ms), and choice phase (i.e. choice images on the screen for 1000-1500 ms when the macaque held the key-touch) of both match and nonmatch trials, were selected for analysis. In each trial, LFPs in each task phase from 1000 ms (as a baseline) before stimulus onset until 1000 ms after stimulus onset were analyzed. The LFP power around the stimulus onset was calculated as follows:

4) Wavelet transform of the signals around the stimulus onset and during the ITI baseline (i.e. a 1000 ms segment) were calculated, yielding $O_{stimulus}$ *and* $O_{baseline}$;
5) The power of the stimulus was calculated as $P_{stimulus} = O_{stimulus}^2$, and the mean power of the baseline was calculated as $P_{baseline}$ = avg($O_{baseline}^2$);
6) The LFP power of the stimulus was calculated as a ration of $P_{stimulus}$ to $P_{baseline}$, i.e.:

$$LFP\ power = \frac{P_{stimulus}}{P_{baseline}} = \frac{{O_{stimulus}}^2}{\text{avg}({O_{baseline}}^2)}$$

As both the power of the stimulus and the baseline have the same units (i.e. μV^2), the above calculated LFP power is dimensionless. Then LFP power in TE, PrC and dlPFC were averaged across corresponding channels and were combined cross sessions.

Timing of spike and LFP responses

To investigate the timing of spike activities and LFP power throughout the recognition memory task, the channels with both significant unit and LFP responses were selected. For unit responses, the instantaneous firing rate was smoothed by convolving the spike counts with a Gaussian kernel with σ =25 ms. The instantaneous LFP power in the theta, alpha/beta and gamma band were calculated by using the squared magnitude of the Hilbert transform of the average LFP filtered at 4-8 Hz (theta), at 12-30 Hz (alpha/beta) and at 40-100 Hz (gamma), individually. The smoothed firing rate and the grand averages of instantaneous theta, alpha/beta and gamma power were calculated across different phases of recognition memory task.

Coherence Analysis

Coherence is a measure of correlation between two continuous signals as a function of frequency. When a coherence value is equal to 1, it indicates that the two signals have a constant relationship; otherwise, a coherence value of 0 indicates the two signals don't have any relationship. It should be noted that coherence is different from phase-locking value as it is a measure of the extent to which one time-series signal can be linearly-predicted from another time-series signal (Lepage and Vijayan 2017). Srinath and Ray further show that, by randomly changing amplitudes of two simulated signals while keeping their phase difference

consistent, coherence between the two signals is decreased whereas the phase-locking value is unaltered (Srinath and Ray 2014), indicating coherence depends upon their amplitudes in addition to their phase difference. Calculation of coherence of two continuous signals is defined as below (algorithms are taken from Chronux Toolbox, *http://chronux.org*):

$$Cxy(f) = \frac{Sxy(f)}{\sqrt{Sx(f)Sy(f)}}$$

Where *Sx(f)* and *Sy(f)* represent the auto-spectra, and *Sxy(f)* represents the cross-spectrum of the two signals x and y. Both auto-spectra and cross-spectra are averaged across trials before calculation on coherence. Data from 200 ms (as a baseline) before stimulus onset until 800 ms after stimulus onset (to avoid the spectral leakage of LFP power when calculated near the margin of a 1000 ms time-window) in each trial were included in the coherence analysis, provided a time window of 1000 ms. LFPs in TE, PrC and dlPFC were firstly averaged across corresponding channels, and then in each recorded session, trial-averaged coherence between TE and PrC, between TE and dlPFC, and between PrC and dlPFC were calculated based on the above algorithm in the novel condition (i.e. sample images only appearing once to the animal within a session) and the familiar condition (i.e. sample images appearing multiple times to the animal within a session) during different phases of recognition memory task (i.e. sample, delay and choice phase).

Statistical analysis of induced LFP power spectra of each recorded brain region and LFP-LFP coherence across three regions between the novel and familiar conditions in different phases of recognition memory task

To investigate (sample) image familiarity on neural activities throughout the recognition memory task, we compared neural signals in the encoding, delay and choice phases of the task between the novel and familiar conditions.

To test for statistical significance of differences of the induced LFP power spectra between the novel and familiar conditions in difference phases of recognition memory task, we performed a nonparametric permutation test, with the median difference between the above conditions as our test statistic. The non-parametric permutation test is an assumption-free method without prescribing underlying distributions (Maris and Oostenveld 2007). As described above in *LFPs pre-processing and spectral analysis*, channel-averaged LFPs across different brain areas were calculated. In each trial, the time window of both the novel and familiar conditions in each task phase for nonparametric permutation test was 0-800 ms (i.e. time zero was the stimulus onset), to avoid the spectral leakage of LFP power when calculated near the margin of a 1000 ms time-window. In each task phase (e.g. encoding, delay, choice), the null hypothesis of this test was assumed that, for each frequency and time bin, there was no significant difference of the LFP power when comparing the observed median difference between the two conditions (i.e. novel and familiar) against a reference distribution. The permutation test for the LFP data was performed in the following steps:

1. The observed median difference between the two conditions was obtained for each time and frequency bin, i.e. $D_{t,f}$;
2. A reference distribution for each time and frequency bin was obtained by performing 10,000 permutations on trial labels to randomly assign the two conditions. That is, each time and frequency bin had its own reference distribution, in the format of $[d_{t,f}] = (d_{t,f,1}, d_{t,f,2}, d_{t,f,3}, \ldots d_{t,f,10000})$.
3. For each time and frequency bin, its $D_{t,f}$ was compared to its own refence distribution (i.e. $[d_{t,f}]$). This bin would be selected if the observed median difference was either larger than the 97.5th or smaller than the 2.5th percentile of its reference distribution.
4. All these selected time and frequency bins were then clustered in connected sets based on adjacency in time and frequency.

6. We calculated the sum of the median differences within each cluster, and kept only the largest cluster (with the largest sum of the median difference) in the cluster-level statistics (Maris and Oostenveld 2007).
7. The above nonparametric permutation procedure was performed separately for each of the brain regions (e.g. TE, PrC and dlPFC) and separately for each task phase (e.g. sample, delay and choice phase).

It's acknowledged that as comparisons between observed data and permutated data have been carried out in all the time and frequency bins separately, multiple comparison problem still exists in this method. To be reasonably conservative, I picked the largest cluster in the real data among other clusters, although by doing so, the sensitivity for detecting smaller clusters is reduced.

To test for statistical significance of differences of the LFP-LFP coherence across different brain areas between the novel and familiar conditions in difference phases of recognition memory task, we also performed a nonparametric permutation test, with the median difference between the above conditions as our test statistic. As described above in *coherence analysis*, trial-averaged and channel-averaged coherence across different brain areas were calculated in each session. For each brain pair, LFP-LFP coherence was then averaged in theta-band (4-6 Hz), alpha/beta-band (12-35 Hz) and gamma-band (35-120 Hz). In each session, the calculated coherence data from 200 ms before stimulus onset until 800 ms after stimulus onset was put into nonparametric permutation test (i.e. providing a time window of 1000 ms). In each task phase (e.g. encoding, delay, choice), the null hypothesis of this test was assumed that, for each time bin, there was no significant difference of the LFP-LFP coherence when comparing the observed median difference between the two conditions (i.e. novel and familiar) against a reference distribution. This reference distribution was obtained by performing 10,000 permutations on session labels to randomly assign the two conditions. A time bin would be selected if its observed median difference was larger than

the 97.5th or smaller than the 2.5th percentile of its permutated data ($p < 0.05$, two-tailed). Then the selected time bins were clustered in connected sets on the basis of temporal adjacency. The above nonparametric permutation procedure was performed separately for each brain pair (e.g. TE- PrC, TE-dlPFC, and PrC-dlPFC) and separately for each task phase (e.g. sample, delay and choice phase).

Results

Behavioural Outcome

A linear regression analysis for the behavioural data shows that accuracy in match trials (i.e. hit-rate) but not in non-match trials (i.e. correct rejection rate) positively correlated with increased familiarity of sample images ($p < 0.05$, Figure 3a); response time decreased with image familiarity in both hit and correct rejection trials ($p < 0.05$, Figure 3b). This indicates image familiarization benefited the responses in match trials but had less impacts on non-match trials.

The equal-variance signal detection (EVSD) model, based on signal detection theory, assumes that novel and old items are represented by two Gaussian functions with equal and unit variance along the dimension of memory strength, in which old-item distribution has a higher memory strength compared to the new-item distribution. The outputs of this model are criterion and d prime (as shown in Figure 3c). Criterion is defined as whenever individual internal response is greater than criterion, subject considers it as an old item; or vice versa. d prime (d') is a discriminative index, which is calculated as the distance from new-item and old-item distributions, reflecting the discrimination between old and new items. After fitting the two types of recognition errors (i.e. miss rate, false alarm rate) into this model, we found that d' significantly increased with image familiarity ($p < 0.05$, Figure 3d); but image

familiarity had no effects on response criterion ($p > 0.05$, Figure 3d). The outcomes from EVSD model further demonstrated image familiarization enhanced discrimination abilities in macaque recognition memory.

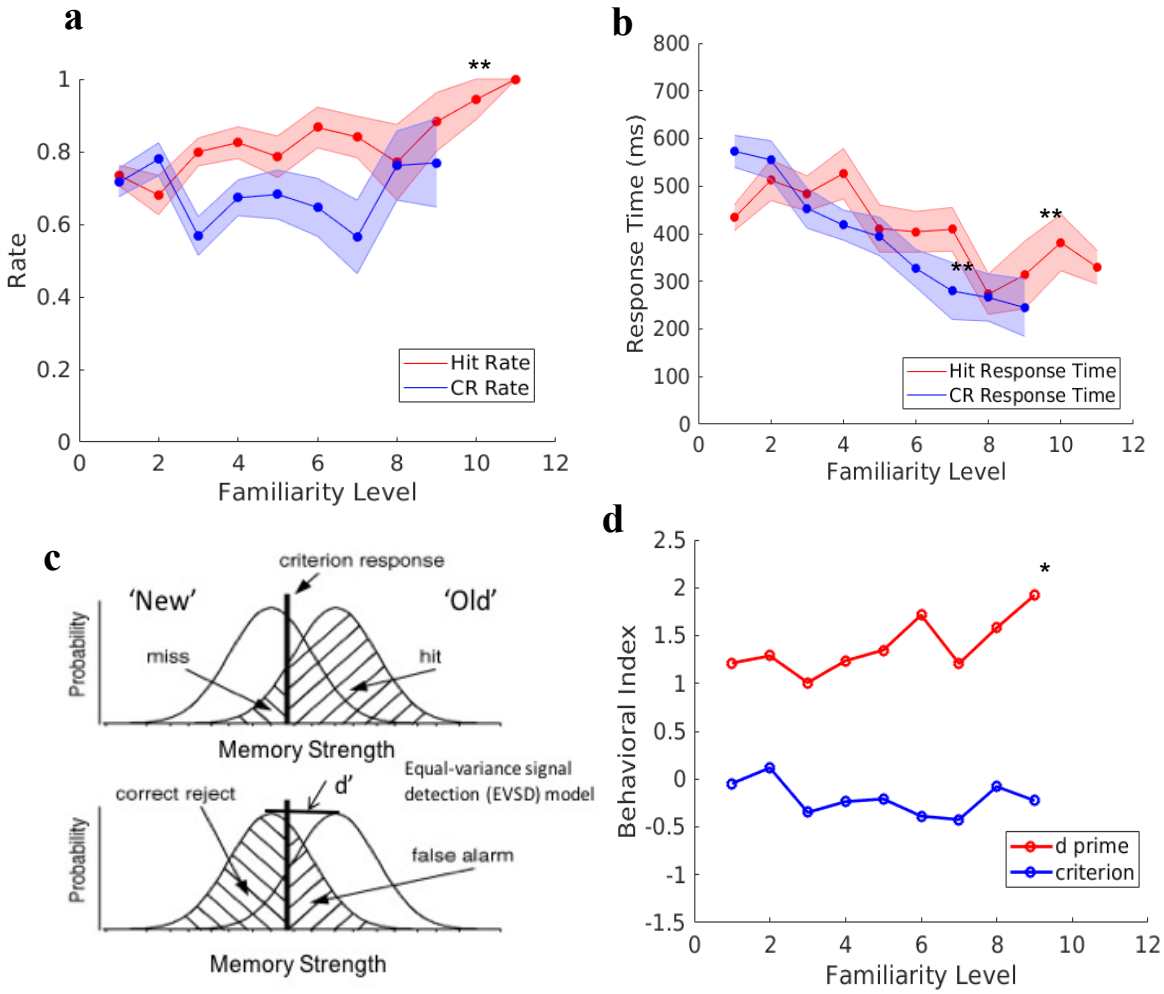


Figure 3. *Behavioural results in recognition memory task. Image familiarization enhanced hit rate but not correct rejection rate (panel a); decreased reaction time in both hit and correct rejection trials (panel b); and increased d' but not response criterion (panel d). * indicates p < 0,05, and ** indicates p < 0.01.*

Modulations of induced LFP spectral power by image familiarity in TE, PrC and dlPFC throughout the recognition memory task

In this LFP spectral power analysis and the below LFP-LFP coherence analysis, the novel condition was defined as trials with the sample image presenting for the first time within a recorded session, and the familiar condition was defined as trials with the sample image presenting multiple times within a session. Data from 29 recorded sessions were put into LFP analysis for each brain region and LFP-LFP coherence analysis for each brain pair (details were described in methods).

In the encoding phase, we have observed an increased LFP power ranging from 4-20 Hz after the onset of sample image in TE, PrC and dlPFC. These brief bursts lasted roughly 300-400ms in both novel (Figure 4, left panel) and familiar conditions (Figure 4, middle panel). It has been observed the power of these brief bursts of low-frequency activities were stronger in dlPFC than in TE and PrC in these two conditions. A nonparametric permutation test (two-tailed) was applied to compare the LFP power in TE, PrC and dlPFC between the novel and familiar conditions (Figure 4, right panel). The test revealed that in TE, two clusters of significant modulations by image familiarity were observed immediately and then around 600 ms after the sample image onset: a gamma power ranging from 70-120 Hz appearing immediately after the presentation of sample image was significantly higher for familiar condition; while a beta power at around 30 Hz occurring at 600 ms was significantly higher for novel condition. In PrC, another two clusters of significant modulations by image familiarity were detected between 100-400 ms and then around 600 ms after the sample image presentation: a low-frequency activity (powering ranging from 10-15 Hz) appearing at 100-400 ms was significantly higher for familiar condition; while at 600 ms, LFP power ranging from 30-40 Hz was significantly higher for novel condition. In dlPFC, a gamma power ranging from 70-120 Hz appearing immediately after sample image onset, which was significantly higher for familiar condition; while still at 600 ms, a gamma power ranging from 50-70 Hz was significantly higher for novel condition.

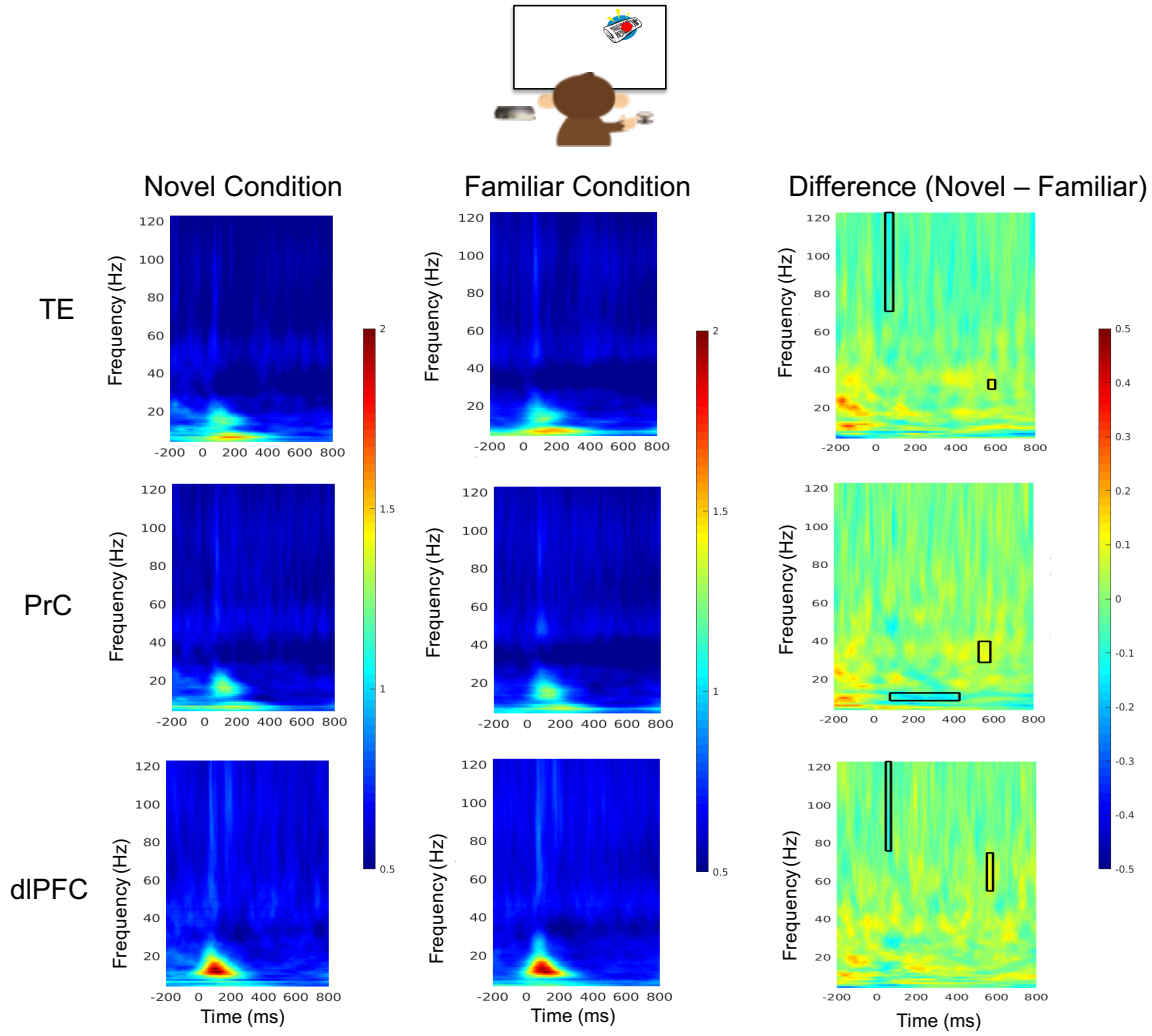


Figure 4. *Induced LFP power and LFP power difference between the novel and familiar conditions after sample image onset in TE, PrC and dlPFC. An increased power ranging from 4-20 Hz after the sample onset in the three regions was found in both novel (left panel) and familiar conditions (middle panel). The significant difference between the two conditions in the three regions were indicated by black squares in the right panel (positive values: Novel > Familiar, negative values: Familiar > Novel).*

In the delay phase, an increased power ranging from 4-20 Hz in TE and PrC, and an increased power ranging from 4-40 Hz in dlPFC were detected around 100-200 ms prior to the offset of sample images (i.e. start of the delay). These brief bursts in those three regions

lasted roughly 300ms for both novel (Figure 5, left panel) and familiar conditions (Figure 5, middle panel). A nonparametric permutation test (two-tailed) revealed that two clusters of significant modulations by image familiarity were found in all the three regions (Figure 5, right panel). In both TE and dlPFC, a gamma power (60-120 Hz in TE and 70-90 Hz in dlPFC) appearing around 100-200 ms relative to delay onset was significantly higher for familiar condition; while at 400 ms, brief bursts of beta power (30 Hz in TE and 30-40 Hz in dlPFC) were found to be significantly higher for novel condition. In PrC, around 400 ms relative to delay onset, power ranging from 20-40 Hz was significantly higher for novel condition; while at 700 ms from the delay onset, a gamma power ranging from 70-120 Hz was significantly higher for familiar condition.

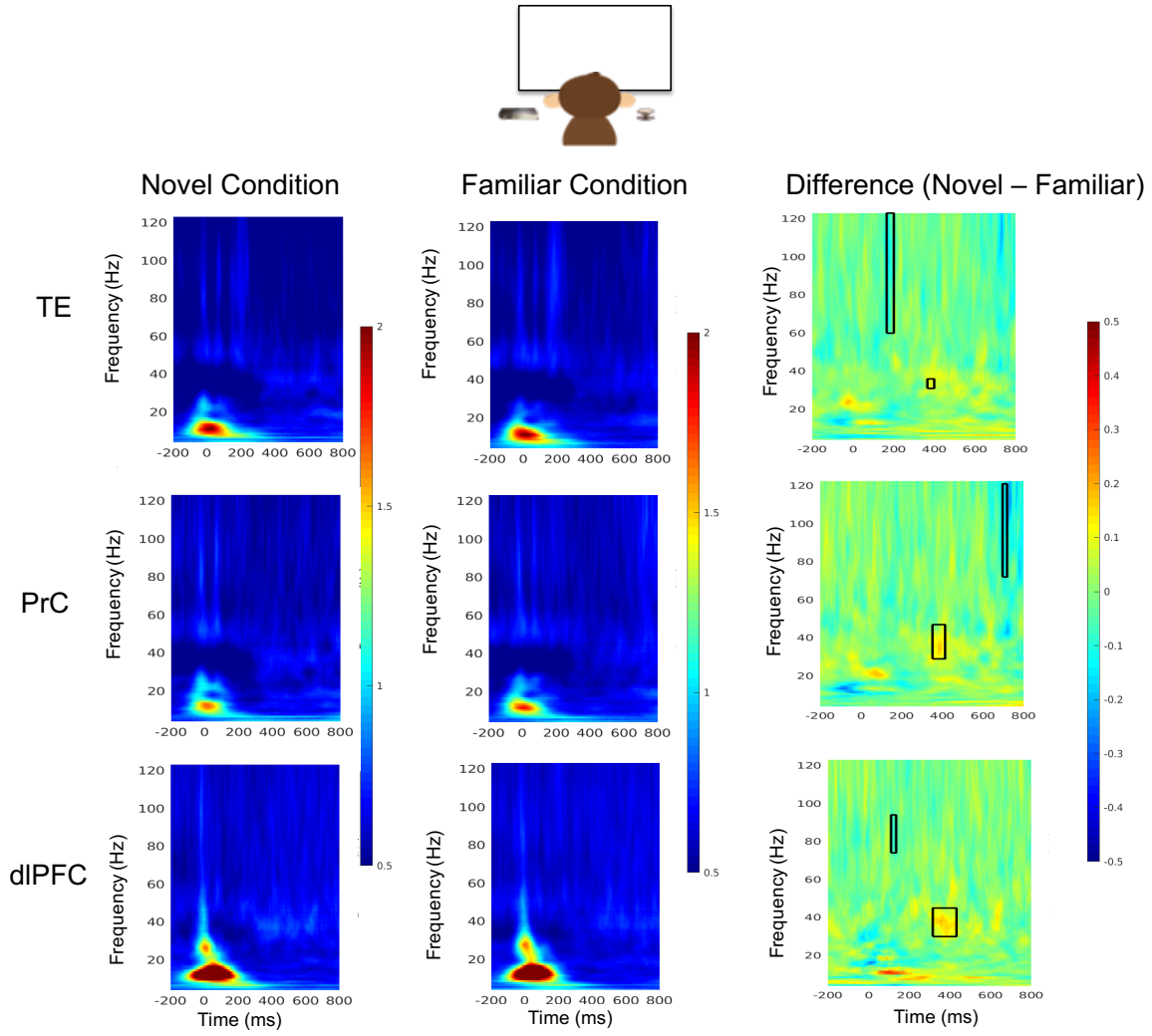


Figure 5. *Induced LFP power and LFP power difference between the novel and familiar conditions after sample image offset (delay onset) in TE, PrC and dlPFC. Increased power ranging from 4-20 Hz in TE and PrC and increased power ranging from 4-40 Hz in dlPFC were detected around 100 ms prior to the start of delay in both novel (left panel) and familiar conditions (middle panel). The significant difference between the two conditions in the three regions were indicated by black squares in the right panel (positive values: Novel > Familiar, negative values: Familiar > Novel).*

In the choice phase of match trials (i.e. sample image was the same as test image), low-frequency bursts of 4-30 Hz and high-frequency bursts of 50-120 Hz were detected in the three regions after the onset of test image in both novel (Figure 6, left panel) and familiar conditions (Figure 6, middle panel). Oscillations at 30-40 Hz were observed in TE and PrC in both conditions and were observed in dlPFC in familiar condition before the presentation of test image, and these oscillations became weaker when the test image appeared. A non-parametric permutation test (two-tailed, shown in Figure 6 right panel) revealed that in TE and PrC, significant clusters of 30-50 Hz were detected immediately after test image onset, which were significantly higher for familiar condition; while other significant clusters (30-40 Hz in TE and 60-90 Hz in PrC) appearing at 400 ms relative to test image were found to be significantly higher for novel condition. In dlPFC, power ranging from 40-60 Hz appearing around 200-400 ms relative to test image was found to be significantly higher for familiar condition; while another power at 40-50 Hz appearing around 700-800 ms relative to test image was significantly higher for novel condition. In the power difference figure of dlPFC (Figure 5, right bottom panel), a LFP power difference ranging from 4-20 Hz between the two conditions has been observed within 0-200 ms, but the permutation test didn't confirm its significance ($p > 0.05$).

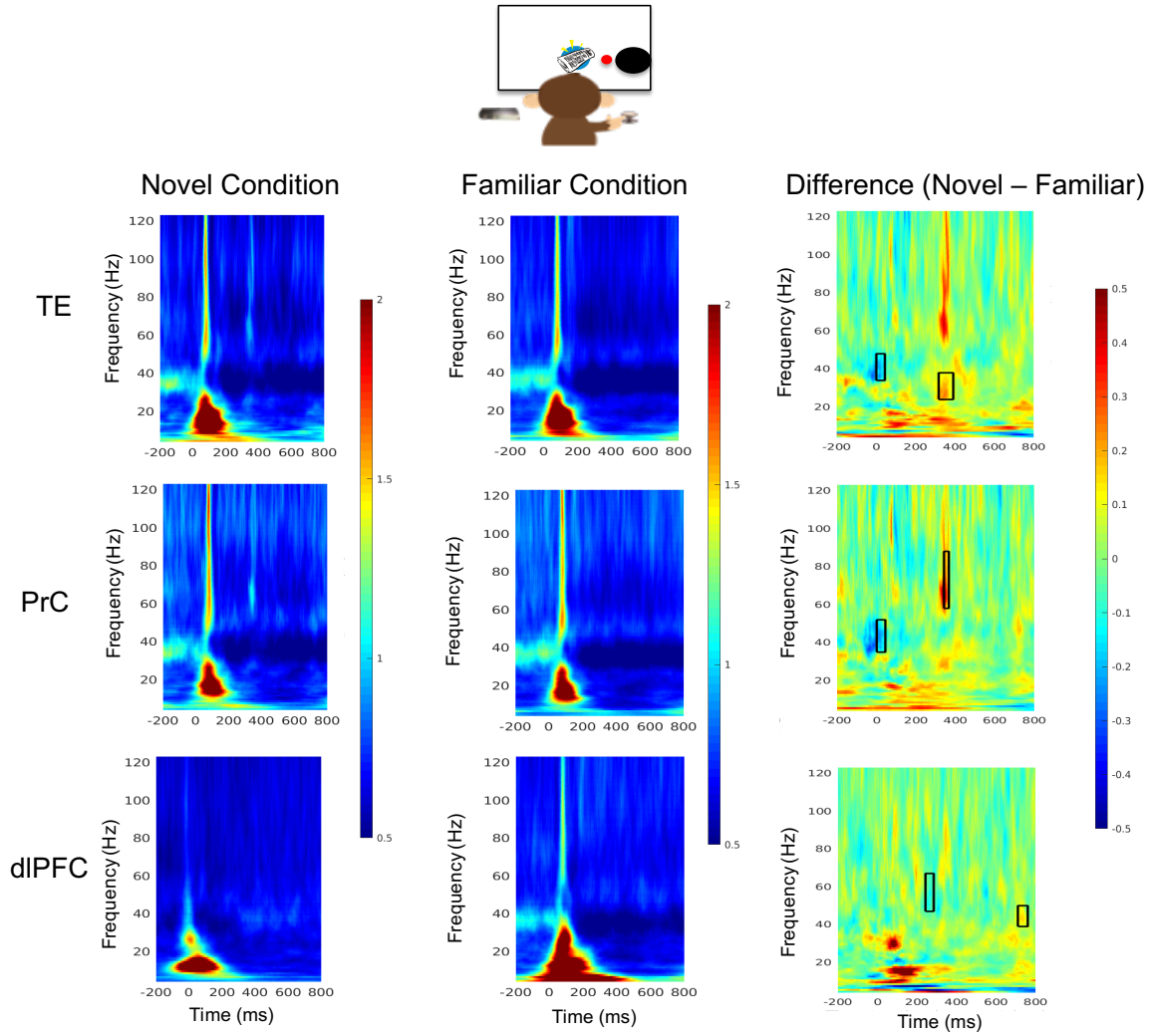


Figure 6. *Induced LFP power and LFP power difference between the novel and familiar conditions in match trials after onset of test image in TE, PrC and dlPFC. An increased power ranging from 4-30 Hz and narrow-band bursts of 50-120 Hz in those three regions after the onset of test image were found in both novel (left panel) and familiar conditions (middle panel). The significant difference between the two conditions in the three regions were indicated by black squares in the right panel (positive values: Novel > Familiar, negative values: Familiar > Novel).*

In the choice phase of non-match trials (i.e. sample image was different from test image), the low-frequency bursts of 4-30 Hz and high-frequency bursts of 50-120 Hz in the

three regions were detected after onset of test image in both novel (Figure 7, left panel) and familiar conditions (Figure 7, middle panel). The 30-40 Hz oscillations were still observed in TE, PrC and dlPFC before the presentation of test image, and became weaker when the test image appeared. A non-parametric permutation test (two-tailed, shown in Figure 7 right panel) revealed that clusters appeared between 100-200 ms relative to test image (with power ranging 50-80 Hz in TE, 40-60 Hz in PrC and 60-80 Hz in dlPFC) were found to be significantly higher for familiar condition. In TE and PrC, other clusters appeared around 300-400 ms (powering ranging 50-60 Hz in TE and 30-40 Hz in PrC) were found to be significantly higher for novel condition. In dlPFC, a narrow band of gamma power (100-120 Hz) appeared around 600 ms relative to test image, which was found to be significantly higher for novel condition.

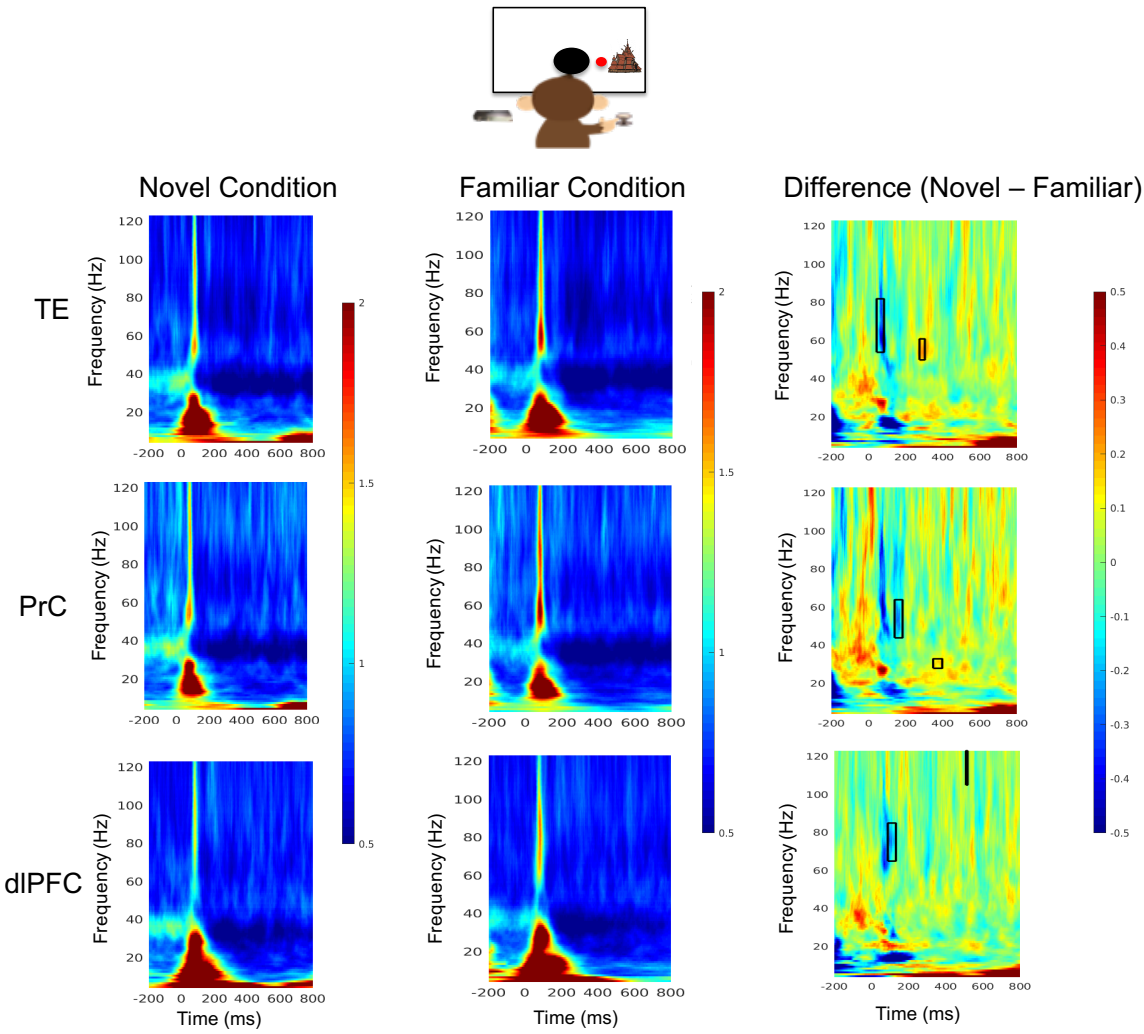


Figure 7. *Induced LFP power and LFP power difference between the novel and familiar conditions in non-match trials after onset of test image in TE, PrC and dlPFC. An increased power ranging from 4-30 Hz and narrow-band bursts of 50-120 Hz in those three regions after the test image onset were found in both novel (left panel) and familiar conditions (middle panel). The significant difference between the two conditions in the three regions were indicated by black squares in the right panel (positive values: Novel > Familiar, negative values: Familiar > Novel).*

Overall LFP activities in TE, PrC and dlPFC across task phases of memory task

To better illustrate the dynamic neural activities of TE, PrC and dlPFC across different phases of memory task in novel sample condition and familiar sample condition, I plotted LFP activities in those three areas across six epochs of memory task. In the top panels of Figure 8A-B, six task epochs were chosen as 1) holding the key-touch to initiate the task (zero ms was when the monkey held the key-touch), 2) viewing the sample image (sample phase, zero ms was when the sample image was on the screen), 3) delay phase (zero ms was when the sample image disappeared), 4) holding the key-touch again to wait for choice stimuli (zero ms was when the monkey held the key-touch), 5) choice images on the screen (choice phase including both match and nonmatch trials, zero ms was when the two choice images were on the screen) and 6) touching the screen to make the responses and getting the reward (response phase including both match and nonmatch trials, zero ms was when the monkey touched the screen).

Figure 8 showed modulations of LFP activities in TE, PrC and dlPFC by novel sample images (Figure 8A) and by familiar sample images (Figure 8B) across six task epochs. In the first task epoch (i.e. holding the key-touch to initiate the task), there was no increase of low-

frequency or high-frequency LFP bursts immediately after the monkey held the key-touch. A slight increase of low-frequency activities (< 20Hz) were detected around 500-750 ms in all the three regions in both conditions. In the second task epoch (i.e. encoding phase), an increased LFP power ranging from 4-20 Hz was found after the onset of sample image in TE, PrC and dlPFC. These brief bursts in those three regions lasted roughly 300-400 ms for both novel (Figure 8A) and familiar conditions (Figure 8B). In the third task epoch (i.e. delay phase), an increased LFP power ranging from 4-20 Hz in TE and PrC, and an increased power ranging from 4-40 Hz in dlPFC were detected around 100-200 ms prior to the offset of sample images. These brief bursts in those three regions lasted roughly 300-400 ms for both novel (Figure 8A) and familiar conditions (Figure 8B). In the fourth task epoch (i.e. holding the key-touch again) and fifth task epoch (i.e. choice phase), oscillations at 30-40 Hz were observed in TE, PrC and dlPFC around 500 ms after the monkey held the key-touch and persisted until choice images were on the screen. When the two choice images were on the screen (i.e. start of the choice phase), bursts of 4-30 Hz and bursts of 50-120 Hz were detected in the three regions after the onset of test image in both novel (Figure 8A) and familiar conditions (Figure 8B). In the sixth task epoch (i.e. response phase), bursts of 4-30 Hz were found in all the three regions immediately after monkey touched the screen to make the response, and high-frequency oscillations at 40-140 Hz were detected in TE and PrC around 500 ms after monkey touched the screen in both novel (Figure 8A) and familiar conditions (Figure 8B). As the delay between touch-screen choice and reward delivery was around 500 ms (i.e. as the smoothie pump was triggered by the computer when touch-screen choice was made by the monkey, and then juice was pumped out and monkey licked it into its mouth), these high-frequency oscillations detected in TE and PrC may be related with reward delivery.

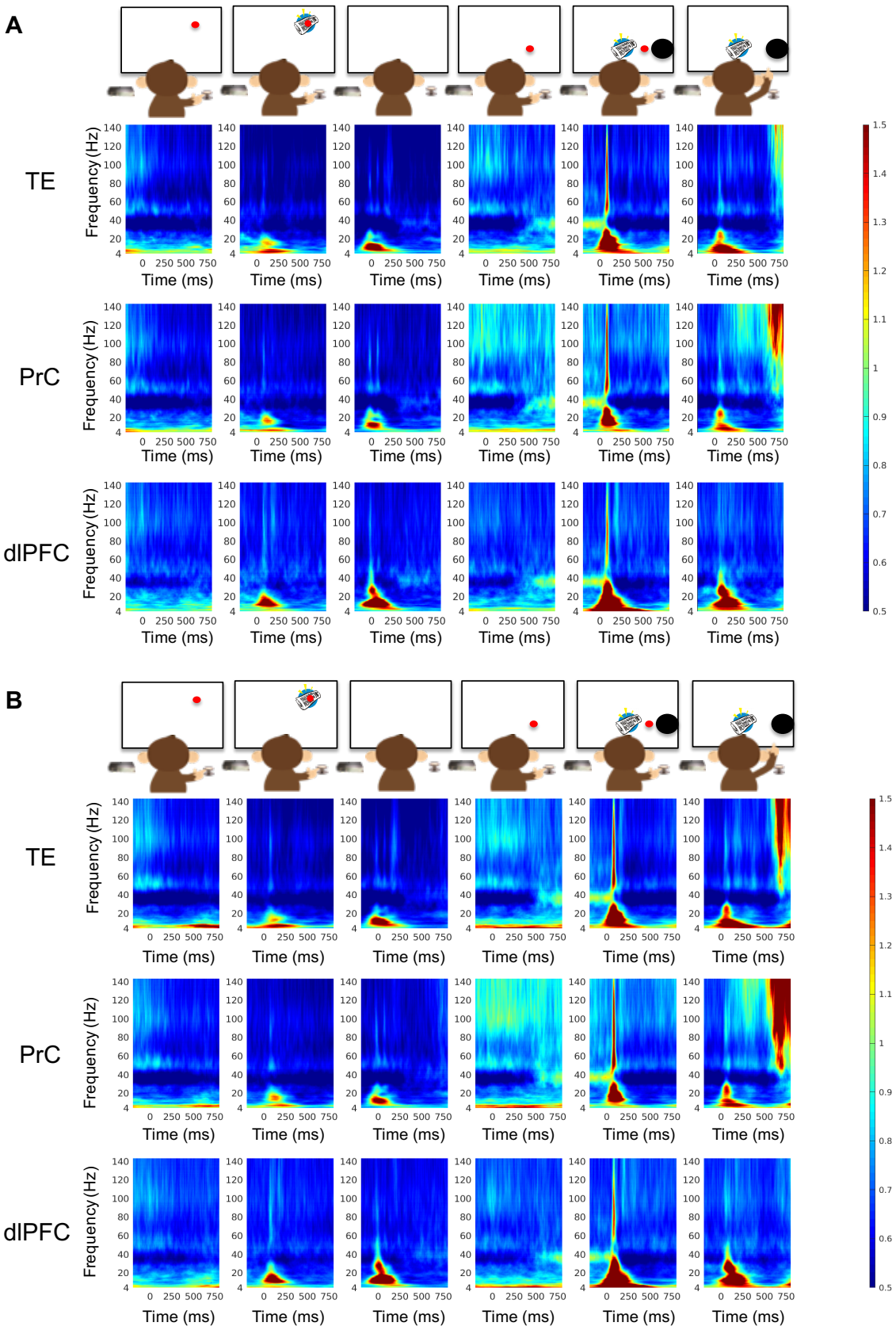

A
TE
PrC
dlPFC
Frequency (Hz)
Time (ms)
B
TE
PrC
dlPFC
Frequency (Hz)
Time (ms)

Figure 8. *Modulation of induced LFPs in TE, PrC and dlPFC by novel sample images (A) and by familiar sample images (B) during the task. In both figures (A-B), top panels are six epochs of memory task: monkey held the key-touch to initiate the task; sample image was on the screen (encoding phase); sample image was off the screen (delay phase); monkey held the key-touch again to wait for choice stimuli; choice images were displayed on the screen (choice phase); and monkey touched the screen to make the responses and got the reward (response phase). In the first task epoch, a slight increase of low-frequency activities (< 20Hz) were detected around 500-750 ms in all the three regions. In the second task epoch (i.e. encoding phase), an increased LFP power ranging from 4-20 Hz was found after the onset of sample image in TE, PrC and dlPFC in both novel (A) and familiar conditions (B). In the third task epoch (i.e. delay phase), an increased power ranging from 4-20 Hz in TE and PrC, and an increased power ranging from 4-40 Hz in dlPFC were detected around 100-200 ms prior to the offset of sample images in both novel (A) and familiar conditions (B). In the fourth and fifth task epoch, oscillations at 30-40 Hz were observed in TE, PrC and dlPFC around 500 ms after monkey held the key-touch and persisted until choice images were on the screen. When the choice images were on the screen (i.e. start of choice phase), bursts of 4-30 Hz and bursts of 50-120 Hz were detected in the three regions after the onset of test image in both novel (A) and familiar conditions (B). In the sixth task phase (i.e. response phase), bursts of 4-30 Hz in all the three regions, and high-frequency oscillations at 40-140 Hz in TE and PrC, were found immediately and around 500 ms after monkey touched the screen to make responses, respectively.*

A linear regression analysis on image repetition and LFP power of TE, PrC and dlPFC during the encoding phase

In the above LFP analysis, I divided familiarity level of sample image into two conditions:

novel condition (i.e. sample images were presented for the first time within a session) and familiar condition (i.e. sample images were presented multiple times within a session). In the above behavior analysis, we found both the hit rate (i.e. correct rate in match trials) and d prime demonstrated a linear relationship with the image repetition time (Figure 3). It would be interesting to know whether the LFP signals in these three areas also demonstrated a similar relationship with image repetition time (i.e. image familiarity).

In the encoding phase of sample image, I observed an increased LFP power ranging from 4-20 Hz after the onset of sample image in TE, PrC and dlPFC. Thus, I defined a region-of-interest (ROI) for each brain region during the encoding phase in each correct trial: frequency range as 4-20 Hz and time range as 0-300 ms (i.e. time zero was the onset of sample image). For the defined ROI in each of the brain regions, I averaged both of its frequency and time range, and called the calculated value as "LFP ROI power". Then for each region, I plotted LFP ROI power against repetition time of the sample image.

A linear regression analysis for each brain region showed image repetition had no effect on LFP ROI power ($p > 0.05$, Figure 9). For all the brain regions, a large increase of LFP ROI power was observed when the sample image was repeated for the third time in a session, and a slight increase of LFP ROI power was observed when the sample image was repeated for the sixth and ninth time in a session.

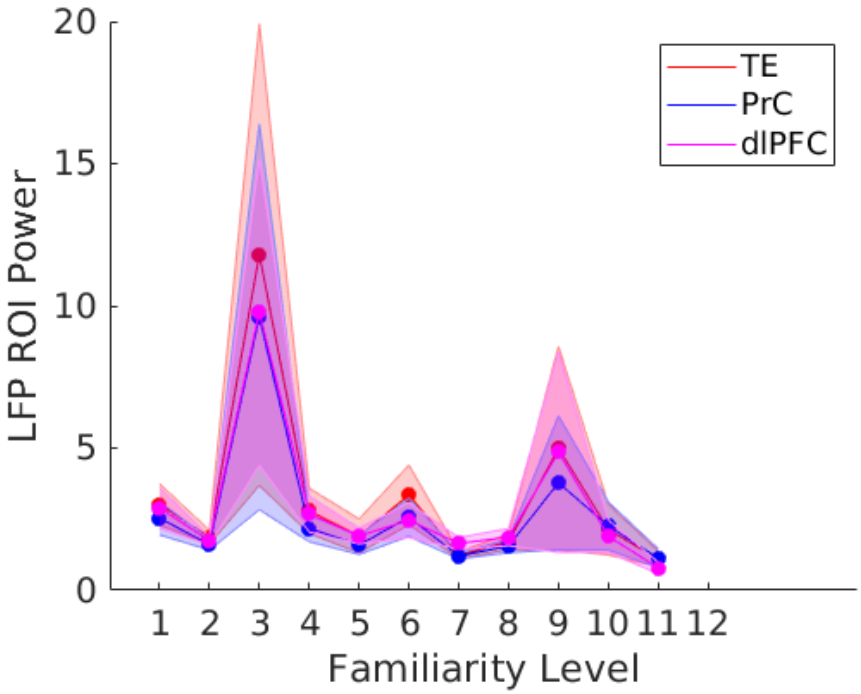


Figure 9. *A linear regression analysis on LFP ROI power (frequency range: 4-12 Hz) against familiarity level (i.e. repetition time) of sample image in TE (red line), PrC (blue line) and dlPFC (purple line) during the encoding phase of recognition memory task. Image familiarization had no effect on LFP ROI power in all the three regions (*$p > 0.05$*). SEM (±) at each familiarity level is indicated by shading over the lines.*

Effects of image familiarity on LFP-LFP coherence across TE, PrC and dlPFC during recognition memory task

When calculating coherence between different brain areas, data from 29 days when simultaneous recordings in TE, PrC and dlPFC were carried out were used. Across all the recorded sessions, 646 trials for novel condition (i.e. trials with the sample image presenting for the first time within a session) and 923 trials for familiar condition (i.e. trials with the sample image presenting multiple times within a session) were included in the analysis. I chose theta band (4-6 Hz), alpha/beta band (12-35 Hz) and gamma band (35-120 Hz) as three

frequency bands for the coherence analysis. For each of the frequency bands, LFPs in each recorded brain region were averaged across corresponding channels, and then trial-averaged LFP-LFP coherence of those three regions in the novel and familiar conditions were calculated in each session. A nonparametric permutation test was applied to compare the significant difference of LFP-LFP coherence in each brain pair (i.e. TE-PrC, TE-dlPFC, PrC-dlPFC) between the novel and familiar conditions in each task phase (details were described in methods).

In the encoding phase, LFP-LFP coherence between TE, PrC and dlPFC in theta band (4-6 Hz), alpha/beta band (12-35 Hz) and gamma band (35-120 Hz) were calculated in both novel and familiar conditions (Figure 10). In both two conditions, a very high coherence value between TE and PrC (around 0.8-0.9) was found in theta, alpha/beta and gamma bands, which may indicate LFP signals in TE and PrC were very similar. To investigate the effects of image familiarity on theta/alpha-beta/gamma-frequency coherence across different brain areas, a non-parametric permutation test (two-tailed) was applied to compare coherence values between the novel (red line) and familiar conditions (blue line). Although a decrease of theta-frequency coherence between TE and dlPFC and a decrease of theta-frequency coherence between PrC and dlPFC were detected from the onset of sample image in novel condition compared with familiar condition, the permutation test didn't confirm its significant difference ($p > 0.05$). A significantly higher coherence in alpha/beta band between TE and dlPFC was detected around 600-700 ms in novel condition compared with familiar condition ($p < 0.05$). Some discontinuous significant differences of gamma-band coherence across three brain regions were found between the two conditions, with each significant area persisting in a very short time period ($p < 0.05$).

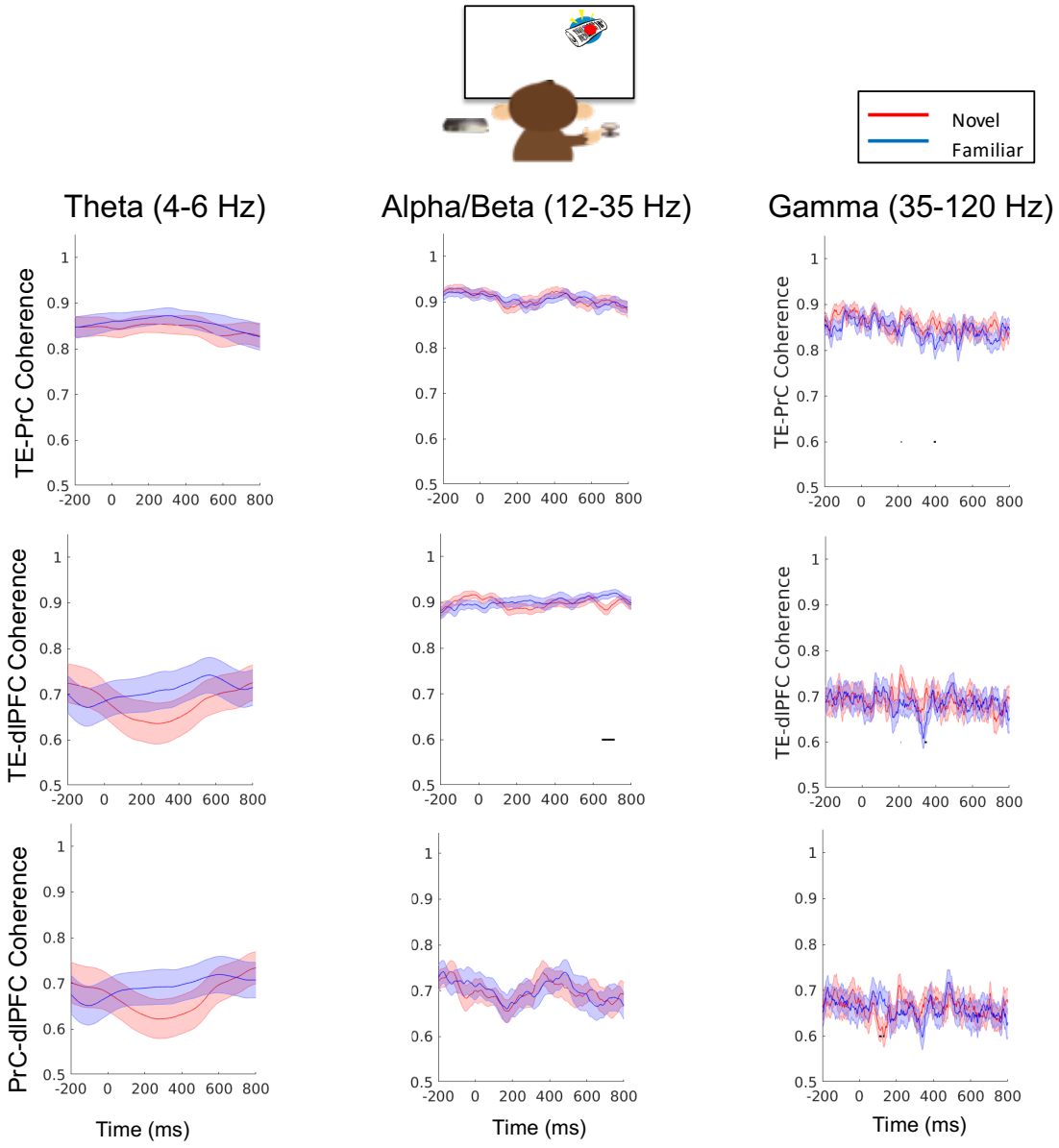


Figure 10. *LFP-LFP coherence across TE, PrC and dlPFC in theta-frequency band (left panel), in alpha/beta-frequency band (middle panel) and in gamma-frequency band (right panel) for both the novel (red line) and familiar (blue line) conditions. No significant difference of coherence in theta band between the two conditions was found during the encoding phase. A significant higher coherence in alpha/beta band between TE and dlPFC was detected around 600-700 ms in novel condition compared with familiar condition (highlighted by black line). Some discontinuous significant differences of gamma-band coherence between TE and PrC, between TE and dlPFC and between PrC and dlPFC were*

found between the two conditions, with each significant area persisting in a very short time period (highlighted by black line). SEM (±) at each time point is indicated by shading over the lines.

In the delay phase (i.e. no stimuli were shown on the screen), LFP-LFP coherence across different areas in different frequency bands were calculated in both the novel and familiar conditions (Figure 11). It seems there was a decrease of theta-frequency coherence between TE and dlPFC after the onset of delay. However, no significant difference of coherence in theta band between the two conditions was found during the delay phase ($p > 0.05$). Additionally, a decrease of alpha/beta-frequency coherence between TE and dlPFC and a decrease of alpha/beta-frequency coherence between PrC and dlPFC after onset of delay were detected, and then both coherence values in the two brain pairs (TE-dlPFC, PrC-dlPFC) slightly increased and reached the peak around 200 ms for familiar condition and around 300 ms for novel condition. Permutation test confirmed a significant higher alpha/beta-band coherence between TE and PrC around 600-700 ms in familiar condition compared with novel condition ($p < 0.05$). Another significant higher gamma-band coherence between TE and PrC was also detected after the delay onset in familiar condition than novel condition, with the significant area persisting in a very short time period ($p < 0.05$).

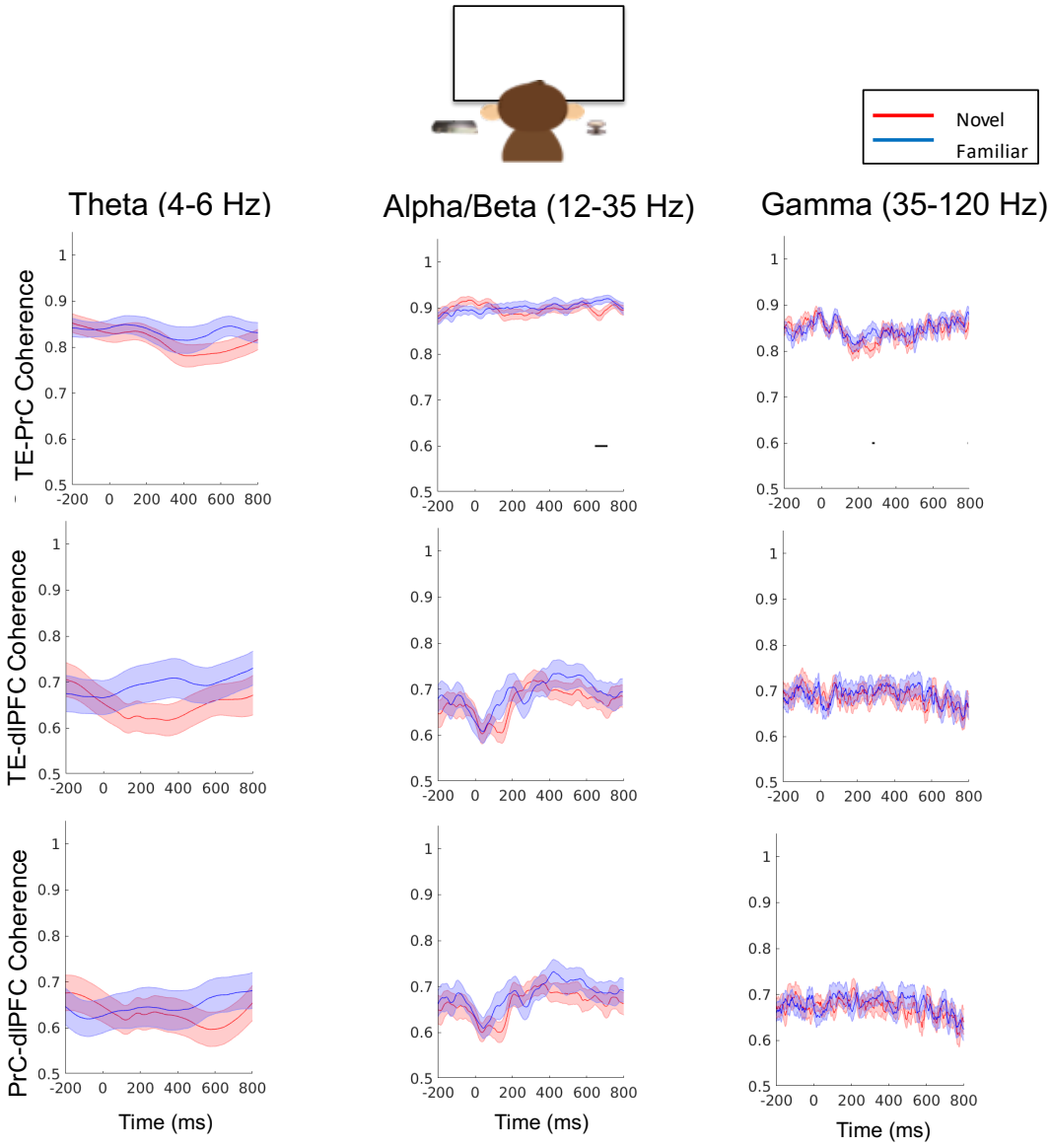


Figure 11. *LFP-LFP coherence between TE, PrC and dlPFC in theta-frequency band (left panel), in alpha/beta-frequency band (middle panel) and in gamma-frequency band (right panel) for both the novel (red line) and familiar (blue line) conditions. No significant difference of coherence in theta band between the two conditions was found. A significant higher coherence in alpha/beta band between TE and PrC was detected around 600-700 ms in familiar condition compared with novel condition (highlighted by black line). A significant higher coherence in gamma band between TE and PrC was also detected after the delay onset in familiar condition than novel condition, with the significant area persisting in a very short time period (highlighted by black line). SEM (±) at each time point is indicated by*

shading over the lines.

In the choice phase of match trials (i.e. sample image was the same as test image), LFP-LFP coherence across different areas in different frequency bands were calculated in both the novel and familiar conditions (Figure 12). It has been observed that the theta-frequency coherence between TE and dlPFC dropped prior to the onset of test image in both novel and familiar conditions. A drop of theta-frequency coherence between PrC and dlPFC has also been detected in both conditions but the fall time to reach the lowest point was earlier in novel condition (around 100 ms relative to test image) than familiar condition (around 200 ms relative to test image). Permutation tests confirmed a significant higher coherence in theta band between TE and PrC around 200-400 ms in familiar condition compared with novel condition ($p < 0.05$). It has also been observed that alpha/beta-frequency coherence between TE and dlPFC and alpha/beta-frequency coherence between PrC and dlPFC decreased after 100 ms relative to test image in both conditions. However, no significant difference of coherence in alpha/beta band between the two conditions was found during the choice phase ($p > 0.05$). Some discontinuous significant differences of gamma-band coherence across three regions were found between the two conditions, with each significant area persisting in a very short time period ($p < 0.05$).

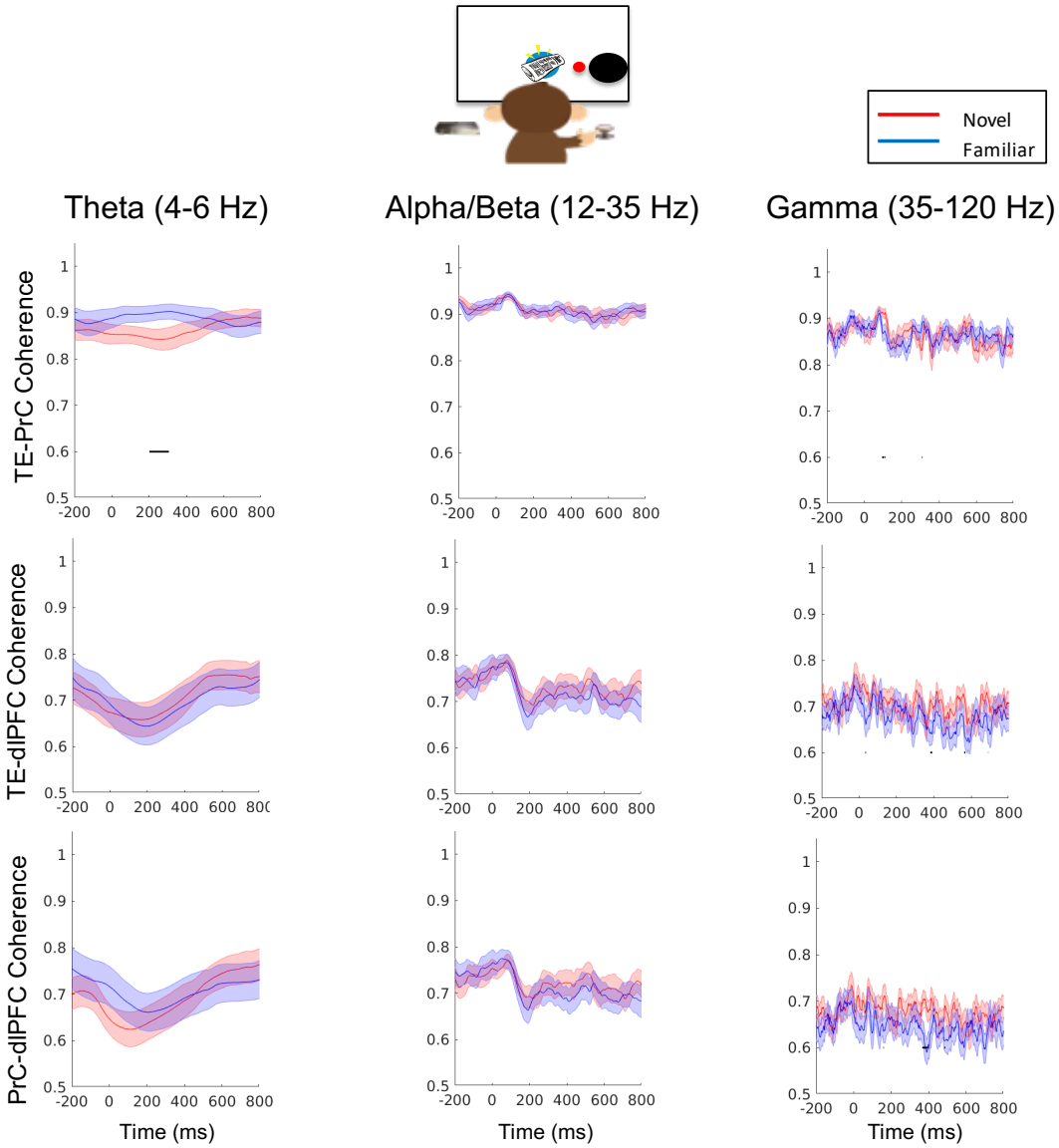


Figure 12. *LFP-LFP coherence between TE, PrC and dlPFC in theta-frequency band (left panel), in alpha/beta-frequency band (middle panel) and in gamma-frequency band (right panel) for both novel (red line) and familiar (blue line) conditions. A significant higher coherence in theta band between TE and PrC was detected around 200-400 ms in familiar condition compared with novel condition (highlighted by black line). No significant difference of coherence in alpha/beta band between the two conditions was found during the choice phase. Some discontinuous significant differences of gamma-band coherence between TE and PrC, between TE and dlPFC and between PrC and dlPFC were found between the two conditions, with each significant area persisting in a very short time period (highlighted*

by black line). SEM (±) at each time point is indicated by shading over the lines.

In the choice phase of non-match trials (i.e. sample image was different from test image), LFP-LFP coherence across different areas in different frequency bands were calculated in both the novel and familiar conditions (Figure 13). No significant difference of coherence in theta band between the two conditions was found during the choice phase ($p > 0.05$). A slight increase of alpha/beta-frequency coherence between TE and dlPFC and alpha/beta-frequency coherence between PrC and dlPFC was found after the onset of test image in both conditions. Permutation test confirmed a significant higher coherence in alpha/beta band between TE and PrC around 500-600 ms in familiar condition compared with novel condition ($p < 0.05$). Some discontinuous significant differences of gamma-band coherence across three regions were found between the two conditions, with each significant area persisting in a very short time period ($p < 0.05$).

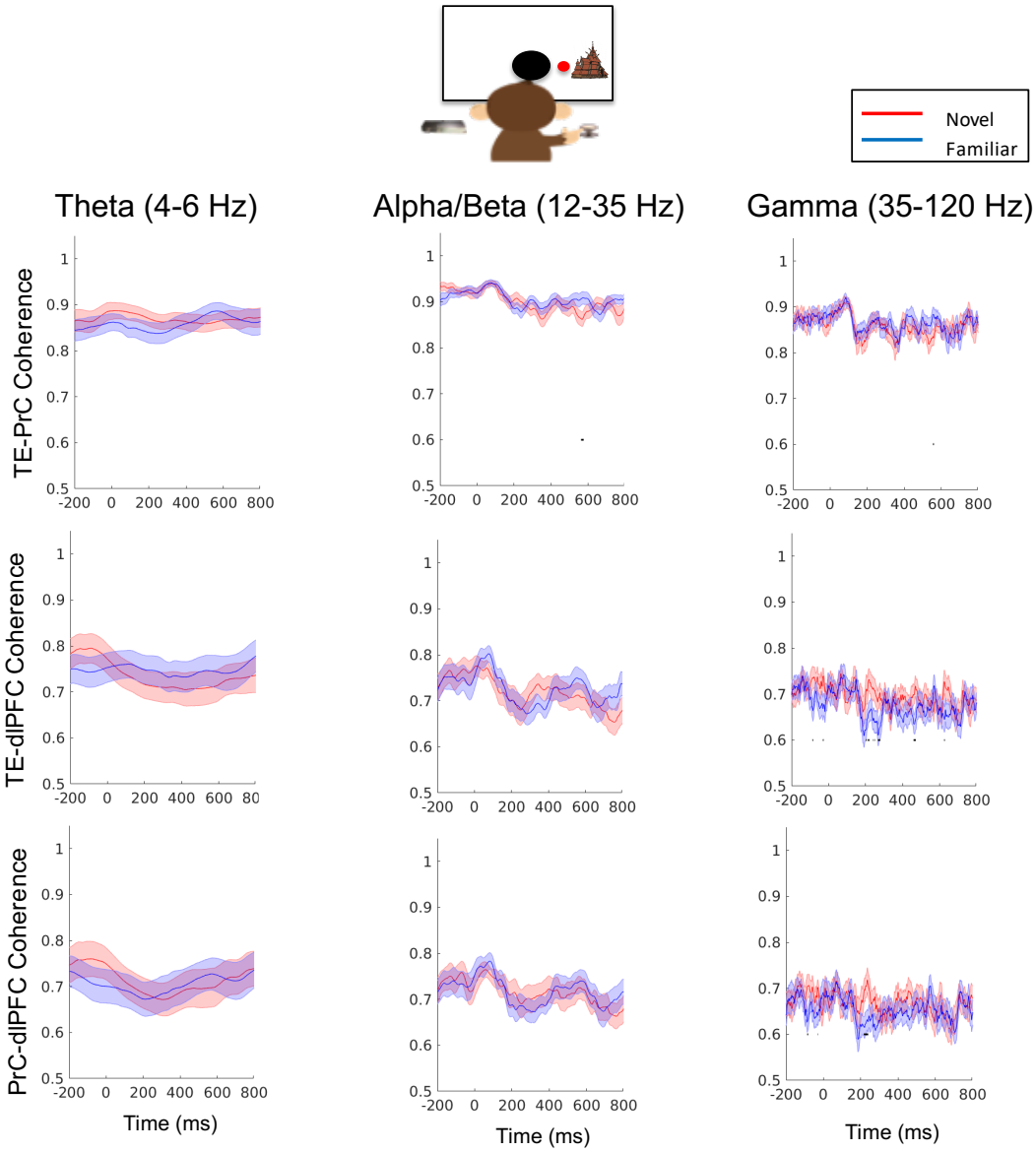


Figure 13. *LFP-LFP coherence between TE, PrC and dlPFC in theta-frequency band (left panel), in alpha/beta-frequency band (middle panel) and in gamma-frequency band (right panel) for both novel (red line) and familiar (blue line) conditions. No significant difference of coherence in theta band between the two conditions was found. A significant higher coherence in alpha/beta band between TE and PrC was detected around 500-600 ms in familiar condition compared with novel condition (highlighted by black line). Some discontinuous significant differences of gamma-band coherence between TE and PrC, between TE and dlPFC and between PrC and dlPFC were found between the two conditions, with each significant area persisting in a very short time period (highlighted by black line).*

SEM (±) at each time point is indicated by shading over the lines.

Overall LFP-LFP coherence across TE, PrC and dlPFC across different phases of memory task

To better illustrate the dynamic change of coherence across TE, PrC and dlPFC across different phases of memory task, I plotted LFP-LFP coherence of those areas across six epochs of the recognition memory task. As visualized in the top panels of Figure 14 A-C, these epochs include: 1) holding the key-touch to initiate the task; 2) display the sample image; 3) the delay phase; 4) holding the key-touch again; 5) display of the choice images (including both match and non-match trials); and 6) making responses by touching the screen and getting the reward. The zero ms of each task epoch was set to when monkey held the key-touch, sample image displayed on the screen, sample image disappeared, monkey held the key-touch again, choice images displayed on the screen, and monkey touched the screen, respectively. The LFP-LFP coherence in theta, alpha/beta, and gamma band were shown in Figure 14 A, B, and C, respectively. In each LFP-LFP coherence plot, it has been given a serial number, in which A-C refer to theta, alpha/beta and gamma coherence; 1-3 refer to brain pair of TE-PrC, TE-dlPFC, PrC-dlPFC; and 1-6 refer to six task epochs. Red and blue lines represent coherence in novel condition and in familiar condition, respectively.

In panels of A-2-2 and A-2-5 of Figure 14A (i.e. theta-band), the coherence between TE- dlPFC in the sample (epoch 2) and choice phases (epoch 5) of novel condition (red) demonstrated decreases prior to visual stimuli onset, followed by increases at 250-500 ms after the stimuli onset. In panels of A-3-2 and A-3-5, a similar pattern was also found for coherence between PrC-dlPFC in the sample (epoch 2) and choice phases (epoch 5). In the panel of A-2-3, a decrease of the TE-dlPFC coherence in the novel condition (red) was

observed before the delay onset, and then an increase at 250-500 ms after the delay onset (epoch 3).

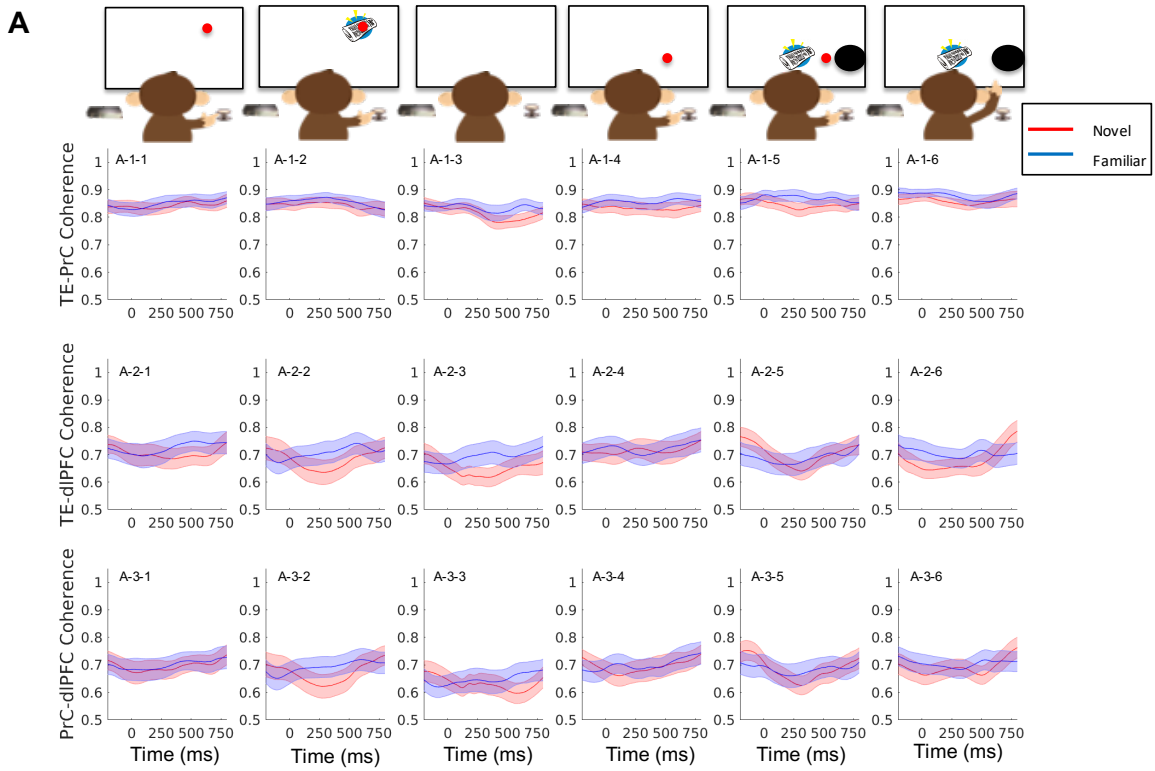


Figure 14A. *LFP-LFP coherence across TE, PrC and dlPFC in theta band (A) for novel sample condition (red line) and familiar sample condition (blue line) during the task. Top panels illustrate six epochs of memory task: monkey held the key-touch to initiate the task; sample image was on the screen (encoding phase); sample image was off the screen (delay phase); monkey held the key-touch again to wait for choice stimuli; choice images were on the screen (choice phase); and monkey touched the screen to make the responses and get the reward (response phase). In panels of A-2-2 (sample phase) and A-2-5 (choice phase), theta-band coherence between TE and dlPFC in the novel condition (red line) were observed to demonstrate a decrease prior to visual stimuli (i.e. sample, choice images) onset, and then show an increase after 250-500 ms relative to stimuli onset. In panels of A-3-2 (sample phase) and A-3-5 (choice phase), theta-band coherence between PrC and dlPFC in the novel condition (red line) were also observed to demonstrate a decrease prior to visual stimuli*

onset, and then show an increase after 250-500 ms relative to stimuli onset. In the panel of A-2-3 (delay phase), a decrease of theta-band coherence between TE and dlPFC in the novel condition (red line) was observed to decease before the delay onset, and then increase after 250-500 ms relative to delay onset. SEM (±) at each time point is indicated by shading over the lines.

In panels of B-2-3 and B-3-3 of Figure 14 B (i.e. alpha/beta-band), decreases in the coherence between TE-dlPFC and coherence between PrC-dlPFC were observed at the beginning of the delay phase (epoch 3). These coherences then bounce and reach their peaks at ~ 200 ms in familiar condition and ~ 300 ms in novel condition. In panels of B-2-5 and B-3-5, decreases of coherences between PrC-dlPFC and coherence between PrC-dlPFC, were observed after the onset of choice images (epoch 5) in both conditions. In panels of B-2-6 and B-3-6, coherence between PrC-dlPFC and coherence between PrC-dlPFC were observed a decrease and then an increase around 250-500 ms after the monkey touched the screen to make responses (epoch 6) in both conditions.

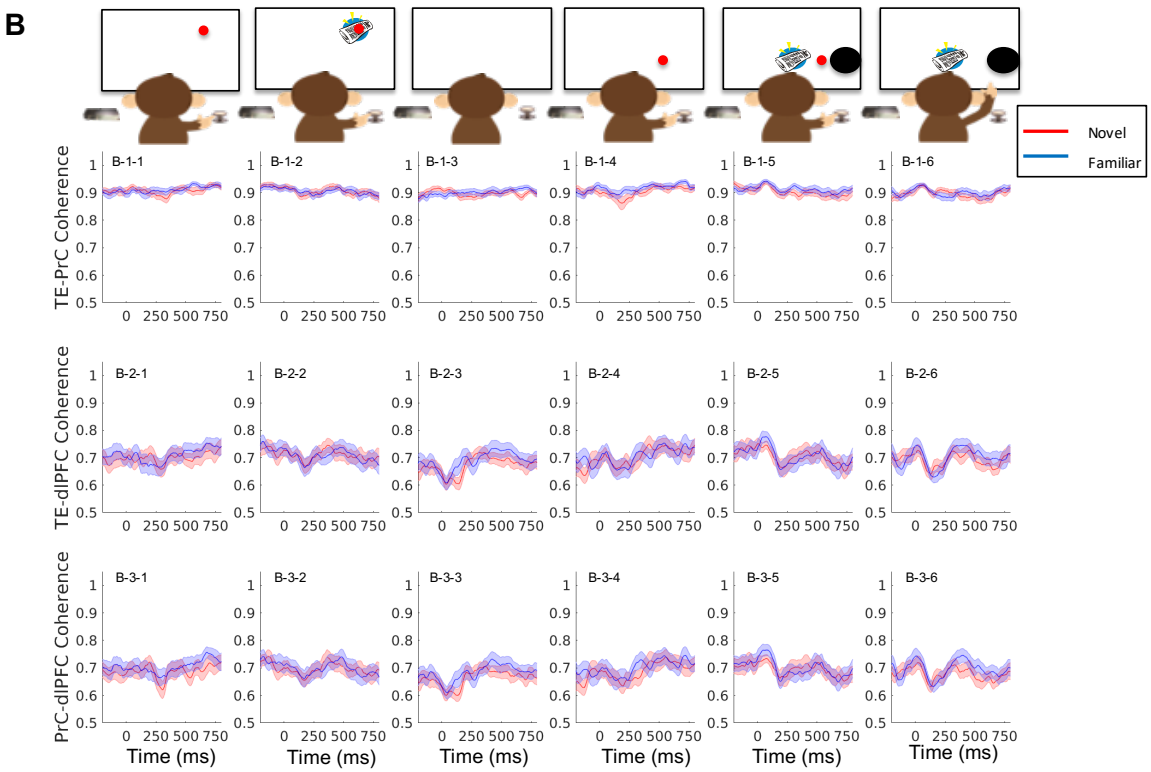


Figure 14B. *LFP-LFP coherence across TE, PrC and dlPFC in alpha/beta band (B) for novel sample condition (red line) and familiar sample condition (blue line) during the task. Top panels illustrate six epochs of memory task, same as top panels in Figure 14A. In panels of B-2-3 and B-3-3 (delay phase), a decrease of alpha/beta-band coherence between TE and dlPFC and a decrease of alpha/beta-band coherence between PrC and dlPFC were observed when delay phase started, and both coherences increased and reached the peak around 200 ms for familiar condition and around 300 ms for novel condition during delay period. In panels of B-2-5 and B-3-5, a decrease of alpha/beta-band coherence between TE and dlPFC and coherence between PrC and dlPFC were observed after the onset of choice images (i.e. start of choice phase) in both conditions. In panels of B-2-6 and B-3-6, a decrease and then an increase (around 250-500 ms) of alpha/beta-band coherence between TE and dlPFC and coherence between PrC and dlPFC were observed after monkey touched the screen to make responses (i.e. start of response phase) in both conditions. SEM (±) at each time point is indicated by shading over the lines.*

In Figure 14 C (gamma-band coherence), no obvious change of coherence across three areas was observed across different task phases.

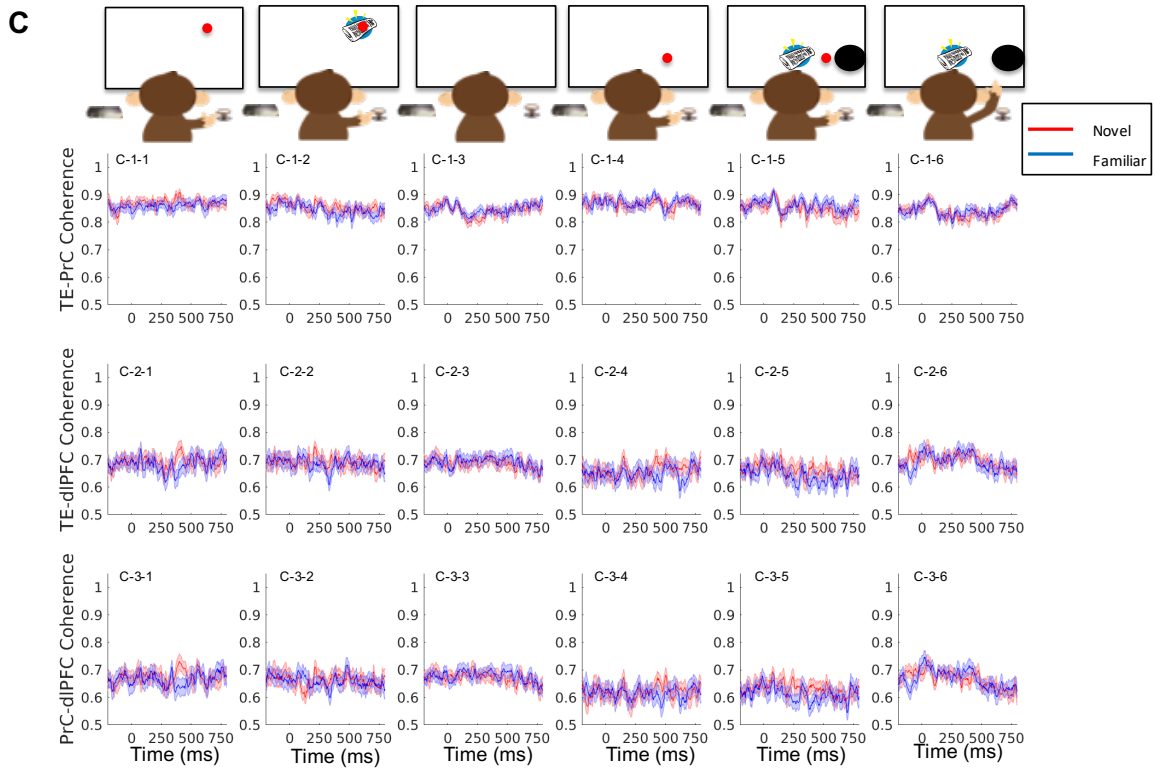


Figure 14C. *LFP-LFP coherence across TE, PrC and dlPFC in gamma band (C) for novel sample condition (red line) and familiar sample condition (blue line) during the task. Top panels illustrate six epochs of memory task, same as top panels in Figure 14A. No obvious change of coherence across three areas was observed in each task phase. SEM (±) at each time point is indicated by shading over the lines.*

Noted in Figure 14A-C, TE and PrC tend to have noticeably good coherence, usually between 0.8 and 0.9, in theta, alpha/beta, and gamma band for both novel and familiar conditions across all the six task epochs. Although this indicates a closer functional

relationship between the two areas, a post-mortem inspection further confirms the array of area TE and array of area PrC were spatially close (see recording sites of the TE array and PrC array in Figure 1), indicating signals from both arrays were similar.

Spike activities of dlPFC and its timing relationship between spike and LFP activities throughout recognition memory task

In total, 3 units in the array of TE and 25 units in the array of dlPFC (both including single- and multi-units) were sorted in different recorded sessions. No unit was detected in the array of PrC in all the recorded sessions, which may suggest the electrodes of this array was not inside the cell layer of PrC. As the above LFP power spectrum analysis showed LFP responses of PrC to visual stimuli during recognition memory task, it suggests the array of PrC was in the cortex. Among the 28 units, only one dlPFC unit demonstrated task-relevant activities. The following spike analysis focused on how this dlPFC unit responded during different epochs of recognition memory task.

In the top panels of Figure 15, six task epochs were chosen to be plotted, which were holding the key-touch to initiate the task (time zero was when monkey held the key-touch), viewing the sample image (sample phase, time zero was when the sample image was on the screen), delay phase (time zero was when the sample image disappeared), holding the key-touch to wait for choice images (time zero was when monkey held the key-touch), choice images on the screen (choice phase, time zero was when the choice images were on the screen) and finally making the choice responses and reward delivery (response phase, time zero was when monkey touched the screen). The middle panels and bottom panels of Figure 15 showed the binned spike activities and the peri-stimulus time histograms (PSTH) of this dlPFC unit across six task epochs. The increased response profile of this dlPFC unit was

found when the monkey correctly touched the choice stimuli and got the reward in the response phase. A slight increase of spike activities was also detected after the onset of sample image (i.e. start of the sample phase) and the onset of choice stimuli (i.e. start of the choice phase). During the delay period, a slight increase of spike activities was detected immediately after the delay onset and then dropped between 250-500 ms.

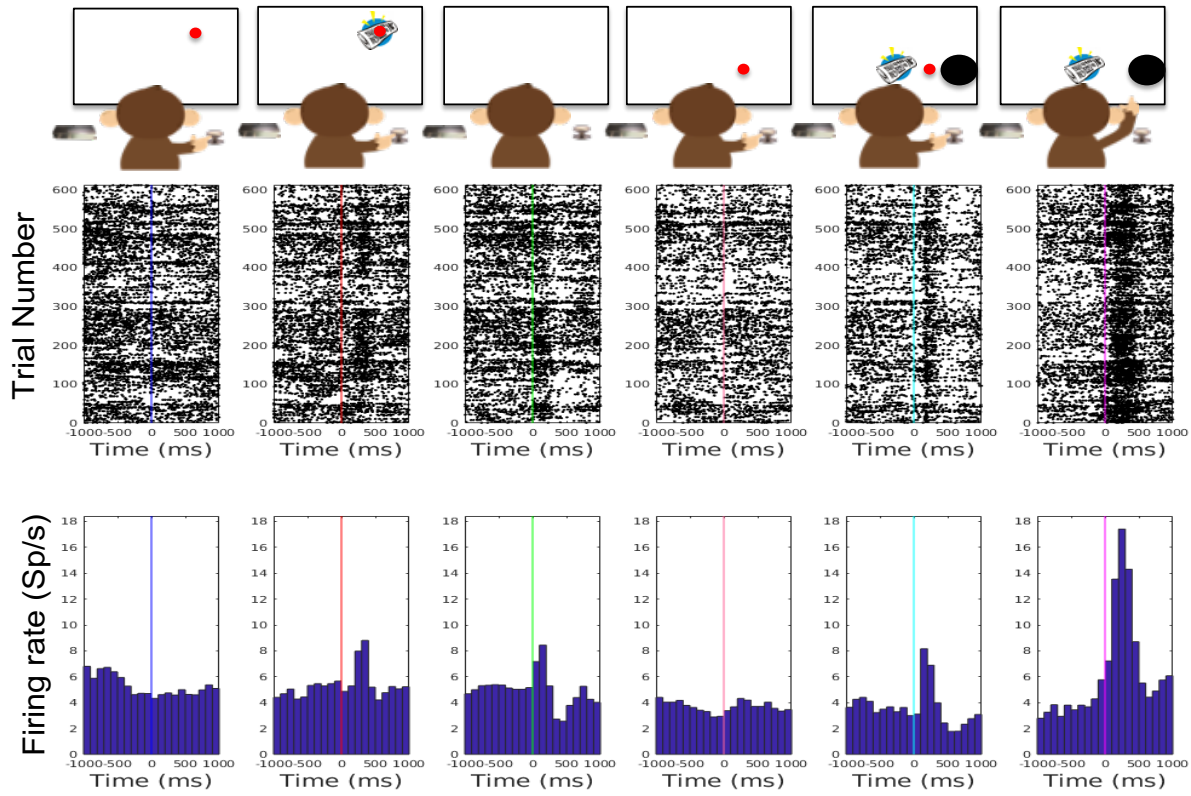


Figure 15. *One dlPFC unit response profile to different epochs of recognition memory. Top panels: six epochs of recognition memory task. First epoch: monkey held the key-touch to initiate the task; Second epoch: sample image was on the screen (i.e. sample phase); Third epoch: sample image disappeared on the screen (i.e. delay phase); Forth epoch: monkey held the key-touch again to wait for choice images; Fifth epoch: choice images were on the screen (i.e. choice phase); Sixth epoch: monkey touched the screen to make the responses (i.e. response phase). Colored line in the middle of each panel indicates time zero of each task epoch. Middle panels: binned spike activities of one dlPFC unit (spike activities were combined across the recorded sessions) across six epochs. Increased spike activities of this*

dlPFC unit following the correct responses (response phase), and slight increases of spike activities were found during the sample, delay, and choice phases. During the delay period, a slight increase of spike activities was detected immediately after the delay onset and then dropped between 250-500 ms. Bottom panels: peri-stimulus time histograms (PSTH) of this dlPFC unit across six epochs. Again, this PSTH shows an increased spike activity during sample, delay and choice phases, and a largely increased spike activity during response phase.

For this dlPFC channel with significant LFPs and unit responses, as stated in the methods (i.e. in the section of *timing of spike and LFP responses*), I computed both instantaneous firing rate using gaussian smoothing and LFP power using the squared magnitude of the Hilbert transform after band-pass filtering the raw data at 4-6 Hz (theta band, first middle panels), 12-30 Hz (alpha/beta band, second middle panels) and 40-100 Hz (gamma band, bottom panels). Across the selected six epochs of recognition memory task (in the top panels of Figure 16), it was found that i) a slight increase in alpha/beta power activation preceded the increase in firing rate by 250 ms in the sample phase; and ii) at the start of delay, increases in alpha/beta power activation shortly proceeded the increase in firing rate appeared by 100-125 ms; and iii) in the choice phase, both the alpha/beta and gamma power activation shortly preceded the increase in firing rate by 100-125 ms, while increases in theta power and firing rate appeared at approximately the same time when test image appeared; and iv) in the response phase, increases in alpha/beta power activation preceded the increase in firing rate by 150 ms.

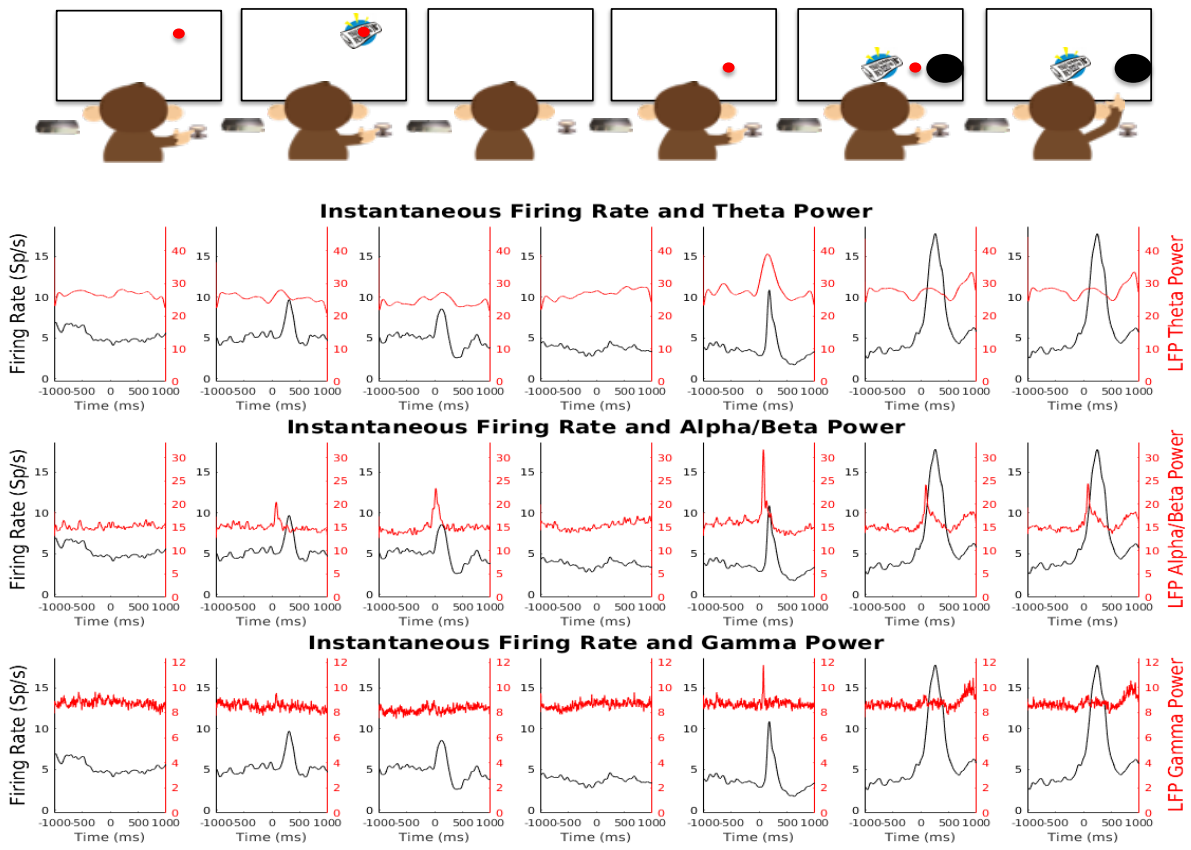


Figure 16. *The instantaneous firing rate, theta-, alpha/beta- and gamma-induced LFP power across six epochs of recognition memory task. Top panels: six epochs of recognition memory task, same as top panels in Figure 15. The bottom three panels illustrate the change of theta-, alpha/beta- and gamma-induced LFP power along with the instantaneous firing rate across six epochs. A slight increase in alpha/beta power activation preceded the increase in firing rate in the sample, delay and response phases. Both alpha/beta and gamma power activation shortly preceded the increase in firing rate while increases in theta power and firing rate appeared at approximately the same time when test image appeared (choice phase).*

Discussion

The MTL is known to support recognition memory (Eichenbaum et al. 2007; Squire et al. 2007); and many neuropsychological and neurophysiological studies have also emphasized the role of PFC in maintaining information about stimuli for upcoming actions (Blumenfeld and Ranganath 2007). However, the dynamics of neural interactions among PFC and MTL, and also inferotemporal cortex (IT), during the encoding, maintenance and retrieval phases of recognition memory are not fully understood. Here I recorded neural activities in an object recognition memory task using simultaneous multi-area, multi-electrode Utah arrays over area TE (an anterior sub-region of IT), PrC and dlPFC in the awake monkey, and investigated the effects of image familiarity on behavior, neural activities of those three regions, and neural interactions between prefrontal and temporal regions throughout the recognition memory task.

Behavioral results indicated an improvement of macaque's performance in recognition memory when the sample images became familiar to the macaque. Specifically, image familiarization significantly benefited responses in match trials, for example, hit rate increased and response time decreased along with the familiarity level of sample images. However, image familiarization had less impacts on non-match trials as only response time decreased along with the familiarity level, which suggests image familiarity may not be necessary for helping the macaque to reject a novel image in non-match trials. Moreover, image familiarization increased d', an indication of discriminative ability between the new and old items in recognition memory. This illustrates that increased familiarity of to-be-remembered items (i.e. sample images) improved recognition in the macaque. A similar improvement on recognition by image familiarity was found in humans (Scapinello and Yarmey 1970), which indicates a common phenomenon of image familiarity on recognition memory performance across species.

Neural data recorded in TE, PrC and dlPFC were analyzed in the form of low-frequency LFP components and high-frequency spike components throughout the recognition memory task. Spike analysis showed that one dlPFC unit demonstrated the largest increasing firing rate when responding to test stimuli, slight increases of firing rate were found to be related to the onset and offset of visual stimuli. Katsuki and Christos found the firing rate of dlPFC peaked around 50-200 ms relative to the stimuli (Figure 17a), and they interpreted their findings as the evidence of an early involvement of macaque dlPFC in the bottom-up attention on salient visual stimuli (Katsuki and Constantinidis 2012). In our macaque spike data (Figure 17b), we detected the response latencies of dlPFC for sample and test image were 100-200 ms, which were well within the time-frame in the study of Katsuki and Christos. Moreover, we also observed an immediate decrease of firing rate in dlPFC after the offset of sample image. Taken together, the early signals we observed in dlPFC reflects both visual and attentional processes to visual stimuli. Additionally, a large increase of firing rate after the monkey responded to choice stimuli was observed, indicating dlPFC signals responses and rewards (Tsujimoto et al. 2012).

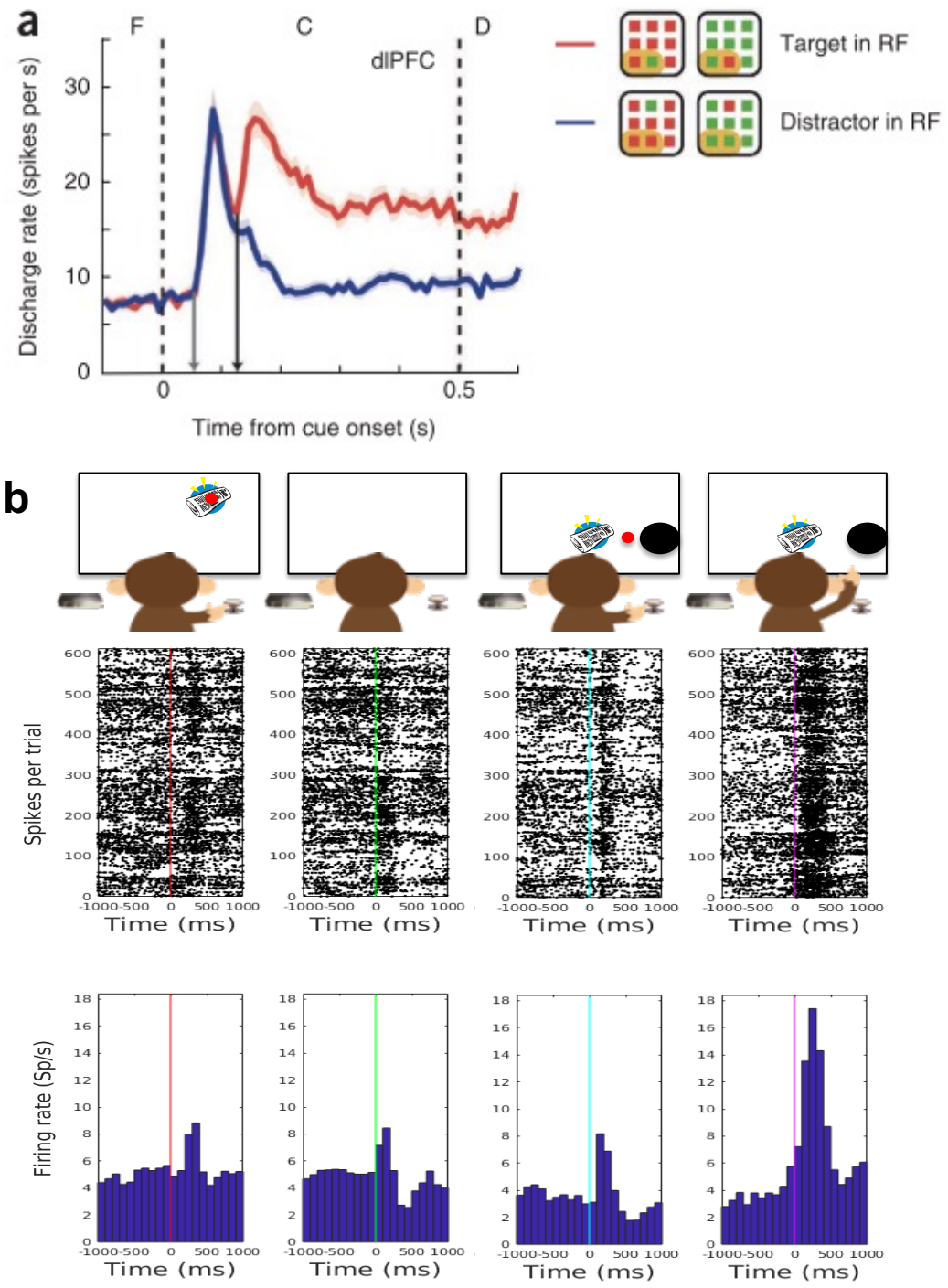


Figure 17. *An early involvement of dlPFC in processing and attending to visual stimuli. Panel a: peristimulus time histogram of dlPFC during the presentation of the target (red line) in the receptive field (RF) and distractor (blue line) in the RF over the fixation (F), cue (C) and delay (D) periods. The gray arrow indicates the population visual response latency for distractor discrimination (around 50-100 ms) and the black arrow indicates the population*

response latency for target discrimination (between 100-200 ms) (adapted from Katsuki and Constantinidis, 2012). Panel b: our peristimulus time histogram of dlPFC during the presentation of sample image (sample epoch), disappearance of sample image (delay epoch), presentation of test image (choice epoch) and touch-screen responses (response epoch). Colored line in the middle of each panel indicates time zero of the above epochs. Response latencies for viewing the sample and test image were around 100-200 ms. After the sample image disappeared on the screen (delay phase), the firing rate in dlPFC immediately increased and then dropped around 300-400 ms. A large increase of firing rate in dlPFC was found immediately after monkey responded to the choice stimuli and got the reward.

LFP activities in the three regions were analyzed and compared between the novel and familiar conditions. In TE, PrC and dlPFC, low-frequency power (ranging from 4-20 Hz, lasting around 300-400 ms) were detected immediately after the sample image onset (encoding phase) and around the sample image offset (delay phase), and low-frequency power (ranging from 4-30 Hz) together with a gamma power (ranging from 50-120 Hz) were found immediately after the test image onset (choice phase in both match and non-match trials). These brief bursts of low- and high-frequency power existed in those three regions and were related to the onset and offset of visual stimuli in different task phases (e.g. encoding, maintenance, choice). It seems these brief bursts were only related to visual stimuli presentation regardless of image familiarity, as permutation tests didn't reveal any significant difference of these bursts between the novel and familiar conditions. One of the interpretations of these brief bursts is that they were involved in visual and attentional processes to the salient stimuli against the background (Doesburg et al. 2008). For dlPFC, I also investigated both the timing of spike activities and instantaneous power of theta/alpha-beta/gamma power throughout recognition memory task. It has been found alpha/beta bursts

peaked prior to the summit of spike activities in the encoding, delay and choice phases; and gamma bursts peaked prior to the summit of spike activities only in the choice phase; and theta bursts and spike activities appeared at approximately the same time when test image appeared in the choice phase. It seems alpha/beta bursts tracked spike activities better than the neural activities of other frequencies during the onset and offset of visual stimuli, indicating a close relationship between spikes and alpha/beta power of dlPFC in visual and attentional processes.

Image familiarity modulated induced LFPs in both beta and gamma bands in TE, PrC and dlPFC throughout the recognition memory task. As delay period was fixed at 1000 ms in the task, and the presentation durations of the sample and test images were varied between 1000-1500 ms, LFP power spectral of each brain region was calculated in a window of 1000 ms, and a time window of 800 ms was chosen (i.e. to avoid LFP spectral leakage in a 1000-ms time window) to compare the induced LFP power between the novel and familiar conditions. In the encoding phase, a linear regression analysis has been carried out to test whether image familiarity could modulate the low-frequency power appearing immediately after the sample onset by image repetition time (i.e. familiarity level), but no linear relationship between the repetition time and the low-frequency power in each brain region was detected. This may be related to the unevenly distributed number of trials in each familiarity level, since there were fewer trials at higher familiarity levels. To balance the number of trials in each condition, I divided trials into novel (1st presentation, 646 trials in total) and familiar (repeated, 923 trials in total) conditions in the LFP power spectra and LFP-LFP coherence analysis. In the encoding phase, novel sample images induced significant larger high-frequency beta activities (30-40 Hz) in temporal regions (e.g. TE and PrC), and gamma activities (50-70 Hz) in dlPFC around 600 ms relative to sample image onset. Familiar sample images induced gamma activities (70-120 Hz) in TE and dlPFC, and alpha/low-beta activities (10-15 Hz) in PrC, which both appeared immediately after the

sample onset. A tentative conclusion can be drawn from the above LFP power comparisons is that modulations of LFPs in temporal and frontal regions by familiar sample images was earlier than modulations of LFPs by novel sample images in the encoding phase.

In the delay phase, a common beta burst (20-40 Hz) in TE, PrC and dlPFC induced by novel images was found at 400 ms relative to sample image offset. The coherence analysis further illustrates that alpha/beta-frequency coherence in TE-dlPFC and in PrC-dlPFC brain pairs peaked around 400 ms relative to delay onset in novel condition. A tentative conclusion can be drawn from here is previously-presented novel images modulated both LFPs and alpha/beta-band coherence between temporal and frontal regions around 400 ms relative to image offset. Bursts of gamma power in those three regions were found significantly higher for familiar images, appearing immediately after delay onset in TE and dlPFC and appearing approximately 700 ms in PrC. It seems previously-presented familiar sample images modulated LFPs of temporal and frontal regions in the gamma band.

In the choice phase of both match and non-match trials, 30-40 Hz oscillations were persistent in TE, PrC and dlPFC prior to the presentation of test image, but became weaker when test image appeared. An electrophysiological study in NHPs has shown a beta range of oscillations (15-20 Hz) was found in IT while macaques maintained sample images in their short-term memory (Tallon-Baudry 2004). Another macaque electrophysiological study using laminar recordings in different layers of PFC showed that a synchronization of alpha/beta bands was found between superficial and deep layers of PFC during memory delay period (Bastos et al. 2018). Taken together, the above two findings and our LFP results show that beta oscillations in frontal and temporal regions were related to maintenance of items in recognition memory. In match trials, we found an early modulation of neural activities in both the temporal and frontal regions by familiar sample images (i.e. familiar condition) than novel sample images (i.e. novel condition). Specifically, in familiar condition, neural

activities in TE (30-50 Hz) and PrC (30-50 Hz) appeared immediately after test image onset, and activities in dlPFC (40-60 Hz) appeared 300 ms relative test image onset; while in novel condition, activities in TE (30-40 Hz) and PrC (60-90 Hz) appeared around 400 ms and activities in dlPFC (40-50 Hz) appeared around 700-800 ms after test image onset. In non-match trials, a similar phenomenon of early modulation by familiar sample images compared with novel sample images was found. To be specific, in familiar condition, gamma activities in the three regions (e.g. 50-80 Hz in TE, 40-60 Hz in PrC, 60-80 Hz in dlPFC) appeared between 100-200 ms relative to test image onset; while in novel condition, activities in TE (50-60 Hz), PrC (30-40 Hz) and dlPFC (100-120 Hz) appeared 300 ms relative to test image. One possible explanation of the early neural modulations by image familiarity is that familiar sample images which were held in macaques' memory may have a priority to be retrieved when comparing them with other test stimuli in the choice phase.

To further illustrate the interaction between temporal and frontal regions throughout the recognition memory task and how the temporal and frontal interaction being modulated by image familiarity, a coherence analysis among TE, PrC and dlPFC was conducted. It has been detected a very high value of coherence between TE and PrC throughout the recognition memory task. This may indicate a closer relationship between TE and PrC in recognition memory as anatomically visual area IT projected to PrC (Aminoff et al. 2013). A further brain extraction operation further confirms the array of TE and array of PrC were spatially close (see recording sites of the TE array and PrC array in Figure 1), indicating signals from the two arrays were similar thus had a high coherence value. Permutation tests (two-tailed) have shown a significantly increased alpha/beta-band coherence between TE and dlPFC during the encoding phase of familiar images; and a significantly increased alpha/beta-band coherence between TE and PrC during the delay phase of maintaining familiar images; and a significantly increased theta-band coherence between TE and PrC in familiar condition than novel condition during the match choice phase of memory task. This indicates low-frequency

coherence (i.e. for theta and alpha/beta bands) between temporal and frontal lobe seem to be more modulated by familiar images than novel images throughout recognition memory task. Although some gamma-band coherence were found to be significantly different between the novel and familiar conditions, most of them had repaid fluctuation and were thus discrete along the time. Admittedly, permutation tests used in our coherence analysis are very sensitive to the fluctuations, indicating a smoothing operation on high-frequency coherence (e.g. gamma-band coherence) may be needed prior to permutation comparison.

In summary, our analyses primarily indicate dynamical interactions between frontal and temporal regions in macaque recognition memory, and also confirm image familiarity modulated both behavioral and neural activities throughout the recognition memory task. Compared with traditional focus of research on individual neurons and individual brain regions in memory, we used simultaneous multi-area multi-neuronal recordings from implanted microelectrode arrays to determine how brain regions in the frontal and temporal lobes causally interact with each other during recognition memory. In the future, interaction between PFC and MTL, especially interaction between PFC and hippocampus (i.e. a topic has been investigated in Chapter 6), in primates will be a central focus to unravel the neural mechanisms of recognition memory and will facilitate decoding analyses of informational content.

Chapter 5. Contributions of prefrontal and temporal lobe cortical areas to recognition memory and perceptual discrimination

Abstract

The function of medial temporal lobe (MTL) was traditionally viewed as containing a system of structures exclusively involved in memory. However, more recent studies have shown that some parts of the system structures (e.g. perirhinal cortex and hippocampus) participate in perception. Recent literature also confirms a role of PFC in both perception and memory. To better understand this scientific issue, a delayed mnemonic task and a hybrid mnemonic and perceptual task were developed for simultaneous multi-area, multi-electrode recordings in non-human primates (NHPs) in this study so that the interaction between MTL and PFC in tasks which draw upon these two processes to greater or lesser extents can be investigated. Behavioral results showed no difference (e.g. correct rate, d prime) was found between the memory and hybrid tasks, indicating the two tasks were matched in term of accuracy. By analyzing the local field potentials (LFPs) of recorded brain areas and LFP-LFP coherence between those regions in both tasks, we found low-frequency LFP activities (i.e. theta and alpha/low-beta activities) in temporal and frontal regions were important for encoding, maintaining and retrieval of visual stimuli in the memory task; and high-frequency gamma activities in temporal regions during the choice phase were more related to perceptual discrimination. Although the limitations (e.g. strong power line interference on recorded data) exist in neural data interpretation, this study benefited future electrophysiological

research on this topic by providing new directions (e.g. task design in animal electrophysiological study) to solve the debate as well as advanced recording methodologies.

Introduction

From convergent neurophysiological evidence, it is widely acknowledged that the medial temporal lobe (MTL) contributes to declarative memory (Squire et al. 2004; Squire 2004). According to canonical MTL memory system theory, the MTL is exclusively involved in declarative memory with little or no contribution to perception (Squire and Zola-Morgan 1991; Buffalo et al. 1998, 1999, 2000; Squire 2004; Squire et al. 2004, 2006; Suzuki 2009). However, there has since been a long-standing debate as to whether some MTL structures, most notably the perirhinal cortex (PrC) and the hippocampus, also contribute to perception (Baxter 2009; Buckley et al. 2001; Buckley 2005; Bussey et al. 2002a; Bussey and Saksida 2002; Bussey et al. 2003, 2005, 2006; Bussey and Saksida 2007; Eacott et al. 1994; Lee et al. 2005a, 2005b, 2005c; Murray and Bussey 1999; Murray and Richmond 2001). A perceptual-mnemonic theory of MTL function has therefore been proposed to explain the MTL also plays an essential role in certain forms of high-level perception (Baxter 2009; Buckley 2005; Buckley and Gaffan 2006).

In the early research investigating the role of MTL in memory and perception, the set-size effects both in recognition memory (Eacott et al. 1994; Gaffan and Eacott 1995) and in concurrent discrimination learning (Buckley et al. 1997; Buckley and Gaffan 1998a) have been investigated. The original study from Eacott et al. (1994) showed that bilateral ablations of macaque rhinal cortex preserved their performance in a delayed matching-to sample (DMS) task with small set-sizes but impaired their performance in both a DMS task and a simultaneous matching-to sample task with large set-sizes (Eacott et al. 1994), indicating rhinal cortex is both involved in recognition memory and visual processing. Eacott et al. (1995) further found lesion of uncinate fascicle (i.e. an area connecting visual association cortex and prefrontal areas) had no effect on monkeys' performance in DMS task with either small or large set-sizes (Gaffan and Eacott 1995), indicating that the intact memory after removal of rhinal cortex in the DMS task with small set-sizes (Eacott et al. 1994) may be

supported by the remaining visual association cortex, which is located medial and posterior to the rhinal cortex (Gaffan and Eacott 1995). In the later research from Buckley and Gaffan, they found that monkeys with lesions of PrC demonstrated impairments in concurrent visual discriminations between pairs of colored shapes with increased numbers of foils or with increased set-sizes (Buckley et al. 1997). Further studies showed that damage to macaque PrC also impaired object concurrent discrimination learning with large-set sizes (Buckley and Gaffan 1998a) but not the performance in recognition memory task with small set-sizes (Eacott et al. 1994; Zola-Morgan et al. 1993). As removal of PrC impairs performance in both concurrent learning task and recognition memory task if set-size is large but not impairs performance if set-size is small, this suggests that set-size of stimulus matters more than task category. This is a slight indication that PrC is important for object identification.

To further investigate the role of PrC in perception, several perceptual discrimination paradigms (i.e. the oddity task, the morph task and the biconditional discrimination task) have been developed and used in both animal lesion studies and human neuropsychology research. The oddity task was invented by Buckley and Gaffan in macaques (Buckley et al. 2001) and used later in human patients (Lee et al. 2005a, 2005b, 2005c; Levy et al. 2005). In this oddity task, simultaneous discriminations are required to be made between simultaneously presented stimuli (Buckley et al. 2001; Lee et al. 2005a, 2005b, 2005c; Levy et al. 2005). It has been found damage to macaque PrC doesn't impair simple discriminations based on color, shape, or size, or same-viewpoint presentations of human/monkey faces; but impairs discriminating oddity objects or oddity human/monkey faces among other objects or faces with different-views and also impairs discriminating oddity scenes among other same-view scenes (Buckley et al. 2001). This indicates a role of macaque PrC involved in perceptual discriminations at an object-level (i.e. involving multiple features configured together) rather than at a simple-feature level (Buckley et al. 2001). Lee and his colleague further applied this oddity task paradigm to human patients, and they found patients with

extensive MTL damage, including PrC, demonstrate severe discrimination deficits in the oddity judgments based on an object level (Lee et al. 2005a, 2005b, 2005c). Although Squire and Suzuki criticized interpretations on the role of PrC in macaque oddity task as they argued that deficits of perceptual discrimination abilities after lesions of PrC can be also interpreted as a leaning or memory deficit (Squire et al. 2006; Suzuki 2009), Buckley et al. further demonstrated that PrC-lesioned macaques showed impairments in the first-trial discrimination between oddity objects/human/monkey faces and other objects/human/monkey faces with different-views, which cannot be interpreted as a memory deficit (Buckley 2005). Bussey and his colleagues designed a morph task, in which subjects are required to discriminate pairs of morphed stimuli with high-degree of feature ambiguity (Bussey et al. 2003, 2006; Bussey and Saksida 2007). It has been shown that lesions of macaque PrC impair discriminating between very similar morphed pictures but not very different morphed pictures (Bussey et al. 2003, 2006). Bussey and his colleagues (2002) also developed a biconditional discrimination task, in which subjects are required to discriminate stimuli with minimum, intermediate and maximum feature ambiguity. It has been found that macaques with selective PrC lesions and patients with ablations of extensive MTL demonstrate impairments in discriminating stimuli in which high degrees of feature overlap are explicitly introduced (Bussey et al. 2002a; Bussey and Saksida 2002; Barense et al. 2005). To summarize the above studies, it seems that PrC is involved in discriminating between objects with high similarities in terms of feature overlap.

What's a key manipulation on perceptual discrimination task to reveal impairments induced by damage to PrC? Several points can be summarized based on the previous lesion literature in macaques and human patients, and some viewpoints from the memory versus perception debate (Baxter 2009; Buckley 2005; Buckley and Gaffan 2006). First of all, the PrC is thought to be sensitive to objects presented in different viewpoints in the oddity task (Baxter 2009; Buckley 2005; Buckley and Gaffan 2006) and the degree of image feature

ambiguity in the morph task (Bussey et al. 2002a; Bussey and Saksida 2002, 2007). In both tasks, discriminating between objects cannot rely on a single feature but a combination or conjunction of different features. Secondly, a larger set-size of stimuli in the oddity task is critical for revealing perceptual deficits, as images with repeated presentations (i.e. small set-size) compromise the interpretation of MTL in perception due to a possible effect of long-term memory in animal research (Baxter 2009; Buckley 2005; Suzuki 2009). In my study, we used trial-unique stimuli with a large set-size for electrophysiological research to examine whether the role of PrC in recognition memory or perceptual discrimination would be different or not.

The canonical memory system theory of MTL has been proposed by Squire and Zola-Morgan in 1991, and they proposed that the MTL is a homogenous system and claimed that MTL does not contribute to perception and exclusively contributes to long-term declarative memory (Squire and Zola-Morgan 1991). After 20 years, Graham et al. have summarized more neuropsychological and neuroimaging findings in both animals and humans, and concludes that '*there is now significant evidence of a functional specialization in how MTL structures contribute to memory and perception of objects and scenes'* (Graham et al. 2010). For example, Lee et al. found a double-dissociation between hippocampus and PrC in processing scenes and processing objects in patients (Lee et al. 2005b). In a recent human neuroimaging study, a functional separation within MTL has been found in a scene-object associative memory task: the PrC is involved in object processing and parahippocampal cortex (PhC) participates in scene processing; while the hippocampus doesn't show any preference to either scene or object processing but integrates the object information from PrC and scene information from PhC during retrieval process (Staresina et al. 2013). Given the evidence of functional specialization of MTL structures above, investigating the ***interaction*** among hippocampus, PrC and PhC is crucial to help us understand how these structures play their roles in recognition memory and perceptual discrimination. Indeed, a more recent

prominent review summarized the recent findings on the role of PrC in memory/perception and concludes with the statement: "*it will be important to record during oddity or concurrent discrimination as well as during other clear memory-demanding tasks to determine if the perirhinal cortex provides similar mnemonic signals across both categories of tasks*" (Suzuki and Naya 2014). This is a key motivating factor and intention in the tasks I developed for simultaneous multi-area, multi-electrode recordings in NHPs in this study. I would investigate whether neuronal interactions within and between areas of the MTL (and also between MTL and PFC) were similar or different in mnemonic versus perceptual tasks. My hypothesis was that the PrC would interact differently with prefrontal areas in mnemonic task and perceptual task. In order to compare different neural mechanisms of PrC and other related regions underlying mnemonic and perceptual processes, two versions of tasks have been designed and used in this study: a delayed mnemonic task (a) (i.e. the same task used in Chapter 4) and a hybrid task (b) involving both delayed memory and simultaneous perception (the simple version of the two tasks was shown in Figure 1). In both tasks, the animal was trained to follow the same rule. The animal viewed the sample image (e.g. a yellow face in Figure 1); then after experiencing a delay period, in the delayed mnemonic task, a test object image and a black circle were shown to the animal; while in the hybrid task, the sample image reappeared along with the test object image and the black circle so to allow performance to be based upon simultaneous perceptual discrimination in addition to (or even instead of) memory to be investigated. In future work underway in other animals we have planned a third task which has the simultaneous discrimination at choice but omits the preceding sample alone phase, so to have a task version that can only draw upon simultaneous perceptual discrimination; regrettably it wasn't possible for this first NHP to learn this third task before the animal was terminated. In the two task versions we did use here the object test image was either the identical stimulus to the sample image (seen earlier in the mnemonic task or seen again in the hybrid task) or it was not identical to the sample

image (e.g. a red heart in Figure 1). The animal was rewarded for touching the test-item image if it matched the sample image (these we refer to as 'match trials'), or it was rewarded for selecting the standard 'non-match button' (i.e. the black circle) if the test-item was a non-match (these we refer to an 'non-match trials') in both tasks. The mnemonic and hybrid tasks had same task structure (i.e. encoding, delay, choice), and the only difference between the two tasks was the possibility for the animal to utilize perceptual discrimination in the choice phase. The presence or absence of the sample image in the choice phase could allow us to compare the neural signals from MTL and PFC in short-term mnemonic processes (a) and combined perceptual-discrimination and short-term mnemonic processes (b).

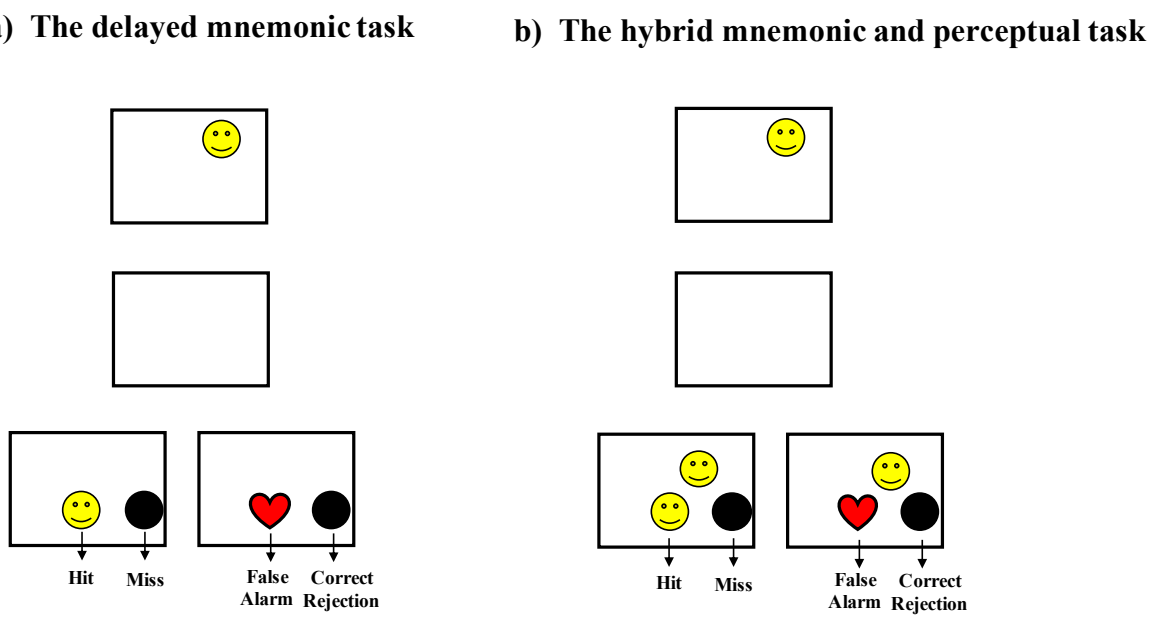


Figure 1. *A highly simplified schematic of the delayed mnemonic task (a) and the hybrid perceptual and mnemonic task (b) for NHPs to illustrate the main difference. In both tasks, the animal viewed the sample image (e.g. a yellow face). Then after a delay period, two choice stimuli were shown on the screen in both the mnemonic and hybrid tasks: either an identical image (e.g. a yellow face) or a novel image (e.g. a red heart) along with a black circle ('non-match' button). In the hybrid task, the sample image re-appeared (e.g. the yellow face) along with the two choice stimuli. Animal was rewarded for either touching the*

identical image to make a 'hit' response or touching the non-match' button to make a 'correct rejection' response.

Materials and Methods

Subject

Neural data was recorded in one young adult female macaque monkey (*Macaca mulatta, age 8 years, weight 10-13 kg*). All animals in our lab are socially housed (or socially housed for as long as possible if later precluded, for example, by repeated fighting with cage-mates despite multiple regrouping attempts) and all are housed in enriched environments (e.g. swings and ropes and objects, all within large pens with multiple wooden ledges at many levels) with a 12hr light/dark cycle. The NHP always had *ad libitum* water access 7 days/week. Most of its daily food ration of wet mash and fruit and nuts and other treats was delivered in the automated testing/lunch-box at the end of each behavioral session (this provided 'jack-pot' motivation for quickly completing successful session performance; supplemented by trial-by-trial rewards for correct choices in the form of drops of smoothie delivered via a sipping tube) and this was supplemented with fruit and foraging mix in the home enclosure. All animal training, array implantation surgery, and experimental procedures were performed in accordance with the guidelines of the UK Animals (Scientific Procedures) Act of 1986, licensed by the UK Home Office, and approved by Oxford's Committee on Animal Care and Ethical Review.

Surgical procedure

The details of *surgical procedures* can be found in Chapter 2. After the basic behavioural and initial task training phase was complete the animal first received a titanium head-post, implanted posteriorly and secured to the cranium with titanium cranial screws through the

legs of the post; the reflected skin and galea was sutured and the wound closed around the base of the head-post. Localizations of the targeted brain areas was based on pre-operative structural MRI scans. During the implantation surgery, one 64-electrode Utah array (the electrodes were arrange on a 8 × 8 grid embedded in silicone) subdurally inserted into area TE, and the other two 32-electrode Utah arrays (the 6 × 6 grid of silicone microelectrodes) inserted into PrC (area 35/36) and dlPFC (area 9/46), separately. All the microelectrodes were made of platinum (Pt). These three arrays were all connected to one pedestal (with 128 output channels) affixed externally to the cranium. The four corner electrodes of this pedestal were 2 reference electrodes and 2 ground electrodes. Recording sites of TE array, PrC array and dlPFC array in the NHP were shown in Figure 2. Another 64-electrode Utah array (the 8 × 8 grid of silicone microelectrodes) subdurally inserted into area vlPFC (area 45), and the other two 32-electrode Utah arrays (the 6 × 6 grid of silicone microelectrodes) inserted into area OFC (area 11/13) and temporal pole, separately. All the microelectrodes were made of platinum-iridium mix. Unfortunately, the neural signals from vlPFC, OFC and temporal pole arrays could not be obtained due to accidental disconnection of the pedestal connecting to those Utah arrays from the cranium (i.e. pulled off by the animal playing with loosened pedestal before we had completed preparations for surgical stabilization of the pedestal which were underway). All the electrode length was 1.0 mm and their separation from each other in the array was 0.4 mm). After array implantation surgery, two reference wires connecting to the two pedestals were left under the dura, and both dura and bone flap were sutured back and covered with the skin.

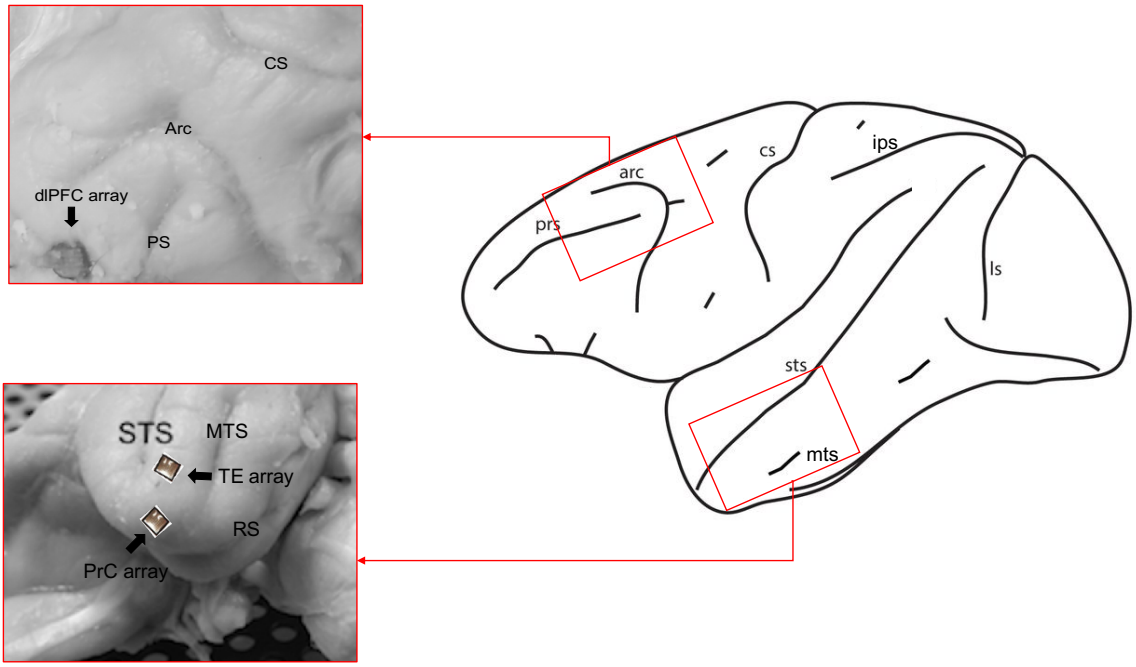


Figure 2. *Recording sites from TE array, PrC array and dlPFC array in lateral view of the NHP brain. NHP recording sites (shown in the upper red square) using the Utah array of dlPFC was above the principle sulcus (PS) and anterior to the arcuate sulcus (Arc). NHP recording sites (shown in the lower red square) using the Utah array of TE was between the superior temporal sulcus (STS) and anterior to the medial temporal sulcus (MTS), and recording sites using the Utah array of PrC was below the STS and above the rhinal sulcus (RS).*

Task stimuli and apparatus

Both the delayed mnemonic task and the hybrid perceptual and mnemonic task were programmed using Turbo Pascal (Borland), run under DOS on a desktop PC. Visual stimuli used in the task were clip-art images in colour, which were presented on a 20.1" colour touch-sensitive screen (TFT LCD TS200H GNR). Those clip-art images used in both tasks were from a large pool of several thousand unique images. Each image subtended 5° of visual angle in width and 5° in height to the subject when presented on the screen. The sample

image was always presented on the right top of the screen, positioned +9 ° horizontal and -9 ° vertical from the center of the screen. The test images were presented on the right bottom of the screen in both tasks: one was positioned 0 ° horizontal and +3 ° vertical from the center of the screen; and the other one was positioned +17 ° horizontal and +3 ° vertical from the center of the screen. The background colour to the screen was white. In each session of recordings, images were randomly chosen from the pool without replacement and were not re-used on the other recording days.

The animal was seated in a primate chair (Rogue Research Inc.) in front of the touch screen with its head-fixated and whilst it performed both tasks in a magnetic-shielded, and partially sound-attended, testing-box. A window in the front of the chair provided its access, both to the touch-screen itself and also to a touch-sensitive knob which we refer to as a 'key-touch' which was positioned low down in front of the touch screen; the animal had to steadily hold the keytouch at various times in each trial (to control for arm movement/position whilst it waited for stimuli, looked at stimuli, and waiting for a visual cue to release keytouch and touch the screen to make a choice). The distance between the monkey and touch screen was fixed at 50 cm enabling the animal to touch the screen easily. An infrared camera was used to monitor the general status of the monkey in the box. A peristaltic pump device located on top of the box fed smoothie reward through a tube and to a spout positioned in the vicinity of the animal's mouth. Below the screen was also an automated lunch-box which contained the majority of the animal's daily meal (wet mash and fruits and nuts etc.) and which opened immediately at the end of the task.

Behavioral Tasks

The macaque participated in both a delayed mnemonic task and a hybrid mnemonic and perceptual task (see Figure 3). In each trial of both tasks, the animal initiated the tasks by holding the key-touch when cued to do so by a small red circular keytouch cue presented on

the screen. The NHP was required to keep holding the keytouch device through a variable delay of 1000-1500 ms (if the keytouch hold was broken the trial aborted) after which a central sample (object image) appeared behind the red key-touch cue. The NHP was required to keep holding the keytouch device through another variable delay of 1000-1500 ms (again, if the keytouch hold was broken the trial aborted) after which the red keytouch cue disappeared which was the cue to the animal it could release its hand from the keytouch at which point the delay (1000ms) between sample and choice-phases began (the maximal time for releasing key-touch was 5000 ms else the trial aborted and the animal received a time-out for 10 s). Then after the 1000 ms delay period another red keytouch cue appeared, this time in the bottom of the screen (close to, and equidistant, from where the two choice items would appear) and animal was required to hold the key-touch again. The NHP was again required to keep holding the keytouch device through a variable delay of 1000-1500 ms (if the keytouch hold was broken the trial aborted) after which two choice stimuli appeared (one an object image and the other a black circle, left-right randomized between trials) in both tasks and the central sample re-appeared on the top of the screen in the hybrid task. In both tasks, the NHP was required to keep holding the keytouch device through another variable delay of 1000-1500 ms (again, if the keytouch hold was broken the trial aborted) after which the red keytouch cue disappeared which was the cue to the animal that it could release holding the keytouch and now make a choice to the touchscreen to either the object test-image stimulus or to the black circle stimulus. The object stimulus was either the identical stimulus to the sample (seen earlier in the mnemonic task and seen again in the hybrid task) in the trial or it was not identical to the sample. The animal was rewarded by delivery of 10 ml of smoothie for touching the test-item image if it matched the sample image (these we refer to as ‘match trials’), or it was rewarded for selecting the standard ‘non-match button’ (i.e. the black circle) if the test-item was a non-match (these we refer to an ‘non-match trials’). The next trial started after a 3000 ms inter-trial interval after a correct response, or after a 10 s ‘time-out’

after any kind of error response (or after any failure to hold keytouch for the required time, or after failure to release when required). A schematic of the delayed mnemonic task (panel a) and a hybrid mnemonic and perceptual task (panel b) is illustrated in Figure 3. Accordingly in both mnemonic and hybrid tasks, on *match trials* the animal could either make a correct response ('hit') or an incorrect response ('miss') whereas on *non-match trials* the animal could either make a correct response ('correct rejection') or an incorrect response ('false alarm'). To make both mnemonic and hybrid task comparable, we also varied the degree to which stimuli were either familiar or novel in the session in both tasks (typically there were up to 80 pairs of novel stimuli that were trial-unique in each session, and six other familiar stimuli, grouped into three pairs, that repeated many times through the session).

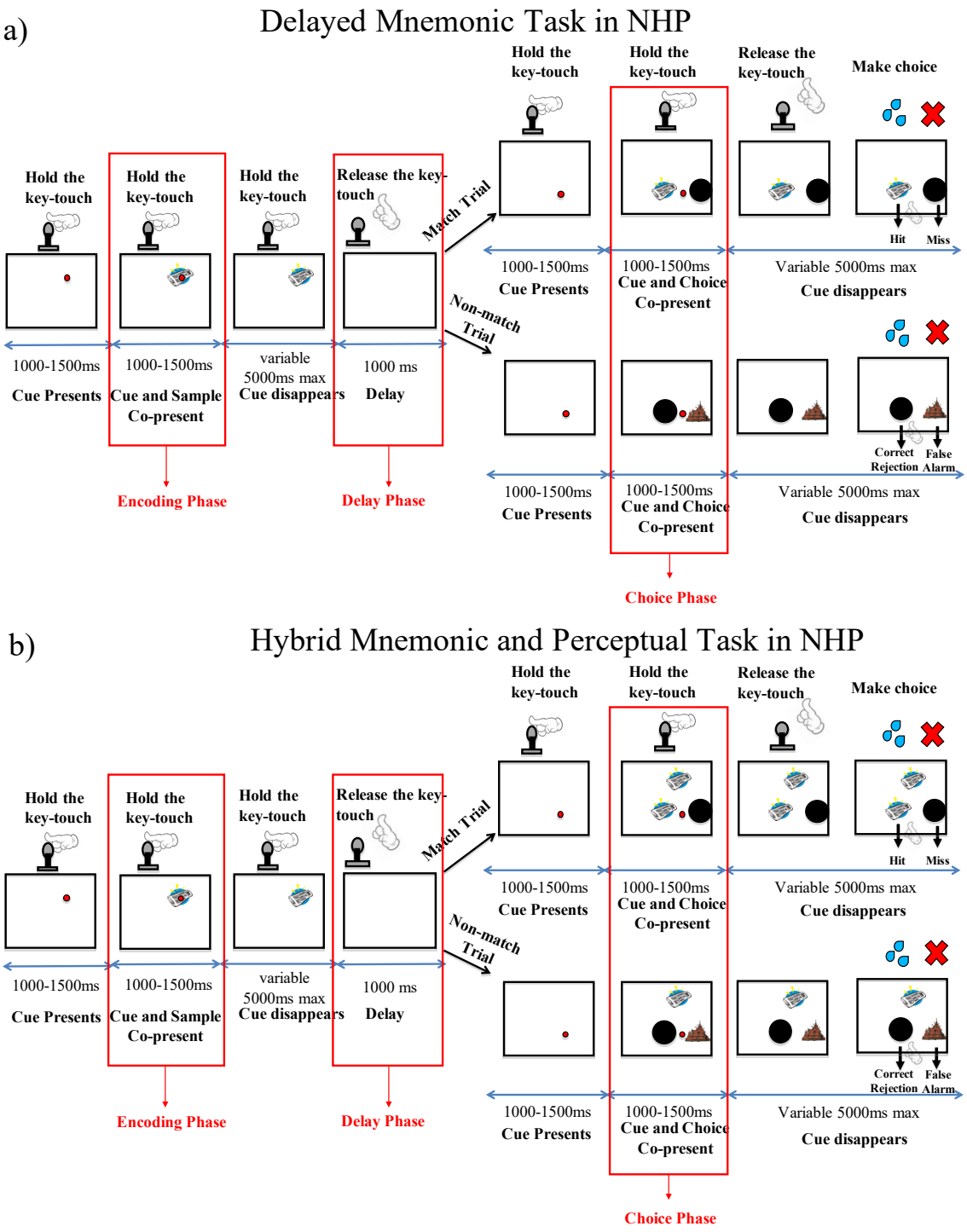


Figure 3. *Delayed mnemonic task (a) and hybrid perceptual and mnemonic task (b) in NHPs. In both tasks, the animal initiated the task by holding the key-touch within a variable time of 1000-1500 ms, then a sample image was shown on the screen below the red cue (encoding phase). The NHP was required to keep holding the keytouch device through another variable delay of 1000-1500 after which the red keytouch cue disappeared then the NHP was trained*

to release its hand from the keytouch prompting the commence of the delay (1000ms) between sample and choice-phases. Then after the 1000 ms delay period another key-touch red dot cue, this time in the bottom of the screen, and the animal was required to hold the key-touch again. The NHP was again required to keep holding the key-touch device through a variable delay of 1000-1500 ms after which choice stimuli appeared. In the mnemonic task (a), two choice images, either an identical image or a novel image along with a black circle were shown on the screen; while in the hybrid task (b), two choice stimuli along with the central sample image were shown on the screen (choice phase). The NHP was required to keep holding the keytouch device through another variable delay of 1000-1500 ms after which the key-touch red dot cue disappeared cueing the animal that it could release holding the key-touch and make a choice to the touchscreen to either the object test-image stimulus or to the black circle. The highlighted sample, delay and choice phases were selected to be time windows for neural data analysis.

Neurophysiological Recordings

Data were recorded simultaneously from the 64-electrodes in the microelectrode array in TE, and the 32-electrodes in PrC and the 32-electrodes in dlPFC throughout both the delayed mnemonic task and the hybrid perceptual and mnemonic task. Recording details were described in Materials and Methods of Chapter 4.

Signal Analysis

The NHP performed, on average, 75 trials (with both trial-unique and repeated stimuli) per day; the total average session duration was 45 minutes. The NHP has completed 29 sessions of delayed mnemonic task (data were also used in Chapter 3 and Chapter 4) and 28 sessions of hybrid mnemonic and perceptual task. In the below analysis, I only focused on trials with

trial-unique stimuli in both tasks (roughly 35 trials with trial-unique stimuli in each recorded session) as repeated stimuli can be learnt about across trials which may promote mnemonic involvement even in the hybrid task. Due to the electrode degrading (the yield from electrodes degrades over time, presumably due to processes occurring at the electrode tip), I didn't get any single-unit or multi-unit activities from all the Utah arrays by the time the animal was tested in the hybrid task. Therefore to compare the neural signals recorded in both mnemonic and hybrid tasks, I analyzed only the local field potential (LFP) activities from the three Utah arrays in TE, PrC and dlPFC and investigated the LFP-LFP coherence between the three recorded areas in both tasks. Details of signal analysis was described in Materials and Methods of Chapter 4. Briefly, in the LFP power spectrum analysis, LFPs of three brain areas in the sample phase (sample image on the screen for 1000-1500 ms when the macaque held the key-touch), delay phase (1000 ms), and choice phase (choice images on the screen for 1000-1500 ms when the macaque held the key-touch) of both memory task and hybrid task were selected for analysis. In each trial, LFPs in each task phase from 1000 ms (as a baseline) before stimulus onset until 1000 ms after stimulus onset were analyzed. The LFP power around the stimulus onset was calculated as follows:

7) Wavelet transform of the signals around the stimulus onset and during the ITI baseline (i.e. a 1000 ms segment) were calculated, yielding $O_{stimulus}$ *and* $O_{baseline}$;
8) The power of the stimulus was calculated as $P_{stimulus} = O_{stimulus}^2$, and the mean power of the baseline was calculated as $P_{baseline} = \text{avg}(O_{baseline}^2)$;
9) The LFP power of the stimulus was calculated as a ratio of $P_{stimulus}$ to $P_{baseline}$, i.e.:

$$LFP\ power = \frac{P_{stimulus}}{P_{baseline}} = \frac{O_{stimulus}{}^2}{\text{avg}(O_{baseline}{}^2)}$$

As both the power of the stimulus and the baseline have the same units (i.e. μV^2), the above calculated LFP power is dimensionless. Then LFP power in TE, PrC and dlPFC were

averaged across corresponding channels and were combined cross sessions.

In the coherence analysis, data from 200 ms (as a baseline) before stimulus onset until 800 ms after stimulus onset (to avoid the spectral leakage of LFP power when calculated near the margin of a 1000 ms time-window) in each trial were included, provided a time window of 1000 ms. LFPs in TE, PrC and dlPFC were averaged across corresponding channels, and then trial-averaged coherence between TE and PrC, between TE and dlPFC, and between PrC and dlPFC were calculated during the sample, delay, and choice phases of memory task and hybrid task in each recorded session.

All the neural data were analyzed with the MATLAB (R2017b, MathWorks), FieldTrip toolbox (*http://www.fieldtriptoolbox.org*, details see Oostenveld et al., 2011), Chronux Toolbox (*http://chronux.org*), and custom-written scripts. As it's important to avoid memory confounds when investigating perceptual discrimination where possible, behavioral and neural data were analyzed from only trial-unique and successfully completed trials.

Statistical analysis of induced LFP power spectra of each recorded brain region and LFP-LFP coherence across three regions between the memory and hybrid tasks

To investigate the task structure on neural activities, we compared induced LFP power from TE, PrC and dlPFC and LFP-LFP coherence between pair-wise regions in the encoding, delay and choice phases of the delayed mnemonic task and the hybrid mnemonic/perceptual task.

To test for statistical significance of differences of the induced LFP power spectra between the two tasks in difference phases, we performed a nonparametric permutation test, with the median difference between the above conditions as our test statistic. As described above in *signal analysis*, channel-averaged LFPs across different brain areas were calculated. In each trial, the time window for nonparametric permutation test was 0-800 ms (i.e. time

zero was the stimulus onset) in each task phase of both tasks, to avoid the spectral leakage of LFP power when calculated near the margin of a 1000 ms time-window. The non-parametric permutation test is an assumption-free method without prescribing underlying distributions (Maris and Oostenveld 2007). In each task phase (e.g. encoding, delay, choice), the null hypothesis of this test was assumed that, for each frequency and time bin, there was no significant difference of the LFP power when comparing the observed median difference between the two conditions (i.e. memory and hybrid) against a reference distribution. The permutation test for the LFP data was performed in the following steps:

1. The observed median difference between the two conditions was obtained for each time and frequency bin, i.e. $D_{t,f}$;
2. A reference distribution for each time and frequency bin was obtained by performing 10,000 permutations on trial labels to randomly assign the two conditions. That is, each time and frequency bin had its own reference distribution, in the format of $[d_{t,f}] = (d_{t,f,1}, d_{t,f,2}, d_{t,f,3}, \ldots d_{t,f,10000})$.
3. For each time and frequency bin, its $D_{t,f}$ was compared to its own refence distribution (i.e. $[d_{t,f}]$). This bin would be selected if the observed median difference was either larger than the 97.5th or smaller than the 2.5th percentile of its reference distribution.
4. All these selected time and frequency bins were then clustered in connected sets based on adjacency in time and frequency.
5. We calculated the sum of the median differences within each cluster, and kept only the largest cluster (with the largest sum of the median difference) in the cluster-level statistics (Maris and Oostenveld 2007).
6. The above nonparametric permutation procedure was performed separately for each of the brain regions (e.g. TE, PrC and dlPFC) and separately for each task phase (e.g. sample, delay and choice phase).

It's acknowledged that as comparisons between observed data and permutated data have been carried out in all the time and frequency bins separately, multiple comparison problem still exists in this method. To be reasonably conservative, I picked the largest cluster in the real data among other clusters, although by doing so, the sensitivity for detecting smaller clusters is reduced.

To test for statistical significance of differences of the LFP-LFP coherence across different brain areas in difference phases of memory hybrid tasks, we performed a nonparametric permutation test, with the median difference between the above task conditions as our test statistic. Prior to nonparametric permutation test, trial-averaged and channel-averaged coherence across different brain areas were calculated in each session. For each brain pair, LFP-LFP coherence was then averaged in theta-band (4-6 Hz), alpha/beta-band (12-35 Hz) and gamma-band (35-120 Hz). In each session, the calculated coherence data from 200 ms before stimulus onset until 800 ms after stimulus onset was put into nonparametric permutation test (i.e. providing a time window of 1000 ms). In each task phase (e.g. encoding, delay, choice), the null hypothesis of this test was assumed that, for each time bin, there was no significant difference of the LFP-LFP coherence when comparing the observed median difference between the two conditions (i.e. memory and hybrid) against a reference distribution. This reference distribution was obtained by performing 10,000 permutations on session labels to randomly assign the two conditions. A time bin would be selected if its observed median difference was larger than the 97.5^{th} or smaller than the 2.5^{th} percentile of its permutated data ($p < 0.05$, two-tailed). Then the selected time bins were clustered in connected sets on the basis of temporal adjacency. The above nonparametric permutation test was performed separately for each brain pair (e.g. TE- PrC, TE-dlPFC, and PrC-dlPFC) and separately for each task phase (e.g. sample, delay and choice phase).

Results

Behavioural comparisons between the mnemonic and hybrid tasks

Accuracy and response time (RT) in match trials (i.e. hit rate) and in non-match trials (i.e. correct rejection rate) were calculated in both mnemonic and hybrid tasks. A mixed-model repeated measures ANOVA was conducted on the rate data, with task-type (2 levels: memory task, hybrid task) as the between-subject factor and rate-type (2 levels: hit rate, correct rejection rate) as the within-subject factor. A main effect of rate-type was significant ($F_{(1,54)}$ = 7.382, p = 0.009, η^2 = 0.120). Neither the main effect of task-type ($F_{(1,54)}$ = 0.216, p = 0.644, η^2 = 0.004) nor the interaction between task-type and rate-type ($F_{(1,54)}$ = 3.162, p = 0.081, η^2 = 0.055) was significant (Figure 4a). Another mixed-model repeated measures ANOVA was conducted on the RT data, with task-type (2 levels: memory task, hybrid task) as the between-subject factor and RT-type (2 levels: hit RT, correct rejection RT) as the within-subject factor. Neither the two main effects (main effect of task-type: $F_{(1,54)}$ = 0.171, p = 0.681, η^2 = 0.003; main effect of RT-type: $F_{(1,54)}$ = 1.392, p = 0.243, η^2 = 0.025) nor the interaction between task-type and RT-type ($F_{(1,54)}$ = 0.031, p = 0.862, η^2 = 0.001) was significant (Figure 4b).

The d prime and response criterion from the equal-variance signal detection (EVSD) model, were also calculated based on recognition errors in both tasks. d prime (d') is a discriminative index, which is calculated as the distance from the new-item and old-item distributions, reflecting the discrimination between the old and new items. Response criterion (cr) is defined as whenever individual internal response is greater than criterion, subject considers it as an old item; or vice versa. A mixed-model repeated measures ANOVA was conducted on the index data, with task-type (2 levels: memory task, hybrid task) as the between-subject factor and index-type (2 levels: dp, cr) as the within-subject factor. A main effect of index-type was significant ($F_{(1,54)}$ = 248.397, p < 0.001, η^2 = 0.821). Neither the

main effect of task-type ($F_{(1,54)} = 1.114$, $p = 0.296$, $\eta^2 = 0.020$) nor the interaction between task-type and index-type ($F_{(1,54)} = 2.254$, $p = 0.139$, $\eta^2 = 0.040$) was significant (Figure 4c). Taken together, no behavioral difference between the two tasks was found.

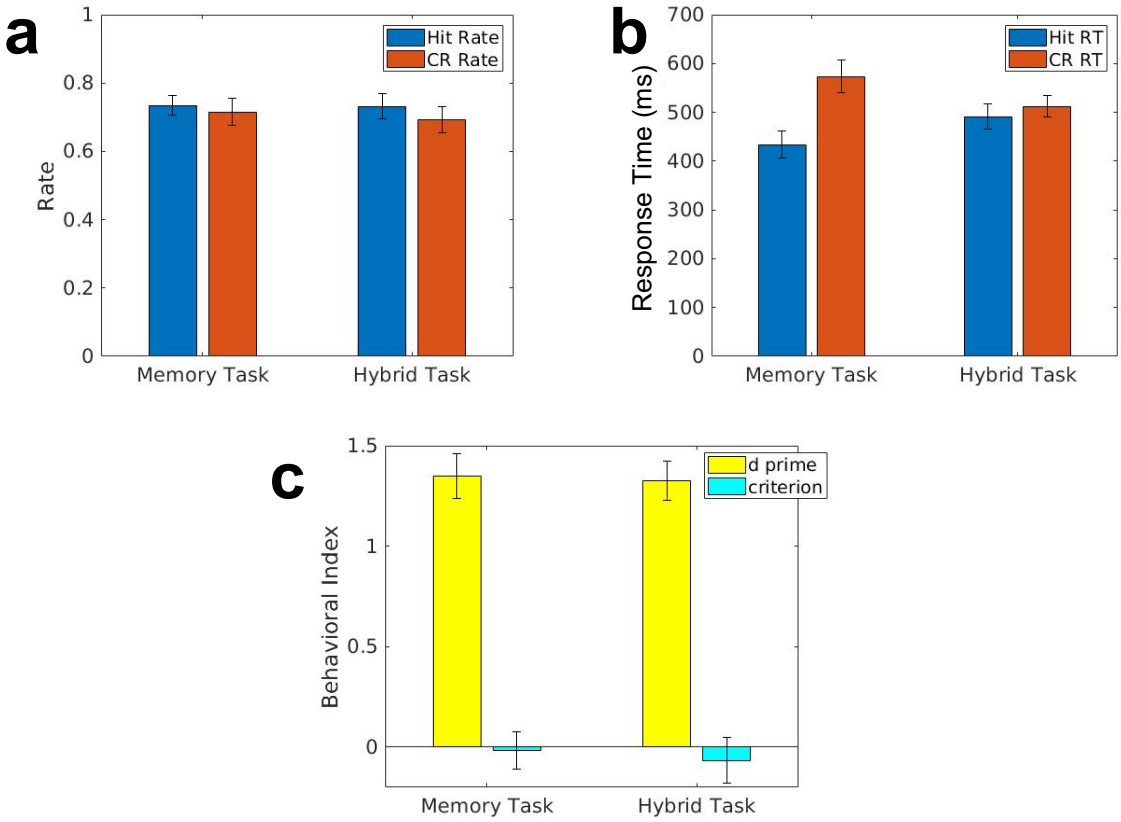


Figure 4. *Comparisons of behavioral performance between the mnemonic and hybrid tasks. No significant difference of the behavioral measurements (e.g. panel A: hit rate, correct rejection rate; panel B: response time of hit trials and correct rejection trials; panel C: d prime, response criterion) was found between the two tasks.*

Modulations of induced LFP spectral power by task category in TE, PrC and dlPFC

I compared induced LFP spectral power in TE, PrC and dlPFC during the encoding, delay and choice phases of the memory and hybrid tasks. In the encoding phase of both tasks, we have observed an increased power ranging from 4-30 Hz after the sample onset in TE, PrC

and dlPFC. These brief bursts lasted roughly 300-400 ms in both memory (Figure 5, left panel) and hybrid tasks (Figure 5, middle panel). It has been observed these brief bursts of low-frequency activities were stronger in dlPFC than in TE and PrC in both tasks. A nonparametric permutation test (two-tailed) was applied to compare the power of LFPs in TE, PrC and dlPFC across the two tasks (Figure 5, right panel). The low-frequency clusters (power ranging from 4-10 Hz in TE and PrC, and 4-20 Hz in dlPFC) were found significantly higher for memory task. These clusters appeared immediately after the sample onset, whose durations were 500-600 ms in TE and PrC and 200-300 ms in dlPFC, respectively. In TE and PrC, another two clusters (power ranging from 40-80 Hz in TE and 40-60 Hz in PrC) appeared around 500-600 ms and around 700-800 ms after the sample onset, which were significantly higher for hybrid task. In dlPFC, a gamma power ranging from 70-120 Hz appearing immediately after the sample onset was significantly higher for hybrid task.

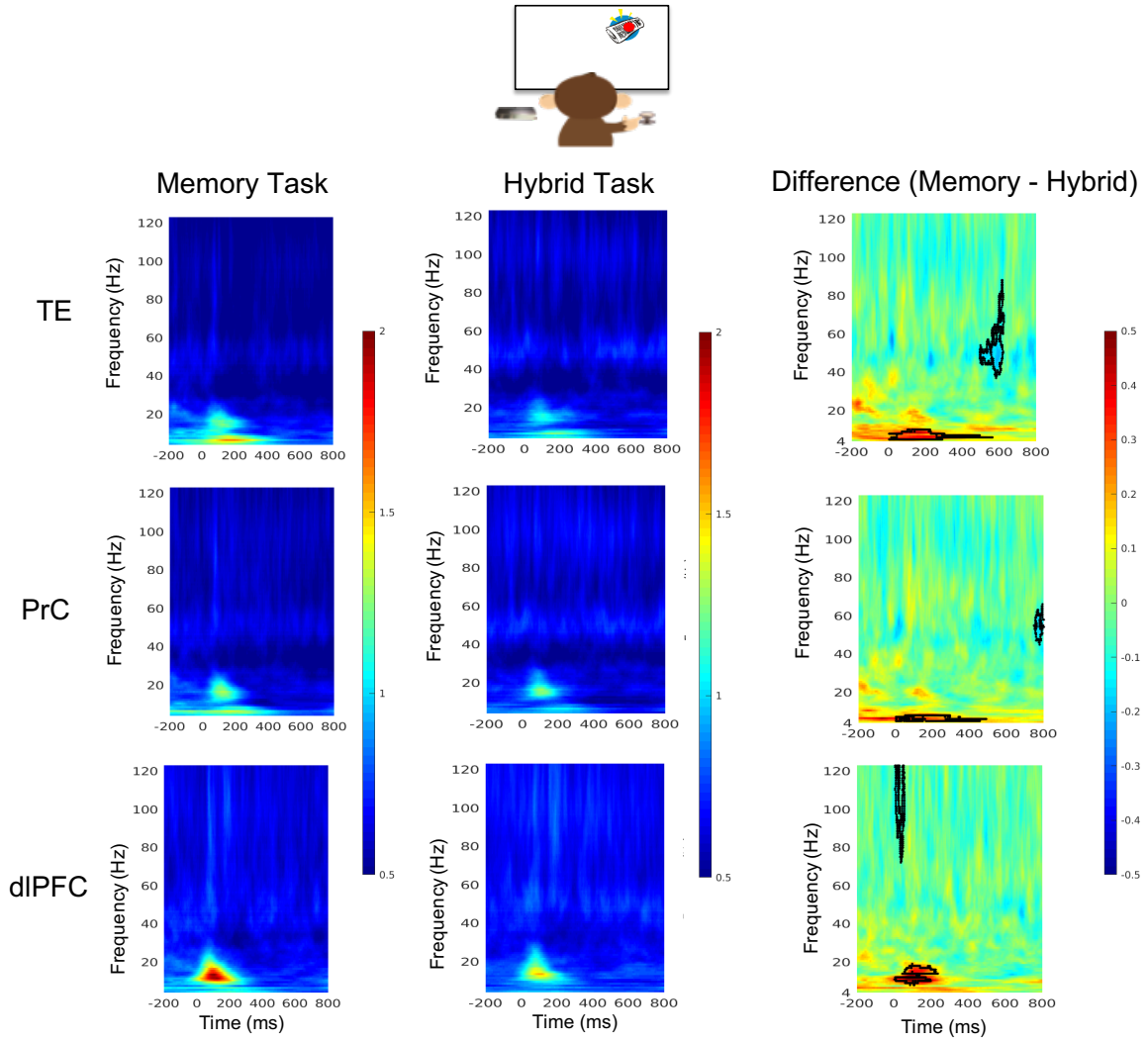


Figure 5. *Induced LFP power and LFP power difference in TE, PrC, dlPFC during the encoding phase of the memory (left panel) and hybrid task (middle panel). An increased power ranging from 4-30 Hz after the sample onset in the three regions was found in both tasks. The significant differences between the two tasks in the three regions were indicated by black lines in the right panel (positive values: Memory> Hybrid, negative values: Hybrid > Memory).*

In the delay phase, an increased power ranging from 4-30 Hz in TE and PrC, and an increased power ranging from 4-40 Hz in dlPFC were detected around 100-200 ms prior to the sample image offset (i.e. start of the delay) in both tasks. These low-frequency bursts in

those three regions lasted roughly 300-400 ms in both memory (Figure 6, left panel) and hybrid tasks (Figure 6, middle panel). Activities with frequency centering at 50 Hz were observed in TE, PrC and dlPFC in the hybrid task before the sample offset, and these activities became weaker when the delay started (i.e. a possible effect of key-touch noise induced by power line interference). A non-parametric permutation test (two-tailed, shown in Figure 6 right panel) revealed that in all the three regions, clusters with power ranging from 4-20 Hz, appeared immediately after the delay onset, which were significantly higher for memory task. Durations of these memory task-related clusters were various in the three regions: 700-800 ms in TE, 300-400 ms in PrC and 500-600 ms in dlPFC, respectively. Other clusters appeared immediately after the delay onset (power ranging from 20-80 Hz in TE, PrC and 20-100 Hz in dlPFC), which were significantly higher for hybrid task. Durations of these hybrid task-related clusters were around 600 ms in TE, 400-500 ms in PrC and 500-600 ms in dlPFC, respectively.

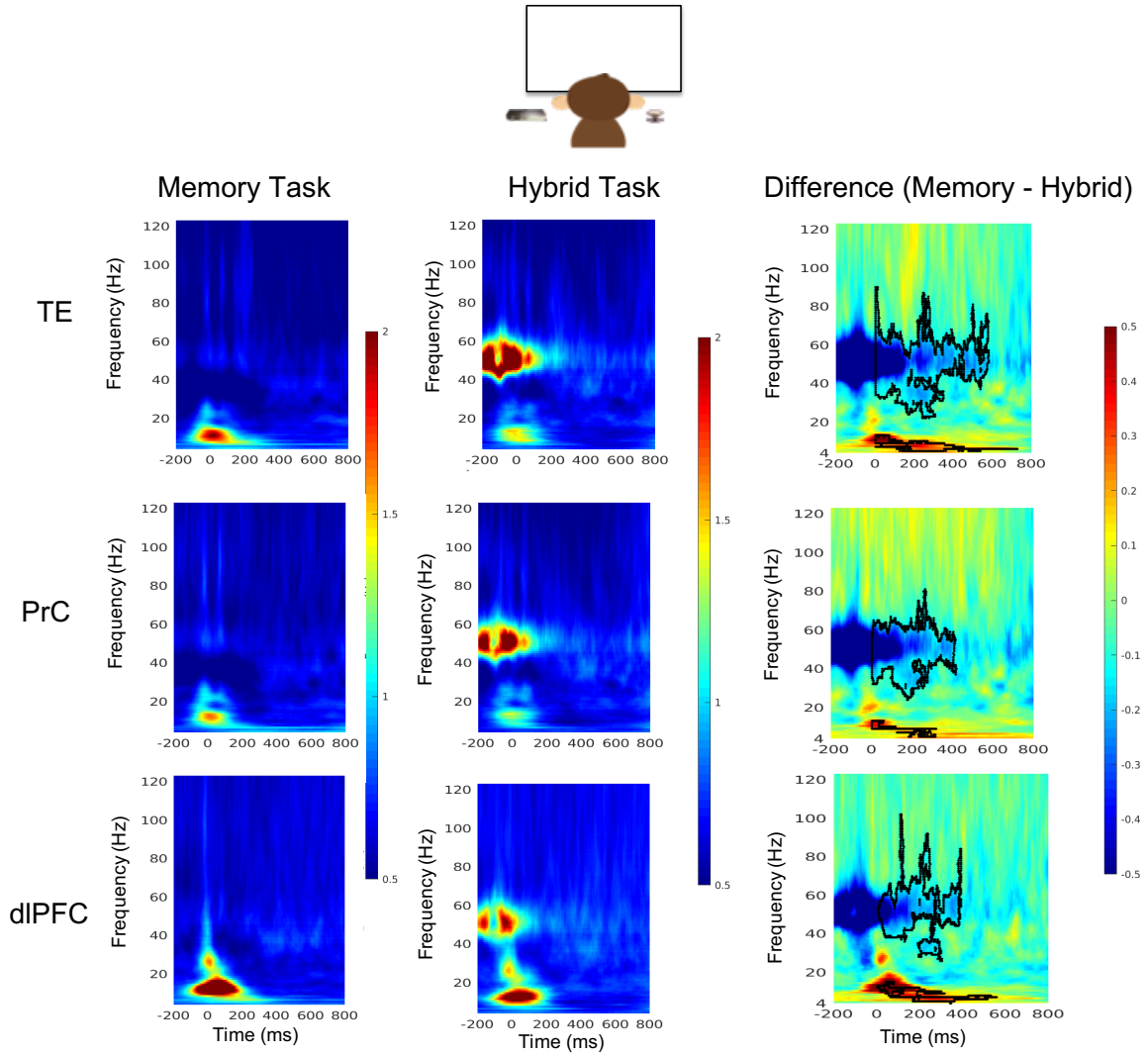


Figure 6. *Induced LFP power and LFP power difference in TE, PrC, dlPFC during the delay phase of the memory (left panel) and hybrid task (middle panel). Increased power ranging from 4-30 Hz in TE and PrC and ranging from 4-40 Hz in dlPFC were detected around 100 ms prior to the start of delay in both tasks. Activities at 50 Hz (i.e. a possible effect of key-touch noise induced by power line interference) were detected in the hybrid task and became weaker when the delay started. The significant differences between the two tasks in the three regions were indicated by black lines in the right panel (positive values: Memory> Hybrid, negative values: Hybrid > Memory).*

In the choice phase of match trials (i.e. sample image was the same as test image) of both tasks, low-frequency bursts of 4-40 Hz and high-frequency bursts of 50-120 Hz in the three regions were detected after the test image onset in both the memory (Figure 7, left panel) and hybrid tasks (Figure 7, middle panel). Oscillations at 30-40 Hz were observed in TE and PrC only in the memory task before the test image onset, and these oscillations became weaker when the test image appeared. A non-parametric permutation test (two-tailed, shown in Figure 7 right panel) revealed that in all the three regions, clusters with power ranging from 4-20 Hz in TE, PrC and dlPFC, appeared immediately after the test image onset, which were significant higher for the memory task. Duration of these memory task-related clusters were 200-300 ms in TE and PrC, and 400-500 ms in dlPFC, respectively. Other clusters of gamma power (30-120 Hz in TE, 30-100 Hz in PrC), appeared 400-500 ms in TE and 100-200 ms in PrC after the test image onset, which were significantly higher for the hybrid task. In dlPFC, alpha/beta bursts of 10-20 Hz appeared 400-600 ms after the test image onset, which was found to be significantly higher for the hybrid task.

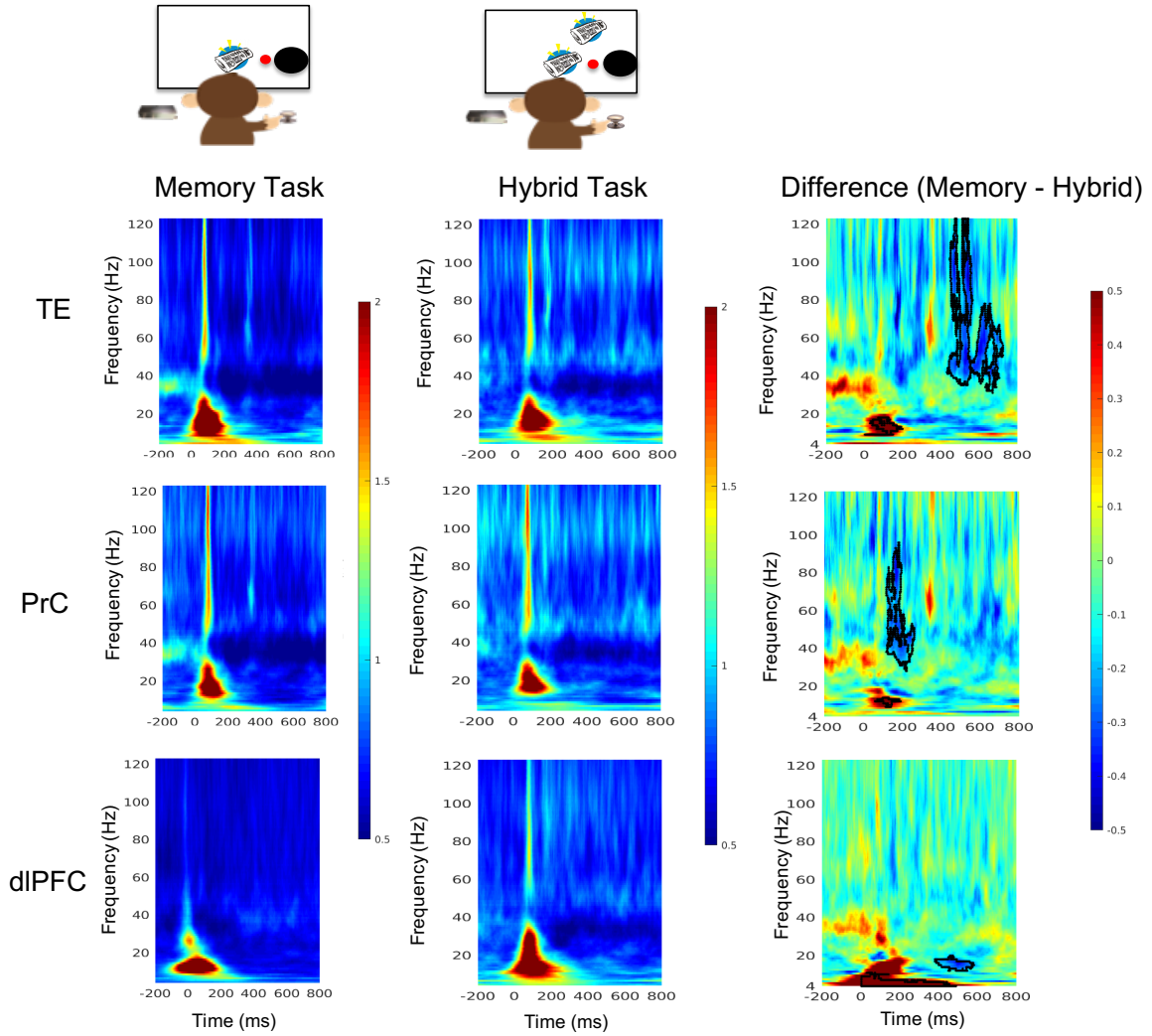


Figure 7. *Induced LFP power and LFP power difference in TE, PrC, dlPFC during the match-choice phase of the memory (left panel) and hybrid task (middle panel). An increased power ranging from 4-40 Hz and narrow-band bursts of 50-120 Hz in those three regions after the test image onset were found in both tasks. Oscillations at 30-40 Hz were detected only in memory task in TE and PrC, and these oscillations became weaker when test image appeared. The significant differences between the two tasks in the three regions were indicated by black lines in the right panel (positive values: Memory> Hybrid, negative values: Hybrid > Memory).*

In the choice phase of non-match trials (i.e. sample image was different from test image) of both tasks, similar low-frequency bursts of 4-40 Hz and high-frequency bursts of 50-120

Hz in the three regions were detected after the test image onset in both memory (Figure 8, left panel) and hybrid task (Figure 8, middle panel). The 30-40 Hz oscillations were still observed in TE, PrC and dlPFC during memory task before the test image onset, and became weaker when test image appeared. A non-parametric permutation test (two-tailed, shown in Figure 8 right panel) revealed that in TE, one cluster (with power ranging 10-20 Hz) appeared immediately after the test image onset, which was found to be significantly higher for the memory task; while another cluster (with power ranging from 30-60 Hz) appeared around 400 ms after the test image onset, which was significantly higher for the hybrid task. In PrC, a very narrow band of gamma power (60-80 Hz) appeared 700-800 ms after the test image onset, which was significantly higher for the memory task; while another cluster (with power ranging 30-60 Hz) appeared around 400 ms after the test image onset, which was significantly higher for the hybrid task. In dlPFC, low-frequency bursts of 4-20 Hz appeared immediately after the test image onset (lasting 500-600 ms), which were found to be significantly higher for the memory task; while another cluster of gamma power (80-120 Hz) appeared 300-400 ms after the test image onset, which was significantly higher for the hybrid task.

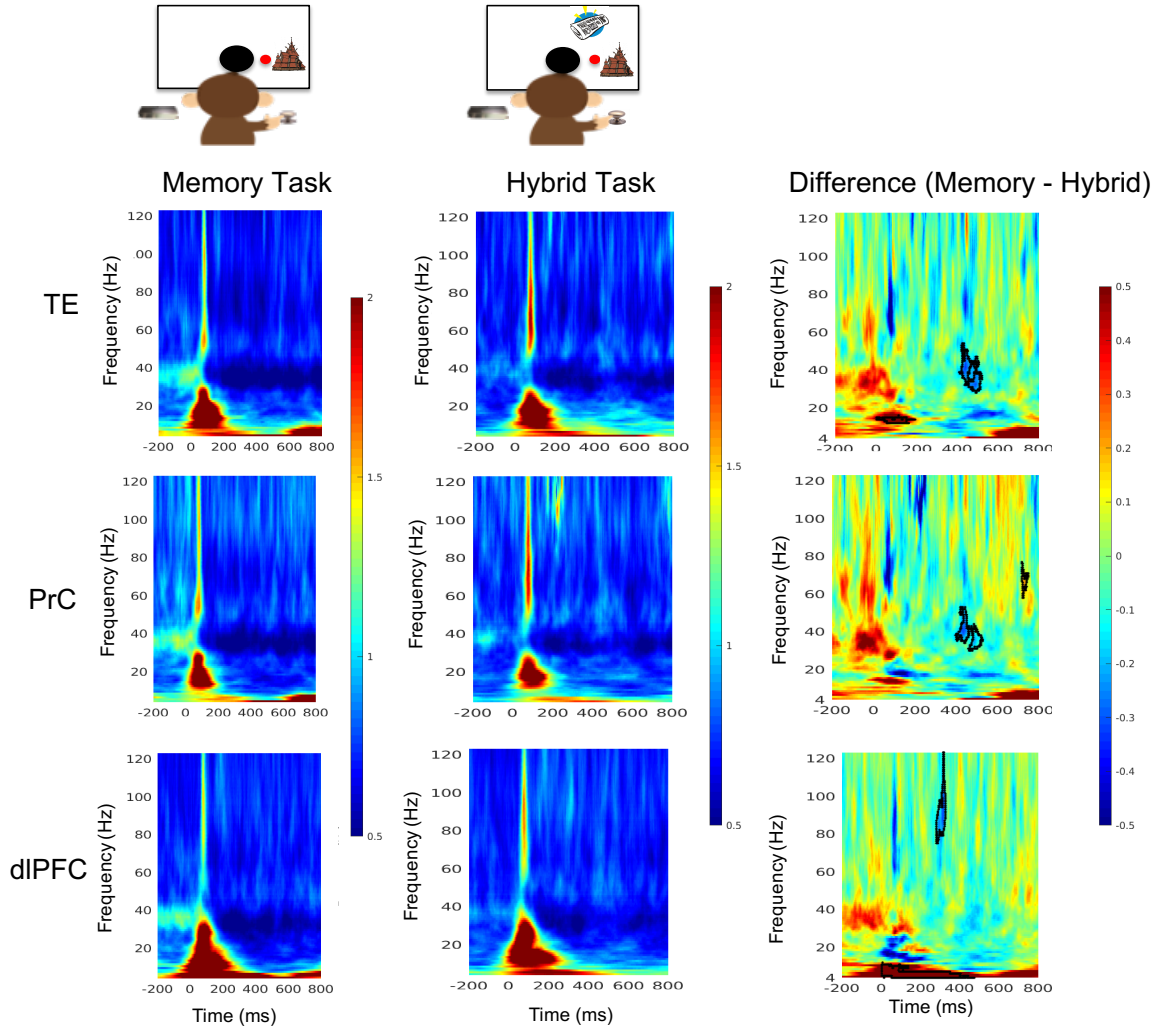


Figure 8. *Induced LFP power and LFP power difference in TE, PrC, dlPFC during the nonmatch-choice phase of the memory (left panel) and hybrid task (middle panel). An increased power ranging from 4-40 Hz and narrow-band bursts of 50-120 Hz in those three regions after the test image onset were found in both tasks. Oscillations at 30-40 Hz were detected in memory task in all the three regions, and these oscillations became weaker when test image appeared. The significant differences between the two tasks in the three regions were indicated by black lines in the right panel (positive values: Memory> Hybrid, negative values: Hybrid > Memory).*

Overall LFP activities in TE, PrC and dlPFC across different phases of memory task and hybrid task

To better illustrate the dynamic neural activities of TE, PrC and dlPFC across different phases of the memory and hybrid tasks, I plotted LFP activities in those three areas across six epochs of both tasks. In the top panels of Figure 9, six task epochs were chosen as 1) holding the key-touch to initiate the task (time zero was when monkey held the key-touch), 2) viewing the sample image (sample phase, time zero was when the sample image was on the screen), 3) delay phase (time zero was when the sample image disappeared), 4) holding the key-touch again to wait for choice images (time zero was when monkey held the key-touch), 5) choice images on the screen (choice phase including both match and nonmatch trials, time zero was when choice images were on the screen) and 6) touching the screen to make the response and getting the reward (response phase including both match and nonmatch trials, time zero was when the monkey touched the screen).

Figure 9 showed modulations of LFP activities in TE, PrC and dlPFC across six task epochs of memory task (Figure 9A) and of hybrid task (Figure 9B). In the first task epoch of hybrid task (Figure 9B), activities at 50 Hz were detected in all the regions when monkey initiated the task, whereas these 50 Hz activities were not found in memory task (Figure 9A). In the second task epoch (i.e. encoding phase), an increased LFP power ranging from 4-30 Hz was found after the onset of sample image in TE, PrC and dlPFC in both memory task (Figure 9A) and hybrid tasks (Figure 9B). These brief bursts in those three regions lasted roughly 300-400 ms. In the third task epoch (i.e. delay phase), an increased power ranging from 4-30 Hz in TE and PrC, and an increased power ranging from 4-40 Hz in dlPFC were detected around 100-200 ms prior to the offset of sample images. Activities at 50 Hz were again found in all the three regions in hybrid task (Figure 9B) when the monkey released the key-touch (i.e. the offset of sample image) and when the monkey held the key-touch again to

wait for choice stimuli (i.e. the forth task epoch). These 50 Hz activities in hybrid task may be related to key-touch noise induced by power line interference (as the array has been degraded to some extent when recording neural signals in the hybrid task). In the fourth and fifth task epoch of memory task (Figure 9A) but not hybrid task, oscillations at 30-40 Hz were observed in TE, PrC and dlPFC around 500 ms after monkey held the key-touch and persisted until choice images were on the screen. When the choice images were on the screen (i.e. start of choice phase), bursts of 4-40 Hz and bursts of 50-120 Hz were detected in the three regions after the onset of test image in both memory task (Figure 9A) and hybrid tasks (Figure 9B). In the sixth task phase (i.e. response phase), bursts of 4-30 Hz were found in all the three regions immediately after the monkey touched the screen to make the response, and high-frequency oscillations at 40-140 Hz were detected in TE and PrC around 500 ms after monkey touched the screen in both memory task (Figure 9A) and hybrid tasks (Figure 9B). As the delay between touch-screen choice and reward delivery was around 500 ms (i.e. as the smoothie pump was triggered by the computer when touch-screen choice was made by the monkey, and then juice was pumped out and monkey licked it into its mouth), these high-frequency oscillations detected in TE and PrC may be related with reward delivery in both tasks.

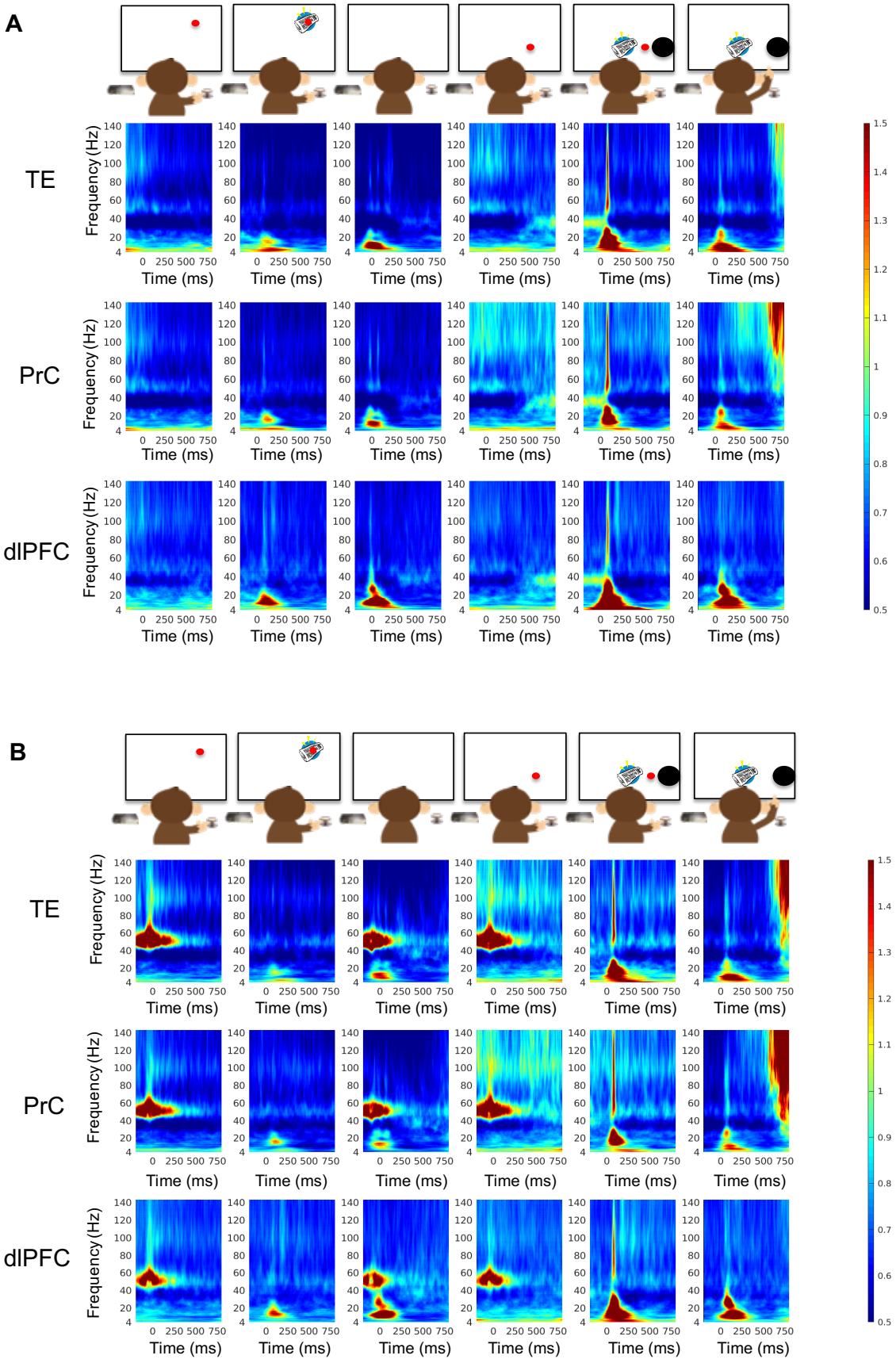

A
TE
PrC
dlPFC
Frequency (Hz)
Time (ms)
B
TE
PrC
dlPFC
Frequency (Hz)
Time (ms)

Figure 9. *Modulation of induced LFPs in TE, PrC and dlPFC across six task epochs of memory task (A) and of hybrid task (B). In both figures, top panels are the six task epochs: monkey held the key-touch to initiate the task; sample image was on the screen (encoding phase); sample image was off the screen (delay phase); monkey held the key-touch again to wait for choice stimuli; choice images were on the screen (choice phase); and monkey touched the screen to make the response and got the reward (response phase). In the first task epoch of hybrid task (B), activities at 50 Hz were detected in all the regions when monkey initiated the task, whereas these 50 activities were not found in memory task (A). In the second task epoch (i.e. encoding phase), an increased LFP power ranging from 4-30 Hz was found after the onset of sample image in TE, PrC and dlPFC in both tasks. In the third task epoch (i.e. delay phase), an increased power ranging from 4-30 Hz in TE and PrC, and an increased power ranging from 4-40 Hz in dlPFC were detected around 100-200 ms prior to the offset of sample images. Activities at 50 Hz were again found in all the three regions in hybrid task (B) when monkey released the key-touch (i.e. offset of sample image) and when monkey held the key-touch again to wait for choice stimuli. These 50 Hz activities detected during the key-touch holding (i.e. first and forth task epoch) and key-touch releasing (i.e. third task epoch) in hybrid task (B) may be related to key-touch noise induced by power line interference. In the fourth and fifth task epoch of memory task (A) but not hybrid task, oscillations at 30-40 Hz were observed in TE, PrC and dlPFC around 500 ms after monkey held the key-touch and persisted until choice images were on the screen. When the choice images were on the screen (i.e. start of choice phase), bursts of 4-40 Hz and bursts of 50-120 Hz were detected in the three regions after the onset of test image in both tasks. In the sixth task phase (i.e. response phase), bursts of 4-30 Hz were found in all the three regions immediately after monkey touched the screen to make the choice, and high-frequency oscillations at 40-140 Hz were detected in TE and PrC around 500 ms after monkey touched the screen in both tasks.*

Effects of task category on LFP-LFP coherence across TE, PrC and dlPFC

When calculating coherence between different brain areas, data from 29 days of mnemonic task and data from 28 days of hybrid task were used (simultaneous recordings in TE, PrC and dlPFC were carried out in all the recorded days). Across all the recorded sessions, 646 trials in mnemonic task (i.e. trial-unique stimuli) and 553 trials in hybrid task (i.e. trial-unique stimuli) were used for the analysis. I chose theta band (4-6 Hz), alpha/beta band (12-35 Hz) and gamma band (35-120 Hz) as three frequency bands for the coherence analysis. For each of the frequency bands, LFPs in each recorded brain region were averaged across corresponding channels, and then LFP-LFP coherence were calculated for each brain pair. A nonparametric permutation test was applied to compare the significant difference of LFP-LFP coherence in each brain pair (i.e. TE-PrC, TE-dlPFC, PrC-dlPFC) between memory and hybrid tasks in each task phase (details were described in methods).

In the encoding phase, LFP-LFP coherence between TE, PrC and dlPFC in theta band (4-6 Hz), alpha/beta band (12-35 Hz) and gamma band (35-120 Hz) were calculated in both memory and hybrid tasks (Figure 10). In both tasks, a very high coherence value between TE and PrC (around 0.8-0.9) was detected in all the frequency bands, which indicated LFP signals in TE and PrC were very similar. To investigate the effects of task category on the theta/alpha-beta/gamma-frequency coherence across different brain areas, a non-parametric permutation test (two-tailed) was applied to compare coherence values across the regions between memory (red line) and hybrid tasks (blue line). Theta-band coherence between TE and dlPFC, and theta-band coherence between PrC and dlPFC demonstrated a decrease prior to the sample onset and then increase around 200-300 ms after the sample onset (left panel in Figure 10). Permutation test confirmed a significant higher coherence in theta band between TE and dlPFC around 700-800 ms in hybrid task compared with memory task ($p < 0.05$). No

significant difference of coherence in alpha/beta band during encoding phase between the two task conditions was found ($p > 0.05$). A significantly higher coherence in gamma band between TE and PrC was detected before the image onset in hybrid task compared with memory task ($p < 0.05$). Some other discontinuous significant differences of gamma-band coherence between TE and PrC, between TE and dlPFC and between PrC and dlPFC after sample image onset were found between the two tasks, with each significant area persisting in a very short time period ($p < 0.05$).

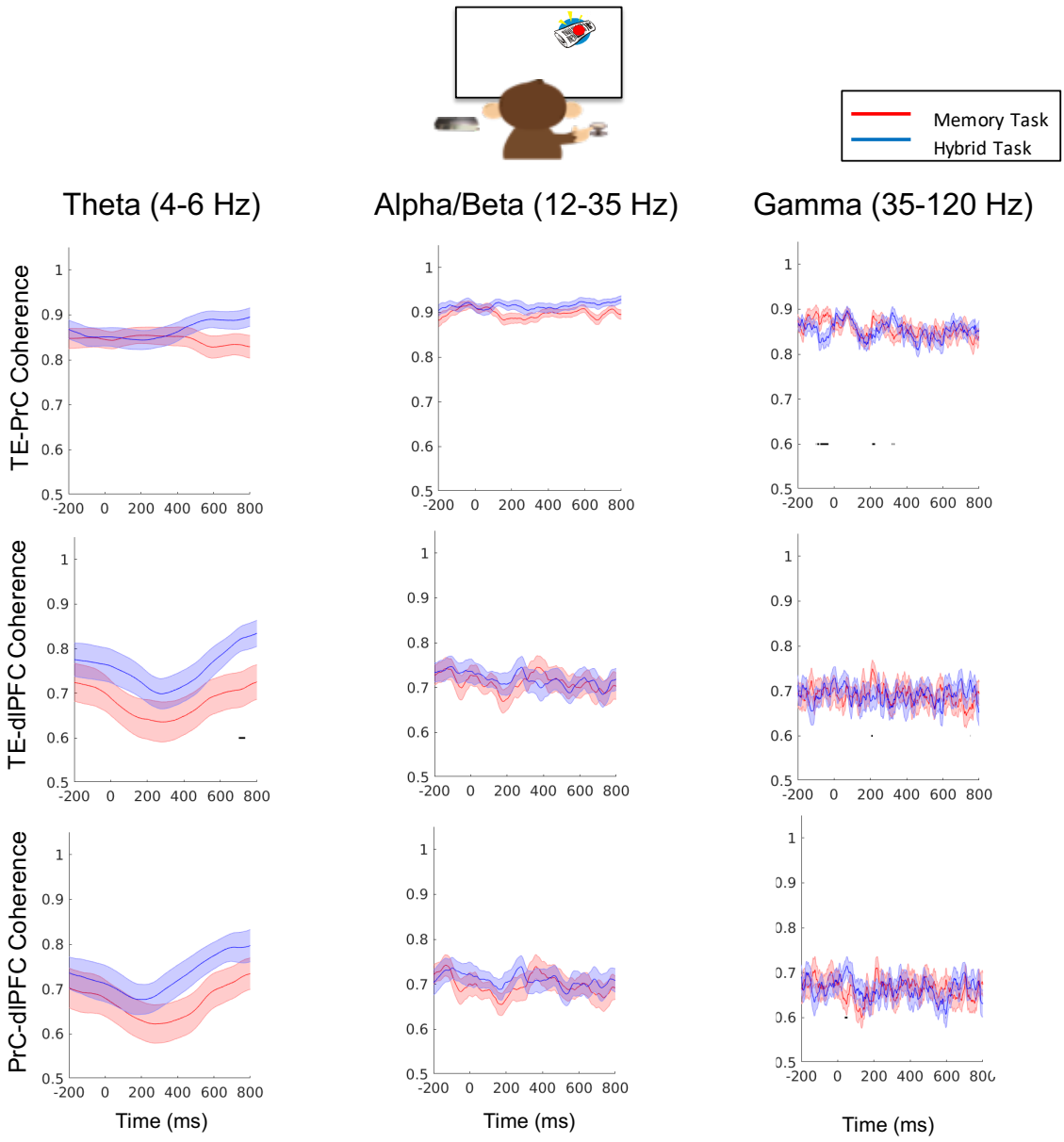


Figure 10. *LFP-LFP coherence across TE, PrC and dlPFC in theta-frequency band (left panel), alpha/beta-frequency band (middle panel) and gamma-frequency band (right panel) during the encoding phase of the memory (red line) and hybrid (blue line) tasks. A significant higher coherence in theta band between TE and dlPFC was detected around 700-800 ms in hybrid task compared with memory task (highlighted by black line). No significant difference of coherence in alpha/beta band between the two tasks was found during encoding phase. A significant higher coherence in gamma band between TE and PrC was detected before the image onset in hybrid task compared with memory task (highlighted by black line). Some other discontinuous significant differences of gamma-band coherence across these regions after sample image onset were found between the two task conditions, with each significant area persisting in a very short time period (highlighted by black line). SEM (±) at each time point is indicated by shading over the lines.*

In the delay phase (i.e. no stimuli were shown on the screen), LFP-LFP coherence across different brain areas in different frequency bands were calculated in both tasks (Figure 11). Decreases of theta-frequency coherence between TE and dlPFC and theta-frequency coherence between PrC and dlPFC prior to delay onset were observed in the memory task (red line) compared with the hybrid task (blue line). Permutation test confirmed a significant higher coherence in theta band between TE and PrC around 200-400 ms in hybrid task compared with memory task, and another significant higher coherence in theta band between TE and dlPFC around 0-500 ms in hybrid task compared with memory task (both $p < 0.05$). Additionally, it has been observed that alpha/beta-frequency coherence between TE and dlPFC and coherence between PrC and dlPFC in both tasks decreased immediately after the delay onset and then increased around 200 ms. Permutation tests confirmed significant higher alpha/beta-band coherence between TE and PrC during 100-200 ms and 600-800 ms of the

delay period in hybrid task; and significant higher alpha/beta-band coherence between TE and dlPFC, and alpha/beta-band coherence between PrC and dlPFC before the delay onset and during 0-200 ms, and 600-700 ms of the delay period in hybrid task (all $p < 0.05$). Some discontinuous significant higher gamma-band coherence across three areas were found before and after the delay onset in hybrid task (all $p < 0.05$). The above results indicate that during the delay phase, theta-, alpha/beta- and gamma-band coherence across three regions seemed to higher in hybrid task than memory task.

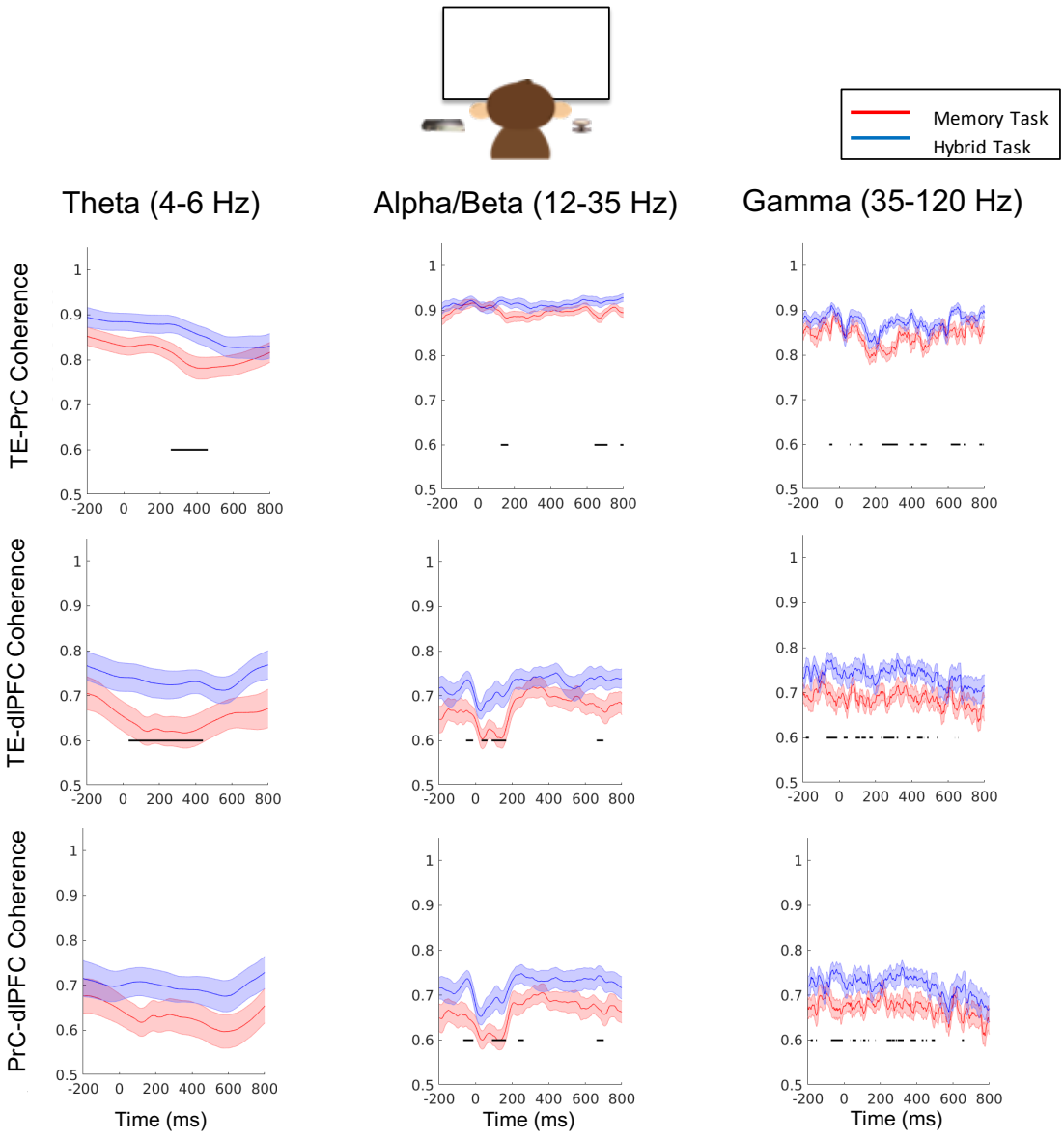


Figure 11. *LFP-LFP coherence across TE, PrC and dlPFC in theta-frequency band (left*

panel), alpha/beta-frequency band (middle panel) and gamma-frequency band (right panel) during the delay phase of the memory (red line) and hybrid (blue line) tasks. A significant higher theta-band coherence between TE and PrC was detected around 200-400 ms in hybrid task compared with memory task, and another significant higher theta-band coherence between TE and dlPFC was found around 0-500 ms in hybrid task compared with memory task (both highlighted by black line). Significant higher alpha/beta-band coherence between TE and PrC was found during 100-200 ms and 600-800 ms of the delay period in hybrid task; and significant higher alpha/beta-band coherence between TE and dlPFC, and alpha/beta-band coherence between PrC and dlPFC were detected prior to delay onset, and during 0-200 ms, and 600-700 ms of the delay period in hybrid task (all highlighted by black line). Significant higher gamma-band coherence between TE and PrC, between TE and dlPFC, and between PrC and dlPFC were found before and after the delay onset in hybrid task (all highlighted by black line). SEM (±) at each time point is indicated by shading over the lines.

In the choice phase of match trials (i.e. sample image was the same as test image), LFP-LFP coherence across different areas in different frequency bands were calculated in both memory (red line) and hybrid tasks (blue line) (Figure 12). Decreases of theta-frequency coherence between TE and dlPFC and theta-frequency coherence between PrC and dlPFC were observed prior to the test image onset in both tasks, and slight increases of theta-frequency coherence of the two brain pairs were observed around 200-400 after test image onset in both tasks. Permutation test confirmed a significant higher coherence in theta band between TE and PrC around 0-400 ms in hybrid task; and another significant higher theta-band coherence between PrC and dlPFC was detected prior to the choice phase in hybrid task compared with memory task (both $p < 0.05$). Additionally, decreases of alpha/beta-frequency coherence between TE and dlPFC and beta-frequency coherence between PrC and dlPFC

were detected around 100 ms after the test image onset in both tasks. However, non-parametric permutation tests (two-tailed) didn't confirm any significant difference of the alpha/beta-band coherence across different areas between the two tasks ($p > 0.05$). Some discontinuous significant differences of gamma-band coherence between TE and PrC, between TE and dlPFC and between PrC and dlPFC were found between the two tasks, with each significant area persisting in a very short time period (all $p < 0.05$).

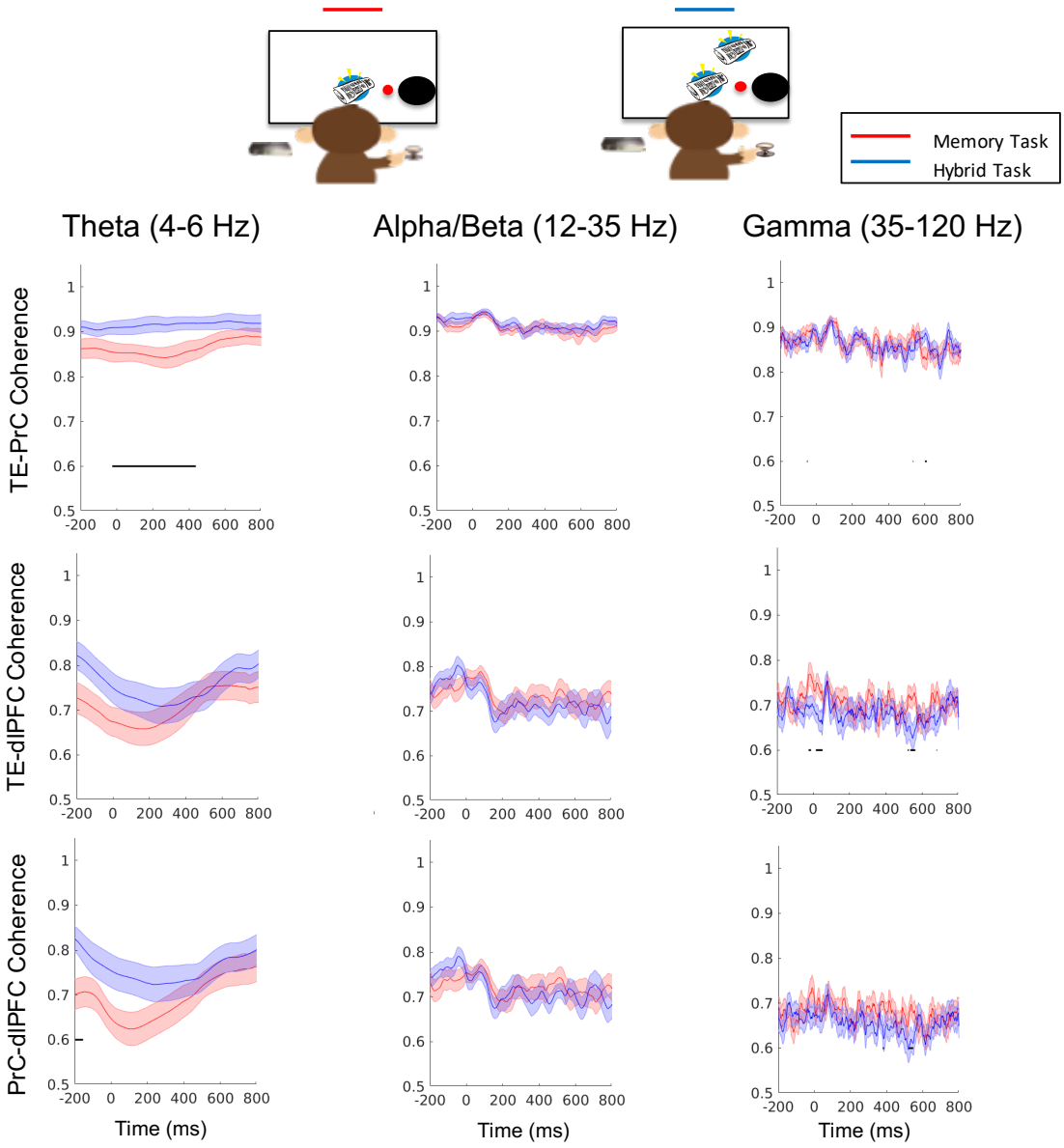


Figure 12. *LFP-LFP coherence across TE, PrC and dlPFC in theta-frequency band (left*

panel), alpha/beta-frequency band (middle panel) and gamma-frequency band (right panel) during the match-choice phase of the memory (red line) and hybrid (blue line) tasks. A significant higher coherence in theta band between TE and PrC was found around 0-400 ms in hybrid task; and another significant higher theta-band coherence between PrC and dlPFC was detected prior to the choice phase in hybrid task (both highlighted by black line). No significant difference of coherence in alpha/beta band between the two tasks was found. Some discontinuous significant differences of gamma-band coherence across three regions were found between the two task conditions, with each significant area persisting in a very short time period (highlighted by black line). SEM (±) at each time point is indicated by shading over the lines.

In the choice phase of non-match trials (i.e. sample image was different from test image), LFP-LFP coherence across different areas in different frequency bands were calculated in in both memory (red line) and hybrid tasks (blue line) (Figure 13). Theta-frequency coherence between TE and dlPFC, and theta-frequency coherence between PrC and dlPFC dropped prior to the test image onset in both tasks, in which valley time (i.e. immediately after choice image onset) in the hybrid task was earlier than the valley time (i.e. around 200 ms after choice image onset) in the memory task. A significantly higher theta-band coherence between TE and PrC was detected around 200-300 ms and 400-800 ms in hybrid task compared with memory task (both $p < 0.05$). Alpha/beta-frequency coherence between TE and dlPFC, and between PrC and dlPFC in both tasks was found to slightly increase immediately after the test image onset, and then dropped around 200 ms after the test image onset. However, non-parametric permutation tests (two-tailed) didn't confirm any significant difference of alpha/beta-band coherence across different areas between the two tasks ($p > 0.05$). Some discontinuous significant differences of gamma-band coherence between TE and PrC were

found between the two task conditions, with each significant area persisting in a very short time period ($p < 0.05$).

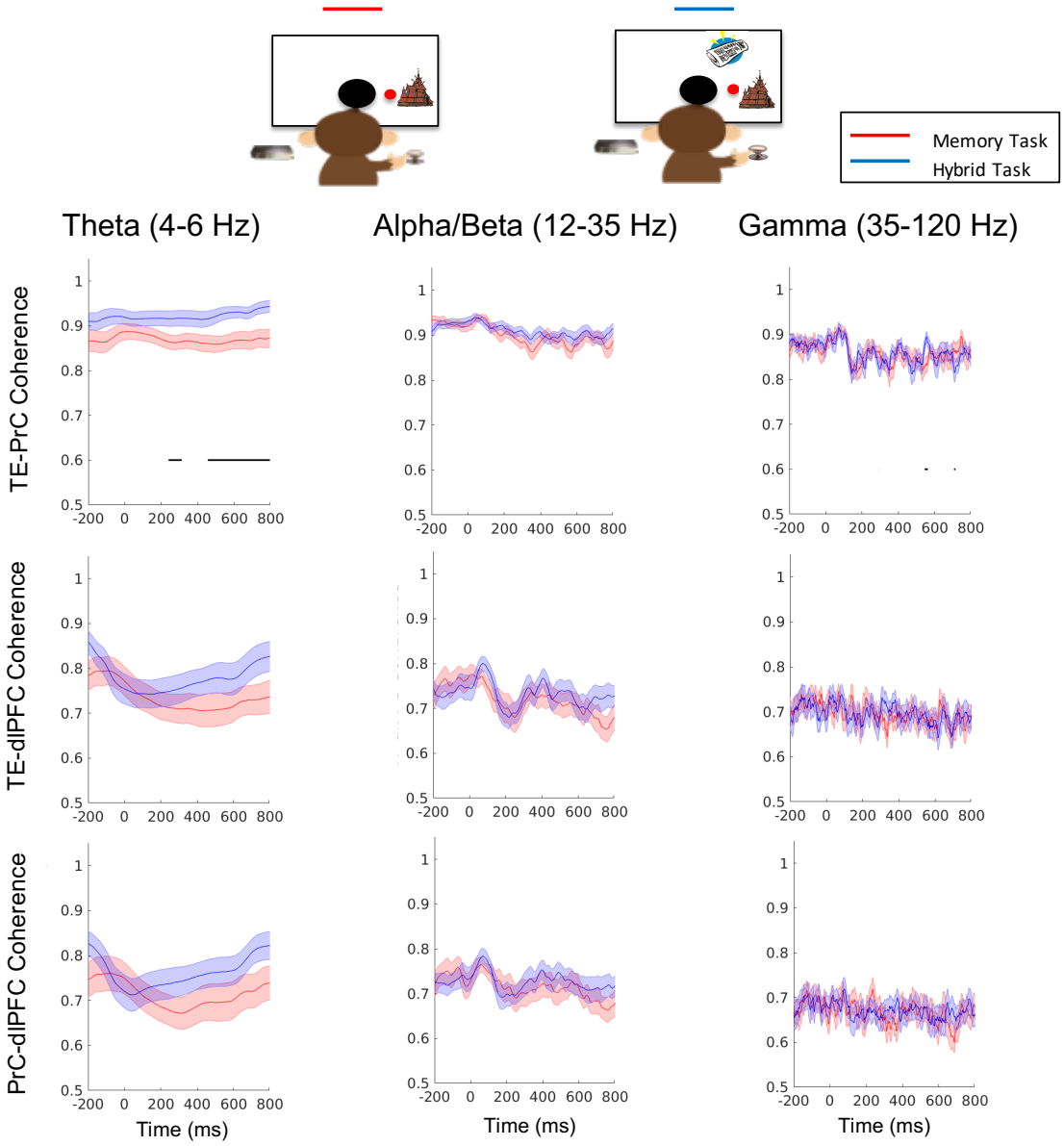


Figure 13. *LFP-LFP coherence across TE, PrC and dlPFC in theta-frequency band (left panel), alpha/beta-frequency band (middle panel) and gamma-frequency band (right panel) during the nonmatch-choice phase of the memory (red line) and hybrid (blue line) tasks. A significant higher theta-band coherence between TE and PrC was detected around 200-300 ms and 400-800 ms in hybrid task compared with memory task (both highlighted by black line). No significant difference of coherence in alpha/beta band between the two tasks was found. Some discontinuous significant differences of gamma-band coherence between TE and*

PrC were found between the two tasks, with each significant area persisting in a very short time period (highlighted by black line). SEM (±) at each time point is indicated by shading over the lines.

Overall LFP-LFP coherence across TE, PrC and dlPFC across different task phases of memory and hybrid tasks

To better illustrate the dynamic change of coherence across TE, PrC and dlPFC across different phases of memory and hybrid tasks, I plotted LFP-LFP coherence among those three areas in six epochs of both tasks. As visualized in the top panels of Figure 14 A-C, these epochs include: 1) holding the key-touch to initiate the task; 2) display the sample image; 3) the delay phase; 4) holding the key-touch again; 5) display of the choice images (including both match and non-match trials); and 6) making responses by touching the screen and getting the reward. The zero ms of each task epoch was set to when monkey held the key-touch, sample image displayed on the screen, sample image disappeared, monkey held the key-touch again, choice images displayed on the screen, and monkey touched the screen, respectively. The LFP-LFP coherence in theta, alpha/beta, and gamma band were shown in Figure 14 A, B, and C, respectively. In each LFP-LFP coherence plot, it has been given a serial number, in which A-C refer to theta, alpha/beta and gamma coherence; 1-3 refer to brain pair of TE-PrC, TE-dlPFC, PrC-dlPFC; and 1-6 refer to six task epochs. Red and blue lines represent coherence in memory and in hybrid tasks, respectively.

In panels of A-2-2 and A-2-5 of Figure 14A (i.e. theta-band), coherence between TE and dlPFC, and in panels of A-3-2 and A-3-5, coherence between PrC and dlPFC, were observed to demonstrate a decrease prior to visual stimuli (i.e. sample, choice images) onset and then an increase around 250-500 ms after the stimuli onset during the sample phase (epoch 2) and

the choice phase (epoch 5) of both tasks. In panels of A-2-6 and A-3-6, a decrease (i.e. prior to touch-screen responses) and then an increase (i.e. around 200-250 ms) of theta-band coherence between TE and dlPFC and coherence between PrC and dlPFC were observed during the response phase (epoch 6) of hybrid task (blue line).

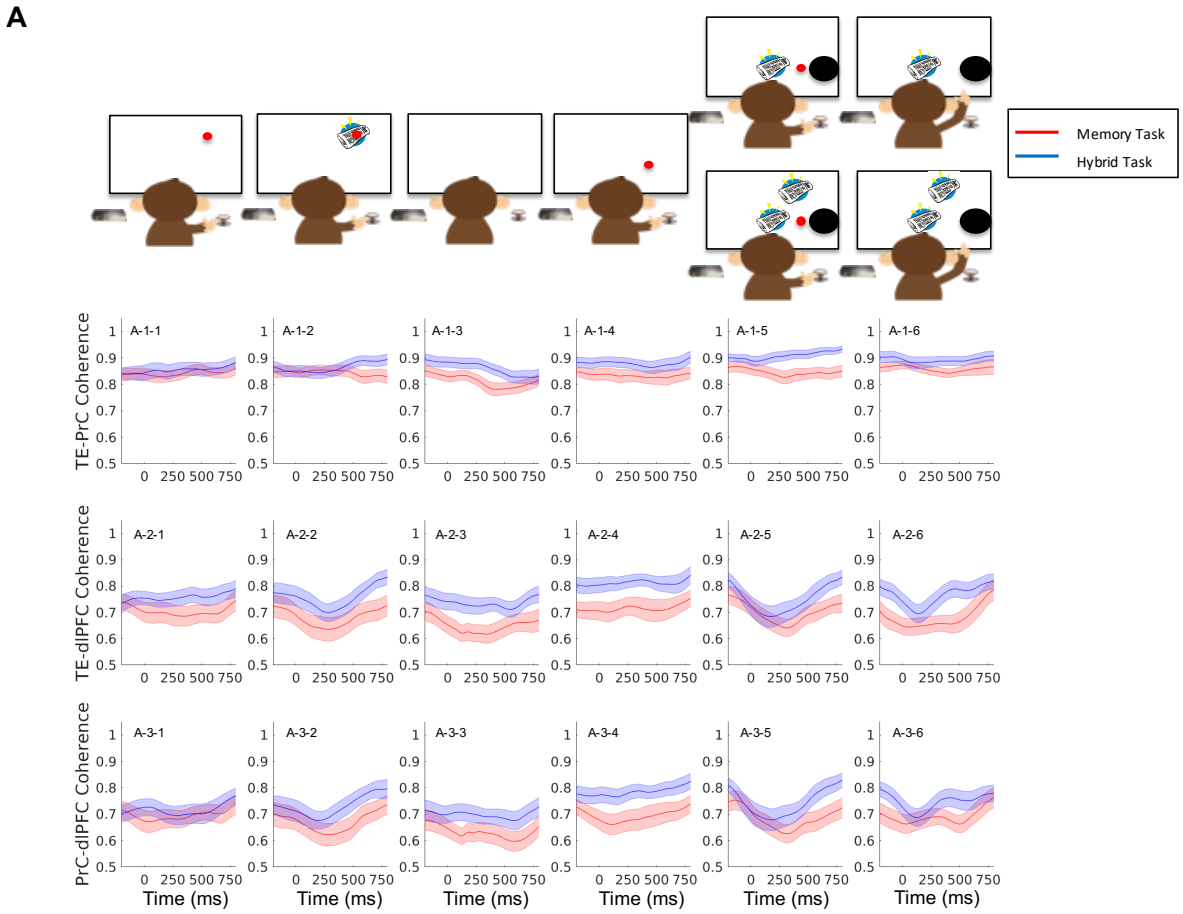


Figure 14A. *LFP-LFP coherence across TE, PrC and dlPFC in theta band (A) across six task phases of memory task (red line) and hybrid task (blue line). Top panels illustrate six epochs of both tasks: monkey held the key-touch to initiate the task; sample image was on the screen (encoding phase); sample image was off the screen (delay phase); monkey held the key-touch again to wait for choice stimuli; choice images were on the screen (choice phase); and monkey touched the screen to make responses and got the reward (response phase). In panels of A-2-2 (sample phase) and A-2-5 (choice phase), theta-band coherence between TE*

and dlPFC was observed to demonstrate a decrease prior to visual stimuli (i.e. sample, choice images) onset and then an increase around 250-500 ms after the stimuli onset. In panels of A-3-2 (sample phase) and A-3-5 (choice phase), theta-band coherence between PrC and dlPFC were also observed to demonstrate a decrease prior to visual stimuli onset and then increase around 250-500 ms after the stimuli onset. In panels of A-2-6 and A-3-6 (response phase), theta-band coherence between TE and dlPFC and coherence between PrC and dlPFC were observed to demonstrate a decrease (i.e. prior to make responses) then an increase (around 200-250 ms) in hybrid task (blue line). SEM (±) at each time point is indicated by shading over the lines.

In panels of B-2-3 and B-3-3 of Figure 14B (i.e. alpha/beta-band), coherence between TE and dlPFC and coherence between PrC and dlPFC in both memory and hybrid tasks were observed to decrease immediately after the delay onset and then increased around 200-250 ms during the delay period (epoch 3). In panels of B-2-5 and B-2-6, decreases of alpha/beta-band coherence between TE and dlPFC, and in panels of B-3-5 and B-3-6, decreases of alpha/beta-band coherence between PrC and dlPFC, were observed after the test image onset during the choice phase (epoch 5) and the response phase (epoch 6) of both tasks.

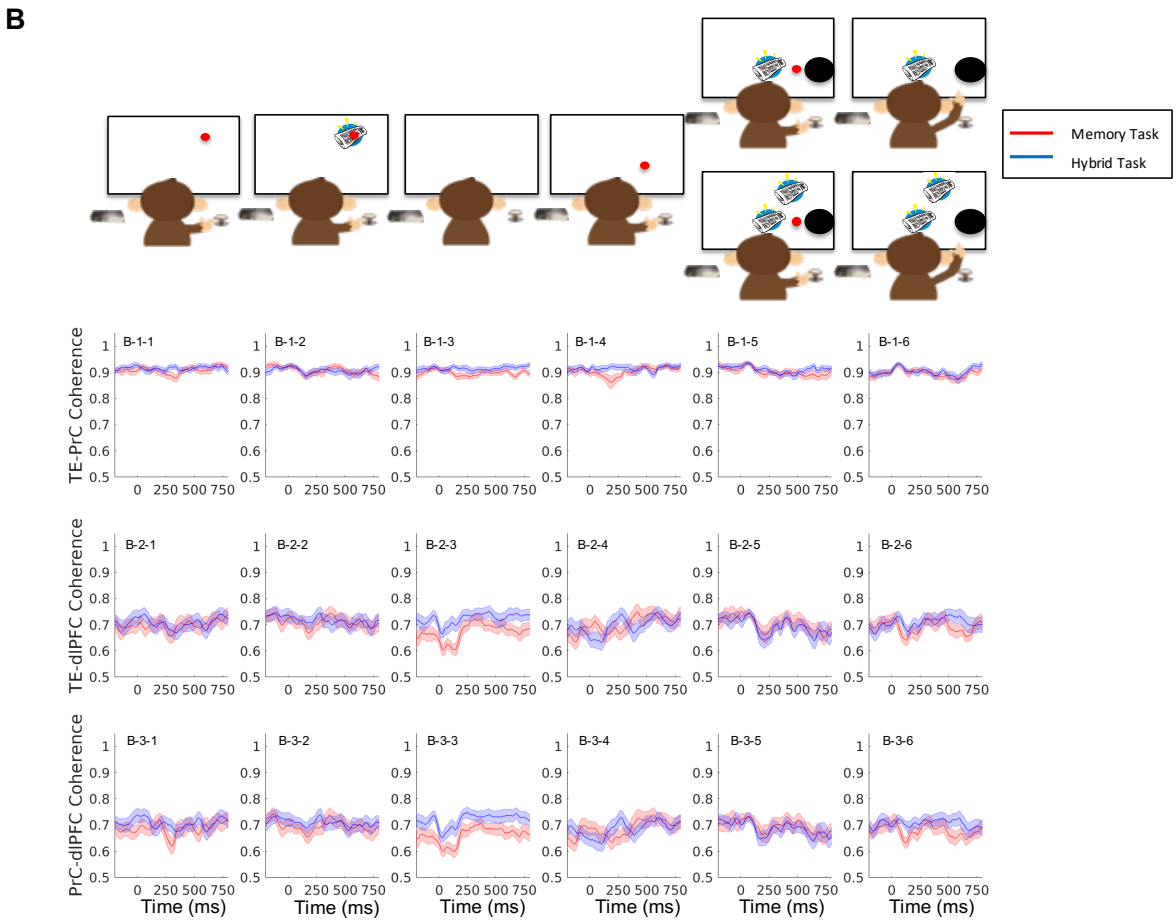


Figure 14B. *LFP-LFP coherence across TE, PrC and dlPFC in alpha/beta band (B) across six task phases of memory task (red line) and hybrid task (blue line). Top panels illustrate six epochs of both tasks, same as the top panels in Figure 14A. In panels of B-2-3 and B-3-3 (delay phase), alpha/beta-band coherence between TE and dlPFC and coherence between PrC and dlPFC in both tasks were observed to decrease immediately after the delay onset and then increased around 200-250 ms during the delay period. In panels of B-2-5 and B-3-5 (choice phase) and B-2-6 and B-3-6 (response phase), decreases of alpha/beta-band coherence between TE and dlPFC and coherence between PrC and dlPFC were observed after the test image onset (i.e. choice phase) and after monkey touched the screen (i.e. response phase) in both tasks. SEM (±) at each time point is indicated by shading over the lines.*

In Figure 14 C (gamma-band coherence), no obvious change of coherence across three areas was observed across different task phases. In panels of C-2-3 and C-3-3, gamma-band coherence between TE and dlPFC and gamma-band coherence between PrC and dlPFC were observed higher during the delay phase (epoch 3) of hybrid task than memory task.

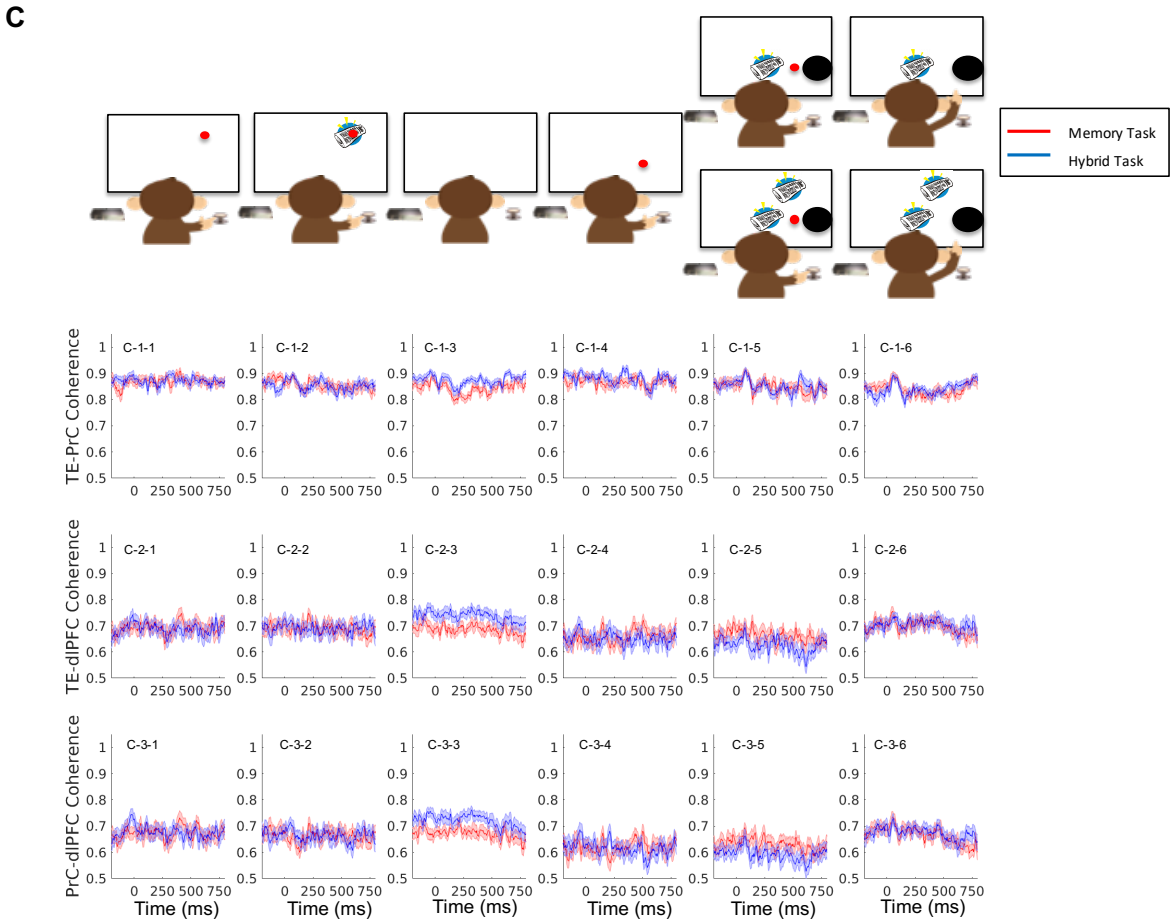


Figure 14C. *LFP-LFP coherence across TE, PrC and dlPFC in gamma band (C) across six task phases of memory task (red line) and hybrid task (blue line). Top panels illustrate six epochs of both tasks, same as the top panels in Figure 14A. In panels of C-2-3 and C-3-3, gamma-band coherence between TE and dlPFC and coherence between PrC and dlPFC were observed higher during the delay phase of hybrid task than memory task. SEM (±) at each time point is indicated by shading over the lines.*

A very high coherence between TE and PrC (between 0.8 and 0.9) in theta, alpha/beta, and gamma band was detected across all the six epochs of both tasks. A post-mortem inspection further confirms the array of area TE and array of area PrC were spatially close (see recording sites of the TE array and PrC array in Figure 2), indicating signals from both arrays were similar.

Discussion

In this study, we compared behavioral and neural signals between a delayed mnemonic task and a hybrid mnemonic and perceptual task. The difference between the two tasks lies in the necessity to encode sample images: in the delayed mnemonic task, the macaque was trained to remember the sample images as the encoding depth of the sample images affected later retrieval performance; in the hybrid task, the macaque didn't need to encode the sample images as the sample images re-appeared with other test stimuli in the choice phase and macaque could rely on perceptual discrimination between the sample and choice stimuli to make the responses.

Behavioral comparisons between the two tasks showed no difference of accuracy (e.g. hit rate, correct rejection rate) and response time between the memory and hybrid tasks. Additionally, after fitting behavioral data to EVSD model (based on signal detection theory), we didn't detect any difference of d prime (an index of discrimination ability) and response criterion between the two tasks. Behavioral results indicate that task category (i.e. memory and hybrid) had no impact on macaque's performance. In other words, macaque's behavioral performance was matched in both the memory and hybrid tasks, thus differences of neural signals in these two tasks cannot be attributed to the differences of task difficulty.

Then induced LFP power spectra in temporal regions (i.e. TE, PrC) and prefrontal region (i.e. dlPFC) were compared across different phases of the memory and hybrid tasks. In

the encoding phase of both tasks, a low-frequency power (i.e. 4-30 Hz) in temporal and frontal regions has been observed in both tasks. These effects which were not absent in the hybrid task probably reflect that encoding may happen naturally in the hybrid task as animal used to encode samples in the memory task or/and encoding samples will help animal's performance in the hybrid task too. In both the encoding and delay phase of memory and hybrid tasks, low-frequency components (i.e. theta and alpha/low-beta power) have been found to be significantly higher for memory task than hybrid task. For example, a significant increase of 4-20 Hz bursts in TE, PrC and dlPFC in memory task has been detected immediately after the sample onset and immediately after the delay onset. It can be tentatively concluded that these low-frequency activities in temporal and prefrontal regions were important for encoding and maintenance of to-be-remembered items in the memory task. Indeed, in a working memory task, beta oscillations (20-35 Hz) in macaque lateral prefrontal cortex have been found to occur in brief and variable bursts during encoding and maintenance of items, which may reflect a default state (Lundqvist et al. 2016, 2018). The significant increased theta and alpha/low-beta bursts in our memory task (compared with hybrid task), and the brief bursts of beta oscillations reported in Lundqvist et al. (2016, 2018), verify the importance of low-frequency activities, particular beta power, in the encoding and maintenance of memory. Our study also showed gamma bursts in the temporal and prefrontal regions during the encoding and delay phases were related to hybrid task. For example, some gamma activities after the sample onset (40-80 Hz in TE, 40-60 Hz in PrC, and 70-120 Hz in dlPFC) and after the delay onset (20-100 Hz in TE, PrC and dlPFC) were found to be significantly higher for hybrid task. As the 50 Hz activities have been detected prior to delay onset, which was more likely associated with key-touch noise, it limited the interpretations of the significant gamma power occurring during the delay phase of hybrid task.

In the memory task but not in the hybrid task, oscillations at 30-40 Hz were detected prior to the test image onset and became weaker when test image appeared, regardless of

following match or nonmatch choices. This further suggests beta oscillations in frontal and temporal regions were related to the maintenance of items in recognition memory (Lundqvist et al. 2016, 2018). Brief bursts of low-frequency activities (i.e. 4-20 Hz in TE, PrC and dlPFC) in match trials and low-frequency activities (i.e. 10-20 Hz in TE and 4-20 Hz in dlPFC) in non-match trials appeared immediately after the test image onset, which were found to be significantly higher for the memory task. These higher low-frequency bursts detected immediately after the test image in the memory task (compared with hybrid task) may reflect a mnemonic processing as the macaque needed to retrieve the sample image and compare it with the test stimuli in the choice phase of memory task. Some gamma activities in temporal regions in both match (30-120 Hz in TE and 30-100 Hz in PrC) and nonmatch trials (30-60 Hz in TE and PrC) have been detected significantly higher for hybrid task than memory task. One of the interpretations of these higher temporal gamma activities during the choice phase was that they may be involved in perceptual discrimination.

To investigate how the interaction between frontal and temporal regions was modulated by task category, I compared LFP-LFP coherence across brain regions in the encoding, delay and choices phases of both tasks. A very high coherence value between TE and PrC has been detected in different phases of both tasks. As stated in the discussion of Chapter 4, this may indicate signals from TE and PrC came from the same source as a post-mortem inspection further confirms the array of TE and array of PrC were spatially close (see recording sites of the TE array and PrC array in Figure 2). Permutation tests (two-tailed) confirmed an increased theta-band coherence between TE and dlPFC during the encoding phase of hybrid task; a larger theta-band, alpha/beta-band and gamma-band coherence between temporal and frontal regions during the delay phase of hybrid task; and a larger theta-band coherence between TE and PrC during both the match-choice and nonmatch-choice phase of hybrid task than memory task. This indicates a stronger interaction between temporal and frontal regions throughout the hybrid task than memory task. Although some gamma-band coherence were

found to be significantly different in different phases of the two tasks, most of them had repaid fluctuation and were thus discrete along the time. As stated in the discussion of Chapter 4, permutation tests used in our coherence analysis are very sensitive to the fluctuations, indicating a smoothing operation on high-frequency coherence (e.g. gamma-band coherence) may be needed prior to permutation comparison. In a human imaging study with matched performance in perceptual and memory tasks for recognizing human faces, functional connectivity analysis showed PrC exhibited stronger connectivities with prefrontal regions in a memory task; while PrC showed stronger connectivities with fusiform areas (a region specifically involved in face discrimination) in a perceptual task (O'Neil et al. 2012). This study indicates the interplay of PrC with other cortical regions differed based on different task demands (memory or perception). As we only investigated interactions between PrC and other temporal/frontal regions in a delayed memory task versus a hybrid perceptual and mnemonic task, it will be important to investigate the interaction between PrC and other MTL brain regions in a simultaneous perceptual task and compare how different task demands affect neural activities of macaque MTL.

Several limitations of this study existed. Firstly, it may be the case that noise polluted the recorded neural data in the hybrid task, which weakened the data interpretation when comparing the results between the two tasks. Due to the electrode degrading, more noise (from mains, EMG signals from eye and muscle movements) appeared to have polluted the recorded LFP data in the hybrid task. For example, huge artifacts from the main noise at 50 Hz has been found when the monkey held and released the key-touch (as electrodes degraded to some extent when recoding the signals in hybrid task), although the key-touch noise should be filtered when pre-processing the raw LFP data (in my study I used *filtfilt* function in MATLAB). A further application of some powerful filters and repeating filtering multiple times may be useful for getting rid of the main noise from the raw data. Secondly, previous lesion literatures have shown that PrC is sensitive to discriminating objects presented in

different viewpoints in the oddity task (Buckley 2005; Buckley and Gaffan 2006) or objects with highly feature ambiguity in the morph task (Bussey et al. 2002a; Bussey and Saksida 2002; Bussey et al. 2006; Bussey and Saksida 2007). However, due to electrode degrading, this animal was not involved in either a mnemonic or a perceptual version of tasks with those kinds of manipulations to objects (the animals in the study with chambers and microdrives, see Chapter 6, will be doing task versions with those kinds of manipulations). In a human neuroimaging study, it has been found that when using morphed human faces as stimuli in both memory and perception tasks, a comparable signal from PrC was detected in both recognition memory and perceptual discrimination when performances in both tasks were matched (O'Neil et al. 2009). This study further indicates that using stimuli with certain degrees of image feature ambiguity is critical to reveal the role of PrC in perception (Bussey et al. 2002a; Bussey and Saksida 2002; Bussey et al. 2006; Bussey and Saksida 2007). Finally, this animal only completed a mnemonic task and a hybrid mnemonic/perceptual task but was not involved in a pure simultaneous perceptual task. Failure to compare neural signals from temporal and prefrontal regions between a pure delayed memory task and a pure simultaneous perceptual task limited our data interpretation. Although this animal demonstrated a matched performance in memory and hybrid tasks with the same task structure, the effects related to mnemonic encoding or maintenance of visual stimuli in the hybrid task cannot be excluded even though the different neural signals between the two tasks have been detected. In some human neuroimaging research, human participants were asked to encode the stimuli prior to fMRI scanning; in other words, participants completed the encoding phase of memory task before they went into the scanner. During fMRI scanning, participants responded to stimuli either based on an instruction of using perceptual discrimination or another instruction of using recognition memory, thus the choice phase of memory (i.e. retrieval phase) was in the same structure as in the perceptual discrimination so signals from a pure memory process and a pure perceptual process can be compared in

humans (Morales et al. 2018; O'Neil et al. 2009). In animal studies, it's hard to train animals encode the stimuli beforehand and then test them in trials with instructing them using either mnemonic rule (i.e. select the choice by recalling the previously encoded stimuli) or perceptual rule (i.e. select the choice by discriminating between presented stimuli). In our study, we aimed to solve this issue by requiring animals to complete three versions of tasks: a delayed mnemonic task, a simultaneous perceptual task and a hybrid mnemonic and perceptual task. By comparing signals from different tasks with different task demands, we could investigate how PrC is involved in memory and perception. Recently, Mendoza-Halliday and Martinez-Trujillo designed a mnemonic and a perceptual task with same structures to investigate a role of lateral PFC in a memory-guided and in a perception-guided motion direction judgment. Their perceptual task was identical to the structure of the memory task in every aspect (e.g. encoding, delay and test phase), except that the sample stimuli remained on the display until the end of test phase. This allowed macaques to have visual access to the sample stimuli at any time during the encoding, delay and test phases in their perception task (Mendoza-Halliday and Martinez-Trujillo 2017). However, their perception task design cannot exclude effects of working memory in perceptual discrimination as monkeys can still automatically encode the stimuli throughout the perceptual task. This suggests comparing mnemonic and perceptual processes in animals cannot be done in one structure due to this criticism. Future investigations on mnemonic and perceptual processes might include three versions of memory and perceptual tasks (i.e. a delayed mnemonic task, a simultaneous perceptual task and a hybrid mnemonic and perceptual task) to cope with the problem of task design in animals.

In summary, this study focused on the role of PrC and the interaction of PrC with other temporal and prefrontal cortical areas in a delayed mnemonic task and a hybrid mnemonic and perceptual task by simultaneously recording these areas throughout both tasks. I got some preliminary findings by investigating the function of PrC and interaction between PrC

and other temporal and prefrontal regions: i) low-frequency neural activities (theta and alpha/low-beta oscillations) in temporal and frontal regions were important for encoding, maintaining and retrieval of visual stimuli in a delayed mnemonic task; and ii) gamma activities in temporal regions during the choice phase was more related to perceptual discrimination. It should be noted that limitations of this electrophysiological research existed: the limited sample size (only one macaque), lack of data in a simultaneous perceptual task, and noise pollulation due to the electrode degrading. This study has nonetheless benefited future electrophysiological research on this topic by providing new directions and advanced recoding technique to tackle with the mnemonic-perceptual debate. For example, it will be essential in future studies to record activities of MTL and PFC in a delayed mnemonic task, a simultaneous perceptual task and a hybrid mnemonic and perceptual task with matched behavioral performance to investigate the mnemonic and perceptual processes and I have already shown that two out of three of these tasks are matched (e.g. no significant difference in d prime measures). Meanwhile, visual stimuli (e.g. objects, scenes) with different viewpoints (i.e. those stimuli were used in the study with chambers and microdrives in Chapter 6) would be usefully employed in those tasks as it has been found damage to PrC affected perceptual discrimination between stimuli with those kinds of manipulations in many studies of the literature (Buckley 2005; Buckley and Gaffan 2006).

Chapter 6. Hippocampal-prefrontal theta coherence during the encoding phase signaling successful recognition memory performance (on-going project)

Abstract

In this final experimental chapter, I describe an ongoing project I developed and led to investigate the interaction between hippocampus and prefrontal cortex in recognition memory using a novel semi-chronic chamber and microdrive recording system in two awake behaving macaques. The recording is still ongoing in the 2nd animal (I trained both NHPs from the point they arrived in the lab, and recorded from the 1st, but the intense daily recording in the 2nd animal has since been taken over by a post-doctoral research assistant as this is a long-term project (longer that the duration of a D.Phil. research program) that is expected to continue throughout 2020, after which the thorough analyses of neural data in both animals will commence and the post-doctoral research assistant and I will continue to collaborate on that in the future) but here I am able to describe the work I have done on the initial stages of this long-term project so far during my D.Phil. research; accordingly, at this point I am only able to present some preliminary analyses from the both animals in the project (using some of the analysis methods detailed in previous thesis chapters). My preliminary data analyses showed that some hippocampal and PFC neurons in two awake monkeys demonstrated visual responses to encoded images during the sample phase of recognition memory task. Moreover, LFP-LFP coherence analyses between hippocampus and PFC further showed that after the sample image appeared, an increase of theta-band coherence in correct trials whereas a decrease of theta-band coherence in error trials was observed. Before and after the sample

image onset, the dynamic change of theta-band coherence between hippocampus and PFC in correct and error trials indicates their theta-band coherence may signal successful memory performance. More thorough and detailed neural analysis will be carried out in the future (after all recordings are complete) to validate these initial findings. Besides focusing on the interaction between hippocampus and PFC in recognition memory, in this ongoing project, we aim to provide electrophysiological evidence that may go some way to help reconcile canonical MTL memory system theory, process-specific theories of MTL function, and domain specific-theories of MTL function including perceptual-mnemonic theory of MTL function. The approach taken is to record from two monkeys in a delayed memory task, a simultaneously perceptual task and a hybrid mnemonic and perceptual task using visual objects and scenes stimuli with manipulation of viewpoints to discover how the neural activities in various MTL structures would differ depending on stimulus type and view.

Introduction

Hippocampal-prefrontal interaction has been largely examined in rodent spatial memory. Spellman et al. (2015) found an afferent pathway between rodent ventral hippocampus and medial prefrontal cortex (mPFC) to be essential for cue-encoding in a spatial memory task. In other maze-based tasks, it has been found theta synchrony between rodent hippocampus and mPFC during spatial memory performance (Jones and Wilson 2005); and rodent mPFC neurons respond to task-related behaviour by dynamically coordinating with hippocampal theta rhythm entrained firing (Hyman et al. 2005). Besides the hippocampal-prefrontal interaction is engaged in spatial memory, Eichenbaum et al. have confirmed its role in episodic memory in rodents (Eichenbaum et al. 1999).

It is still unclear, that in primates, how the hippocampus and prefrontal cortex interact in episodic memory. Up to date, there are only a few studies recoding both hippocampus and PFC in non-human primates (NHPs) (Brincat and Miller 2015; Naya et al. 2017). Naya et al. (2017) simultaneously recorded macaque lateral PFC and some MTL areas, including hippocampus, entorhinal cortex and perirhinal cortex, in a temporal memory task. They found that both regions of PFC and hippocampus signaled timing information that appeared to represent the continuous passage of time during the encoding phase, while they didn't explicitly look for interaction between the two brain regions during the temporal memory task (Naya et al. 2017). In another study Brincat and Miller (2015) recorded macaque hippocampus and PFC activities whilst monkeys learned associations between different object pairs, and they found during the feedback of this associative memory task, an increased theta hippocampal-PFC synchrony was detected in error trials while an incremental alpha/beta hippocampal-PFC synchrony was found in correct trials, which indicates a frequency-specific role of hippocampal-prefrontal interaction in macaque associative memory. In humans, a MEG study has shown that a theta-band coherence between hippocampus and medial PFC increased during the encoding phase of an associative memory

task, and this theta-band coherence predicated subsequent performance of memory integration (Backus et al. 2016). As the above findings in primates focused on the timing or association information in declarative memory, it's still unclear how the interaction between hippocampus and PFC is involved in recognition memory and perceptual discrimination (i.e. the scientific issues have been investigated in Chapter 4 and Chapter 5). In this chapter, I will further investigate this issue by simultaneously recording neural activities of the hippocampus and other MTL structures (e.g. entorhinal cortex, perirhinal cortex and parahippocampal cortex) and lateral and medial PFC in an object recognition memory task using a simultaneous multi-area, multi-electrode recording paradigm in two awake behaving macaques. As the neural data recording is still ongoing and the data analysis has not been completed yet, here, I describe my methods and present some preliminary results on the activities of macaque hippocampus and PFC during the encoding phase of object recognition memory.

This is an ongoing electrophysiological project where several inter-related scientific issues (that I have reviewed throughout my thesis) will be investigated in the future. One of these key issues is how to reconcile canonical MTL memory system theory which maintains the MTL is not functionally sub-divided and not involved in stimulus perception (Squire and Zola-Morgan 1991; Buffalo et al. 1998, 1999, 2000; Squire 2004; Squire et al. 2004, 2006; Suzuki 2009) with perceptual-mnemonic theory of MTL which maintains there is a stimulus domain-specific functional subdivision on the MTL and that MTL structures also contribute to both memory and perception on account of it being primarily a representational theory involving hierarchical levels of representations running through so-called visual-related and mnemonic-related brain regions (Baxter 2009; Buckley et al. 2001; Buckley 2005; Bussey et al. 2002a; Bussey and Saksida 2002; Bussey et al. 2003, 2005, 2006; Bussey and Saksida 2007; Eacott et al. 1994; Lee et al. 2005a, 2005b, 2005c; Murray and Bussey 1999; Murray and Richmond 2001). Although this issue has been investigated in Chapter 5, some

limitations (e.g. power line interference, lack of recording in a simultaneous perceptual task, lack of stimuli from different viewpoints used in memory and perception tasks) existed. To further investigate this issue, and importantly in the context of this broader study to record from hippocampus as well as other MTL cortical areas as well as PFC regions, we used a different approach to recording that the multi-electrode array method described in previous chapters. I pioneered the first use, in Oxford, of a 96 channel semi-chronic microdrive system to record from deep MTL structures including the hippocampus (together with an anterior 32 channel system to target prefrontal cortical regions) in two macaques so to access not only superficial cortical regions (e.g. lateral PFC) but deep brain areas of PFC too (e.g. frontopolar cortex) in addition to the already mentioned deep brain regions of MTL (e.g. hippocampus, entorhinal cortex, perirhinal cortex and parahippocampal cortex). We also recorded from these two monkeys in a hybrid perceptual and mnemonic task, and in an object recognition memory task with object stimulus from different viewpoints. By employing different task structures (i.e. different task demands) and task stimuli (i.e. object stimulus with different views), we aimed to investigate how perirhinal cortex interacted differently with other MTL structures and with other PFC structures depending on the manipulations.

Graham et al. have summarized some neuropsychological and neuroimaging findings in both animals and humans, and concludes that '*there is now significant evidence of a functional specialization in how MTL structures contribute to memory and perception of objects and scenes'* (Graham et al. 2010). The domain-specific theory of MTL proposed that PrC is more involved in object processing whilst hippocampus and parahippocampal cortex are involved in spatial/temporal processing (Graham et al. 2010; Epstein et al. 2003; Hodgetts et al. 2016; Lee et al. 2005b; Staresina et al. 2013). To investigate the domain-specific role of different MTL structures, I recorded from the two monkeys in both an object recognition memory task and a scene recognition memory task, to illustrate how the neural activities in the targeted regions differed depending on stimulus type.

Materials and Methods

Subjects

Two male rhesus monkeys (*Macaca mulatta*), weighing 10-14 kg (Monkey A) and 11-15 kg (Monkey B), were used in this project. All animals in our lab are socially housed (or socially housed for as long as possible if later precluded, for example, by repeated fighting with cage-mates despite multiple regrouping attempts) and all are housed in enriched environments (e.g. swings and ropes and objects, all within large pens with multiple wooden ledges at many levels) with a 12hr light/dark cycle. The two NHPs always had *ad libitum* water access 7 days/week. Most of their daily food ration of wet mash and fruit and nuts and other treats was delivered in the automated testing/lunch-box at the end of each behavioral session (this provided 'jack-pot' motivation for quickly completing successful session performance; supplemented by trial-by-trial rewards for correct choices in the form of drops of smoothie delivered via a sipping tube) and this was supplemented with fruit and foraging mix in the home enclosure. All animal training, titanium headpost, chamber and microdrive implantation surgery, and experimental procedures were performed in accordance with the guidelines of the UK Animals (Scientific Procedures) Act of 1986, licensed by the UK Home Office, and approved by Oxford's Committee on Animal Care and Ethical Review.

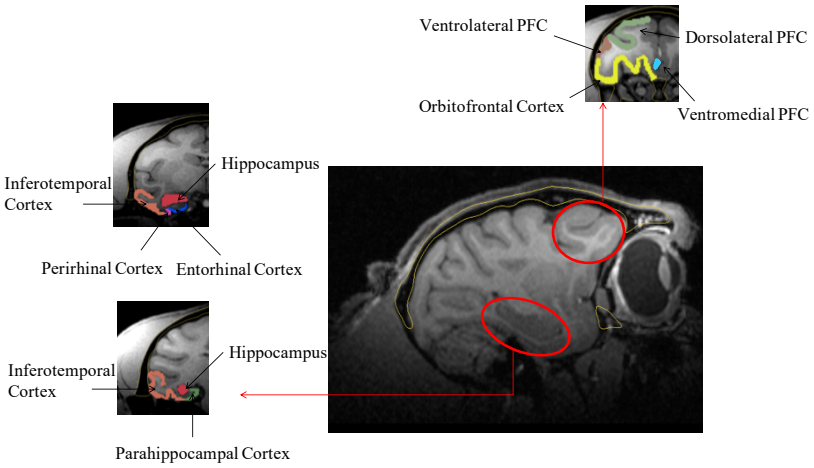
Surgical procedures and recordings

After the basic behavioural and initial task training phase was complete, monkey A first received a titanium head-post, implanted on the right side of the skull and secured to the cranium with titanium cranial screws through the legs of the post (the legs of the head-post were pre-shaped to fit the precise morphology of the skull in the region according to a 3D printed skull model based on pre-operative structural MRI scans); later monkey B received a

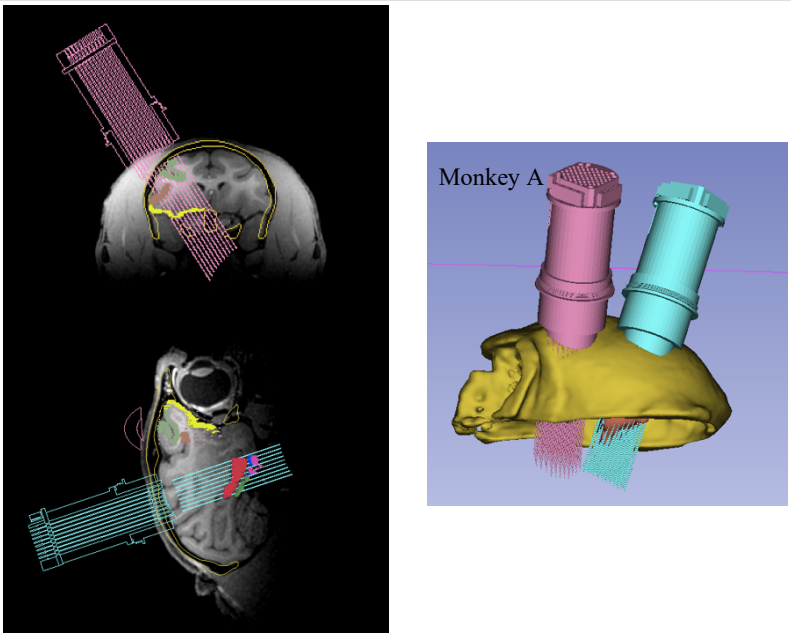
custom-designed PEEK head-post (i.e. MRI compatible implant), implanted posteriorly and secured to the cranium with titanium cranial screws through the legs of the post. In both monkeys, the reflected skin and galea was sutured and the wound closed around the base of the head-post.

After more behavioural training with head-fixation was complete and task-performance satisfactory, chamber and microdrive system design were carried out in both monkeys. Recording locations and targeted brain areas are shown in Figure 1 for monkey A and monkey B. The bespoke chambers (and internal microdrive system) were designed to fit each animal by creating a 3D model of each animal's skull. To achieve this, I constructed an MRI-based 3D graphical model of each monkey's skull using Brainsight software (https://www.rogue-research.com/tms/brainsight-tms/). And then I outlined all the targeted cortical and sub-cortical regions in 3D Slicer software (https://www.slicer.org). As depicted by the arrows in Figure 1, the frontal chambers along with the microdrives were designed to target dorsolateral (light green colour),ventrolateral (incarnadine colour), ventromedial PFC (light blue colour) and orbitofrontal cortex (yellow colour); the posterior chambers along with the microdrives were designed to target inferotemporal cortex (IT) (orange colour), hippocampus (red colour), perirhinal cortex (pink colour), entorhinal cortex (dark blue colour) and parahippocampal cortex (blackish green colour). All the locations of chambers and microdrives were then completed in 3D Slicer software.

a. Targeted cortical and sub-cortical brain regions



b. Locations of chamber and microdrive recording systems in two monkeys



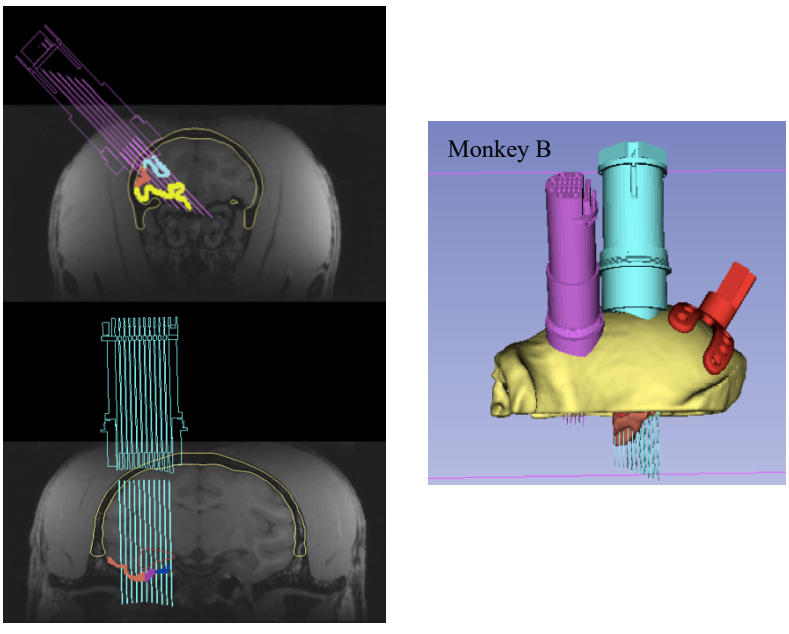


Figure 1. *Targeted cortical and sub-cortical brain areas (a) and locations of recording chamber and microdrive systems (b) in monkey A and monkey B. Panel a: frontal chambers (pink/purple chambers in panel b) along with the microdrives are designed to target dorsolateral (light green colour),ventrolateral (incarnadine colour), ventromedial PFC (light blue colour) and orbitofrontal cortex (yellow colour); the posterior chambers (blue chambers in panel b) along with the microdrives are designed to target inferotemporal cortex (IT) (orange colour), hippocampus (red colour), perirhinal cortex (pink colour), entorhinal cortex (dark blue colour) and parahippocampal cortex (blackish green colour). Panel b: locations of the frontal chamber and microdrive recording systems (pink/purple) and posterior chamber and microdrive recording systems (blue) in two monkeys.*

After the above design was complete, both monkeys were implanted with two recording chambers (GrayMatter Research). Frontal chambers were placed over the lateral prefrontal cortex of the left hemisphere, and posterior chambers were placed over the MTL of the left hemisphere. Before chamber implantation surgeries, MRI-based skull models with stereotaxic coordinates were initially marked by a point and each chamber outline was marked by a circle (Fig 2.a). In this step, the stereotaxic coordinates of each chamber location were recorded. During chamber implantation surgeries, once the chamber location was identified in a stereotaxic frame, holes could be drilled (Fig 2.b) and titanium bone screws were then anchored on the skull (Fig 2.c). Then chambers were positioned using the stereotaxic chamber holder mounted onto a coarse manipulator on the stereotaxic system (Fig2. d), and then were sealed by a thin bead of superbond bone cement (Fig 2.e). Once the sealing was complete, a thin layer of bone cement was applied to connect the chambers to the surrounding bone screws (Fig 2.f) and the stereotaxic chamber holder could be removed (Fig 2.g). Additional layers of bone cement were built up to complete the coverage of the screws

(Fig 2.h). Then the o-ring, short plug and chamber cap were placed in order (i.e. the sequence was shown in Fig 2.i) to ensure the sterilization of the chamber interior; and the chamber implantation was complete (Fig 2.j).

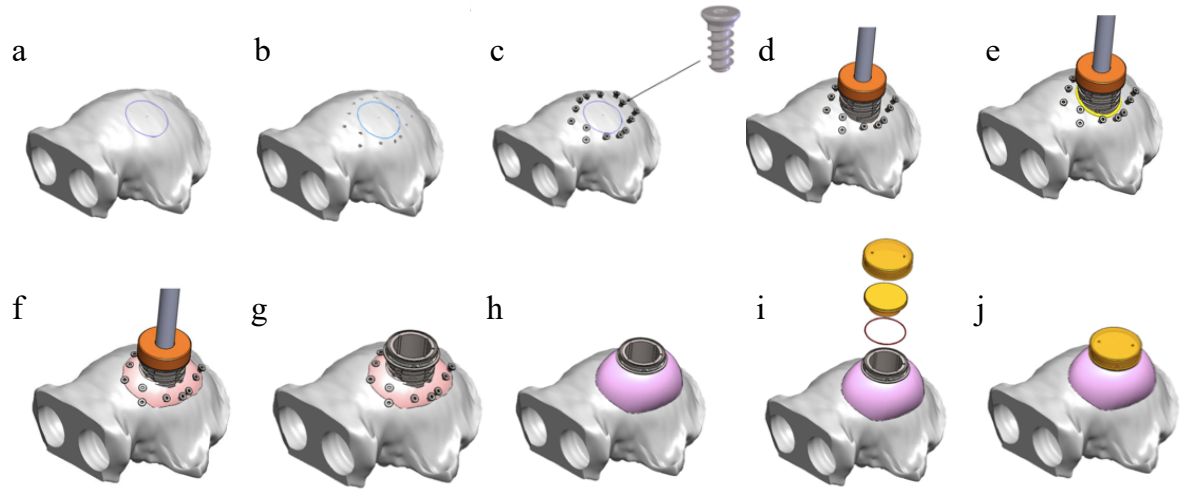


Figure 2. Steps of chamber implantation surgery. *Panel a: stereotaxic coordinates of chamber location were identified. Panel b-c: in a stereotaxic system, holes were drilled, and bone screws were anchored on the skull. Panel d-e: chambers were positioned using the stereotaxic chamber holder mounted onto a coarse manipulator on the stereotaxic system, and then were sealed by a thin bead of superbond bone cement. Panel f-g: bone cement was applied to link the chamber and bone screws, and then the stereotaxic chamber holder was removed. Panel h-j: additional bone cement was built up; the o-ring, short plug and chamber cap were placed in order to ensure the sterilization of the chamber interior (adapted from the manual from Grey Matter Research).*

After the chamber implantation surgeries, unfortunately, monkey A got the bone infection from its frontal chamber. The infected bones were quickly ripped off in another surgery, and a regular cleaning (i.e. 4-6 times a week) both inside the infected frontal chamber and around the skin margin was carried out in a sterile environment for this monkey. After 2 months, his health condition was maintained and was ready for posterior microdrive

implantation surgery. The anterior microdrive implantation of this monkey was not carried out in the same surgery as we worried the previous infection may not be completely gone and we thought regular cleaning was still required to maintain a good condition of the frontal chamber interior. After recording from the posterior microdrive for six months, monkey A received the anterior microdrive implantation surgery (although unfortunately, after the surgery the infection between the bone and dura continued and we had to euthanize him after recording for two weeks). Monkey B recovered well after chamber implantations, and after 1-2 months, he received both anterior and posterior microdrive implantations in one surgery.

During microdrive implantation surgeries, a craniotomy was made within the interior of each chamber. A starter hole was made in the center of the chamber using a bone drill, and then all of the remaining bone were removed using a rongeur. The dura beneath the removed bones was then punctured by the grid using a stainless needle, to guarantee in the later stage, the microdrive electrodes could be driven through the dura smoothly and to minimize the possibility of bending the tips. After dura puncture, the frontal microdrives (SC32) were mounted within the anterior chambers, and posterior microdrives (SC96) were mounted within the posterior chambers. All the implanted microdrives were fixed in place by tightening the retaining caps onto the chambers. An additional layer of bone cement was applied to reinforce the microdrives. In monkey A, we directly lowered some electrodes to the deep brain structures of MTL (e.g. hippocampus) and PFC (e.g. medial prefrontal regions), in a worry of a limited recording schedule available due to his health issue; while in monkey B, all electrodes were gradually lowered to the targeted areas in daily recordings. Distances to which the electrodes should be lowered to reach the target regions were estimated in our design which was compiled using the 3D Slicer software. Finally, all the microdrives were fully assembled with protective caps, with fixation screws tightening on the chambers.

In both frontal and posterior microdrives, I used 34 Platinum/Iridium (Microprobes, USA) and 94 tungsten microelectrodes (Alpha Omega, USA) in monkey A, and the corresponding numbers were 36 and 92 in monkey B. All the electrodes were mounted on a grid inside the recording chambers. Each of the electrodes in the frontal recording chambers were independently controlled by a 32 channel microdrive which can travel up to 32 mm, and each of the 96 electrodes in the posterior recording chambers were independently controlled by a 96 channel microdrive which can travel up to 42 mm (GrayMatter Research). In each of the daily recording sessions, if no cell was found in the electrodes, electrodes were manually turned to travel to the cell layers of targeted brain regions. Monkey A completed all the recordings we were able to obtain in six months, and Monkey B is still under recording (long-term from both chambers).

Behavioral Tasks

To-date, both monkeys went through an object recognition memory task (task used in Chapter 4) and a hybrid perceptual and mnemonic task (task used in Chapter 5). Monkey A has also completed a scene recognition memory task and a same/different-view object recognition memory task.

Object recognition memory task

This task is the same task used in Chapter 4. In each trial, the animals initiated the object recognition memory task by holding the key-touch when cued to do so by a small red circular keytouch cue presented on the screen. The animals were required to keep holding the keytouch device through a variable delay of 1000-1500 ms (if the keytouch hold was broken the trial aborted) after which a central sample (clip-art object image, see Figure 3A) appeared behind the red key-touch cue. The NHPs were required to keep holding the keytouch device

through another variable delay of 1000-1500 ms (again, if the keytouch hold was broken the trial aborted) after which the red keytouch cue disappeared which was the cue to the animal it could release its hand from the keytouch at which point the delay (1000ms) between sample and choice-phases began (the maximal time for releasing key-touch was 5000 ms else the trial aborted and the animal received a time-out for 10 s). Then after the 1000 ms delay period another red keytouch cue appeared, this time in the bottom of the screen (close to, and equidistant, from where the two choice items would appear) and animal was required to hold the key-touch again. The NHPs were again required to keep holding the keytouch device through a variable delay of 1000-1500 ms (if the keytouch hold was broken the trial aborted) after which two choice stimuli appeared (one an object image and the other a black circle, left-right randomized between trials). The NHPs were required to keep holding the keytouch device through another variable delay of 1000-1500 ms (again, if the keytouch hold was broken the trial aborted) after which the red keytouch cue disappeared which was the cue to the animal that it could release holding the keytouch and now make a choice to the touchscreen to either the object test-image stimulus (object image) or to the black circle stimulus. The NHPs were rewarded by delivery of 10 ml of smoothie for touching the test-item image if it matched the sample image (i.e. 'match trials'), or it was rewarded for selecting the standard 'non-match button' (i.e. the black circle) if the test-item was a non-match (i.e. 'non-match trials'). The next trial started after a 3000 ms inter-trial interval after a correct response, or after a 10 s 'time-out' after any kind of error response (or after any failure to hold keytouch for the required time, or after failure to release when required). We used larger sets moreover we also varied the degree to which stimuli were either familiar or novel in the session (typically there were up to 80 pairs of novel stimuli that were trial-unique in each session, and six other familiar stimuli, grouped into three pairs, that repeated many times through the session). Specifically, in any given session 50% of the trials used trial-unique object stimuli and 50% were 'repeat' object stimuli used previously in the session (but

not used in any previous session); in each session there were six repeat object stimuli sorted into 3 pairs such that in each trial with repeat object stimuli one pair was chosen at random and one member of the pair was randomly chosen to be the sample. Each session typically consisted of 150 trials so the six repeat object stimuli got steadily more familiar across the session. A schematic of the object recognition memory task is illustrated in Figure 4A.

Object hybrid perceptual and mnemonic task

This task is the same task used in Chapter 5. Briefly, in each trial, the two animals initiated the task by holding the key-touch when cued to do so by a small red circular keytouch cue presented on the screen. The two animals were required to keep holding the keytouch device through a variable delay of 1000-1500 ms after which a central sample (clip-art object image, see Figure 3A) appeared behind the red key-touch cue. The NHPs were required to keep holding the keytouch device through another variable delay of 1000-1500 ms after which the red keytouch cue disappeared which was the cue to the animal it could release its hand from the keytouch at which point the delay (1000ms) between sample and choice-phases began. Then after the 1000 ms delay period another red keytouch cue appeared, this time in the bottom of the screen and NHPs were required to hold the key-touch again. The NHPs were again required to keep holding the keytouch device through a variable delay of 1000-1500 ms after which two choice stimuli appeared (one an object image and the other a black circle, left-right randomized between trials) and the previously-presented central sample image re-appeared on the top of the screen. The NHPs were required to keep holding the keytouch device through another variable delay of 1000-1500 ms after which the red keytouch cue disappeared which was the cue to the animal that it could release holding the keytouch and now make a choice to the touchscreen to either the object test-image stimulus or to the black circle stimulus. The object test-image stimulus was either the identical stimulus to the central

sample in the trial or it was not identical to the central sample. The animal was rewarded by delivery of 10 ml of smoothie for touching the test-item image if it matched the sample image (these we refer to as 'match trials'), or it was rewarded for selecting the standard 'non-match button' (i.e. the black circle) if the test-item was a non-match (these we refer to an 'non-match trials'). The next trial started after a 3000 ms inter-trial interval after a correct response, or after a 10 s 'time-out' after any kind of error response. In any given session 50% of the trials used trial-unique object stimuli and 50% were 'repeat' object stimuli used previously in the session (but not used in any previous session); in each session there were six repeat object stimuli sorted into 3 pairs such that in each trial with repeat object stimuli one pair was chosen at random and one member of the pair was randomly chosen to be the sample. Each session typically consisted of 150 trials so the six repeat object stimuli got steadily more familiar across the session. A schematic of the hybrid mnemonic and perceptual task is illustrated in Figure 4B.

Scene recognition memory task

The structure of scene recognition memory task was exactly the same as the object recognition memory task except for the different stimuli type (nature scene images, see Figure 3B). In any given session 50% of the trials used trial-unique scene stimuli and 50% were 'repeat' scene stimuli used previously in the session (but not used in any previous session); in each session there were six repeat scene stimuli sorted into 3 pairs such that in each trial with repeat scene stimuli one pair was chosen at random and one member of the pair was randomly chosen to be the sample. Each session typically consisted of 150 trials so the six repeat scene stimuli got steadily more familiar across the session. A schematic of the scene recognition memory task is illustrated in Figure 4C.

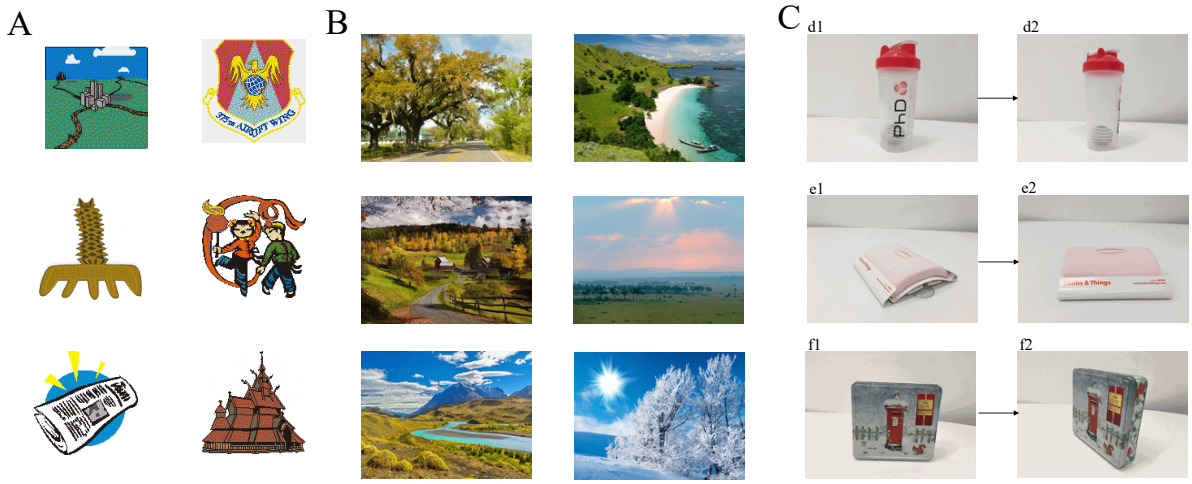
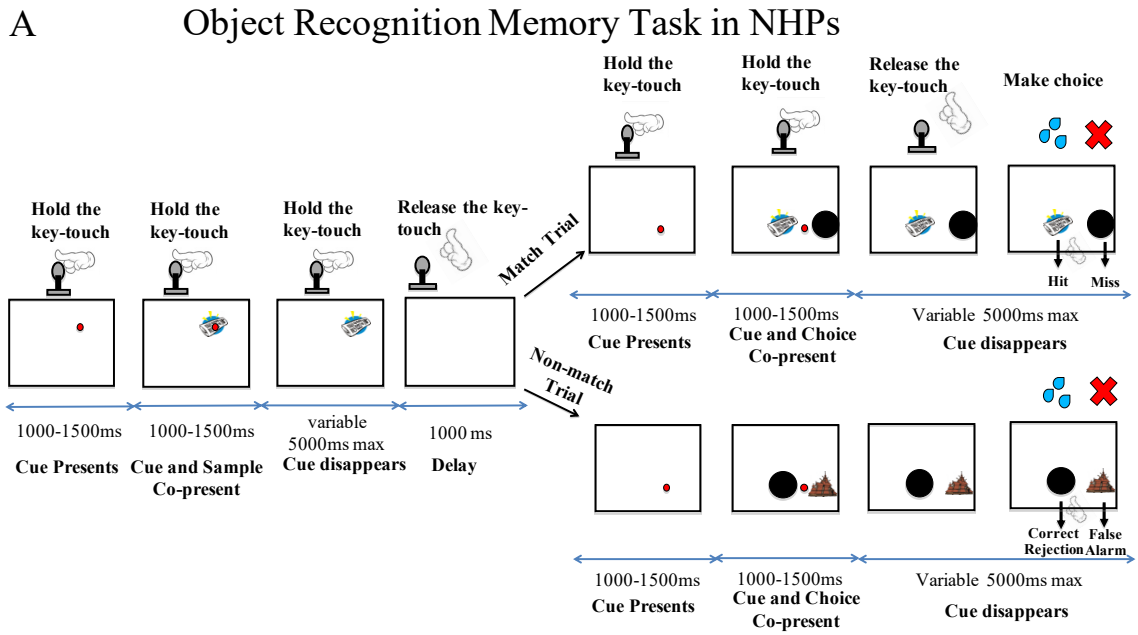


Figure 3. Stimuli used in a series of NHP behavioral tasks. *Panel A: clip-art object images used in the object recognition memory task and in the object hybrid perceptual and memory task. Panel B: nature scene images used in the scene recognition memory task. Panel C: three example photographic object stimuli (d, e, f) with two different views (d1-d2; e1-e2; f1-f2), used in the same- or different view object recognition memory task,*

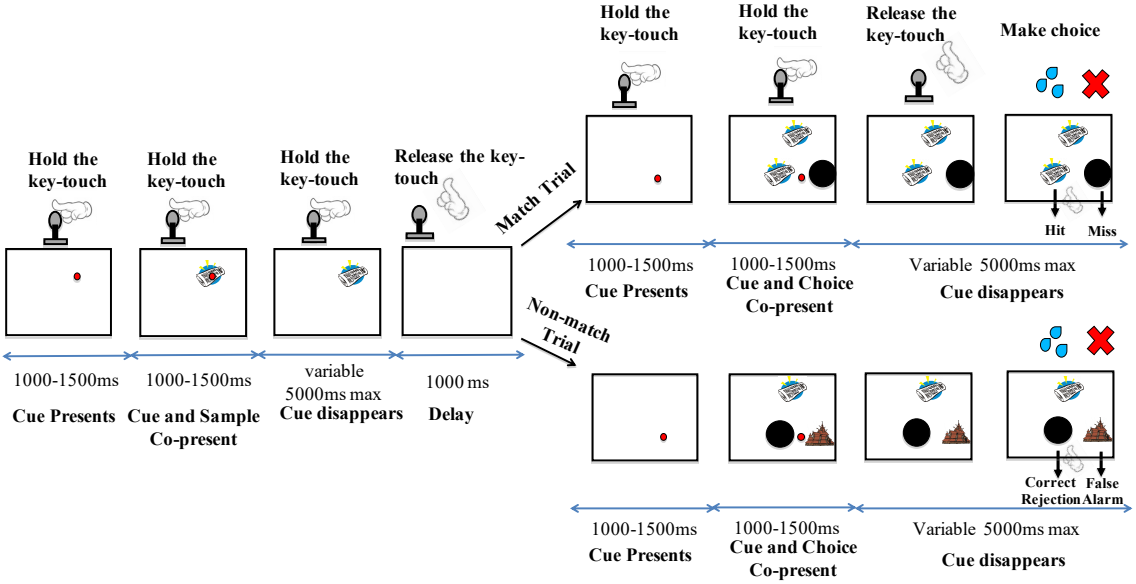
Same- or different-view object recognition memory task

In this task, we used photographic object test-stimuli with same or different views as sample-stimuli in a recognition memory task (see Figure 3C). This task structure was identical to the object recognition memory task in the sample and delay phase. During the choice phase, the test-image stimulus was either the identical stimulus with same view (e.g. d1, e1, f1 in Figure 3C) to the central sample (e.g. d1, e1, f1) or identical stimulus with different view (e.g. d2, e2, f2) to the central sample in the trial (i.e. the proportion of different-view object stimulus in match trials is 50% or 100% within a session); or it was a completely novel stimulus to the central sample. In a given session which sets proportion of different-view object stimulus in match trials is 50%, same-view and different-view object stimulus appeared equally in the total number of match trials. In a given session which sets proportion of different-view object

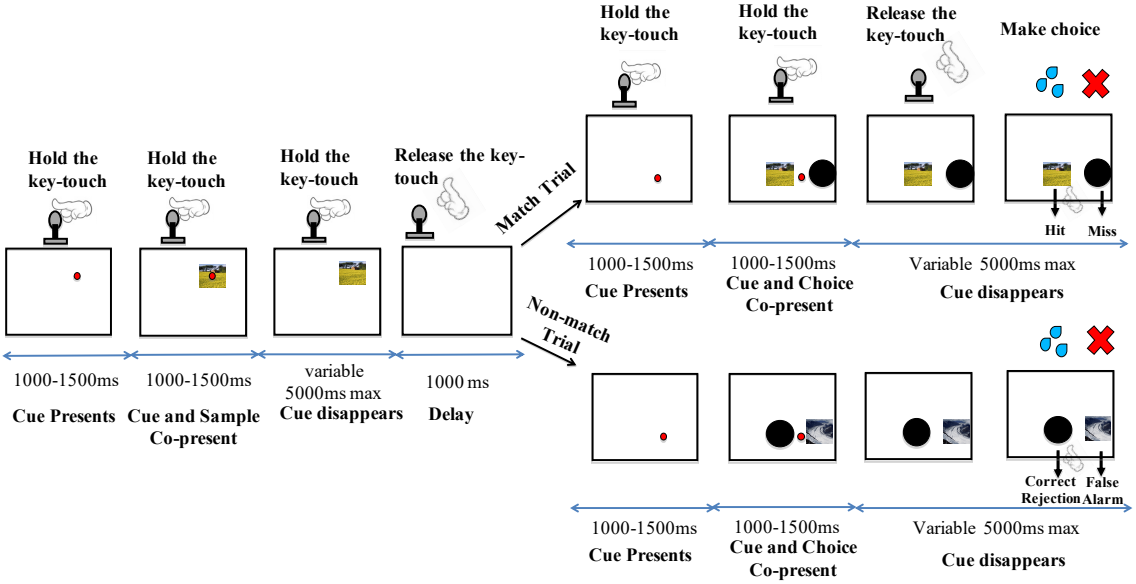
stimulus in match trials is 100%, different-view object stimulus always appeared in match trials. The animal was rewarded by delivery of 10 ml of smoothie for touching the test-item image if it matched the sample image either with the same-view or different-view (these we refer to as 'match trials'), or it was rewarded for selecting the standard 'non-match button' (i.e. the black circle) if the test-item was a non-match (these we refer to an 'non-match trials'). In any given sessions 50% of the trials used trial-unique object stimuli and 50% were 'repeat' object stimuli used previously in the session; in each session there were six repeat object stimuli sorted into 3 pairs such that in each trial with repeat stimuli one pair was chosen at random and one member of the pair was randomly chosen to be the sample. Each session typically consisted of 150 trials so the six repeat stimuli got steadily more familiar across the session. A schematic of the same- or different-view object recognition memory task is illustrated in Figure 4D.



B Object Hybrid Mnemonic and Perceptual Task in NHPs



C Scene Recognition Memory Task in NHPs



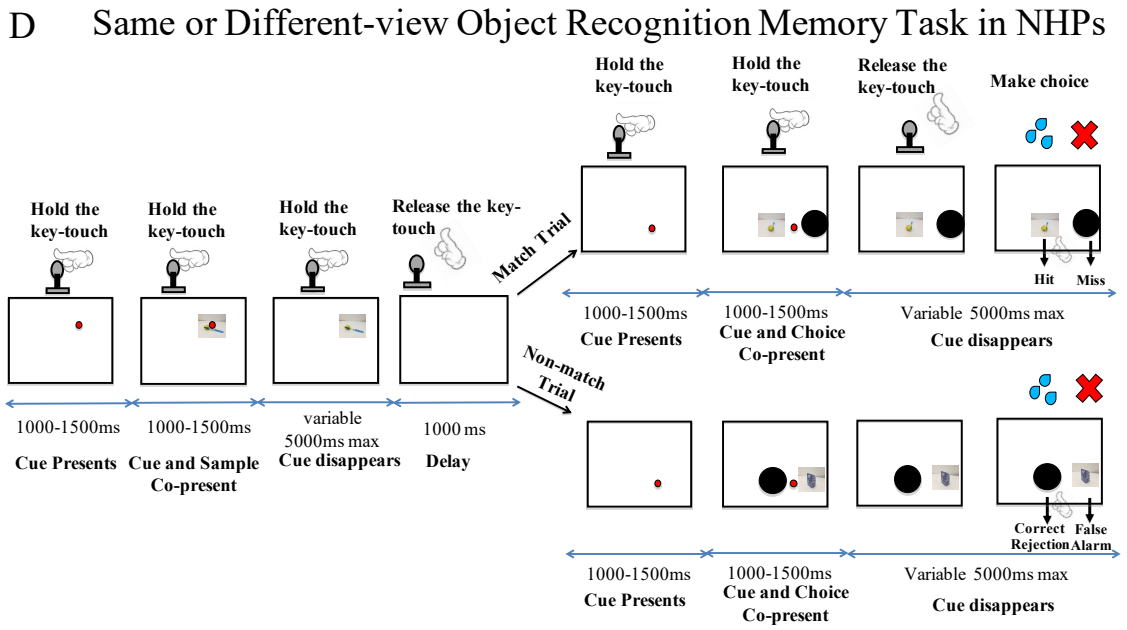


Figure 4. A series of NHP behavioral tasks. *Panel A: object recognition memory task. Panel B: object hybrid perceptual and mnemonic task. Panel C: scene object recognition memory task. Panel D: same- or different-view object recognition memory task. The above four tasks had similar task structures. In each trial, the NHPs initiated the task by holding the key-touch device once the red dot cue appeared through a variable time of 1000-1500 ms, after which a sample image (object image in panel A, B and D, and scene image in panel C) was shown on the screen behind the red dot cue. The NHPs were required to keep holding the keytouch device through another variable delay of 1000-1500 after which the red keytouch cue disappeared then the NHPs were trained to release its hand from the keytouch prompting the commence of the delay (1000ms) between sample and choice-phases. Then after the 1000 ms delay period another key-touch red dot cue, this time in the bottom of the screen, and the animals were required to hold the key-touch again. The NHPs were again required to keep holding the key-touch device through a variable delay of 1000-1500 ms after which two choice stimuli (one a test-stimulus image and the other a black circle, left-right randomized between trials) appeared in panel A, C and D; while two choice stimuli (one a test-stimulus*

image and the other a black circle, left-right randomized between trials) appeared on the bottom and the previously-presented sample stimuli re-appeared on the top in panel B. In panel A and B, the test-stimulus image was either an identical object image in the trial (i.e. 'Match Trials') or a novel object image to the sample in the trial (i.e. 'Non-match Trials'). In panel C, the test-stimulus image was either an identical scene image in the trial (i.e. 'Match Trials') or a novel scene image to the sample in the trial (i.e. 'Non-match Trials'). In panel D, the test-image stimulus was either the identical stimulus with same view to the central sample (i.e. exactly the same as the central sample) or identical stimulus with different view to the central sample in the trial (i.e. 'Match Trials'); or it was a completely novel stimulus to the central sample in the trial (i.e. 'Non-match Trials'). The NHPs were required to keep holding the keytouch device through another variable delay of 1000-1500 ms after which the key-touch red dot cue disappeared cueing the animal that it could release holding the key-touch and make a choice to the touchscreen to either the test-image stimulus or to the black circle. Animals were trained to touch the test-item if they remembered or perceived the test-item was a match in 'Match Trials' but to touch the black circle if they thought the test-item was a non-match in 'Non-match Trials'; accordingly the responses could be separated into hits, misses, correct rejections, and false alarms as indicted separately in the four panels.

Data Analysis

In this ongoing project, Monkey B is still under recording while Monkey A has completed all the recordings from MTL in the above four tasks (object recognition memory task: 33 sessions; object hybrid perceptual and mnemonic task: 31 sessions; scene recognition memory task: 23 sessions; same- or different-view object recognition memory task: 1 session with different-view object proportion set as 50%; 1 session with different-view object proportion set as 100%). Monkey A has also completed the recordings from both MTL and

PFC in one session of object recognition memory task and one session of object hybrid perceptual and mnemonic task. In this chapter, I present a preliminary analysis of neural data from one MTL recording session in Monkey A and another PFC/MTL recording session in Monkey B in an object recognition memory task to illustrate how the 'big data' from both animals (when complete) may be exploited. In these two sessions, both monkeys successfully completed around 200 trials. In the neural data analysis, and to draw comparisons with earlier chapters in this thesis, I focused on the sample phase of recognition memory task (i.e. sample image was on the screen) in both correct and error trials.

In the included sessions, Monkey A had hippocampal/MTL signals from the posterior microdrive, while monkey B had both PFC and hippocampal/MTL neural signals from both microdrives. I present analyses of single-unit activities from the hippocampus (from both monkeys) and from lateral PFC (from monkey B) in correct trials. I also present LFP coherence analyses and a non-parametric permutation test (as described in detail in Chapter 4 and Chapter 5) from the hippocampus and lateral PFC from monkey B in both correct and error trials. All the neural data were analyzed with MATLAB (R2017b, MathWorks), FieldTrip toolbox (*http://www.fieldtriptoolbox.org*, details see Oostenveld et al., 2011), Chronux Toolbox (*http://chronux.org*), and custom-written scripts.

Results

Spike activities of hippocampus and lateral prefrontal cortex

Details of spiking sorting were described in the methods of Chapter 4. After spike sorting the single sessions (note that in future complete data-set analyses we will have many sessions, and a key issue will become rating units as likely to be 'same' or 'different' as in previous sessions if the electrodes were not moved on that day) I detected 3 hippocampal units in monkey A, and 4 hippocampal units and 17 lateral PFC units in monkey B (both monkeys had other units in other MTL structures, IT and parietal cortex, and here, I just focused on the

hippocampal and PFC units). Among the sorted hippocampal units in the two monkeys, 2 hippocampal units in monkey A and 1 hippocampal unit in monkey B showed visual responses to the sample image during recognition memory task (which augurs well for the future as this is currently ~43% of visually responsive hippocampal units). As shown in Figure 5, two example hippocampal units in monkey A showed increased spike activities after the sample image onset (left: onset latency around 200-400 ms, right: onset latency around 100-200 ms); and another example hippocampal unit in monkey B also demonstrated increased spike activities after sample image onset (onset latency around 100-200 ms). The response latencies in some hippocampal units (e.g. 100-200 ms) were consistent with the finding from Jutras et al. (2010), as they found onset latencies of 131 recorded hippocampal units were in a range of 100-250 ms.

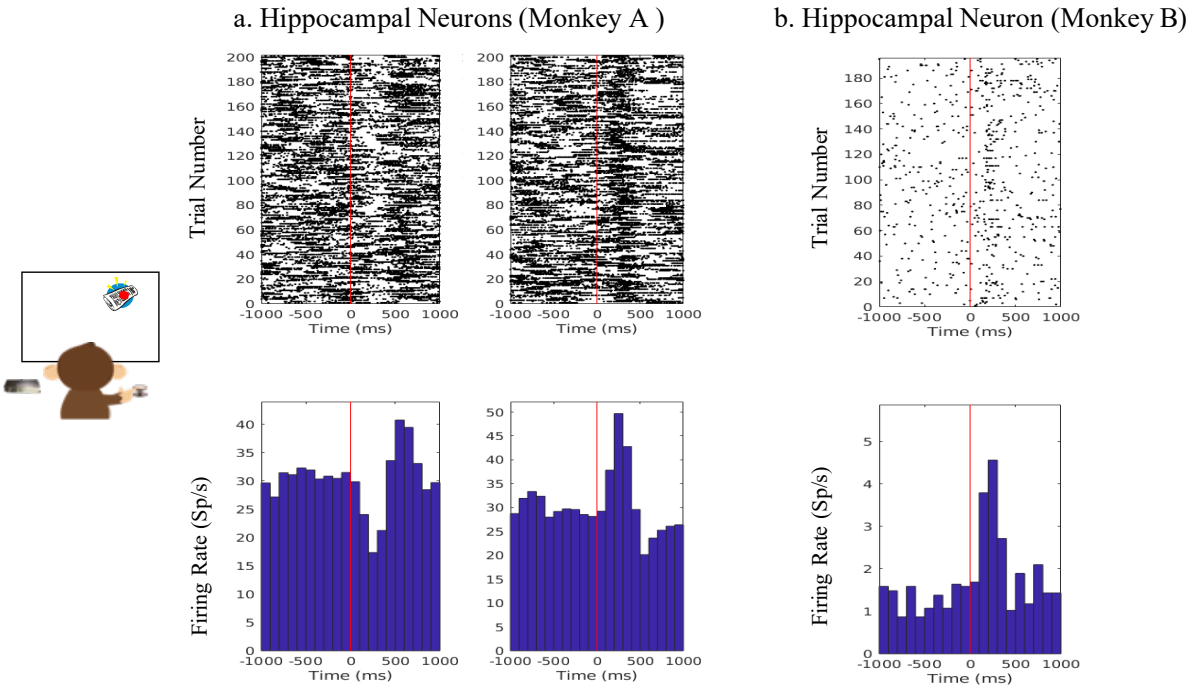


Figure 5. *Two example hippocampal neurons in monkey A and one example hippocampal neuron in monkey B demonstrated increased spike activities after sample image onset. Top*

panel: binned spike activities of hippocampal units in the sample phase of recognition memory. Bottom panel: peri-stimulus time histograms of the same hippocampal units in the sample phase of recognition memory. Red line in the middle of each panel indicates the onset of sample image (time zero). Duration of pre-sample and post-sample phase in each panel was set to 1000 ms, respectively, as during this period monkeys were holding the key-touch all the time.

In Monkey B, 7 lateral PFC neurons (which augurs well for the future as this is currently ~41% of visually responsive PFC units) showed visual responses (i.e. either increased or decreased firing rate) to the sample image during the recognition memory task. As shown in below Figure 6, two example PFC units in monkey B showed visual responses to visual stimuli: one PFC unit showed increased spike activities (onset latency around 100-200 ms) while another PFC unit showed decreased spike activities (onset latency around 300-500 ms) after sample image onset.

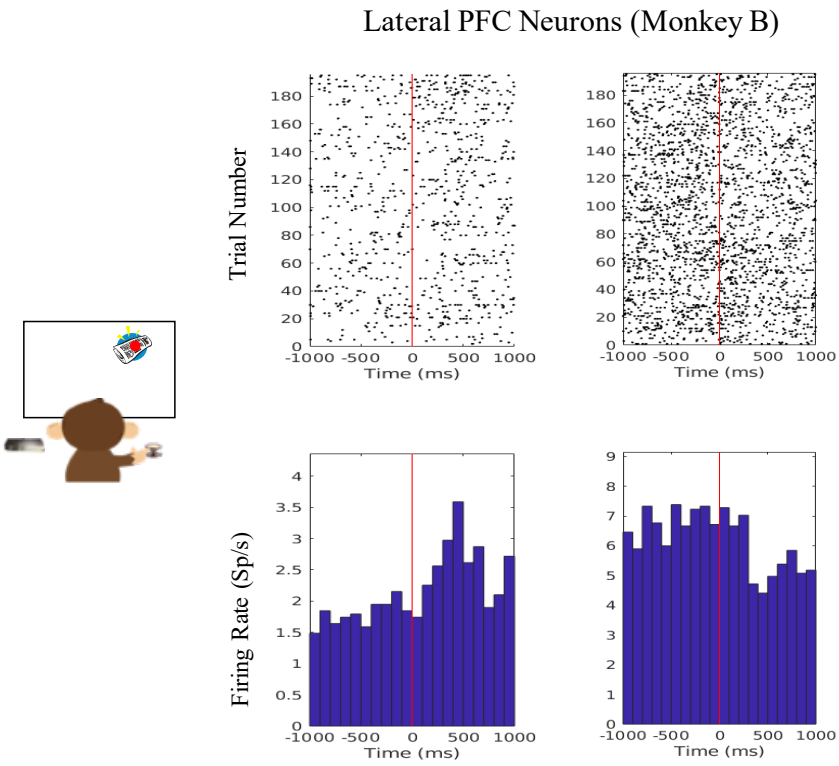


Figure 6. *Two example PFC neurons in monkey B demonstrated visual response to the sample image: the left one showed increased activities whole the right one showed decreased activities after sample image onset. Top panel: binned spike activities of lateral PFC units in the sample phase of recognition memory. Bottom panel: peri-stimulus time histograms of the same lateral PFC in the sample phase of recognition memory. Red line in the middle of each panel indicates the onset of sample image (time zero). Duration of pre-sample and post-sample phase in each panel was set to 1000 ms, respectively, as during this period monkeys were holding the key-touch all the time.*

Hippocampal-prefrontal coherence during sample phase of recognition memory

As I am interested in how the visual responses of hippocampus and PFC to the sample image affect the recognition memory performance, LFPs were analyzed in the electrodes which

contained units (indicating those electrodes were inside the cell layers), which showed responses to visual stimuli. As monkey A didn't have PFC units in this session, the hippocampal-PFC coherence analysis was carried out in monkey B. In each trial, LFPs (1 hippocampal LFP and 7 PFC LFPs) in the sample phase from 1000 ms (as a baseline) before stimulus onset until 1000 ms after stimulus onset were analyzed. Then LFP data from 200 ms (as a baseline) before stimulus onset until 800 ms after stimulus onset (to avoid the spectral leakage of LFP power when calculated near the margin of a 1000 ms time-window) in each trial were included in the coherence analysis, provided a time window of 1000 ms. In this recorded session in monkey B, correct trials (N=195) and error trials (N=23) were used for calculation of coherence for 7 hippocampus-PFC brain pairs. Trial-averaged LFP-LFP coherence of those brain pairs in correct condition and error condition were calculated, and then were averaged in the theta frequency band (4-6 Hz). To test for statistical significance of differences of the LFP-LFP theta-band coherence across hippocampus and PFC between correct and error conditions in the sample phase of recognition memory task, a nonparametric permutation test was applied, with the median difference between the above conditions as our test statistic. In the encoding phase, the null hypothesis of this test was assumed that, for each time bin, there was no significant difference of the LFP-LFP theta-band coherence when comparing the observed median difference between the two conditions (i.e. correct and error) against a reference distribution. This reference distribution was obtained by performing 10,000 permutations on brain pair labels to randomly assign the two conditions. A time bin would be selected if its observed median difference was larger than the 97.5^{th} or smaller than the 2.5^{th} percentile of its permutated data ($p < 0.05$, two-tailed). Then the selected time bins were clustered in connected sets on the basis of temporal adjacency. As shown in Figure 7, permutation test (two-tailed) confirmed a significant difference of coherence between correct and error conditions prior to the sample image onset (error > correct, $p < 0.05$). After sample image appeared on the screen, an increase of coherence was found in correct condition

whereas a decrease of coherence in was found error condition. Permutation test (two-tailed) further confirmed a significant difference between correct and error conditions between 200-500 ms, in which coherence in correct condition was significantly larger than coherence in error condition (correct > error, $p < 0.05$). Then around 500 ms, coherence in correct condition decreased while coherence in error condition increased, and the significant difference between the two conditions appeared around 600-800 ms (error > correct, $p < 0.05$). This preliminary coherence analysis indicates theta-coherence between hippocampus and PFC may signal monkey's recognition memory performance.

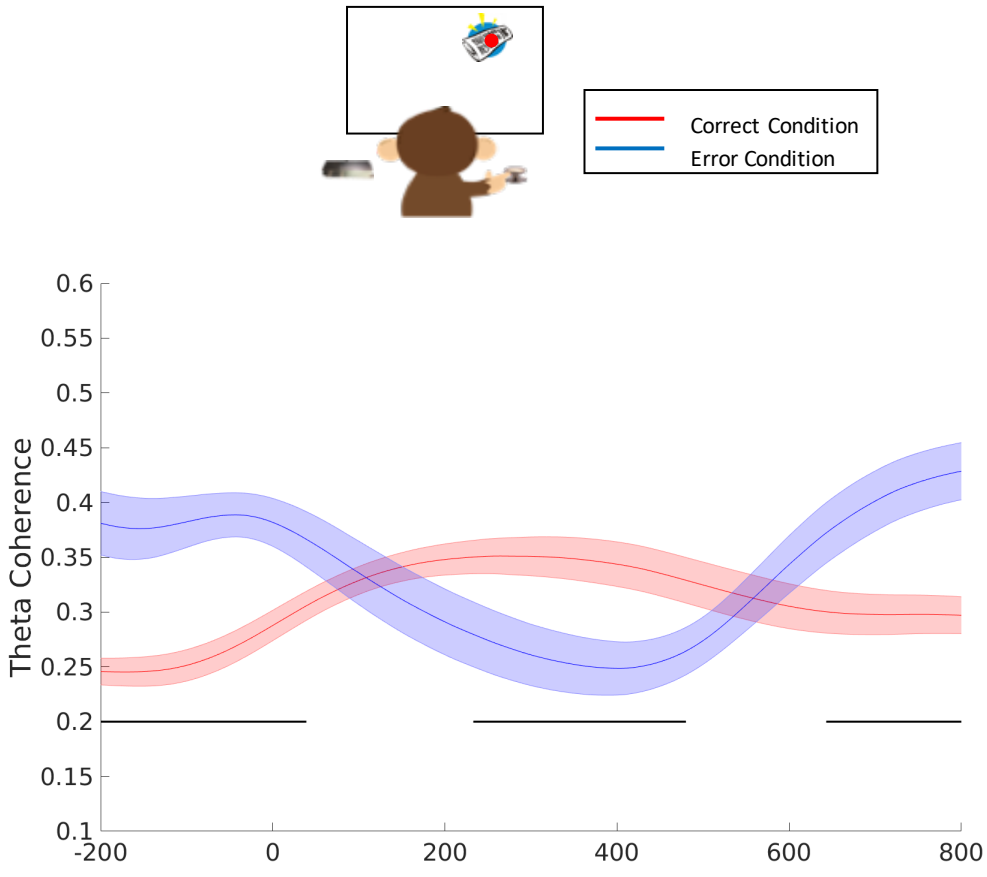


Figure 7. *LFP-LFP coherence between macaque hippocampus and lateral PFC in theta-frequency band for both correct (red line) and error conditions (blue line), with black line underneath indicating the significant difference between the two trial-type conditions.*

Permutation test confirmed a significant difference of coherence prior to the sample image onset (error > correct, highlighted in black line). After sample image appeared on the screen (time zero was set to sample image onset), an increase of coherence was found in correct condition whereas a decrease of coherence was detected in error condition, and the significant difference between the two conditions was found during 200-500 ms, in which coherence in correct condition was significantly larger than coherence in error condition (highlighted in black line). Then around 500 ms, coherence in correct condition decreased while coherence in error condition increased, and the significant difference of coherence between the two conditions appeared around 600-800 ms (error > correct, highlighted in black line).

Discussion

Recent electrophysiological studies in the macaque hippocampus have shown hippocampal neural activities and oscillations are associated with memory encoding and reactivation (Jutras et al. 2009, 2010, 2013; Jutras and Buffalo 2014), associative learning (Brincat and Miller 2015), and temporal-order memory (Naya and Suzuki 2011; Naya et al. 2017). Our preliminary results in two NHPs, which performed an object recognition memory task, demonstrated hippocampal cells showed visual responses to the sample image presented during the encoding phase. Both our study and Jutras et al. (2010) have shown some hippocampal neurons demonstrated selective activities to visual stimuli (Figure 8). Jutras et al. (2010) have further shown that 67% of recorded macaque hippocampal neurons responded to visual stimulus presentation, and 36% of those visually responsive neurons showed firing rate modulations by either novel or repeated stimuli, indicating hippocampus is associated with processing stimulus novelty (Jutras and Buffalo 2010). It will be of interest to know how these novelty or familiarity responsive neurons correlate to monkeys' performance on

recognition memory, which is a topic we will investigate in our recorded neural data-set when it is complete.

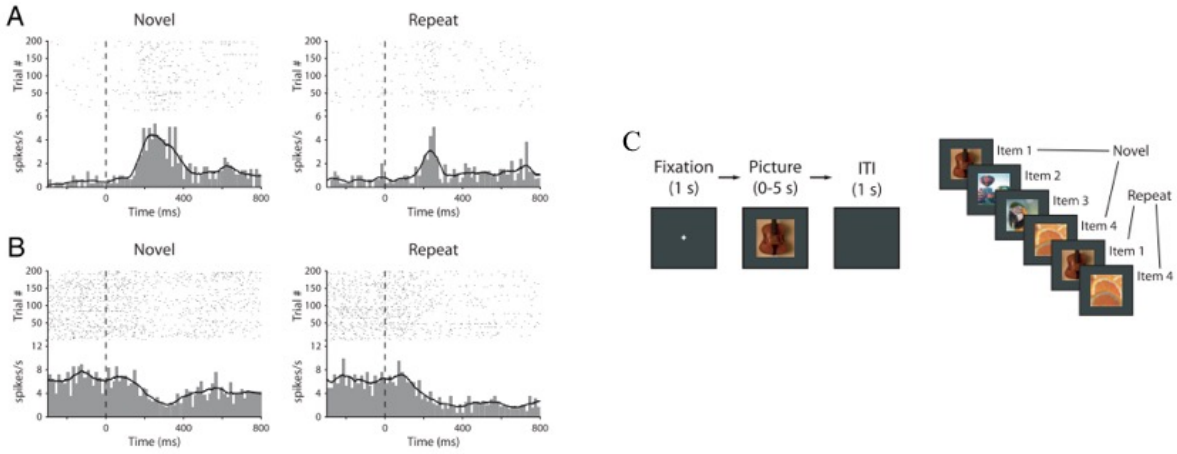


Figure 8. *Raster plots and peristimulus time histograms for two example hippocampal neurons (A and B). Neuron A showed increased firing rate while neuron B showed decreased firing rate to both novel and repeated visual stimuli. C. Behavioral task. Each trial began with a required 1-s fixation period, and then either a novel or repeated stimuli presentation for a maximum of 5 s. Intertrial interval was fixed as 1 s (adapted from Jutras et al., 2010).*

Theta oscillations in hippocampus have been linked to spatial navigation/exploration in rodent. For example, previous studies showed that the hippocampal theta oscillations were found to be related to exploration behaviour, such as twitching behaviour (Komisaruk 1970) and sniffing movement (Macrides et al. 1982). In 1993, O'Keefe and Recce found a relationship between spikes of hippocampal pyramidal cells and theta-band LFPs during rats' spatial navigation. Hippocampal pyramidal cells are also termed as place cells, as each

individual cell fires most rapidly (i.e. maximal firing rate) at a particular position, also termed as place field of this cell. As rats approaching to the place field of a given cell, the firing rate of this cell increases, and its phase begins to be out of synchrony with the theta-band LFP oscillations (i.e. theta wave). At the center of the place field, where the firing rate of this cell reaches its maximum, firing of this place cell and theta wave are anti-phased. When rats move away from the place field, the firing rate of this cell decreases, and its action potentials continue to occur gradually earlier than the theta wave, until they become synchronized. This phenomena is termed as "phase precession" (O'Keefe and Recce 1993; Skaggs et al. 1996). Further study showed that when the rats came to a new environment, the place fields were remapped to represent the new surroundings (Bose and Recce 2001). Besides involvement in spatial navigation, a recent electrophysiological research has linked hippocampal theta oscillation to recognition memory performance in primates. Specifically, preceding the encoded novel stimulus presentation, the magnitude of theta power during the baseline fixation period predicated how well the monkeys remembered the stimulus in the retrieval phase (Jutras et al. 2013). Recent studies have started to focus on the theta coherence or synchrony between hippocampus and PFC in primates to further illustrate the role of theta oscillations in memory. For instance, one electrophysiological study has found the theta synchrony between hippocampus and PFC increased after error responses during associative learning in NHPs (Brincat and Miller 2015). Another human magnetoencephalography research has shown during the encoding phase of an associative memory task, a stronger theta coherence between hippocampus and medial PFC was found during successful memory performance (Backus et al. 2016). In our recognition memory task, we preliminarily found hippocampal-PFC coherence in theta band during the sample phase was relevant to monkey's recognition memory performance. When the sample image was on the screen, an increased theta coherence was observed in trials that ended up being correct trials while a decreased coherence was found in trials that ended up being error trials, and their significant difference

was reached after 200 ms relative to sample image onset. This preliminary coherence analysis, along with the non-parametric permutation test, indicates theta coherence may signal successful performance in macaque recognition memory. As only the data from one session and from one monkey was included in this analysis, more data will need to be analyzed to give weight to this preliminary significant observation.

In summary, we provided some preliminary results to show how interactions between macaque hippocampus and PFC during the sample phase of an object recognition memory task, and how the hippocampal-prefrontal interaction was related to memory performance. As macaque hippocampus is a deep structure which cannot be accessed by Utah arrays, this chapter also describes the alternate recording methodology I pioneered in Oxford (i.e. this study was the first in Oxford to implant a NHP with a 96 channel multi-electrode microdrive) which we believe will be important to guide future studies intent on targeting macaque hippocampus and surrounding MTL structures in combination. In the future, more thorough and sophisticated neural analyses on spike (single- and multi-units) activities, and LFPs, and spike-spike, LFP-LFP and spike-LFP analysis across all the recorded MTL and PFC regions in these two monkeys will be carried out to further validate our initial findings.

General Discussion

According to the MTL long-term declarative memory system, Squire and Zola-Morgan proposed that MTL is a homogenous memory system and is exclusively involved in long-term declarative memory (Squire and Zola-Morgan 1991). This theory is not accurate as there is now significant evidence that the MTL is not a homogenous system as i) it may be divided by stimulus domain (e.g. hippocampus and parahippocampal cortex more involved in spatial/temporal relational mnemonic encoding and perirhinal cortex more involved in object memory processes); and ii) it may be divided by process domain (e.g. hippocampus more involved in recollection and perirhinal cortex more involved in familiarity); and iii) some MTL structures (i.e. perirhinal cortex and hippocampus) may be involved in both mnemonic and perceptual processes. The above issues of domain and process division of function also apply to PFC where it is even less clear its divisions along those dimensions exist. In this thesis, I provided some clues to the considerations and controversies related to those issues, by investigating interactions both within MTL and PFC and also between MTL and PFC in a range of perceptual and mnemonic tasks by using different stimuli (objects for the most part and scenes in the latest ongoing work) in NHPs, and by investigating the mechanisms of recollection and familiarity processes in both humans and NHPs based on a series of homologous paradigms.

One key scientific issue is that MTL is divided by stimulus domain, although the underlying neural mechanism is not fully understood. In Chapter 4 and Chapter 6, I investigated how different sub-regions of MTL (e.g. perirhinal cortex, hippocampus) participated in an object delayed matching-to-sample task (i.e. a short-term memory task). In Chapter 4, I found dynamic neural activities of different temporal structures (i.e. visual area TE, perirhinal cortex) and PFC across different epochs (i.e. encoding, delay, choice) of the object recognition memory task; moreover, those MTL and PFC structures interacted

differently in various task epochs. In Chapter 6, I found some hippocampal neurons in macaques demonstrated visual responses to encoded object images during the sample phase of recognition memory task; moreover, a dynamic change of theta-band coherence between hippocampus and PFC during the sample phase signaled the success of monkey's retrieval performance. These two chapters indicate different MTL sub-regions interacted differently within MTL and interacted differently with other brain regions of prefrontal cortex in different epochs of object recognition memory. I also recorded neural signals of MTL and PFC from two monkeys in a scene recognition memory task (i.e. ongoing project in Chapter 6). Comparison on neural activities of MTL and PFC in different epochs of both tasks will be made as future analysis, in an attempt to provide more insights to the stimulus domain theory of MTL (and PFC).

A second key scientific issue is how to reconcile process-specific theories with domain-specific theories of MTL in memory. According to dual-process theory, recognition memory is assumed to draw upon familiarity (i.e. a feeling of familiarity or knowing of encountered items without too much details) and recollection (i.e. a vivid recall of encountered items and episodes) (Dede et al. 2014; Parks and Yonelinas 2007; Scalici et al. 2017; Wixted 2007; Yonelinas 2001, 2002; Yonelinas and Parks 2007). In process-specific theory, there is good evidence that PrC is involved in familiarity whereas hippocampus is involved in recollection (Fortin et al. 2004; Sauvage et al. 2008; Yonelinas et al. 2002; Eichenbaum et al. 2007). In domain-specific theory, more evidence have been found to show that PrC is involved in object processing while hippocampus and parahippocampal cortex are involved in spatial/temporal processing (Graham et al. 2010; Epstein et al. 2003; Hodgetts et al. 2016; Lee et al. 2005b; Staresina et al. 2013). These two theories are mutually exclusive as it doesn't seem credible that people cannot be familiar with scenes and cannot recollect objects. How can both theories be so well supported by an extensive literature? One proposed answer is that perirhinal cortex and hippocampus may interact differently with each other and with

other MTL structures and with other PFC regions depending on task demands. In humans, the relative contribution of familiarity and recollection to recognition memory are commonly distinguished by analysing receiver-operating-characteristics (ROC) curves; while analogous methods are more complex and very rare in animals. In Chapter 2, I proposed a response time derived paradigm and applied it to both humans and NHPs to show a common behavioral profile (i.e. time course) of both species in recollection and familiarity processes. This cross-species paradigm developed in Chapter 2 can be applied to NHP's electrophysiological research to further investigate neural substrates within the regions involved in process-specific theory. In Chapter 3, I investigated how human dorsolateral PFC and dorsomedial PFC mediated recollection and familiarity processes. I found that low beta-frequency rTMS caused decreased recollection when targeted to human dlPFC, but enhanced familiarity when targeted to dorsomedial prefrontal cortex. Then in Chapter 6 (an ongoing project), I compared different neural activities of hippocampus and PFC in an object memory task. To better understand the domain-specific theory of MTL, more neural data acquisition and analysis need to be done in the future of this project. I primarily aim to compare different neural activities of hippocampus (and other surrounding MTL structures) and PFC in an object versus scene task, and to determine how these areas interact at the neural level when animals discriminate between different types of stimuli (e.g. objects versus scenes). Moreover, if we can apply the response time derived paradigm developed in Chapter 2 to this project, then we aim to investigate whether neural activities within MTL and PFC areas, and between MTL and PFC areas, differ depending on whether individual discriminations are indexed as being based more upon familiarity and/or recollection.

Finally, returning to the issue of MTL structures contributing to short versus long-term memory, that debate has extended into one also considering the extent to which MTL structures contribute to perceptual discrimination (Baxter 2009; Buckley et al. 2001; Buckley 2005; Bussey et al. 2002a; Bussey and Saksida 2002; Bussey et al. 2003, 2005, 2006; Bussey

and Saksida 2007; Eacott et al. 1994; Lee et al. 2005a, 2005b, 2005c; Murray and Bussey 1999; Murray and Richmond 2001). The perineal cortex (PrC) is functionally distinct from other MTL structures as it is interconnected both with the ventral visual processing stream (e.g. area TE) and with other structure in the MTL (e.g. hippocampus), which makes it a prominent target for experiments and discussion in the context of debates about perceptual-mnemonic theory versus MTL declarative memory system theory (Buckley 2005). Previous studies in macaques and human patients confirmed damage to PrC induced perceptual deficits in discriminating objects on the basis of a combining of different features (i.e. object-level representation) in the oddity task (Baxter 2009; Buckley 2005; Buckley and Gaffan 2006) and in the morph task (Bussey et al. 2002a; Bussey and Saksida 2002, 2007). It is therefore argued that PrC is important for object-level perceptual discrimination, and also object-level memory if the underlying representation for 'object-level' needs to be maintained in PrC. Here, we hypothesized that PrC could be both involved both in memory and perception processes by interacting differently with other different MTL structures and PFC structures depending on task demands. In Chapter 5, I used a delayed memory task versus a hybrid memory and perception task to compare different neural activities of MTL and PFC underlying the memory and perception processes. I found macaque perirhinal cortex and dorsolateral PFC interacted differently in different epochs (e.g. sample, delay, choice) of the two tasks. In Chapter 6 (an ongoing project), I applied object stimuli with different viewpoints to a recognition memory task as previous literature has shown perirhinal cortex was sensitive to objects with different views in the oddity task (Buckley et al. 2001; Lee et al. 2005b). In this ongoing project, I will continue to investigate how the perirhinal cortex and hippocampus interact differently with other MTL or PFC brain regions when discriminating between objects with same view (i.e. on the basis of a single feature) or different views (i.e. on the basis of a conjunction of different features) (Buckley 2005).

The above neuropsychological and stimulation research in both humans and NHPs highlights a synchronized brain network involving different MTL and PFC brain structures in both memory and perceptual discrimination tasks. What does a macaque brain network look like during resting state without any task demand? In Chapter 1, I applied neuroimaging technique to anaesthetized NHPs to investigate their resting-state brain network. I also investigated the extent to which that network was influenced or mediated by area 10 (frontopolar cortex, FPC). The reason to investigate NHP area 10 is that the cognitive function of this region is not yet fully understood. Functional connectivity analysis along with lesion manipulations in NHPs (used in Chapter 1) provides another approach to look at how causal interactions between areas were mediated by area 10. By investigating FPC-mediated brain networks during resting state, we could reveal which brain regions were involved in those networks and how those regions interacted in absence of external tasks. The next step (in the ongoing electrophysiological research), would be to record from those areas simultaneously in awake animals before and after selective inactivation/lesions of FPC in specific tasks, as a further attempt to investigate the causal network dynamics in the process of perception, memory and decision making in NHPs.

Summary and implications of investigations of primate area 10 in Chapter 1

We know remarkably little about the crucial contributions to cognition of one of the largest cytoarchitectural areas in the human brain, namely area 10 of FPC, which on anatomical and connectivity grounds appears to sit a atop a hierarchy of prefrontal cortical regions in primates (as rodents do not have an equivalent to area 10). Understanding how this region contributes to cognition may be of particular importance for furthering understanding of some of the more advanced cognitive processes in non-human and human primates.

There are several reasons for this acute scarcity of knowledge of FPC functions. First of all, current knowledge mostly derives from correlational human neuroimaging which has failed to reach consensus as to key functions as so many disparate functions have been related to FPC using neuroimaging (Badre and Wagner 2004; Bunge et al. 2009; Burgess 2000; Burgess et al. 2011; Christoff et al. 2001, 2003; Koechlin et al. 1999, 2000; Okuda et al. 2003, 2007; Ryals et al. 2015; Yokoyama et al. 2010). Secondly, selective damage to FPC is remarkably rare in humans as there exist only extremely rare case studies of individual patients with lesions restricted to within FPC and we are aware of only one case study of a single patient (Hoffmann and Bar-On 2012). Thirdly, unlike all other prefrontal brain regions in primates which have been investigated for many decades with combinations of detailed electrophysiological neuronal recordings and selective cortical lesions, there are only two published studies that have recorded from FPC neurons in non-human primates (Tsujimoto et al. 2010, 2012) and only two studies that have examined the behavioural deficits of selective FPC lesions in non-human primates (Boschin et al. 2015; Mansouri et al. 2015).

A recent review on the function of FPC, taking into account the non-human and human primate literature, proposes a functional model of FPC in which FPC contributes to disengaging cognitive control from the current task and redistributing resources to other potential goals for 'exploration'; while the posterior parts of the prefrontal cortex are involved in staying on the focus on the current task to facilitate 'exploitation' (Mansouri et al. 2017). This review indicates a potential interaction between FPC and other posterior parts of the prefrontal cortex in mediating the optimum balance between 'explorative' and 'exploitative' tendencies. Additionally, one anatomical study confirms FPC has a unique pattern of reciprocal connections to other posterior cortical areas (i.e. superior temporal sulcus and superior temporal gyrus region, anterior and medial temporal lobe including perirhinal cortex, and anterior and posterior cingulate and retrosplenial cortices) (Petrides and Pandya 2007). To better illustrate the function of FPC in cognition, it's essential to

investigate the functional relationship between FPC and other cortical regions, which is a key motivation of the study in Chapter 1.

In this chapter, I investigated the causal effects of FPC lesions on functional connectivity between cortical areas within and beyond prefrontal cortex to examine the necessity of FPC to maintain networks of functional connectivity in the non-human primate brain. By using cluster analyses of network interaction functional connectivity data, I found that the primate brain without FPC present cannot maintain as many separable but overlapping networks as the primate brain with a fully functioning PFC present, and illustrated that FPC is a mediator of network modularity in the primate brain. A very important aspect of this study is that it provides causal evidence (i.e. via the intervention) as to the influence of FPC on brain networks and such causal evidence does not exist in the literature yet with respect to FPC.

Our research on primate FPC upon resting-state brain network has some implications on the future investigations of FPC function in awake and behaving animals. As shown in previous FPC lesion studies, FPC-lesioned animals demonstrated specific impairments in first-trials (i.e. rapid one-trial learning stage) of both concurrent objects-in-scenes learning and successive single problem learning (in both cases involving considering the relative values of alternative novel stimuli); learning new abstract rules (which involves considering the relative value of novel alternative rules), however, they didn't show any behavioural deficits in tasks with established and familiar rules or stimuli (Boschin et al. 2015). This line of behavioural evidence indicates that FPC contributes to rapid learning about the relative value of alternatives of a broad kind. In addition, Mansouri et al. have found macaques with lesions of FPC didn't show any behavioural difference in a standard Wisconsin Card Sorting Test (WCST, switch between well-established abstract rules) compared with control animals, but rather they showed enhancements in WCST task performance if trials involved conflict, or an intended distracting interrupting task that delivered reward, or even a distracting free-reward (Mansouri et al. 2015). This evidence further suggests that in absence of FPC, animals

can more easily resist attending to the relative value of potential behavioural 'alternatives' and perform better in the current tasks; in other words (as suggested in the recent review), FPC contributes to disengaging executive control from the current task and redistributing it to explore any other potential goals (Mansouri et al. 2017). Those specific behavioural deficits induced by lesion to FPC suggests that lesion effects of FPC cannot be simply understood as a loss of function in the specific area removed. Indeed, in our resting state fMRI data, we showed a unique functional and spatial separation of a frontal-temporal-anterior parietal network and a cingulate-occipital-posterior parietal network in absence of FPC, the disengagement of these two brain networks indicates a possible and potential interaction between these two brain networks when mediating behaviour. One of the limitations of this study is that at the current stage, we only considered one lesioned area (i.e. FPC), as it would be important to validate this approach and test its generality by examining another lesion group where a different cortical area other than FPC is lesioned. Such work is currently undergoing, and we are introducing a lesion group of dlPFC to the existing analysis approach and conducting brain network analysis based on both dlPFC- and FPC-lesioned groups.

Given the complexity of FPC-related behavioural deficits, the outstanding puzzle is how to relate the very selective behavioural deficits observed after FPC lesions with widespread FPC mediated influence on the brain (as evidenced by these rsfc changes). This will require future electrophysiological research examining the causal influences of FPC exerts at the neuronal level on interconnected areas in the awake behaving animals. As most neurological and neuropsychological disorders are increasingly understood as being due to network dysfunction (altered interactions) as opposed to due to dysfunction of individual brain areas (Stam 2014), a combined multi-area recording and brain intervention could be the key to understand the mechanism behind them (and we're carrying out a big electrophysiological research to investigate the neural activities of FPC and its interactions with frontal, parietal and temporal regions in memory and perception).

Summary and implications of the investigations of recollection and familiarity processes in Chapters 2-3

According to the dual-process theory, recognition memory draws upon both familiarity and recollection. In Chapter 2, I investigated the time course of these two processes in humans and non-human primates (NHPs); and in Chapter 3, I investigated different roles of prefrontal neural activities on familiarity and recollection in humans. One advantage of both studies is using a complementary cross-species approach (e.g., electrophysiological recordings in macaques vs. direct brain manipulation methods in humans) under a homologous behavioral task, which benefits translation between species for advancing basic scientific knowledge of familiarity and recollection processes.

We know remarkably little about how neural activities in different sub-regions of primate prefrontal cortex underlies these two processes. Understanding the inherent neural oscillations in brain areas will likely be an essential component in revealing the kinds of mechanisms by which different sub-areas of PFC contribute to recollection and familiarity. In Chapter 3, by first recording macaque local field potentials (LFPs), I observed modulation of low-beta power in dorsolateral PFC during the sample stimulus encoding, and further revealed an increased alpha/beta power in the 10-15 Hz range observed in correct versus error trials. Then, in an analogous recognition memory task in humans, I targeted dorsolateral PFC with repetitive TMS at beta frequency (i.e. 12.5 Hz as the intermediate of the range of low-beta power) and succeeded in causally influencing mnemonic function during encoding of targeted samples. Moreover, I revealed a dissociation between the effects of beta-frequency stimulation to dorsolateral PFC in suppressing recollection process and dorsomedial PFC in enhancing familiarity process. These cross-species translational studies demonstrate a causal role of beta-frequency oscillations in PFC to primate recognition memory performance. This combined report of electrophysiological recordings in macaques

and TMS intervention in humans under a similar behavioral paradigm also provides cross-species validations for the importance of prefrontal oscillations in recollection and familiarity processes in primate.

As in the study of Chapter 3, I didn't investigate familiarity and recollection-like processes in the NHP, I turned to these two processes in both NHP and humans in Chapter 2 with a focus on their time course for reasons discussed in the chapter. Scant data exists as to the neural basis underlying recollection, as many of the most informative neuroscientific investigative techniques primarily exist in animal models, yet at the same time robust animal models of episodic memory in general and of recollection per se are either difficulty to achieve in practice, controversial in interpretation, or both. The relative contribution to recognition memory is commonly distinguished in humans by analysing receiver-operating-characteristics (ROC) curves (Parks and Yonelinas 2007; Eichenbaum et al. 2007; Yonelinas and Jacoby 1994; Yonelinas 2001, 2002; Yonelinas and Parks 2007; Yonelinas et al. 2010). Analogous methods are more complex and rarer in animals (Fortin et al. 2004; Guderian et al. 2011; Sauvage et al. 2008) but another approach, namely the classification of fast familiarity and slow recollective-like processes (FF/SR) have been detected in NHPs based on analysing recognition error response time profiles (Basile and Hampton 2013). The relative utility of these methods to investigate familiarity and recollection/recollection-like processes across species is uncertain though and addressing this is a key purpose of this study in Chapter 2. In brief, in this study a broadly similar recognition memory task was exploited in both humans and NHPs to investigate the time course of the two recognition processes. I first showed that the FF/SR dissociation existed in this task in human participants and then I demonstrated a similar profile in NHPs which suggests that FF/SR processes are comparable across species. I then verified, using ROC-derived indices for each response time bin in the FF/SR profile, that the ROC and FF/SR measures are related. Hence I argue that the FF/SR approach, which is procedurally easier in animals than ROC, can indeed be used as a decent proxy to investigate

these two recognition processes. This behavioural study validates the use of these paradigms for future studies that may use invasive neuroscientific methodologies (e.g. lesion studies and/or electrophysiological studies) because such studies, being invasive, need to depend on robust behavioural methodologies. Furthermore, this study points to a good way to bridge the species divide in investigations of elements of episodic memory and recollection versus familiarity.

Summary and implications of the electrophysiological investigations of memory and perception in Chapters 4-6

The medial temporal lobe (MTL) was traditionally viewed as containing a system of structures exclusively involved in declarative memory (Squire and Zola-Morgan 1991). However, more recent studies have shown that parts of the MTL structures (e.g. perirhinal cortex) participate in perception. And more recent findings suggest a role of prefrontal cortex (PFC) in maintaining information during working memory. To better illustrate the different interactions between MTL and in PFC underlying memory and perception, here we recorded neural activities in an object recognition memory task and an object hybrid mnemonic and perceptual task using a simultaneous multi-area, multi-electrode recording paradigm in three awake behaving macaques in Chapter 4-6. In the first animal (i.e. participating in Chapter 4-5), we recorded simultaneously from 32-electrodes in dorsolateral prefrontal cortex (dlPFC) in PFC, 32-electrodes in in perirhinal cortex (PrC) in MTL, and 64-electrodes in area TE (part of inferotemporal cortex and involved in visual processing) throughout both tasks. In the other two animals (i.e. participating in Chapter 6), we recorded hippocampus, entorhinal cortex, perirhinal cortex, parahippocampal cortex and inferotemporal cortex using semi-chronic 96-channel recording chamber systems and simultaneously recorded dorsolateral, ventrolateral, orbital and polar prefrontal cortex using semi-chronic 32-channel recording chamber systems. I analyzed the spike activities (e.g. including both single- and multi-units),

local field potentials (LFPs), and coherence analysis from both the three Utah arrays and the microdrive systems.

In Chapter 4 and Chapter 6, I mainly investigated the dynamic interactions between MTL and PFC during different task epochs (i.e. encoding, delay and choice) of the object recognition memory task. In Chapter 4, I found brief bursts of low-frequency activities (e.g. 4-40 Hz) in TE, PrC and dlPFC appeared around the onset of encoding and delay phase; and brief bursts of low-frequency activities (e.g. 4-30 Hz) and narrow-band gamma activities (e.g. 50-120 Hz) in TE, PrC and dlPFC appeared around the onset of choice phase. Previous electrophysiological investigation in NHPs have found an early involvement of dlPFC in the representation of salient stimuli, for example visual responses were observed with a latency as early as 52 ms in the population peristimulus time histogram and linked to bottom-up visual attention (Katsuki and Constantinidis, 2012). Early signals with a somewhat longer latency (around 120 ms) observed in dlPFC have also been linked with top-down visual attention (Buschman and Miller 2007). In area TE, neurons responded to visual stimuli was earlier (around 75 ms) than PrC, whereas the response latencies of PrC neurons were 75-135 ms (Xiang and Brown 1998). As the latencies of our low- or high-frequency bursts of TE, PrC and dlPFC occurring during the stimulus onset and offset were very short in my study, it is possible that the early signals I observed in those areas reflects both visual and attentional processes of sample and choice stimuli during recognition memory task. A further spike analysis in dlPFC showed a slight increase of firing rate occurred after the sample image and choice image onset and after the sample image offset, and a large increase of firing rate happened when the NHP touched the screen to make the choice and got the reward. Timing analysis of spike and LFPs confirmed the change of instantaneous firing rate of dlPFC were consistent with the change of alpha/beta power across the encoding, delay, choice and response phases, which further illustrates an early involvement of dlPFC in processing visual stimuli via spiking activities and low-beta power. In Chapter 6, I preliminarily found a

portion of both hippocampal and PFC neurons demonstrated visual responses to the sample image during the encoding phase of recognition memory; a theta coherence between hippocampus and PFC may signal successful performance in macaque recognition memory. These preliminary results (data were analyzed from one session per NHP) may indicate an important role of theta synchrony across hippocampus and PFC in recognition memory.

In Chapter 4, I also compared the modulation effects of sample image familiarity on the LFPs and LFP-LFP coherence across MTL and PFC regions. I found during the encoding phase, an early modulation of induced LFP power was detected after familiar sample presentation compared with novel presentation; during the delay phase, previously-presented novel sample images modulated both LFPs and alpha/beta-band coherence between temporal and frontal regions while familiar sample images modulated LFPs in the gamma band between these regions; and during the choice phase, an early LFP modulation by familiar image than novel image has been found in temporal and frontal regions, which indicates familiar encoded images may have a priority to be retrieved when comparing them with other test stimuli. These analyses indicate that prefrontal and temporal neural activities (particularly beta power) were related with encoding and decoding the familiarity of visual stimulus in recognition memory.

In Chapter 5, I investigated the function of MTL and PFC in both memory and perception by developing a delayed mnemonic task and a hybrid mnemonic and perceptual task for simultaneous multi-area, multi-electrode recordings in NHPs. The first investigation on the behavioral performance in the two tasks showed a matched performance between the memory and hybrid tasks. Then by analysing and comparing LFPs and LFP-LFP coherence in temporal and prefrontal regions between these two tasks, I found low-frequency neural activities (theta and alpha/low-beta oscillations) in temporal and frontal regions were important for encoding, maintaining and retrieval of visual stimuli in a mnemonic-demanding task. Furthermore, brief burst of beta oscillations (30-40 Hz) were persistent in area TE, PrC

and dlPFC prior to the presentation of test image and then became weaker when the test image appeared. As these beta oscillations appeared only in the memory task, it seems beta oscillations in the temporal and frontal regions were more related to maintenance of items in recognition memory. Moreover, it has been found gamma activities in temporal regions during the choice phase was more related to perceptual discrimination. Taken together, it seems the low-beta and gamma power in temporal and frontal regions play different roles in memory and perception processes.

It is acknowledged that some limitations of our task design and data interpretation exist in the electrophysiological studies of Chapter 4-5. For example, I found larger main noise pollution on the recorded neural data in the latter conducted experiment (i.e. when animal was tested in the hybrid task). Additionally, as there was only one animal participating in electrophysiological studies of the two chapters, I will still need another animal's data to replicate our findings. However, these electrophysiological studies in Chapter 4-5 have nonetheless benefited future electrophysiological research (i.e. the on-going project in Chapter 6) and I will continue to investigate the MTL-PFC interaction underlying memory and perception. As our neural data analysis mainly focused on LFPs in Chapter 4-5 as only a few units of dlPFC have been recorded, in the future on-going project, a spike-spike, LFP-LFP and spike-LFP analysis across the MTL and PFC regions will be implemented to better illustrate their dynamic interactions in recognition memory and perceptual discrimination and will facilitate the decoding analyses of informational content.

Concluding remarks

This thesis has contributed to understanding the neural mechanisms of memory and perception by investigating interactions between different MTL and PFC regions underlying different processes, and by investigating different combinations of those areas (networks and

sub-networks) recruited for different processes. We first found several macaque resting-state brain networks mediated by frontopolar cortex, and results of this study show that animals with an intact FPC can maintain more distinct sets of brain networks than animals without FPC. Then using a cross-species approach, we found a dissociation of dorsolateral and dorsomedial prefrontal contributions to familiarity and recollective processes in humans; and using the same homologous behavioral tasks, we found similar time course of fast familiarity and slow recollection processes existing in humans and macaques. To further illustrate the dynamic interactions between MTL and PFC in memory and perception, we recorded neural activities in both a delayed memory task and a hybrid memory and perception task using a simultaneous multi-area, multi-electrode recording paradigm in three awake behaving macaques. Our neural data analysis indicated that prefrontal and temporal low-frequency activities (e.g. theta, alpha/low-beta power) were more related to encoding, maintenance and retrieval of visual stimuli during memory; and gamma activities were more involved in perceptual discrimination; and a role of theta oscillations in hippocampus and PFC signaled successful memory performance. An electrophysiological project involving a novel chamber and microdrive recording system in two macaques is on-going. By targeting both superficial cortical regions (e.g. lateral PFC) and deep brain areas of PFC (e.g. frontopolar cortex) and deep brain regions of MTL (e.g. hippocampus, entorhinal cortex, perirhinal cortex and parahippocampal cortex), the neural substrates and neural mechanism of memory and perception can be better revealed.

References

Aggleton JP, Brown MW. 1999. Episodic memory, amnesia, and the hippocampal-anterior thalamic axis. *Behav Brain Sci* **22**: 425–444.

Aggleton JP, Brown MW. 2006. Interleaving brain systems for episodic and recognition memory. *Trends Cogn Sci* **10**: 455–463.

Aggleton JP, Dumont JR, Warburton EC. 2011. Unraveling the contributions of the diencephalon to recognition memory: A review. *Learn Mem* **18**: 384–400.

Aguirre GK, Detre JA, Alsop DC, D'Esposito M. 1996. The parahippocampus subserves topographical learning in man. *Cereb Cortex* **6**: 823–829.

Ainsworth M, Browncross H, Mitchell DJ, Mitchell AS, Passingham RE, Buckley MJ, Duncan J, Bell AH. 2018. Functional reorganisation and recovery following cortical lesions: A preliminary study in macaque monkeys. *Neuropsychologia* **119**: 382–391. https://doi.org/10.1016/j.neuropsychologia.2018.08.024.

Albert NB, Robertson EM, Mehta P, Chris Miall R. 2009. Resting state networks and memory consolidation. *Commun Integr Biol* **2**: 530–532.

Albouy P, Weiss A, Baillet S, Zatorre RJ. 2017. Selective Entrainment of Theta Oscillations in the Dorsal Stream Causally Enhances Auditory Working Memory Performance. *Neuron* 1–14. http://linkinghub.elsevier.com/retrieve/pii/S0896627317301988.

Alvarado MC, Bachevalier J. 2005. Comparison of the effects of damage to the perirhinal and parahippocampal cortex on transverse patterning and location memory in rhesus macaques. *J Neurosci* **25**: 1599–1609.

Alvarez-Royo P, Zola-Morgan S, Squire LR. 1992. Impairment of long-term memory and sparing of short-term memory in monkeys with medial temporal lobe lesions: a response to Ringo. *Behav Brain Res* **52**: 1–5.

Aly M, Yonelinas AP, Kishiyama MM, Knight RT. 2011. Damage to the lateral prefrontal cortex impairs familiarity but not recollection. *Behav Brain Res* **225**: 297–304.

http://dx.doi.org/10.1016/j.bbr.2011.07.043.

Aminoff EM, Kveraga K, Bar M. 2013. The role of the parahippocampal cortex in cognition. *Trends Cogn Sci* **17**: 379–390. https://linkinghub.elsevier.com/retrieve/pii/S1364661313001423.

Anderson B, Mruczek REB, Kawasaki K, Sheinberg D. 2008. Effects of Familiarity on Neural Activity in Monkey Inferior Temporal Lobe. *Cereb Cortex* **18**: 2540–2552. https://academic.oup.com/cercor/article-lookup/doi/10.1093/cercor/bhn015.

Anderson MC, Ochsner KN, Kuhl B, Cooper J, Robertson E, Gabrieli SW, Glover GH, Gabrieli JDE. 2004. Neural Systems Underlying the Suppression of Unwanted Memories. *Science (80-)* **303**: 232–235.

Apurva Ratan Murty N, Arun SP. 2015. Dynamics of 3D view invariance in monkey inferotemporal cortex. *J Neurophysiol* **113**: 2180–2194.

Bachevalier J, Mishkin M. 1986. Visual recognition impairment follows ventromedial but not dorsolateral prefrontal lesions in monkeys. *Behav Brain Res* **20**: 249–261.

Backus AR, Schoffelen JM, Szebényi S, Hanslmayr S, Doeller CF. 2016. Hippocampal-prefrontal theta oscillations support memory integration. *Curr Biol* **26**: 450–457.

Badre D, Wagner AD. 2004. Selection, Integration, and Conflict Monitoring. *Neuron* **41**: 473–487.

Barbas H, Ghashghaei H, Dombrowski SM, Rempel-Clower NL. 1999. Medial prefrontal cortices are unified by common connections with superior temporal cortices and distinguished by input from memory-related areas in the rhesus monkey. *J Comp Neurol* **410**: 343–367.

Barbm H, Pandya DN. 1989. Architecture and Intrinsic Connections of the Prefrontal Cortex i n the Rhesus Monkey. **375**.

Barense MD, Bussey TJ, Lee ACH, Rogers TT, Davies RR, Saksida LM, Murray EA, Graham KS. 2005. Functional Specialization in the Human Medial Temporal Lobe. **25**:

10239–10246.

Barredo J, Öztekin I, Badre D. 2015. Ventral fronto-temporal pathway supporting cognitive control of episodic memory retrieval. *Cereb Cortex* **25**: 1004–1019.

Basile BM, Hampton RR. 2011. Monkeys recall and reproduce simple shapes from memory. *Curr Biol* **21**: 774–778. http://dx.doi.org/10.1016/j.cub.2011.03.044.

Basile BM, Hampton RR. 2013. Recognition errors suggest fast familiarity and slow recollection in rhesus monkeys. *Learn Mem* **20**: 431–437. http://learnmem.cshlp.org/cgi/doi/10.1101/lm.029223.112.

Basile BM, Hampton RR, Suomi SJ, Murray EA. 2009. An assessment of memory awareness in tufted capuchin monkeys (Cebus apella). *Anim Cogn* **12**: 169–180.

Bastos AM, Loonis R, Kornblith S, Lundqvist M, Miller EK. 2018. Laminar recordings in frontal cortex suggest distinct layers for maintenance and control of working memory. *Proc Natl Acad Sci* 201710323. http://www.pnas.org/lookup/doi/10.1073/pnas.1710323115.

Baxter MG. 2009. Review : Point / Counterpoint Involvement of Medial Temporal Lobe Structures in Memory and Perception Review : Point / Counterpoint. *Neuron* **61**: 667–677. http://dx.doi.org/10.1016/j.neuron.2009.02.007.

Baxter MG, Murray EA. 2001. Opposite relationship of hippocampal and rhinal cortex damage to delayed nonmatching-to-sample deficits in monkeys. *Hippocampus* **11**: 61–71.

Beam W, Borckardt JJ, Reeves ST, George MS. 2009. An efficient and accurate new method for locating the F3 position for prefrontal TMS applications. *Brain Stimul* **2**: 50–54. http://dx.doi.org/10.1016/j.brs.2008.09.006.

Beason-Held LL, Rosene DL, Killiany RJ, Moss MB. 1999. Hippocampal formation lesions produce memory impairment in the rhesus monkey. *Hippocampus* **9**: 562–574.

Behzadi Y, Restom K, Liau J, Liu TT. 2007. A component based noise correction method

(CompCor) for BOLD and perfusion based fMRI. *Neuroimage* **37**: 90–101. https://www.ncbi.nlm.nih.gov/pmc/articles/PMC2214855/pdf/nihms-27952.pdf.

Benn A, Barker GRI, Stuart SA, Roloff EVL, Teschemacher AG, Clea Warburton E, Robinson ESJ. 2016. Optogenetic stimulation of prefrontal glutamatergic neurons enhances recognition memory. *J Neurosci* **36**: 4930–4939.

Blumenfeld RS, Ranganath C. 2007. Prefrontal cortex and long-term memory encoding: An integrative review of findings from neuropsychology and neuroimaging. *Neuroscientist* **13**: 280–291.

Boorman ED, Behrens TEJ, Woolrich MW, Rushworth MFS. 2009. How Green Is the Grass on the Other Side? Frontopolar Cortex and the Evidence in Favor of Alternative Courses of Action. *Neuron* **62**: 733–743. http://dx.doi.org/10.1016/j.neuron.2009.05.014.

Boschin EA, Piekema C, Buckley MJ. 2015. Essential functions of primate frontopolar cortex in cognition. *Proc Natl Acad Sci* **112**: E1020–E1027. http://www.pnas.org/lookup/doi/10.1073/pnas.1419649112.

Bose A, Recce M. 2001. Phase precession and phase-locking of hippocampal pyramidal cells. *Hippocampus* **11**: 204–215. papers3://publication/uuid/77DAEE99-4876-4CCA-A005-EBA9EBCD32C9.

Boussaoud D, Desimone R, Ungerleider LG. 1992. Subcortical connections of visual areas MST and FST in macaques. *Vis Neurosci* **9**: 291–302.

Bowles B, Crupi C, Pigott S, Parrent A, Wiebe S, Janzen L, Köhler S. 2010. Double dissociation of selective recollection and familiarity impairments following two different surgical treatments for temporal-lobe epilepsy. *Neuropsychologia* **48**: 2640–2647. http://dx.doi.org/10.1016/j.neuropsychologia.2010.05.010.

Brainerd CJ, Gomes CFA, Moran R. 2014. The two recollections. *Psychol Rev* **121**: 563–599.

Brainerd CJ, Nakamura K, Lee W-FA. 2019. Recollection is fast and slow. *J Exp Psychol Learn Mem Cogn* **45**: 302–319. http://doi.apa.org/getdoi.cfm?doi=10.1037/xlm0000588.

Brainerd CJ, Reyna VF. 2005. *The science of false memory*. Oxford University Press, New York.

Brincat SL, Miller EK. 2015. Frequency-specific hippocampal-prefrontal interactions during associative learning. *Nat Neurosci* **18**: 576–581. http://dx.doi.org/10.1038/nn.3954.

Brown MW. 1996. Neuronal responses and recognition memory. *Semin Neurosci* **8**: 23–32.

Brown MW, Aggleton JP. 2001. Recognition memory: What are the roles of the perirhinal cortex and hippocampus? *Nat Rev Neurosci* **2**: 51–61.

Brown VJ, Bowman EM. 2002. Rodent models of prefrontal cortical function. *Trends Neurosci* **25**: 340–343.

Buckley MJ. 2005. The role of the perirhinal cortex and hippocampus in learning , memory , and perception. 246–268.

Buckley MJ, Booth MCA, Rolls ET, Gaffan D. 2001. Selective Perceptual Impairments After Perirhinal Cortex Ablation. **21**: 9824–9836.

Buckley MJ, Gaffan D. 1997. Impairment of visual object-discrimination learning after perirhinal cortex ablation. *Behav Neurosci* **111**: 467–475.

Buckley MJ, Gaffan D. 1998a. Learning and transfer of object-reward associations and the role of the perirhinal cortex. *Behav Neurosci* **112**: 15–23.

Buckley MJ, Gaffan D. 1998b. Perirhinal cortex ablation impairs configural learning and paired-associate learning equally. *Neuropsychologia* **36**: 535–546.

Buckley MJ, Gaffan D. 1998c. Perirhinal cortex ablation impairs visual object identification. *J Neurosci* **18**: 2268–2275.

Buckley MJ, Gaffan D. 2006. Perirhinal cortical contributions to object perception. *Trends Cogn Sci* **10**: 100–107. https://linkinghub.elsevier.com/retrieve/pii/S136466130600026X.

Buckley MJ, Gaffan D, Murray EA. 1997. Functional double dissociation between two inferior temporal cortical areas: Perirhinal cortex versus middle temporal gyrus. *J Neurophysiol* **77**: 587–598.

Buffalo EA, Ramus SJ, Clark RE, Teng E, Squire LR, Zola SM. 1999. Dissociation between the effects of damage to perirhinal cortex and area TE. *Learn Mem* **6**: 572–599.

Buffalo EA, Ramus SJ, Squire LR, Zola SM. 2000. Perception and recognition memory in monkeys following lesions of area TE and perirhinal cortex. *Learn Mem* **7**: 375–382.

Buffalo EA, Reber PJ, Squire LR. 1998. The human perirhinal cortex and recognition memory. *Hippocampus* **8**: 330–339. http://doi.wiley.com/10.1002/%28SICI%291098-1063%281998%298%3A4%3C330%3A%3AAID-HIPO3%3E3.0.CO%3B2-L.

Bunge SA, Helskog EH, Wendelken C. 2009. Left, but not right, rostrolateral prefrontal cortex meets a stringent test of the relational integration hypothesis. *Neuroimage* **46**: 338–342. http://dx.doi.org/10.1016/j.neuroimage.2009.01.064.

Burgess PW. 2012. *Rostral prefrontal cortex: What neuroimaging can learn from human neuropsychology*. New York: Oxford University Press.

Burgess PW. 2000. Strategy application disorder: The role of the frontal lobes in human multitasking. *Psychol Res* **63**: 279–288.

Burgess PW, Gonen-Yaacovi G, Volle E. 2011. Functional neuroimaging studies of prospective memory: What have we learnt so far? *Neuropsychologia* **49**: 2246–2257. http://dx.doi.org/10.1016/j.neuropsychologia.2011.02.014.

Burman KJ, Reser DH, Richardson KE, Gaulke H, Worthy KH, Rosa MGP. 2011a. Subcortical projections to the frontal pole in the marmoset monkey. *Eur J Neurosci* **34**: 303–319.

Burman KJ, Reser DH, Yu HH, Rosa MGP. 2011b. Cortical input to the frontal pole of the marmoset monkey. *Cereb Cortex* **21**: 1712–1737.

Buschman TJ, Miller EK. 2007. Top-Down Versus Bottom-Up Control of Attention in the Prefrontal and. *Science (80-)* **315**: 1860–1863.

Bussey TJ, Saksida ÃLM, Murray EA. 2003. Impairments in visual discrimination after perirhinal cortex lesions : testing ‘ declarative ’ vs . ‘ perceptual-mnemonic ’ views of

perirhinal cortex function. **17**: 649–660.

Bussey TJ, Saksida LM. 2007. Memory , Perception , and the Ventral Visual-Perirhinal-Hippocampal Stream : Thinking Outside of the Boxes. **908**: 898–908.

Bussey TJ, Saksida LM. 2002. The organization of visual object representations : a connectionist model of effects of lesions in perirhinal cortex. **15**.

Bussey TJ, Saksida LM, Murray EA. 2006. Perirhinal cortex and feature-ambiguous discriminations. 103–105.

Bussey TJ, Saksida LM, Murray EA. 2002a. Perirhinal cortex resolves feature ambiguity in complex visual discriminations. **15**.

Bussey TJ, Saksida LM, Murray EA. 2005. The perceptual-mnemonic/feature conjunction model of perirhinal cortex function. *Q J Exp Psychol Sect B Comp Physiol Psychol* **58**: 269–282.

Bussey TJ, Wise SP, Murray EA. 2002b. Interaction of ventral and orbital prefrontal cortex with inferotemporal cortex in conditional visuomotor learning. *Behav Neurosci* **116**: 703–715.

Buzsáki G, Anastassiou CA, Koch C. 2012. The origin of extracellular fields and currents-EEG, ECoG, LFP and spikes. *Nat Rev Neurosci* **13**: 407–420.

Buzsáki G, Schomburg EW. 2015. What does gamma coherence tell us about inter-regional neural communication? *Nat Neurosci* **18**: 484–489.

Carmichael ST, Price JL. 1994. Architectonic subdivision of the orbital and medial prefrontal cortex in the macaque monkey. *J Comp Neurol* **346**: 366–402. http://doi.wiley.com/10.1002/cne.903460305.

Cavada C. 2000. The Anatomical Connections of the Macaque Monkey Orbitofrontal Cortex. A Review. *Cereb Cortex* **10**: 220–242. https://academic.oup.com/cercor/article-lookup/doi/10.1093/cercor/10.3.220.

Chanes L, Quentin R, Tallon-Baudry C, Valero-Cabre A. 2013. Causal Frequency-Specific

Contributions of Frontal Spatiotemporal Patterns Induced by Non-Invasive Neurostimulation to Human Visual Performance. *J Neurosci* **33**: 5000–5005. http://www.jneurosci.org/cgi/doi/10.1523/JNEUROSCI.4401-12.2013.

Chén OY, Cao H, Reinen JM, Qian T, Gou J, Phan H, De Vos M, Cannon TD. 2019. Resting-state brain information flow predicts cognitive flexibility in humans. *Sci Rep* **9**: 1–16.

Christoff K, Prabhakaran V, Dorfman J, Zhao Z, Kroger JK, Holyoak KJ, Gabrieli JDE. 2001. Rostrolateral prefrontal cortex involvement in relational integration during reasoning. *Neuroimage* **14**: 1136–1149.

Christoff K, Ream JM, Geddes LPT, Gabrieli JDE. 2003. Evaluating Self-Generated Information: Anterior Prefrontal Contributions to Human Cognition. *Behav Neurosci* **117**: 1161–1168.

Clark AM, Bouret S, Young AM, Murray EA, Richmond BJ. 2013. Interaction between orbital prefrontal and rhinal cortex is required for normal estimates of expected value. *J Neurosci* **33**: 1833–1845.

Cochin S. 1999. Observation and execution of movement: Similarities demonstrated by quantified electroencephalography. *Eur J Neurosci* **11**: 1839–1842.

Compte A, Constantinidis C, Tegnér J, Raghavachari S, Chafee M V., Goldman-Rakic PS, Wang XJ. 2003. Temporally Irregular Mnemonic Persistent Activity in Prefrontal Neurons of Monkeys during a Delayed Response Task. *J Neurophysiol* **90**: 3441–3454.

Curran T. 2000. Brain potentials of recollection and familiarity. *Mem Cognit* **28**: 923–938. http://link.springer.com/10.3758/BF03209340.

Cusack R, Vicente-Grabovetsky A, Mitchell DJ, Wild CJ, Auer T, Linke AC, Peelle JE. 2015. Automatic analysis (aa): Efficient neuroimaging workflows and parallel processing using Matlab and XML. *Front Neuroinform* **8**: 1–13.

Daw ND, O'Doherty JP, Dayan P, Seymour B, Dolan RJ. 2006. Cortical substrates for

exploratory decisions in humans. *Nature* **441**: 876–879.

De Araujo IE, Simon SA. 2009. The gustatory cortex and multisensory integration. *Int J Obes* **33**: S34–S43.

Dede AJO, Squire LR, Wixted JT. 2014. A novel approach to an old problem: Analysis of systematic errors in two models of recognition memory. *Neuropsychologia* **52**: 51–56. http://dx.doi.org/10.1016/j.neuropsychologia.2013.10.012.

DeVito LM, Eichenbaum H. 2011. Memory for the order of events in specific sequences: Contributions of the hippocampus and medial prefrontal cortex. *J Neurosci* **31**: 3169–3175.

Doesburg SM, Roggeveen AB, Kitajo K, Ward LM. 2008. Large-scale gamma-band phase synchronization and selective attention. *Cereb Cortex* **18**: 386–396.

Dosher BA. 1984. Discriminating preexperimental (semantic) from learned (episodic) associations: A speed-accuracy study. *Cogn Psychol* **16**: 519–555.

Dosher BA, Rosedale G. 1991. Judgments of semantic and episodic relatedness: Common time-course and failure of segregation. *J Mem Lang* **30**: 125–160. https://linkinghub.elsevier.com/retrieve/pii/0749596X9190001Z.

Dreher JC, Koechlin E, Tierney M, Grafman J. 2008. Damage to the fronto-polar cortex is associated with impaired multitasking. *PLoS One* **3**.

Duarte A, Ranganath C, Knight RT. 2005. Effects of unilateral prefrontal lesions on familiarity, recollection, and source memory. *J Neurosci* **25**: 8333–8337.

Eacott MJ, Gaffan D, Murray EA. 1994. Preserved Recognition Memory for Small Sets, and Impaired Stimulus Identification for Large Sets, Following Rhinal Cortex Ablations in Monkeys. *Eur J Neurosci* **6**: 1466–1478.

Eichenbaum H, Dudchenko P, Wood E, Shapiro M, Tanila H. 1999. The Hippocampus, Memory, Review and Place Cells: Is It Spatial Memory or a Memory Space? might occur at different locations. Olton and colleagues Neuron 210 Figure 1. Schematic

Overhead Views of Four Different Types of Apparatus and Examples of Location-S. *Neuron* **23**: 209–226. http://cogs200.pbworks.com/f/Eichenbaum 99 Hippocampus.pdf.

Eichenbaum H, Fortin NJ, Ergorul C, Wright SP, Agster KL. 2005. Episodic recollection in animals: "If it walks like a duck and quacks like a duck..." *Learn Motiv* **36**: 190–207.

Eichenbaum H, Sauvage MM, Fortin NJ, Yonelinas AP. 2008. ROCs in rats? Response to wixted and squire. *Learn Mem* **15**: 691–693.

Eichenbaum H, Yonelinas AP, Ranganath C. 2007. The Medial Temporal Lobe and Recognition Memory. *Annu Rev Neurosci* **30**: 123–152. http://www.annualreviews.org/doi/10.1146/annurev.neuro.30.051606.094328.

Elkin-Frankston S, Fried P, Rushmore RJ, Valero-Cabré A. 2011. From qualia to quantia: A system to document and quantify phosphene percepts elicited by non-invasive neurostimulation of the human occipital cortex. *J Neurosci Methods* **198**: 149–157. http://dx.doi.org/10.1016/j.jneumeth.2011.02.013.

Epstein R, Graham KS, Downing PE. 2003. Viewpoint-specific scene representations in human parahippocampal cortex. *Neuron* **37**: 865–876.

Epstein R, Kanwisher N. 1998. The parahippocampal place area: A cortical representation of the local visual environment. *Neuroimage* **7**: 6–9.

Fell J, Axmacher N. 2011. The role of phase synchronization in memory processes. *Nat Rev Neurosci* **12**: 105–118.

Feuerriegel D. 2016. Selecting appropriate designs and comparison conditions in repetition paradigms. *Cortex* **80**: 196–205. http://dx.doi.org/10.1016/j.cortex.2015.10.022.

Fortin NJ, Wright SP, Eichenbaum H. 2004. Recollection-like memory retrieval in rats is dependent on the hippocampus. *Nature* **431**: 188–191.

Freedman DJ. 2005. Experience-Dependent Sharpening of Visual Shape Selectivity in Inferior Temporal Cortex. *Cereb Cortex* **16**: 1631–1644. https://academic.oup.com/cercor/article-lookup/doi/10.1093/cercor/bhj100.

Fries P. 2005. A mechanism for cognitive dynamics: Neuronal communication through neuronal coherence. *Trends Cogn Sci* **9**: 474–480.

Fries P. 2015. Rhythms for Cognition: Communication through Coherence. *Neuron* **88**: 220–235. http://dx.doi.org/10.1016/j.neuron.2015.09.034.

Fujita I. 2002. The inferior temporal cortex: Architecture, computation, and representation. *J Neurocytol* **31**: 359–371.

Fuster JM, Alexander GE. 1971. Neuron Activity Related to Short-Term Memory. *Science (80-)* **173**: 652–654. http://www.sciencemag.org/cgi/doi/10.1126/science.173.3997.652.

Fuster JM, Jervey JP. 1982. Neuronal firing in the inferotemporal cortex of the monkey in a visual memory task. *J Neurosci* **2**: 361–375.

Gaffan D. 1994a. Dissociated effects of perirhinal cortex ablation, fornix transection and amygdalectomy: evidence for multiple memory systems in the primate temporal lobe. *Exp Brain Res* **99**: 411–422.

Gaffan D. 1994b. Scene-specific memory for objects: A model of episodic memory impairment in monkeys with fornix transection. *J Cogn Neurosci* **6**: 305–320.

Gaffan D, Eacott MJ. 1995. Uncinate fascicle section leaves delayed matching-to-sample intact, with both large and small stimulus sets. *Exp Brain Res* **105**: 175–180.

Gaffan D, Wilson CRE. 2008. Medial temporal and prefrontal function: Recent behavioural disconnection studies in the macaque monkey. *Cortex* **44**: 928–935.

Gardiner JM, Ramponi C, Richardson-Klavehn A. 1998. Experiences of Remembering, Knowing, and Guessing. *Conscious Cogn* **7**: 1–26.

Giap BT, Jong CN, Ricker JH, Cullen NK, Zafonte RD. 2000. The hippocampus: Anatomy, pathophysiology, and regenerative capacity. *J Head Trauma Rehabil* **15**: 875–894.

Glanzer M, Adams JK. 1990. The Mirror Effect in Recognition Memory: Data and Theory. *J Exp Psychol Learn Mem Cogn* **16**: 5–16.

Graham KS, Barense MD, Lee ACH. 2010. Going beyond LTM in the MTL: A synthesis of

neuropsychological and neuroimaging findings on the role of the medial temporal lobe in memory and perception. *Neuropsychologia* **48**: 831–853. http://dx.doi.org/10.1016/j.neuropsychologia.2010.01.001.

Gregoriou GG, Gotts SJ, Zhou H, Desimone R. 2009. High-Frequency, Long-Range Coupling Between Prefrontal and Visual Cortex During Attention. *Science (80-)* **324**: 1207–1210. http://www.sciencemag.org/cgi/doi/10.1126/science.1171402.

Gronlund SD, Ratcliff R. 1989. Time Course of Item and Associative Information: Implications for Global Memory Models. *J Exp Psychol Learn Mem Cogn* **15**: 846–858.

Guderian S, Brigham D, Mishkin M. 2011. Two processes support visual recognition memory in rhesus monkeys. *Proc Natl Acad Sci* **108**: 19425–19430. http://www.pnas.org/cgi/doi/10.1073/pnas.1117078108.

Hallett M. 2007. Transcranial Magnetic Stimulation: A Primer. *Neuron* **55**: 187–199.

Hampton RR. 2005. Monkey perirhinal cortex is critical for visual memory, but not for visual perception: Reexamination of the behavioural evidence from monkeys. *Q J Exp Psychol Sect B Comp Physiol Psychol* **58**: 283–299.

Hampton RR. 2001. Rhesus monkeys know when they remember. *Proc Natl Acad Sci U S A* **98**: 5359–5362.

Hampton RR, Hampstead BM. 2006. Spontaneous behavior of a rhesus monkey (Macaca mulatta) during memory tests suggests memory awareness. *Behav Processes* **72**: 184–189.

Hampton RR, Murray EA. 2002. Learning of discriminations is impaired, but generalization to altered views is intact, in monkeys (Macaca mulatta) with perirhinal cortex removal. *Behav Neurosci* **116**: 363–377.

Hampton RR, Zivin A, Murray EA. 2004. Rhesus monkeys (Macaca mulatta) discriminate between knowing and not knowing and collect information as needed before acting. *Anim Cogn* **7**: 239–246.

Hanslmayr S, Matuschek J, Fellner MC. 2014. Entrainment of prefrontal beta oscillations induces an endogenous echo and impairs memory formation. *Curr Biol* **24**: 904–909. http://dx.doi.org/10.1016/j.cub.2014.03.007.

Hanslmayr S, Spitzer B, Bäuml KH. 2009. Brain oscillations dissociate between semantic and nonsemantic encoding of episodic memories. *Cereb Cortex* **19**: 1631–1640.

Hanslmayr S, Staudigl T, Fellner M-C. 2012a. Oscillatory power decreases and long-term memory: the information via desynchronization hypothesis. *Front Hum Neurosci* **6**: 1–12.

Hanslmayr S, Volberg G, Wimber M, Oehler N, Staudigl T, Hartmann T, Raabe M, Greenlee MW, Bauml K-HT. 2012b. Prefrontally Driven Downregulation of Neural Synchrony Mediates Goal-Directed Forgetting. *J Neurosci* **32**: 14742–14751. http://www.jneurosci.org/cgi/doi/10.1523/JNEUROSCI.1777-12.2012.

Hanslmayr S, Volberg G, Wimber M, Raabe M, Greenlee MW, Bauml K-HT. 2011. The Relationship between Brain Oscillations and BOLD Signal during Memory Formation: A Combined EEG-fMRI Study. *J Neurosci* **31**: 15674–15680. http://www.jneurosci.org/cgi/doi/10.1523/JNEUROSCI.3140-11.2011.

Hay JF, Moscovitch M, Levine B. 2002. Dissociating habit and recollection: evidence from Parkinson's disease, amnesia and focal lesion patients. *Neuropsychologia* **40**: 1324–1334.

Healy MR, Light LL, Chung C. 2005. Dual-process models of associative recognition in young and older adults: Evidence from receiver operating characteristics. *J Exp Psychol Learn Mem Cogn* **31**: 768–788.

Henson RNA, Rugg MD, Shallice T, Josephs O, Dolan RJ. 1999a. Recollection and familiarity in recognition memory: An event-related functional magnetic resonance imaging study. *J Neurosci* **19**: 3962–3972.

Henson RNA, Shallice T, Dolan RJ. 1999b. Right prefrontal cortex and episodic memory

retrieval: A functional MRI test of the monitoring hypothesis. *Brain* **122**: 1367–1381.

Herweg NA, Apitz T, Leicht G, Mulert C, Fuentemilla L, Bunzeck N. 2016. Theta-alpha oscillations bind the hippocampus, prefrontal cortex, and striatum during recollection: Evidence from simultaneous EEG–fMRI. *J Neurosci* **36**: 3579–3587.

Hintzman DL, Caulton DA, Levitin DJ. 1998. Retrieval dynamics in recognition and list discrimination: Further evidence of separate processes of familiarity and recall. *Mem Cogn* **26**: 449–462.

Hintzman DL, Curran T. 1994. Retrieval Dynamics of Recognition and Frequency Judgments: Evidence for Separate Processes of Familiarity and Recall. *J Mem Lang* **33**: 1–18. https://linkinghub.elsevier.com/retrieve/pii/S0749596X84710011.

Hodgetts CJ, Shine JP, Lawrence AD, Downing PE, Graham KS. 2016. Evidencing a place for the hippocampus within the core scene processing network. *Hum Brain Mapp* **37**: 3779–3794.

Hoffmann M, Bar-On R. 2012. Isolated frontopolar cortex lesion: A case study. *Cogn Behav Neurol* **25**: 50–56.

Holmes CD, Papadimitriou C, Snyder LH. 2018. Dissociation of LFP power and tuning in the frontal cortex during memory. *J Neurosci* **38**: 8177–8186.

Horner AJ, Bisby JA, Bush D, Lin WJ, Burgess N. 2015. Evidence for holistic episodic recollection via hippocampal pattern completion. *Nat Commun* **6**: 1–11. http://dx.doi.org/10.1038/ncomms8462.

Huang YZ, Edwards MJ, Rounis E, Bhatia KP, Rothwell JC. 2005. Theta burst stimulation of the human motor cortex. *Neuron* **45**: 201–206.

Hyman JM, Zilli EA, Paley AM, Hasselmo ME. 2005. Medial prefrontal cortex cells show dynamic modulation with the hippocampal theta rhythm dependent on behavior. *Hippocampus* **15**: 739–749.

Insausti R, Juottonen K, Soininen H, Insausti AM, Partanen K, Vainio P, Laakso MP,

Pitkänen A. 1998. MR volumetric analysis of the human entorhinal, perirhinal, and temporopolar cortices. *Am J Neuroradiol* **19**: 659–671.

Jacoby LL. 1991. A process dissociation framework: Separating automatic from intentional uses of memory. *J Mem Lang* **30**: 513–541. https://linkinghub.elsevier.com/retrieve/pii/0749596X9190025F.

Jacoby LL. 1999. Ironic Effects of Repetition: Measuring Age-Related Differences in Memory. *J Exp Psychol Learn Mem Cogn* **25**: 3–22.

Jacoby LL, Jones TC, Dolan PO. 1998. Two effects of repetition: Support for a dual-process model of know judgments and exclusion errors. *Psychon Bull Rev* **5**: 705–709.

Janssen P. 2000. Selectivity for 3D Shape That Reveals Distinct Areas Within Macaque Inferior Temporal Cortex. *Science (80-)* **288**: 2054–2056. http://www.sciencemag.org/cgi/doi/10.1126/science.288.5473.2054.

Janzen G, Wagensveld B, Van Turennout M. 2007. Neural representation of navigational relevance is rapidly induced and long lasting. *Cereb Cortex* **17**: 975–981.

Johnson JD, Suzuki M, Rugg MD. 2013. Recollection, familiarity, and content-sensitivity in lateral parietal cortex: a high-resolution fMRI study. *Front Hum Neurosci* **7**: 1–15.

Jones MW, Wilson MA. 2005. Theta rhythms coordinate hippocampal-prefrontal interactions in a spatial memory task. *PLoS Biol* **3**: 1–13.

Jones TC, Jacoby LL. 2001. Feature and Conjunction Errors in Recognition Memory: Evidence for Dual-Process Theory. *J Mem Lang* **45**: 82–102. https://linkinghub.elsevier.com/retrieve/pii/S0749596X0092761X.

Jutras MJ, Buffalo EA. 2014. Oscillatory correlates of memory in non-human primates. *Neuroimage* **85**: 694–701. http://dx.doi.org/10.1016/j.neuroimage.2013.07.011.

Jutras MJ, Buffalo EA. 2010. Recognition memory signals in the macaque hippocampus. *Proc Natl Acad Sci* **107**: 401–406. http://www.pnas.org/cgi/doi/10.1073/pnas.0908378107.

Jutras MJ, Fries P, Buffalo E a. 2013. Oscillatory activity in the monkey hippocampus during visual exploration and memory formation. *Proc Natl Acad Sci* **110**: 13144–13149.

Jutras MJ, Fries P, Buffalo EA. 2010. NIH Public Access. *October* **29**: 12521–12531.

Jutras MJ, Fries P, Buffalo EA, Rr BG, Stru E. 2009. Gamma-Band Synchronization in the Macaque Hippocampus and Memory Formation. **29**: 12521–12531.

Kaas JH, Collins CE. 2004. The primate visual system system.

Kafkas A, Montaldi D. 2012. Familiarity and recollection produce distinct eye movement, pupil and medial temporal lobe responses when memory strength is matched. *Neuropsychologia* **50**: 3080–3093. http://dx.doi.org/10.1016/j.neuropsychologia.2012.08.001.

Katsuki F, Constantinidis C. 2012. Early involvement of prefrontal cortex in visual bottom-up attention. *Nat Neurosci* **15**: 1160–1166. http://dx.doi.org/10.1038/nn.3164.

Kesner RE, Hunt ME, Williams JM, Long JM. 1996. and Visual Object Information in the Rat. *Cereb Cortex* 0–7.

Ketz NA, Jensen O, Reilly RCO. 2015. Thalamic pathways underlying prefrontal cortex – medial temporal lobe oscillatory interactions. *Trends Neurosci* **38**: 3–12. http://dx.doi.org/10.1016/j.tins.2014.09.007.

Khader PH, Rösler F. 2011. EEG power changes reflect distinct mechanisms during long-term memory retrieval. *Psychophysiology* **48**: 362–369.

Kiyoshi Kurata. 1991. Corticocortical inputs to the dorsal and ventral aspects of the premotor cortex of macaque monkeys. *Neurosci Res* **12**: 263–280.

Koechlin E, Basso G, Pietrini P, Panzer S, Grafman J. 1999. The role of the anterior prefrontal cortex in human cognition. *Nature* **399**: 148–151.

Koechlin E, Corrado G, Pietrini P, Grafman J. 2000. Dissociating the role of the medial and lateral anterior prefrontal cortex in human planning. *Proc Natl Acad Sci U S A* **97**: 7651–7656.

Koen JD, Barrett FS, Harlow IM, Yonelinas AP. 2017. The ROC Toolbox: A toolbox for analyzing receiver-operating characteristics derived from confidence ratings. *Behav Res Methods* **49**: 1399–1406. http://dx.doi.org/10.3758/s13428-016-0796-z.

Kolb B, Buhrmann K, Mcdonald R, Sutherland RJ. 1994. Dissociation of the medial prefrontal, posterior parietal, and posterior temporal cortex for spatial navigation and recognition memory in the rat. *Cereb Cortex* **4**: 664–680.

Komisaruk BR. 1970. Synchrony between limbic system theta activity and rhythmical behavior in rats. *J Comp Physiol Psychol* **70**: 482–492. http://doi.apa.org/getdoi.cfm?doi=10.1037/h0028709.

Kornblith S, Buschman TJ, Miller EK. 2016. Stimulus load and oscillatory activity in higher cortex. *Cereb Cortex* **26**: 3772–3784.

Köster M, Friese U, Schöne B, Trujillo-Barreto N, Gruber T. 2014. Theta-gamma coupling during episodic retrieval in the human EEG. *Brain Res* **1577**: 57–68.

Kowalska DM, Bachevalier J, Mishkin M. 1991. The role of the inferior prefrontal convexity in performance of delayed nonmatching-to-sample. *Neuropsychologia* **29**: 583–600.

Lee ACH, Barense MD, Graham KS. 2005a. The Contribution of the Human Medial Temporal Lobe to Perception: Bridging the Gap between Animal and Human Studies. *Q J Exp Psychol Sect B* **58**: 300–325. http://journals.sagepub.com/doi/10.1080/02724990444000168.

Lee ACH, Buckley MJ, Pegman SJ, Spiers H, Scahill VL, Gaffan D, Bussey TJ, Davies RR, Kapur N, Hodges JR, et al. 2005b. Specialization in the medial temporal lobe for processing of objects and scenes. *Hippocampus* **15**: 782–797. http://doi.wiley.com/10.1002/hipo.20101.

Lee ACH, Bussey TJ, Murray EA, Saksida LM, Epstein RA, Kapur N, Hodges JR, Graham KS. 2005c. Perceptual deficits in amnesia: challenging the medial temporal lobe 'mnemonic' view. *Neuropsychologia* **43**: 1–11.

https://linkinghub.elsevier.com/retrieve/pii/S0028393204001939.

Leonard BW, Amaral DG, Squire LR, Zola-Morgan S. 1995. Transient memory impairment in monkeys with bilateral lesions of the entorhinal cortex. *J Neurosci* **15**: 5637–5659.

Lepage KQ, Vijayan S. 2017. The relationship between coherence and the phase-locking value. *J Theor Biol* **435**: 106–109.

Levy DA, Shrager Y, Squire LR. 2005. Intact visual discrimination of complex and feature-ambiguous stimuli in the absence of perirhinal cortex. 61–66.

Levy R, Goldman-Rakic PS. 1999. Association of storage and processing functions in the dorsolateral prefrontal cortex of the nonhuman primate. *J Neurosci* **19**: 5149–5158.

Lewis JW, Van Essen DC. 2000. Corticocortical connections of visual, sensorimotor, and multimodal processing areas in the parietal lobe of the macaque monkey. *J Comp Neurol* **428**: 112–137.

Li L, Miller EK, Desimone R. 1993. The representation of stimulus familiarity in anterior inferior temporal cortex. *J Neurophysiol* **69**: 1918–1929.

Lundqvist M, Herman P, Warden MR, Brincat SL, Miller EK. 2018. Gamma and beta bursts during working memory readout suggest roles in its volitional control. *Nat Commun* **9**: 1–12. http://dx.doi.org/10.1038/s41467-017-02791-8.

Lundqvist M, Rose J, Herman P, Brincat SLL, Buschman TJJ, Miller EKK. 2016. Gamma and Beta Bursts Underlie Working Memory. *Neuron* **90**: 152–164. http://dx.doi.org/10.1016/j.neuron.2016.02.028.

MacPherson SE, Bozzali M, Cipolotti L, Dolan RJ, Rees JH, Shallice T. 2008. Effect of frontal lobe lesions on the recollection and familiarity components of recognition memory. *Neuropsychologia* **46**: 3124–3132. http://dx.doi.org/10.1016/j.neuropsychologia.2008.07.003.

Macrides F, Eichenbaum HB, Forbes WB. 1982. Temporal relationship between sniffing and the limbic θ rhythm during odor discriminatin reversal learning. *J Neurosci* **2**: 1705–

1717.

Málková L, Bachevalier J, Webster M, Mishkin M. 2000. Effects of neonatal inferior prefrontal and medial temporal lesions on learning the rule for delayed nonmatching-to-sample. *Dev Neuropsychol* **18**: 399–421.

Malmberg KJ. 2008. Recognition memory : A review of the critical findings and an integrated theory for relating them. *Cogn Psychol* **57**: 335–384. http://dx.doi.org/10.1016/j.cogpsych.2008.02.004.

Mansouri FA, Buckley MJ, Fehring DJ, Tanaka K. 2019. The Role of Primate Prefrontal Cortex in Bias and Shift Between Visual Dimensions. *Cereb Cortex* 1–15.

Mansouri FA, Buckley MJ, Mahboubi M, Tanaka K. 2015. Behavioral consequences of selective damage to frontal pole and posterior cingulate cortices. *Proc Natl Acad Sci* **112**: E3940–E3949. http://www.pnas.org/lookup/doi/10.1073/pnas.1422629112.

Mansouri FA, Koechlin E, Rosa MGP, Buckley MJ. 2017. Managing competing goals - A key role for the frontopolar cortex. *Nat Rev Neurosci* **18**: 645–657. http://dx.doi.org/10.1038/nrn.2017.111.

Mántylá T, Cornoldi C. 2002. Remembering changes: Repetition effects in face recollection. *Acta Psychol (Amst)* **109**: 95–105.

Maris E, Oostenveld R. 2007. Nonparametric statistical testing of EEG- and MEG-data. *J Neurosci Methods* **164**: 177–190.

Markov NT, Gomes ARR, Lamy C, Magrou L, Vezoli J, Misery P. 2014. A Weighted and Directed Interareal Connectivity Matrix for Macaque Cerebral Cortex. 17–36.

Mars RB, Jbabdi S, Sallet J, O'Reilly JX, Croxson PL, Olivier E, Noonan MAP, Bergmann C, Mitchell AS, Baxter MG, et al. 2011. Diffusion-weighted imaging tractography-based parcellation of the human parietal cortex and comparison with human and macaque resting-state functional connectivity. *J Neurosci* **31**: 4087–4100.

Matzen LE, Taylor EG, Benjamin AS. 2011. Contributions of familiarity and recollection

rejection to recognition: Evidence from the time course of false recognition for semantic and conjunction lures. *Memory* **19**: 1–16.

McLaren DG, Kosmatka KJ, Oakes TR, Kroenke CD, Kohama SG, Matochik JA, Ingram DK, Johnson SC. 2009. A population-average MRI-based atlas collection of the rhesus macaque. *Neuroimage* **45**: 52–59.

Mendoza-Halliday D, Martinez-Trujillo JC. 2017. Neuronal population coding of perceived and memorized visual features in the lateral prefrontal cortex. *Nat Commun* **8**: 1–13. http://dx.doi.org/10.1038/ncomms15471.

Messinger A, Squire LR, Zola SM, Albright TD. 2001. Neuronal representations of stimulus associations develop in the temporal lobe during learning. *Proc Natl Acad Sci U S A* **98**: 12239–12244.

Meunier M, Bachevalier J, Mishkin M. 1997. Effects of orbital frontal and anterior cingulate lesions on object and spatial memory in rhesus monkeys. *Neuropsychologia* **35**: 999–1015.

Meunier M, Bachevalier J, Mishkin M, Murray EA. 1993. Effects on visual recognition of combined and separate ablations of the entorhinal and perirhinal cortex in rhesus monkeys. *J Neurosci* **13**: 5418–5432.

Meunier M, Barbeau E. 2013. Recognition memory and the medial temporal lobe: From monkey research to human pathology. *Rev Neurol (Paris)* **169**: 459–469. http://dx.doi.org/10.1016/j.neurol.2013.01.623.

Meyer T, Walker C, Cho RY, Olson CR. 2014. Image familiarization sharpens response dynamics of neurons in inferotemporal cortex. *Nat Neurosci* **17**: 1388–1394. http://dx.doi.org/10.1038/nn.3794.

Miller E, Li L, Desimone R. 1993. Activity of neurons in anterior inferior temporal cortex during a short- term memory task. *J Neurosci* **13**: 1460–1478. http://www.jneurosci.org/lookup/doi/10.1523/JNEUROSCI.13-04-01460.1993.

Miller EK, Desimone R. 1994. Neuronal Mechanisms. *Science (80-)* **263**: 520–523.

Miller EK, Erickson CA, Desimone R. 1996. Neural mechanisms of visual working memory in prefrontal cortex of the macaque. *J Neurosci* **16**: 5154–5167.

Mishkin M. 1978. Memory in monkeys severely impaired by combined but not by separate removal of amygdala and hippocampus. *Nature* **273**: 297–298.

Mishkin M, Manning FJ. 1978. Non-spatial memory after selective prefrontal lesions in monkeys. *Brain Res* **143**: 313–323.

Mitchell DJ, Bell AH, Buckley MJ, Mitchell AS, Sallet J, Duncan J. 2016. A Putative Multiple-Demand System in the Macaque Brain. *J Neurosci* **36**: 8574–8585. http://www.jneurosci.org/lookup/doi/10.1523/JNEUROSCI.0810-16.2016.

Miyamoto K, Setsuie R, Osada T, Miyashita Y. 2018. Reversible Silencing of the Frontopolar Cortex Selectively Impairs Metacognitive Judgment on Non-experience in Primates. *Neuron* **97**: 980-989.e6. https://doi.org/10.1016/j.neuron.2017.12.040.

Miyashita Y. 2019. Perirhinal circuits for memory processing. *Nat Rev Neurosci* **20**: 577–592. http://dx.doi.org/10.1038/s41583-019-0213-6.

Miyashita Y, Chang HS. 1988. Neuronal correlate of pictorial short-term memory in the primate temporal cortexYasushi Miyashita. *Nature* **331**: 68–70. http://dx.doi.org/10.1038/335817a0.

Montaldi D, Spencer TJ, Roberts N, Mayes AR. 2006. The neural system that mediates familiarity memory. *Hippocampus* **16**: 504–520. http://doi.wiley.com/10.1002/hipo.20178.

Morales J, Lau H, Fleming SM. 2018. Domain-General and Domain-Specific Patterns of Activity Supporting Metacognition in Human Prefrontal Cortex. *J Neurosci* **38**: 2360–17. http://www.jneurosci.org/lookup/doi/10.1523/JNEUROSCI.2360-17.2018.

Morici JF, Bekinschtein P, Weisstaub N V. 2015. Medial prefrontal cortex role in recognition memory in rodents. *Behav Brain Res* **292**: 241–251.

http://dx.doi.org/10.1016/j.bbr.2015.06.030.

Muhammad R, Wallis JD, Miller EK. 2006. A comparison of abstract rules in the prefrontal cortex, premotor cortex, inferior temporal cortex, and striatum. *J Cogn Neurosci* **18**: 974–989.

Mundy ME, Downing PE, Dwyer DM, Honey RC, Graham KS. 2013. A critical role for the hippocampus and perirhinal cortex in perceptual learning of scenes and faces: Complementary findings from amnesia and fMRI. *J Neurosci* **33**: 10490–10502.

Murray EA, Bussey TJ. 1999. Perceptual-mnemonic functions of the perirhinal cortex. *Trends Cogn Sci* **3**: 142–151.

Murray EA, Mishkin M. 1998. Object recognition and location memory in monkeys with excitotoxic lesions of the amygdala and hippocampus. *J Neurosci* **18**: 6568–6582.

Murray EA, Richmond BJ. 2001. Role of perirhinal cortex in object perception, memory, and associations. *Curr Opin Neurobiol* **11**: 188–193.

Naya Y, Chen H, Yang C, Suzuki WA. 2017. Contributions of primate prefrontal cortex and medial temporal lobe to temporal-order memory. *Proc Natl Acad Sci* 201712711. http://www.pnas.org/lookup/doi/10.1073/pnas.1712711114.

Naya Y, Suzuki WA. 2011. Integrating What and When Across the Primate Medial Temporal Lobe. *Science (80-)* **333**: 773–776. http://www.sciencemag.org/cgi/doi/10.1126/science.1206773.

Neubert F, Mars RB, Sallet J, Rushworth MFS. 2015. Connectivity reveals relationship of brain areas for reward-guided learning and decision making in human and monkey frontal cortex.

Neubert FX, Mars RB, Thomas AG, Sallet J, Rushworth MFS. 2014. Comparison of Human Ventral Frontal Cortex Areas for Cognitive Control and Language with Areas in Monkey Frontal Cortex. *Neuron* **81**: 700–713. http://dx.doi.org/10.1016/j.neuron.2013.11.012.

Nichols TE, Holmes AP. 2002. Nonparametric permutation tests for functional neuroimaging: A primer with examples. *Hum Brain Mapp* **15**: 1–25.

Norman KA, O'Reilly RC. 2003. Modeling hippocampal and neocortical contributions to recognition memory: A complementary-learning-systems approach. *Psychol Rev* **110**: 611–646. http://doi.apa.org/getdoi.cfm?doi=10.1037/0033-295X.110.4.611.

O'Keefe J, Recce ML. 1993. Phase relationship between hippocampal place units and the EEG theta rhythm. *Hippocampus* **3**: 317–330.

O'Neil EB, Cate AD, Kohler S. 2009. Perirhinal Cortex Contributes to Accuracy in Recognition Memory and Perceptual Discriminations. *J Neurosci* **29**: 8329–8334. http://www.jneurosci.org/cgi/doi/10.1523/JNEUROSCI.0374-09.2009.

O'Neil EB, Protzner AB, McCormick C, McLean DA, Poppenk J, Cate AD, Köhler S. 2012. Distinct patterns of functional and effective connectivity between perirhinal cortex and other cortical regions in recognition memory and perceptual discrimination. *Cereb Cortex* **22**: 74–85.

Okuda J, Fujii T, Ohtake H, Tsukiura T, Tanji K, Suzuki K, Kawashima R, Fukuda H, Itoh M, Yamadori A. 2003. Thinking of the future and past: The roles of the frontal pole and the medial temporal lobes. *Neuroimage* **19**: 1369–1380.

Okuda J, Fujii T, Ohtake H, Tsukiura T, Yamadori A, Frith CD, Burgess PW. 2007. Differential involvement of regions of rostral prefrontal cortex (Brodmann area 10) in time- and event-based prospective memory. *Int J Psychophysiol* **64**: 233–246.

Oostenveld R, Fries P, Maris E, Schoffelen JM. 2011. FieldTrip: Open source software for advanced analysis of MEG, EEG, and invasive electrophysiological data. *Comput Intell Neurosci* **2011**.

Parker A. 1998. Interaction of frontal and perirhinal cortices in visual object recognition memory in monkeys. *Eur J Neurosci* **10**: 3044–3057.

Parker A, Gaffan D. 1998. Memory after frontal/temporal disconnection in monkeys:

Conditional and non-conditional tasks, unilateral and bilateral frontal lesions. *Neuropsychologia* **36**: 259–271.

Parks CM, Yonelinas AP. 2007. Moving beyond pure signal-detection models: Comment on wixted (2007). *Psychol Rev* **114**: 188–201.

Paxton R, Hampton RR. 2009. Tests of planning and the Bischof-Köhler hypothesis in rhesus monkeys (Macaca mulatta). *Behav Processes* **80**: 238–246.

Peltier SJ, Kerssens C, Hamann SB, Sebel PS, Byas-Smith M, Hu X. 2005. Functional connectivity changes with concentration of sevoflurane anesthesia. *Neuroreport* **16**: 285–288.

Petrides M. 2000. Dissociable roles of mid-dorsolateral prefrontal and anterior inferotemporal cortex visual working memory. *J Neurosci* **20**: 7496–7503.

Petrides M. 1995. Impairments on nonspatial self-ordered and externally ordered working memory tasks after lesions of the mid-dorsal part of the lateral frontal cortex in the monkey. *J Neurosci* **15**: 359–375.

Petrides M, Pandya DN. 1999. Dorsolateral prefrontal cortex: comparative cytoarchitectonic analysis in the human and the macaque brain and corticocortical connection patterns. *Eur J Neurosci* **11**: 1011–1036. http://doi.wiley.com/10.1046/j.1460-9568.1999.00518.x.

Petrides M, Pandya DN. 2007. Efferent Association Pathways from the Rostral Prefrontal Cortex in the Macaque Monkey. **27**: 11573–11586.

Pipa G. 2009. Performance- and stimulus-dependent oscillations in monkey prefrontal cortex during short-term memory. *Front Integr Neurosci* **3**: 1–7. http://journal.frontiersin.org/article/10.3389/neuro.07.025.2009/abstract.

Pitarque A, Sales A, Meléndez JC, Algarabel S. 2015. Repetition increases false recollection in older people. *Scand J Psychol* **56**: 38–44. http://doi.wiley.com/10.1111/sjop.12168.

Place R, Farovik A, Brockmann M, Eichenbaum H. 2016. Bidirectional prefrontal-hippocampal interactions support context-guided memory. *Nat Neurosci* **19**: 992–994.

Ploner CJ. 2000. Lesions Affecting the Parahippocampal Cortex Yield Spatial Memory Deficits in Humans. *Cereb Cortex* **10**: 1211–1216.

Pollmann S, Mahn K, Reimann B, Weidner R, Tittgemeyer M, Preul C, Müller HJ, Von Cramon DY. 2007. Selective visual dimension weighting deficit after left lateral frontopolar lesions. *J Cogn Neurosci* **19**: 365–375.

Preuss TM. 1995. Do rats have prefrontal cortex? The Rose-Woolsey-Akert program reconsidered. *J Cogn Neurosci* **7**: 1–24.

Quiroga RQ, Nadasdy Z, Ben-Shaul Y. 2004. Unsupervised spike detection and sorting with wavelets and superparamagnetic clustering. *Neural Comput* **16**: 1661–1687.

Ranganath C, Yonelinas AP, Cohen MX, Dy CJ, Tom SM, D'Esposito M. 2004. Dissociable correlates of recollection and familiarity within the medial temporal lobes. *Neuropsychologia* **42**: 2–13.

Rao SC, Rainer G, Miller EK. 1997. Integration of what and where in the primate prefrontal cortex. *Science (80-)* **276**: 821–824.

Ringo JL. 1996. Stimulus specific adaptation in inferior temporal and medial temporal cortex of the monkey. *Behav Brain Res* **76**: 191–197.

Ritchey M, Wing EA, LaBar KS, Cabeza R. 2013. Neural similarity between encoding and retrieval is related to memory via hippocampal interactions. *Cereb Cortex* **23**: 2818–2828.

Roca M, Torralva T, Gleichgerrcht E, Woolgar A, Thompson R, Duncan J, Manes F. 2011. The role of Area 10 (BA10) in human multitasking and in social cognition: A lesion study. *Neuropsychologia* **49**: 3525–3531.

Rossi S, Hallett M, Rossini PM, Pascual-Leone A, Avanzini G, Bestmann S, Berardelli A, Brewer C, Canli T, Cantello R, et al. 2009. Safety, ethical considerations, and application guidelines for the use of transcranial magnetic stimulation in clinical practice and research. *Clin Neurophysiol* **120**: 2008–2039.

http://dx.doi.org/10.1016/j.clinph.2009.08.016.

Rossi S, Rossini PM. 2004. TMS in cognitive plasticity and the potential for rehabilitation. *Trends Cogn Sci* **8**: 273–279.

Rossini PM, Barker AT, Berardelli A, Caramia MD, Caruso G, Cracco RQ, Dimitrijević MR, Hallett M, Katayama Y, Lücking CH, et al. 1994. Non-invasive electrical and magnetic stimulation of the brain, spinal cord and roots: basic principles and procedures for routine clinical application. Report of an IFCN committee. *Electroencephalogr Clin Neurophysiol* **91**: 79–92. http://www.elsevier.com/inca/publications/store/6/0/1/5/2/8%5Cnhttp://ovidsp.ovid.com/ovidweb.cgi?T=JS&PAGE=reference&D=emed13&NEWS=N&AN=2015834610.

Rotello CM, Heit E. 2000. Associative recognition: A case of recall-to-reject processing. *Mem Cogn* **28**: 907–922.

Rotello CM, MacMillan NA, Van Tassel G. 2000. Recall-to-Reject in Recognition: Evidence from ROC Curves. *J Mem Lang* **43**: 67–88.

Ryals AJ, Wang JX, Polnaszek KL, Voss JL. 2015. Hippocampal contribution to implicit configuration memory expressed via eye movements during scene exploration. *Hippocampus* **25**: 1028–1041.

Sakai K, Passingham RE. 2006. Prefrontal set activity predicts rule-specific neural processing during subsequent cognitive performance. *J Neurosci* **26**: 1211–1218.

Saleem KS, Logothetis N. 2012. A combined MRI and histology atlas of the rhesus monkey brain in stereotaxic coordinates.

Sallet J, Mars RB, Noonan MP, Neubert FX, Jbabdi S, O'Reilly JX, Filippini N, Thomas AG, Rushworth MF. 2013. The organization of dorsal frontal cortex in humans and macaques. *J Neurosci* **33**: 12255–12274.

Saunders RC, Aggleton JP. 2007. Origin and topography of fibers contributing to the fornix in macaque monkeys. *Hippocampus* **17**: 396–411.

http://doi.wiley.com/10.1002/hipo.20276.

Sauvage MM, Fortin NJ, Owens CB, Yonelinas AP. 2014. on Recollection and Familiarity. **11**: 16–18.

Sauvage MM, Fortin NJ, Owens CB, Yonelinas AP, Eichenbaum H. 2008. Recognition memory: Opposite effects of hippocampal damage on recollection and familiarity. *Nat Neurosci* **11**: 16–18.

Scalici F, Caltagirone C, Carlesimo GA. 2017. The contribution of different prefrontal cortex regions to recollection and familiarity. A review of fMRI data. *Neurosci Biobehav Rev* **83**: 240–251.

Scapinello KF, Yarmey AD. 1970. The role of familiarity and orientation in immediate and delayed recognition of pictorial stimuli. *Psychon Sci* **21**: 329–330.

Semendeferi K, Armstrong E, Schleicher A, Zilles K, Van Hoesen GW. 2001. Prefrontal cortex in humans and apes: A comparative study of area 10. *Am J Phys Anthropol* **114**: 224–241.

Sherman SJ, Hasselmo ME, Atri A, Stern CE, Howard MW. 2003. Scopolamine impairs human recognition memory: Data and modeling. *Behav Neurosci* **117**: 526–539.

Shrager Y, Gold JJ, Hopkins RO, Squire LR. 2006. Intact visual perception in memory-impaired patients with medial temporal lobe lesions. *J Neurosci* **26**: 2235–2240.

Skaggs WE, McNaughton BL, Wilson MA, Barnes CA. 1996. Theta phase precession in hippocampal neuronal populations and the compression of temporal sequences. *Hippocampus* **6**: 149–172. http://doi.wiley.com/10.1002/%28SICI%291098-1063%281996%296%3A2%3C149%3A%3AAID-HIPO6%3E3.0.CO%3B2-K.

Skinner EI, Fernandes MA. 2007. Neural correlates of recollection and familiarity : A review of neuroimaging and patient data. **45**: 2163–2179. http://dx.doi.org/10.1016/j.neuropsychologia.2007.03.007.

Solstad T, Moser EI, Einevoll GT. 2006. RAPID COMMUNICATION From Grid Cells to

Place Cells: A Mathematical Model. *Hippocampus* **1031**: 1026–1031.

Squire L, Zola-Morgan S. 1991. The medial temporal lobe memory system. *Science (80-)* **253**: 1380–1386. https://www.sciencemag.org/lookup/doi/10.1126/science.1896849.

Squire LR. 2004. Memory systems of the brain: A brief history and current perspective. *Neurobiol Learn Mem* **82**: 171–177.

Squire LR, Shrager Y, Levy DA. 2006. Lack of evidence for a role of medial temporal lobe structures in visual perception [2]. *Learn Mem* **13**: 106–107.

Squire LR, Stark CEL, Clark RE. 2004. the Medial Temporal Lobe. *Annu Rev Neurosci* **27**: 279–306.

Squire LR, Wixted JT. 2011. *The Cognitive Neuroscience of Human Memory Since H.M.*

Squire LR, Wixted JT, Clark RE. 2007. Recognition memory and the medial temporal lobe: A new perspective. *Nat Rev Neurosci* **8**: 872–883.

Srinath R, Ray S. 2014. Effect of amplitude correlations on coherence in the local field potential. *J Neurophysiol* **112**: 741–751.

Stam CJ. 2014. Modern network science of neurological disorders. *Nat Rev Neurosci* **15**: 683–695. http://dx.doi.org/10.1038/nrn3801.

Staresina BP, Cooper E, Henson RN. 2013. Reversible Information Flow across the Medial Temporal Lobe: The Hippocampus Links Cortical Modules during Memory Retrieval. *J Neurosci* **33**: 14184–14192.

Staresina BP, Davachi L. 2008. Selective and shared contributions of the hippocampus and perirhinal cortex to episodic item and associative encoding. *J Cogn Neurosci* **20**: 1478–1489.

Stark CEL. 2000. Intact Visual Perceptual Discrimination in Humans in the Absence of Perirhinal Cortex. *Learn Mem* **7**: 273–278. http://www.learnmem.org/cgi/doi/10.1101/lm.35000.

Stettler DD, Axel R. 2009. Representations of Odor in the Piriform Cortex. *Neuron* **63**: 854–

864. http://dx.doi.org/10.1016/j.neuron.2009.09.005.

Stokes MG. 2015. “Activity-silent” working memory in prefrontal cortex: A dynamic coding framework. *Trends Cogn Sci* **19**: 394–405. http://dx.doi.org/10.1016/j.tics.2015.05.004.

Stokes MG. 2005. Simple Metric For Scaling Motor Threshold Based on Scalp-Cortex Distance: Application to Studies Using Transcranial Magnetic Stimulation. *J Neurophysiol* **94**: 4520–4527. http://jn.physiology.org/cgi/doi/10.1152/jn.00067.2005.

Stokes MG, Barker AT, Dervinis M, Verbruggen F, Maizey L, Adams RC, Chambers CD. 2013. Biophysical determinants of transcranial magnetic stimulation: Effects of excitability and depth of targeted area. *J Neurophysiol* **109**: 437–444.

Stokes MG, Chambers CD, Gould IC, English T, McNaught E, McDonald O, Mattingley JB. 2007. Distance-adjusted motor threshold for transcranial magnetic stimulation. *Clin Neurophysiol* **118**: 1617–1625.

Suzuki WA. 1996a. Neuroanatomy of the monkey entorhinal, perirhinal and parahippocampal cortices: Organization of cortical inputs and interconnections with amygdala and striatum. *Semin Neurosci* **8**: 3–12.

Suzuki WA. 2009. Perception and the Medial Temporal Lobe: Evaluating the Current Evidence. *Neuron* **61**: 657–666. http://dx.doi.org/10.1016/j.neuron.2009.02.008.

Suzuki WA. 1996b. The anatomy, physiology and functions of the perirhinal cortex. *Curr Opin Neurobiol* **6**: 179–186.

Suzuki WA, Amaral DG. 1994a. Topographic organization of the reciprocal connections between the monkey entorhinal cortex and the perirhinal and parahippocampal cortices. *J Neurosci* **14**: 1856–1877.

Suzuki WA, Naya Y. 2014. The Perirhinal Cortex. *Annu Rev Neurosci* **37**: 39–53. http://www.annualreviews.org/doi/10.1146/annurev-neuro-071013-014207.

Suzuki WA, Zola-Morgan S, Squire LR, Amaral DG. 1993. Lesions of the perirhinal and parahippocampal cortices in the monkey produce long-lasting memory impairment in

the visual and tactual modalities. *J Neurosci* **13**: 2430–2451.

Suzuki WL, Amaral DG. 1994b. Perirhinal and parahippocampal cortices of the macaque monkey: Cortical afferents. *J Comp Neurol* **350**: 497–533. http://doi.wiley.com/10.1002/cne.20079.

Tallon-Baudry C. 2004. Oscillatory Synchrony in the Monkey Temporal Lobe Correlates with Performance in a Visual Short-term Memory Task. *Cereb Cortex* **14**: 713–720. https://academic.oup.com/cercor/article-lookup/doi/10.1093/cercor/bhh031.

Tanaka K. 1996. Inferotemporal Cortex and Object Vision. *Annu Rev Neurosci* **19**: 109–139. http://www.annualreviews.org/doi/10.1146/annurev.ne.19.030196.000545.

Thut G, Veniero D, Romei V, Miniussi C, Schyns P, Gross J. 2011. Rhythmic TMS causes local entrainment of natural oscillatory signatures. *Curr Biol* **21**: 1176–1185. http://dx.doi.org/10.1016/j.cub.2011.05.049.

Tompa T, Sáry G. 2010. A review on the inferior temporal cortex of the macaque. *Brain Res Rev* **62**: 165–182. http://dx.doi.org/10.1016/j.brainresrev.2009.10.001.

Tsujimoto S, Genovesio A, Wise SP. 2010. Evaluating self-generated decisions in frontal pole cortex of monkeys. *Nat Neurosci* **13**: 120–126.

Tsujimoto S, Genovesio A, Wise SP. 2012. Neuronal activity during a cued strategy task: Comparison of dorsolateral, orbital, and polar prefrontal cortex. *J Neurosci* **32**: 11017–11031.

Tulving E. 1985. Memory and consciousness. *Can Psychol Can* **26**: 1–12. http://doi.apa.org/getdoi.cfm?doi=10.1037/h0080017.

Tulving E, Stuss DT, Tulving E. 1995. Frontal Lobe Damage Produces Episodic Memory Impairment. *J Int Neuropsychol Soc* **1**: 525–536.

Van Essen DC, Glasser MF, Dierker DL, Harwell J. 2012. Cortical parcellations of the macaque monkey analyzed on surface-based atlases. *Cereb Cortex* **22**: 2227–2240.

Vighneshvel T, Arun SP. 2015. Coding of relative size in monkey inferotemporal cortex. *J*

Neurophysiol **113**: 2173–2179.

Vogt BA. 2005. Pain and emotion interactions in subregions of the cingulate gyrus. *Nat Rev Neurosci* **6**: 533–544.

Volle E, Gonen-Yaacovi G, de Lacy Costello A, Gilbert SJ, Burgess PW. 2011. The role of rostral prefrontal cortex in prospective memory: A voxel-based lesion study. *Neuropsychologia* **49**: 2185–2198. http://dx.doi.org/10.1016/j.neuropsychologia.2011.02.045.

Voytko M Lou. 1985. Cooling orbital frontal cortex disrupts matching-to-sample and visual discrimination learning in monkeys. *Physiol Psychol* **13**: 219–229.

Wais PE, Wixted JT, Hopkins RO, Squire LR. 2006. The hippocampus supports both the recollection and the familiarity components of recognition memory. *Neuron* **49**: 459–466.

Waldhauser GT, Johansson M, Hanslmayr S. 2012. Alpha/beta oscillations indicate inhibition of interfering visual memories. *J Neurosci* **32**: 1953–1961.

Wallis JD, Anderson KC, Miller EK. 2001. Single neurons in prefrontal cortex encode abstract roles. *Nature* **411**: 953–956.

Warburton EC, Brown MW. 2010. Neuropsychologia Findings from animals concerning when interactions between perirhinal cortex , hippocampus and medial prefrontal cortex are necessary for recognition memory. *Neuropsychologia* **48**: 2262–2272. http://dx.doi.org/10.1016/j.neuropsychologia.2009.12.022.

Wheeler MA, Stuss DT. 2003. Remembering and knowing in patients with frontal lobe injuries. *Cortex* **39**: 827–846.

Wilson FAW, Scalaidhe SP., Goldman-Rakic PS. 1993. Dissociation of object and spatial processing domains in primate prefrontal cortex. *Science (80-)* **260**: 1955–1958.

Wixted JT. 2007. Dual-process theory and signal-detection theory of recognition memory. *Psychol Rev* **114**: 152–176.

Wixted JT, Squire LR. 2008. Constructing receiver operating characteristics (ROCs) with experimental animals: Cautionary notes. *Learn Mem* **15**: 687–690.

Wixted JT, Stretch V. 2004. In defense of the signal detection interpretation of remember/know judgments. *Psychon Bull Rev* **11**: 616–641.

Womelsdorf T, Schoffelen JM, Oostenveld R, Singer W, Desimone R, Engel AK, Fries P. 2007. Modulation of neuronal interactions through neuronal synchronization. *Science (80-)* **316**: 1609–1612.

Xiang J-Z, Brown MW. 1998. Differential neuronal encoding of novelty, familiarity and recency in regions of the anterior temporal lobe. *Neuropharmacology* **37**: 657–676. https://linkinghub.elsevier.com/retrieve/pii/S0028390898000306.

Xiang JZ, Brown MW. 2004. Neuronal responses related to long-term recognition memory processes in prefrontal cortex. *Neuron* **42**: 817–829.

Yokoyama O, Miura N, Watanabe J, Takemoto A, Uchida S, Sugiura M, Horie K, Sato S, Kawashima R, Nakamura K. 2010. Right frontopolar cortex activity correlates with reliability of retrospective rating of confidence in short-term recognition memory performance. *Neurosci Res* **68**: 199–206. http://dx.doi.org/10.1016/j.neures.2010.07.2041.

Yonelinas AP. 2001. Components of episodic memory: The contribution of recollection and familiarity. *Philos Trans R Soc B Biol Sci* **356**: 1363–1374.

Yonelinas AP. 1994. Receiver-Operating Characteristics in Recognition Memory: Evidence for a Dual-Process Model. *J Exp Psychol Learn Mem Cogn* **20**: 1341–1354.

Yonelinas AP. 2002. The nature of recollection and familiarity: A review of 30 years of research. *J Mem Lang* **46**: 441–517.

Yonelinas AP, Aly M, Wang W, Koen JD. 2010. Recollection and familiarity: Examining controversial assumptions and new directions. *Hippocampus* **20**: 1178–1194. http://doi.wiley.com/10.1002/hipo.20864.

Yonelinas AP, Jacoby LL. 1994. Dissociations of processes in recognition memory: Effects of interference and of response speed. *Can J Exp Psychol Can Psychol expérimentale* **48**: 516–535. http://doi.apa.org/getdoi.cfm?doi=10.1037/1196-1961.48.4.516.

Yonelinas AP, Kroll NEA, Dobbins I, Lazzara M, Knight RT. 1998. Recollection and familiarity deficits in amnesia: Convergence of remember-know, process dissociation, and receiver operating characteristic data. *Neuropsychology* **12**: 323–339.

Yonelinas AP, Kroll NEA, Quamme JR, Lazzara MM, Sauvé MJ, Widaman KF, Knight RT. 2002. Effects of extensive temporal lobe damage or mild hypoxia on recollection and familiarity. *Nat Neurosci* **5**: 1236–1241.

Yonelinas AP, Parks CM. 2007. Receiver Operating Characteristics (ROCs) in Recognition Memory: A Review. *Psychol Bull* **133**: 800–832.

Zhivago KA, Arun SP. 2014. Texture discriminability in monkey inferotemporal cortex predicts human texture perception. *J Neurophysiol* **112**: 2745–2755.

Zola-Morgan S, Squire LR, Clower RP, Rempel NL. 1993. Damage to the perirhinal cortex exacerbates memory impairment following lesions to the hippocampal formation. *J Neurosci* **13**: 251–265.

Zola-Morgan S, Squire LR, Ramus SJ. 1994. Severity of memory impairment in monkeys as a function of locus and extent of damage within the medial temporal lobe memory system. *Hippocampus* **4**: 483–495.

Zola SM, Squire LR, Teng E, Stefanacci L, Buffalo EA, Clark RE. 2000. Impaired recognition memory in monkeys after damage limited to the hippocampal region. *J Neurosci* **20**: 451–463.

Supplemental Materials

Table 1. List of cortical ROIs revealed by non-parametric permutation to be significantly different in the 2-month post-FPC-lesion group vs. control group in Chapter 1.

ROI labels from LV-FOA-PHT composite parcellation	Cortical regions	MRI Coordinates of central voxel (mm)			Cluster number across animal groups		
		x	y	z	Control group	2-month Post-FPC lesion group	40-month post-FPC lesion group
Left GustCtx (LV00)	Gustatory cortex (LV00 atlas)	-20.4	3.1	3.3	2	1	2
Left GustCtx (PHT00)	Gustatory cortex (PHT atlas)	-20.4	9.1	1.1	2	1	2
Left PrCO	Precentral opercular area of the frontal operculum	-25.6	2.8	0.9	2	1	2
Left ProM	Proisocortical motor cortex	-23.0	10.8	-0.5	2	1	2
Left area 12	Area 12	-23.1	11.9	3.8	3	1	2
Left area 12o	Area 12 orbital subdivision	-18.4	12.9	1.2	3	1	2
Left area 12r	Area 12 rostral subdivision	-14.0	21.5	10.2	3	1	1
Left area 4C	Premotor area 4C	-16.8	2.1	17.1	3	1	3
Left area 6Val	Ventral premotor area subdivision al	-21.5	4.5	12.2	3	1	3
Left area 6Vam	Ventral premotor area subdivision am	-18.1	8.3	7.9	3	1	3

Left area 6Vb	Ventral premotor area subdivision b	-26.1	3.9	6.8	2	1	2
Left InsPro	Proisocortex	-18.5	5.8	-2.7	2	1	2
Left granInsula	Granular insula cortex	-18.8	-2.6	3.3	2	1	2
Left AIP	Anterior intraparietal area	-18.6	-12.7	14.6	3	1	3
Left LIPd	Lateral intraparietal area	-15.0	-22.5	18.7	3	1	3
Left S2	Somatosensory area 2 (complex)	-23.7	-7.8	6.5	4	1	2
Left area 1	Somatosensory area 1	-14.3	-11.6	21.3	1	1	3
Left area 2	Somatosensory area 2	-14.8	-12.9	19.7	1	1	3
Left area 3a	Somatosensory area 3a	-12.2	-8.4	17.7	1	1	3
Left area 3b	Somatosensory area 3b	-15.7	-9.0	15.8	1	1	2
Left area 5V	Somatosensory area 5v	-15.1	-18.8	18.9	3	1	3
Left area 7b	Visual area 7b	-24.5	-13.9	15.2	3	1	3
Left area 7op	Parietal operculum	-22.8	-17.9	13.0	3	1	3
Left area 7t	Transitional area 7	-23.3	-9.9	14.8	3	1	3
Left A1	Auditory cortex area 1	-24.2	-8.5	2.0	1	1	2
Left PiriCtx	Piriform cortex	-13.6	5.3	-6.0	2	1	2
Left ST2g	Superior temporal sulc area 2, gyral	-25.6	3.3	-5.1	4	1	2
Left TLR area 36R	Area 36 of perirhinal	-15.5	4.8	-16.7	3	1	1

	cortex (rostral subregion)						
Left Tpt	Temporo-parietal area	-28.7	-15.5	7.7	1	1	2
Left Ts	Superior temporal cortex	-28.4	-4.8	-0.6	4	1	2
Left area 35 (PHT00)	Area 35 of perirhinal cortex (PHT atlas)	-11.3	-4.3	-18.4	3	1	2
Right GustCtx (LV00)	Gustatory cortex (LV00 atlas)	21.3	2.3	3.9	2	1	2
Right GustCtx (PHT00)	Gustatory cortex (PHT atlas)	21.6	8.2	1.6	2	1	2
Right PrCO	Precentral opercular area of the frontal operculum	26.7	1.7	1.6	2	1	2
Right ProM	Proisocortical motor cortex	24.2	9.7	0.1	2	1	2
Right area 12	Area 12	24.2	10.9	4.5	3	1	2
Right area 12r	Area 12 rostral subdivision	15.0	20.9	10.6	3	1	1
Right area 13l	Area 13 lateral subdivision	14.6	12.9	4.1	1	1	1
Right area 6Val	Ventral premotor area 6a (lateral)	22.1	3.6	12.7	3	1	3
Right area 6Vam	Ventral premotor area 6a (medial)	18.9	7.5	8.4	3	1	3
Right area 6Vb	Ventral premotor area 6b	26.9	2.7	7.4	2	1	2
Right InsPro	Proisocortex	19.8	5.0	-2.2	2	1	2
Right granInsula	Granular insular cortex	19.6	-3.4	3.8	2	1	2
Right AIP	Anterior intraparietal area	18.7	-13.5	15.0	3	1	3

Right LIPd	Lateral intraparietal area	14.8	-23.1	19.0	3	1	3
Right S2	Somatosensory area 2 (complex)	24.3	-8.8	7.1	4	1	2
Right area 2	Somatosensory area 2	14.7	-13.5	20.1	1	1	3
Right area 3b	Somatosensory area 3b	15.9	-9.6	16.2	1	1	2
Right area 5V	Somatosensory area 5v	14.9	-19.4	19.3	3	1	3
Right area 7b	Visual area 7b	24.6	-15.0	15.9	3	1	3
Right area 7t	Transitional area 7	23.5	-10.9	15.4	3	1	3
Right A1	Auditory cortex area 1	25.0	-9.6	2.6	1	1	2
Right ST2g	Superior temporal sulc area 2, gyral	27.0	2.2	-4.5	4	1	2
Right ST2s	Superior temporal sulc area 2	23.9	2.7	-4.4	4	1	2
Right Ts	Superior temporal cortex	29.4	-6.0	0.1	4	1	2
Left V3A	Visual area 3a	-15.5	-32.1	13.1	2	2	1
Left area 18 (V2)	Visual area 2	-13.5	-37.0	1.5	2	2	3
Left DP	Dorsal prelunate area	-13.0	-33.3	19.1	4	2	1
Left PO	Parieto-occipital area	-4.5	-33.8	12.6	2	2	1
Left area 30	Retrosplenial cortex area 30	-1.9	-20.4	7.2	4	2	1
Left area 7a	Visual area 7a	-17.9	-24.9	18.2	3	2	3
Left MSTdp	Medial superior temporal	-15.2	-27.1	13.7	3	2	1

	area (subdivision dp)						
Left MT	Middle temporal area	-20.2	-22.7	4.5	1	2	1
Left V4ta	V4 transitional area (anterior)	-26.0	-17.8	2.9	1	2	1
Left VP	Ventral posterior area	-23.0	-29.5	-4.8	3	2	3
Left TPOr	Superior temporal sulcus dorsal bank (rostral)	-24.5	-9.3	-3.7	1	2	1
Right 46v	Area 46 (ventral subdivision)	13.1	16.3	12.7	3	2	1
Right 8as	Area 8A	11.3	12.3	17.3	4	2	1
Right V3A	Visual area 3a	15.3	-32.8	13.5	2	2	1
Right V4tp	V4 transitional area (posterior)	22.4	-26.2	9.1	3	2	1
Right area 18 (V2)	Visual area 2	13.8	-37.5	1.9	2	2	3
Right DP	Dorsal prelunate area	12.5	-33.9	19.5	2	2	1
Right PO	Parieto-occipital area	4.3	-34.0	12.7	2	2	1
Right area 23	Posterior cingulate area 23	4.2	-26.4	2.8	4	2	1
Right area 23b	Posterior cingulate cortex area 23b	1.7	-16.4	13.4	4	2	1
Right area 29d	Retrosplenial cortex area 29d	2.6	-18.5	7.3	4	2	1
Right area 30	Retrosplenial cortex area 30	2.2	-20.5	7.3	4	2	1

Right area 7a	Visual area 7a	17.6	-25.7	18.7	3	2	1
Right FST	Floor of superior temporal area	20.9	-18.3	0.7	1	2	1
Right MSTda	Medial superior temporal area (subdivision da)	19.5	-23.7	9.8	1	2	1
Right MSTdp	Medial superior temporal area (subdivision dp)	15.1	-27.8	14.1	2	2	1
Right MT	Middle temporal area	20.6	-23.5	5.1	1	2	1
Right V4	Visual area 4	26.2	-27.6	4.6	3	2	1
Right V4ta	V4 transitional area (anterior)	26.6	-19.0	3.6	1	2	1
Right VP	Ventral posterior area	23.8	-30.5	-4.2	3	2	3
Right TPOr	Superior temporal sulcus dorsal bank (rostral)	25.5	-10.4	-3.0	1	2	1